UNIVERSITÉ DU QUÉBEC À TROIS-RIVIÈRES

INTÉGRATION DE DIVERSES CONDITIONS DE FONCTIONNEMENT DANS L'IDENTIFICATION EN TEMPS RÉEL ET LA GESTION ÉNERGETIQUE D'UN VÉHICULE À PILE À COMBUSTIBLE

THÈSE PRÉSENTÉE
COMME EXIGENCE PARTIELLE DU

DOCTORAT EN GÉNIE ÉLECTRIQUE

PAR
MOHSEN KANDIDAYENI

MAI 2020

Université du Québec à Trois-Rivières

Service de la bibliothèque

UNIVERSITÉ DU QUÉBEC À TROIS-RIVIÈRES

INTEGRATING VARIOUS OPERATING CONDITIONS INTO REAL-TIME
IDENTIFICATION AND ENERGY MANAGEMENT OF A FUEL CELL VEHICLE

A THESIS PRESENTED
IN PARTIAL FULFILLMENT OF
THE REQUIREMENTS FOR THE DEGREE

DOCTOR OF PHILOSOPHY IN ELECTRICAL ENGINEERING

BY
MOHSEN KANDIDAYENI

MAY 2020

UNIVERSITÉ DU QUÉBEC À TROIS-RIVIÈRES

DOCTORAT EN GENIE ÉLECTRIQUE (Ph.D.)

Direction de recherche :

Loïc Boulon	directeur de recherche

Sousso Kelouwani	codirecteur de recherche

Jury d'évaluation

Nadia Yousfi Steiner	évaluateur externe (Université de Franche-Comté)

Kamal Al-Haddad	évaluateur externe (École de technologie supérieure)

François Nougarou	président du jury (Université du Québec à Trois-Rivières)

Loïc Boulon	directeur de recherche (Université du Québec à Trois-Rivières)

Sousso Kelouwani	codirecteur de recherche (Université du Québec à Trois-Rivières)

Thèse soutenue le 27 Avril 2020

UNIVERSITÉ DU QUÉBEC À TROIS-RIVIÈRES

DOCTOR OF PHILOSOPHY IN ELECTRICAL ENGINEERING (Ph.D.)

Research Supervision:

Loïc Boulon	research director

Sousso Kelouwani	research co-director

Evaluation jury

Nadia Yousfi Steiner	external evaluator (Université de Franche-Comté)

Kamal Al-Haddad	external evaluator (École de technologie supérieure)

François Nougarou	jury president (Université du Québec à Trois-Rivières)

Loïc Boulon	research director (Université du Québec à Trois-Rivières)

Sousso Kelouwani	research co-director (Université du Québec à Trois-Rivières)

Thesis defended on 27 April 2020

Abstract

The autonomy and lifetime of a fuel cell hybrid electric vehicle (FCHEV) depend on the design of an appropriate energy management strategy (EMS), which is normally premised on the proton exchange membrane (PEM) fuel cell (FC) model. However, dependency of the PEMFC energetic performance on its operating conditions and impact of aging have made the design of a precise model immensely complicated. In this respect, a new paradigm has been proposed to avoid the complex modeling of PEMFCs. The idea is to integrate an online PEMFC model identification into the EMS loop to use updated models with close performance to reality. Driven by this motivation, this thesis is meant to contribute to the integration of such online modeling into the design of EMSs. In this respect, firstly, the potential of EMS adaptation into PEMFC performance drifts and systemic management is investigated in terms of fuel economy. After indicating the importance of the hypothesis, a benchmark problem is conducted to select a suitable multi-input PEMFC model and an online identification method. Moreover, the challenges regarding the initialization of the identification methods are investigated. However, this analysis only deals with the electrical side of the FC generator while PEMFC is a multiphysics system with multi inputs and outputs. Therefore, next, a concurrent temperature and current management strategy is developed to consider the PEMFC as a complete system and not just an electric generator. The main objective is to enhance the efficiency of the system, while supplying the requested power, by choosing the right combination of reference temperature and current levels through an updatable 3D power map. The last stage of this work copes with the incorporation of the above-mentioned phases into the design of an EMS. The necessity of updating the PEMFC model while designing an EMS as well as the influence of the discussed simultaneous systemic management over the efficiency upgrade of a FCHEV are thoroughly scrutinized in this phase. The experimental outcomes of this thesis indicate that the performance drifts occurred in a FC system can cause considerable mismatches on the operation of a FCHEV and they can be avoided by using the proposed online PEMFC model in the first stage of this work. Moreover, the put forward concurrent management in the second phase can enhance the fuel economy of a FCHEV up to almost four percent in the tested driving cycles.

Acknowledgement

Undertaking this PhD has been a truly life-changing experience for me, and it would not have been possible without the support and guidance that I received from many people.

Firstly, I would like to express my sincere gratitude to my supervisor Prof. Loïc Boulon for the continuous support of my PhD study and related research, for his patience, motivation, and immense knowledge. Moreover, I would like to say a sincere thanks to my co-supervisor Prof. Sousso Kelouwani. His guidance helped me in all the time of research and writing of this thesis. I could not have imagined having a better supervisor and co-supervisor for my PhD study.

Besides my supervisors, I would like to thank the rest of my thesis committee: Prof. Kamal Al-Haddad, Prof. Nadia Yousfi Steiner, and Prof. François Nougarou, for their insightful comments and encouragement.

My sincere thanks also go to Prof. Hicham Chaoui, who provided me with an opportunity to join his team as intern, and who gave access to the laboratory and research facilities.

I gratefully acknowledge the funding received from Fonds de recherche du Québec - Nature et technologies (FRQNT), a granting agency of the Quebec government, which enabled me to do my PhD without financial concerns.

A very special thanks to my fellow labmate (Alvaro Macias) for the stimulating discussions, for the sleepless nights we were working together before deadlines, and for all the fun we had in the last three years. I also thank all my friends in the Institut de recherche sur l'hydrogène (IRH) who were always so helpful in numerous ways.

My heartfelt thanks to my lovely wife who has been by my side throughout this PhD, living every single minute of it, and without her, I would not have had the courage to embark on this journey in the first place.

Last but not the least, I would like to thank my family to whom I am indebted all my success: my parents, my brothers, and my sisters for supporting me spiritually throughout my life from the first step until now.

Table of Contents

List of Tables

List of Figures

List of Symbols

B	Parametric coefficient
BOL	Beginning of life
CYC_WVUINTER	West Virginia Interstate Driving Schedule
DP	Dynamic programming
ECMS	Equivalent consumption minimization
EKF	Extended Kalman filter
EMS	Energy management strategy
EOL	End of life
FC	Fuel cell
FCHEV	Fuel cell hybrid electric vehicle
FLC	Fuzzy logic controller
FOA	Firefly optimization algorithm
GA	Genetic algorithm
HIL	Hardware-in-the-loop
ICA	Imperialist competitive algorithm
IRH	Hydrogen Research Institute
KF	Kalman filter
ME	Maximum efficiency

| MLP | Multi-layer perceptron |
| QP_{Outdated} | QP using commercial controller and an outdated map |

MLP   Multi-layer perceptron

MP   Maximum power

NiMH   Nickel-metal hydride

PEM   Proton exchange membrane

PMP   Pontryagin's minimum principle

Q Covariance matrix of the process noise

QP   Quadratic programming

$QP_{Outdated}$ QP using commercial controller and an outdated map

QP_{Sys} Systemic management based QP

$QP_{Updated}$ QP using commercial controller and the updated map

R Covariance matrix of the measurement noise

RLS   Recursive Least Square

$R_{internal}$ Internal resistor

SC   Supercapacitor

SFLA   Shuffled frog-leaping algorithm

SOC   State of charge

SOH   State of the health

SSE   Sum of squared errors

SSO   Slap swarm optimizer

ΔSOC   Difference between initial and final SOC

ξ_1 Semi-empirical coefficient

ξ_2	Semi-empirical coefficient
ξ_3	Semi-empirical coefficient
ξ_4	Semi-empirical coefficient
$1D - New\ FC$	Unidimensional DP for new PEMFC
$1D - FI$	Unidimensional DP with the false input
$2D - New\ FC$	Bidimensional DP for new PEMFC
WLTC_class 2	Worldwide harmonized light-duty vehicles test cycles

Chapter 1 - Introduction

1.1 Motivation

Anthropogenic emission of carbon dioxide has been voiced as one of the underlying causes of global warming. In this light, transportation sector is widely blamed for the combustion of petroleum-derived commodities, like gasoline, in internal combustion engines, which produce a fair amount of this heat-trapping gas. Passenger cars are perceived as the most significant source of transportation-related greenhouse gas discharge. Hence superseding the dirty energy sources by cleaner ones in order for powering the vehicles is an important measure to tackle this worldwide crisis [1, 2].

Electric and hybrid electric vehicles could be appropriate substitutes for conventional vehicles. However, the latter still relies on fossil fuels and the former suffers from restricted driving range as well as long charging time. These pitfalls have paved the way for the emergence of alternative power sources like fuel cells (FCs), which are run on hydrogen, in vehicular applications. Among various types of fuel cells, proton exchange membrane fuel cell (PEMFC) possesses a great potential (low-temperature operation, high power density, and solid electrolyte [3]) to be employed in vehicular application.

However, challenges keep arising in the evolution of the hydrogen vehicles and have stopped them from a full penetration into the automotive markets [4]. Some of the key challenges facing these vehicles are hydrogen production, infrastructures, storage, cost, reliability, and performance. In this regard, ongoing researches and projects are being

conducted with the aim of delivering renewable hydrogen to market at less than the cost of fueling a conventional vehicle, providing thousands of hydrogen stations, and shifting the hydrogen storage technology from high-pressure tanks to material-based storage. Apart from the mentioned ongoing objectives, hydrogen vehicles need to win consumers' trust by providing them with a feasible alternative, particularly in terms of performance, reliability, and cost, to survive in this ultra-competitive market. The stated indexes are related to some of the inherent shortcomings of the PEMFCs as follows:

- Slow response to the demanded power

- Fluctuation of output voltage with respect to the load variations

- Self-Cold start issues in cold weather countries

- Incapability of energy recovery through regenerative braking, compared to other sources such as batteries

Therefore, utilizing a sole fuel cell system as a power source cannot satisfy all the requirements of a vehicle due to its intrinsic characteristics and employing a secondary power source, such as battery, supercapacitor (SC), etc., is necessary in order of satisfying the fast dynamic load in vehicles, reducing degradation rate of the PEMFC by absorbing the power peaks, increasing the fuel economy, powering the load during cold start, and energy recovery. Common structures for hybridization of hydrogen vehicles are FC-battery, FC-SC, and FC-battery-SC. The vehicles with such structures are known as fuel cell hybrid electric vehicles (FCHEVs) in which a PEMFC stack acts as the primary power source and a battery pack or/and supercapacitor bank as the secondary power source. FCHEVs do not have the limitations of their competitors and benefit from definite merits, such as high efficiency,

pollution free essence, and convenient maintenance, by comparison [5]. Forklifts have already given PEMFC technology a welcome boost as the early adopters of this energy system. Moreover, FCHEVs are presenting a steadily growing division of the road vehicles market to the extent that a large number of prototypes of different brands and sizes have been developed, such as Hyundai Nexo, Honda Clarity, Mercedes-Benz F-Cell, and Toyota Mirai.

All of the above-mentioned hybrid structures have their own advantages and disadvantages [6]. However, among them, FC-battery structure has been widely employed in practical FCHEVs [7, 8]. This structure benefits from a low cost of powertrain and a low fuel consumption in comparison to the FC-SC system. FC-battery-SC structures have lower fuel consumption and are able to extend the battery lifetime compared to FC-battery systems [6]. Nevertheless, the latter has lower powertrain cost, less mass, and more compact volume, due to using solely one converter without a SC. Among the existing rechargeable batteries, Li-ion battery is considered as a potential secondary source in FCHEVs since it is being used in many hydrogen cars, such as Hyundai Nexo, Honda Clarity, and Mercedes-Benz F-Cell, due to the merits of high capacity, several charge–discharge cycles and acceptable cost [9]. Toyota has tried to be flexible since it uses Li-ion battery in some models (Prius Prime) and Nickel-metal hydride (NiMH) in others (Mirai).

With all the favorable attributes of hybridizing the sources, the performance of an FCHEV is impacted by several interrelated factors, which put the design of an energy management strategy (EMS) in a critical position to enhance the performance and reduce cost [10].

1.2   Literature study

The overall performance of FCHEVs regarding fuel or energy consumption heavily relies on the particular powertrain components efficiency and accurate coordination. Traditionally, the overall aim of an EMS design is to ameliorate fuel economy and lifetime during a driving profile, without sacrificing vehicle performance, by controlling the power flow between the PEMFC, battery, and the drive train. The EMS should ensure the following goals:

- The output power of the electric motor always satisfies the demanded power.

- The level of energy is always maintained within the good operating region in the battery.

- The PEMFC system operates within its efficient operating region.

Several EMSs have been utilized for splitting the power in the previously-discussed structures in FCHEVs. These EMSs fall under three categories of rule-based, optimization-based and intelligent-based [11-16]. The rule-based EMSs are typically designed based on human intelligence and heuristic techniques which are not guaranteed to be optimal or perfect, but instead adequate for attaining an immediate purpose [17]. Optimization-based strategies aim at minimizing a defined cost function. They can be divided into two groups of global and real-time strategies. The former optimizes the cost function over a fixed driving cycle. The latter, however, employs an instantaneous cost function based on the variables of the system. Optimization-based EMSs theoretically offer near-optimal solutions and are also capable of drawing up new guidelines for revising the set of rules and inferential knowledge of the rule-based methods [18]. Depending on the purpose of the project, dynamic programming (as an optimal theory-based strategy) [19, 20] and metaheuristic algorithms,

such as genetic algorithm (GA) [21], (as near optimal strategies) have been abundantly used for the development of off-line global EMSs. Real-time strategies have been also formulated by using optimal theory-based methods, such as quadratic programming (QP) [22-25], Pontryagin's minimum principle (PMP) [26, 27], and equivalent consumption minimization strategy (ECMS) [28, 29] with respect to the formulation of the cost function. Intelligent-based strategies normally use the car navigation data and the history of motion for recognizing and predicting the driving condition [30, 31]. They can be incorporated into the both of ruled-based and optimization-based strategies to compensate for sensitivities and problems related to the driving condition prediction. Several EMSs based on the discussed categories and their combinations are available in the literature for hybrid vehicles. A brief summary of the very recent developed strategies is given in the following paragraph to clearly highlight the contribution of this manuscript.

In [32], a multi-mode fuzzy logic controller (FLC) is used to perform the power split in a FCHEV. The mode of the FLC is determined by a multi-layer perceptron (MLP) neural network using the historical velocity window and the rule base is optimized by GA. This strategy has improved fuel economy by 8.89%, compared to a single-mode fuzzy EMS. In [33], a multi-state (i.e., coasting, braking, and station parking) ECMS is formulated by using a quadratic form energy consumption curve of the PEMFC stack in a tram which has led to 2.5% energy consumption decline compared to a rule-based power following EMS. In [34], convex optimization is proposed to minimize the cost of energy by optimizing the control decisions and the cost power sources (PEMFC stack and battery pack) by finding the optimum size of the components. This study shows that appropriate rated power of the PEMFC can decrease the hydrogen cost up to 61%. In [35], the performance of an ECMS for

a FC-SC tram is improved by combining the ECMS with a rule-based state machine strategy to increase the PEMFC operating time in the high-efficiency range. In [36], an EMS is proposed premised on slap swarm algorithm, which is a recent metaheuristic optimization method. This strategy attempts to minimize the total hydrogen consumption by maximizing the power supplied by the SC and battery pack and shows a superior performance compared to state machine, FLC, GA, and ECMS. In [37], a heuristic strategy called bounded load following strategy is proposed for a FC-battery vehicle where the PEMFC power is bounded between two limits according to the efficiency curve of the stack. The boundaries of this strategy are also refined with respect to the optimal trajectory obtained by dynamic programming (DP) and it is indicated that its performance is very close to DP. An online EMS based on data fusion approach has been suggested in [38]. In this work, three FLCs have been optimized for three different driving conditions, namely highway, suburban and city offline by means of genetic algorithm. Afterwards, probabilistic support vector machine is used to provide probabilistic prediction of the driving condition. Finally, Dempster-Shafer evidence theory is used to fuse the offline optimized FLC parameters to adapt to the driving prediction. It should be noted that the considered constraints to design the controller in this work come from a static efficiency-power map of a PEMFC. In [39], an adaptive control method based on tuning the FLC parameters for normal, regenerative, and overload driving conditions is proposed. It has been mentioned in this work that the output voltage of the PEMFC will decline after long periods of driving and under this condition some of the rule-based values should be reconsidered. In [40], an online EMS based on extremum seeking method is suggested to maintain the PEMFC operating points in high efficiency region and thus increase the fuel economy. Three schemes of first-order, high-pass filter based, and band-pass filter based extremum seeking method are compared and concluded that the band-

pass filter is preferred to enhance both performance and durability of the system. A two-layer EMS composed of rule-based approach and particle swarm optimization has been proposed for real-time control of FCHEVs in [41]. The rule-based layer is responsible for restricting the search space to ensure a fast convergence of the metaheuristic layer. The metaheuristic layer purpose is to determine the optimal PEMFC power and battery state of charge to reach the minimum fuel consumption. The rule-based of this work has been designed based on a static PEMFC map. In [42], an EMS based on neural networks is introduced for a FC-battery vehicle. In this respect, the neural networks have been trained by means of the obtained optimal power splitting between a PEMFC and a battery system, which minimizes the overall equivalent energy consumption. The optimal solution has been achieved by conducting a gradient-based method minimization over eight various driving profiles. In [43], a rule-based EMS based on frequency decoupling is proposed, in which the SC serves as high frequency power backup. The frequency-based approach utilizes the energy sources in different frequency ranges and avoid oxygen starvation or operation outside the safe limits. In [44], an EMS is proposed based on short-term energy estimation to maintain the state of energy of the SC within an active limits in a FC-battery structure. The PEMFC limit is based on a quasi-static model in this work and it has been stated that it is not obvious how to precisely establish the power rate limits to avoid premature ageing of PEMFC. In [45], an EMS, based on stochastic dynamic programming, is suggested to optimize the fuel consumption as well as the PEMFC lifetime. A simple model is proposed in this work to estimate the effect of EMS on the PEMFC degradation. In [46], a multi-objective strategy is proposed to enhance the fuel economy and system durability of a FC-battery vehicle. In this work, a so-called soft-run strategy, which is a rule-based strategy derived from the results of an offline dynamic programming optimization, is proposed for real-time EMS purposes.

In the light of the above-discussed articles, it is evident that the majority of the existent EMSs in the literature, namely rule-based, optimization-based, and intelligent based, are premised upon PEMFC parametric models, especially static models [47-49]. In this respect, PEMFC modeling is of vital importance and a wise selection of the model should be made with regard to the particular goals of the project. However, some factors such as dependency of a PEMFC energetic performance on its operating conditions (temperature, pressure, current, etc.), impact of aging and degradation phenomena on its performance, and so forth have made the design of a complete PEMFC model immensely complicated. In other words, a complete model of a fuel cell system is not still available and is considered as a study limitation. It should be noted that various models have been proposed for a fuel cell system which are capable of dealing with the variations of the operating conditions [50]. These models are by some means convincing, though not perfect, with regard to coping with the operating conditions influences. However, aging phenomenon, which is a very complicated process, has not been resolved yet and there is no model to perfectly consider the effect of aging.

In this respect, some considerable efforts have been made to make the EMS design immune to PEMFC performance drifts by adding a degradation model to the system [51-54]. However, degradation and ageing mechanisms are very complex to be modeled. Moreover, the operation parameters and conditions which are not included in the PEMFC model, such as humidity or ambient temperature, can also change the maximum efficiency (ME) and maximum power (MP) ranges of the stack that are normally among the utilized limitations in the EMS design. To evade the mentioned issues regarding the degradation and conditions modeling, two approaches of extremum seeking and PEMFC model parameters online

identification have come under attention. The former consists in the use of extremum seeking methods in which an optimal operating point is sought after using a periodic perturbation signal in real-time [40, 55, 56]. Such strategies are of interest mostly due to their straightforward implementation while they are not very effective when concurrent identification of several operating points is required in online applications. The thing is that a separate search line for each intended characteristic such as ME and MP is needed in this method. To avoid this problem, some researches have been conducted by utilizing recursive filters for online identification of the PEMFC parameters and extracting the necessary characteristics from the updated model. [57-61] have been done in the Hydrogen Research Institute (IRH). In [57], Ettihir et al. have proposed the utilization of a semi-empirical model, which is only a function of current, with a recursive least square method to get the characteristics of the PEMFC online. They have integrated this work into the EMS design of a FCHEV as well and achieved interesting results [58-60]. Kelouwani et al. have suggested an experimental study based on tracing the maximum efficiency of the PEMFC. In this study, a polynomial model of the PEMFC efficiency is introduced and the best efficiency is looked after by adjusting the control variables, namely current, stoichiometry, and temperature [61]. Methekar et al. has introduced an adaptive control of a fuel cell system with a Wiener model and suggested a numerical validation [62]. Dazi et al. have developed a predictive control to ascertain the maximum power operation of a fuel cell system [63]. In [64], an adaptive supervisory control strategy for a FC-battery bus based on equivalent consumption minimization is proposed. In this paper, an algorithm has been used for charge-sustaining and a recursive least square has been employed for performance identification of the PEMFC. The utilized PEMFC model of this work is a very simple semi-empirical model, which is

only a function of current, and there is no experimental validation for the PEMFC performance.

1.3 Problem statement and conceptual framework of the thesis

With respect to the investigated works, it can be inferred that the employment of real-time techniques needs to be paid more attention with a specific view to adapting the design of EMSs to the real behavior of the PEMFCs. As pointed out earlier, some operational characteristics of the PEMFC stack, such as maximum efficiency and maximum power points, are typically considered as the design variables while developing an EMS. Nevertheless, these characteristics vary through time owing to several reasons, such as operating conditions variation (temperature, pressure, humidity etc.), ageing, and degradation phenomena. Figure 1.1 shows the performance drifts of a 500-W Horizon PEMFC stack in terms of power delivery. Moreover, the change of rated power of the stack with regard to the variation of the operating current and stack temperature is visible in this figure. Figure 1.1a indicates a 20-percent drift in the maximum power of the stack based on which the beginning of life (BOL) and end of life (EOL) have been defined. Figure 1.1b represents the drifts as the result of season change which means the ambient conditions have mostly altered (27°C in Summer and 20°C in Winter). The stars represent the location of maximum power which changes in each case. Regardless of the reason for the variations of the PEMFC stack characteristics, it is vital to consider them in the EMS as they act like uncertainties. When these variations are not tracked, they cause mismanagement in the operation of the vehicle since they change the assumed limits in the controller. There exists several proposed online and real-time EMSs for the application of FCHEVs. However, only few of them have tried to take the real characteristics of the PEMFC into account while designing the EMS.

Moreover, the few existing works regarding the PEMFC investigation behavior are mainly simulation based and lack the experimental validation.
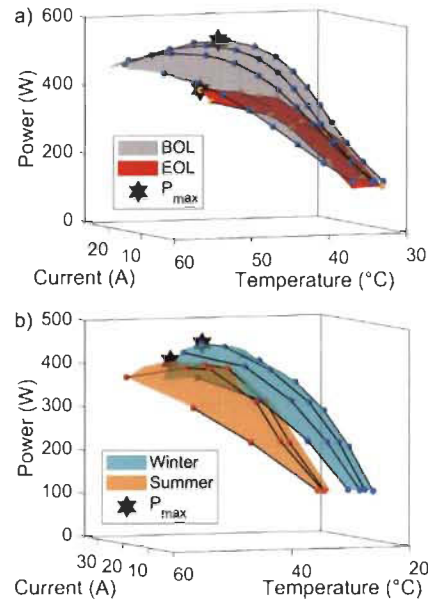
Figure 1.1   The variation of a PEMFC stack characteristics through time, a) lifetime variation, b) seasonal variation.

Another aspect that has escaped the attention of many researchers in the domain of EMS design for FCHEVs is adopting a systemic approach towards the management of the PEMFC stack while developing a strategy. The existing EMSs normally define the required current from the PEMFC stack. Nonetheless, regarding the PEMFC as a system provides several degrees of freedom in terms of supplying the power since the influential operating points in the performance of the PEMFC, such as current and temperature, can come under control in this way. A specific requested power from the PEMFC can be supplied by different combinations of these operating conditions to improve the efficiency [65]. It should be noted there exists many works concerning the thermal/current management of the PEMFC stacks [66-69]. However, to the best of the authors' knowledge, the integration of a simultaneous current and temperature management, which have different physical dynamics, into the

design of an EMS has not been considered so far. Figure 1.2 indicates the general concept put forward by this thesis to upgrade the efficiency of the existing EMSs and make them more robust against the performance drifts of a PEMFC stack. The whole process is conducted online while the PEMFC is under operation. The global EMS comprises three stages, namely parameter identification along with the local management, information extraction, and power split strategy. The objective is to do an online parameter identification to adapt the model to the performance drifts of the PEMFC, and then define the best operating points in the information extraction stage while having a local management over the operating parameters of the stack. Afterwards, the obtained data can be used in the power split strategy stage to control the power flow between the sources. This three-stage process is called global EMS.
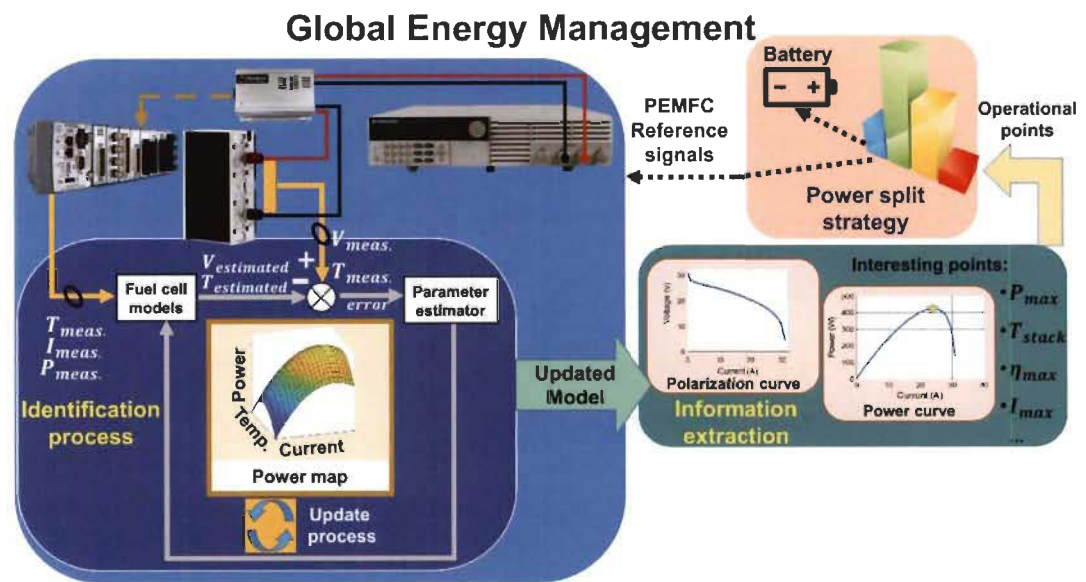
Figure 1.2   The general concept for designing a global EMS for a FCHEV.

1.4   Contribution of the project

Literature consideration indicates that there are a variety of approaches, online and offline, to distribute the power between two sources in a FCHEV. Moreover, there are several research methods to determine the best performance of the PEMFCs or improve its efficiency through local managements of the stack. However, it should be noted that there are only a few EMSs that attempt to link the power splitting in a FCHEV with the real-time performance identification of the PEMFC. In this regard, this work aims to utilize parameter estimation algorithms, which has been suggested to deal with the problems caused by operating conditions variations, degradation and aging, to cope with performance drifts of the PEMFC. It should be noted there are some works in this regard [57-60], as discussed in the previous section. However, a meticulous attention has not been paid to the choice of model and estimation method since the aim has been to reach the proof of concept by applying it to the EMS design.

Apart from the mentioned point, one central feature that the researchers have failed to notice so far in the domain of EMS design for FCHEVs is to consider a systemic method for the management of a PEMFC stack while developing a strategy. In literature, operating current and stack temperature are normally perceived as independent control variables where the existing works focus on controlling either of them. Nevertheless, PEMFC is a multi-physical system with strong dynamic interactions between current and temperature. Having a systemic look at the PEMFC stack makes the design of multi-output EMSs possible which means the requested power from the stack can be supplied by higher efficiency as it can use different combinations of operating parameters such as current and temperature.

In this regard, two principal directions have been followed in this thesis:

- Providing a scientific rigor for the proposed basis by the previous studies, to choose a proper PEMFC model and identification method, by performing a benchmark analysis.

- Pushing the concept forward by integrating a multi-input model and its current and thermal managements into the EMS design.

1.4.1 Aims and objectives

This thesis attempts to bridge the gaps which have been brought into attention by pursuing the above-mentioned directions. In this respect, the main objective is to integrate the online parameters estimation and systemic management of a PEMFC stack into the design of an online EMS in a FCHEV. To this end, the following goals are set:

➢ Performing a benchmark analysis to give a strong structure to the concept:

The previous studies are based on a single-input model, which is only dependent on the current, and the other operating conditions, such as temperature, pressure, etc., are considered as perturbations. In this work, a benchmark analysis is conducted with the aim of selecting a multi-input model, which embraces the main operating conditions, such as current, temperature, and pressure, and integrate a suitable parameter identification method into it to compensate the model uncertainties due to degradation and the operating conditions which are not considered in the model, like humidity. Since this work aims at designing a multi-input EMS, it is necessary to have a dependable multi-input model.

➢ Concurrent thermal and current management of the PEMFC stack:

The benchmark analysis leads to the selection of a parameter estimation method as well as a multi-input model for predicting the behavior of the PEMFC. Temperature is one of the inputs of the chosen multi-input electrochemical model, and its value comes from the measurement from a real PEMFC. However, the regulation of temperature, which has an important role in its performance since very low or high operating temperature can deteriorate the performance and decrease the lifetime of the PEMFC, is not possible with only the electrochemical model. In this regard, a thermal model of the PEMFC, which allows controlling the temperature by acting on the fan, is in demand. The second objective of this work is to use a thermal model besides the PEMFC electrochemical model to provide a local thermal and current management. This systemic management helps to reach the desired power level efficiently by choosing the right level for temperature and current.

➢ Integration into EMS design for a FCHEV:

The package of online voltage model and the thermal model along with the local management over the stack is used to design a global EMS. The main idea is to perform a real-time model identification to find the best operating points through an information extraction stage. Subsequently, the power split strategy can use the provided data from the updated PEMFC model to optimally distribute the power flow. In addition to work with the updated data, the other contribution of this EMS compared to the available ones in the literature is that it works with more than one reference signal. In fact, it determines the reference temperature of

the PEMFC through the defined local management as well as the reference operating current.

1.5   Methodology

After discussing the motivation and conducting a comprehensive literature survey to highlight the gaps in this line of work in the first step (Chapter 1), the second step deals with providing a concrete basis for supporting the hypothesis that online modeling of a PEMFC stack and its systemic management can lead to the performance enhancement of an EMS in a FCHEV. In this respect, an optimal EMS based on DP is formulated to compare the hydrogen consumption of a simulated FCHEV for different scenarios. In the first scenario, the fuel economy of the vehicle is investigated by developing a unidimensional DP to determine the optimal trajectory of the PEMFC current while using two PEMFC stacks with different levels of degradation in which the rated powers are not the same. This analysis will show the effect of PEMFC stack degradation on the vehicle's fuel economy. In the second scenario, a bidimensional DP is developed for the new PEMFC case in the first scenario to determine the optimal trajectory of PEMFC current and cooling fan duty cycle. Then the results are compared with the unidimensional EMS to realize the influence of conceiving the PEMFC as a system while designing an EMS.

The third step of this work focuses on the online parameters' identification of a PEMFC stack. As there are a few studies within this scope, this step provides a conclusive rigor to this methodology by: 1) Reviewing the literature to determine the present-day state of information about the proposed topic. Subsequently, the considered methods are categorized in terms of precision, applicability in online situations and energy management purposes; 2) performing a benchmark problem analysis based on the suitable recognized candidates of the

first step to select a suitable multi-input PEMFC model and an identification method for further stages; 3) experimental validation of the selected model and identification technique.

The fourth step of this thesis copes with the initialization and customization of recursive filters for the online PEMFC parameters' estimation problem. In this respect, a benchmark study of three well-known metaheuristic optimization algorithms is performed to introduce a dependable technique for the initial tuning of the model parameters and the recursive filter variables. It should be noted that metaheuristic algorithms are the most common approach in the literature to extract the parameters of a PEMFC model. The quality of online PEMFC characteristics estimation is scrutinized for different initial tuning of the parameters.

The last step of this work deals with the development of a simultaneous current and temperature management through mapping the PEMFC characteristics and the integration of this approach to the EMS design of a FCHEV. The main challenge for the systemic management development is different physical dynamics of current, which is very fast, and temperature, which is very slow. The systemic management provides the opportunity to have a local control over the PEMFC system to enhance its performance in real-time. Such a systemic management is suitable for energy management purposes. In this respect, the obtained temperature and current management from this stage paves the way for designing EMSs which can lead to very realistic outcomes. The put forward EMS in this stage mainly attempts to enhance the performance of a FCHEV in terms of fuel economy by utilizing an online systemic management of the PEMFC stack. This strategy is in fact the ultimate goal of this thesis as it takes into consideration both the performance drifts of a PEMFC system and its thermal management. One distinguishing feature of this EMS is generating two reference signals (PEMFC current and temperature) to achieve optimality in power splitting,

as opposed to the existing EMSs which only have one control variable (PEMFC current). It is worth reminding that the designed energy management is tested on a developed hardware-in-the-loop (HIL) set-up of Némo vehicle of the IRH, which is a laboratory-scaled hydrogen vehicle for validation.

1.6 Thesis structure

The remainder of this thesis is organized as follows. Chapter 2 describes the importance of adapting the EMS to the real performance of a PEMFC stack as well as adopting a systemic approach for EMS design through presenting an article entitled ''Investigating the Impact of Aging and Thermal Management of a Fuel Cell System in Energy Management Strategies''. Chapter 3 reviews the modelling and parameter estimation approaches of the PEMFC, along with the discussion of the achieved results of a performed benchmark analysis through presenting an article entitled ''Overview and Benchmark Analysis of Fuel Cell Parameters Estimation for Energy Management Purposes'' respectively. Chapter 4 explains the customization of recursive filters for online parameters identification of PEMFC stacks by presenting an article entitled ''Benchmark of Proton Exchange Membrane Fuel Cell Parameters Extraction with Metaheuristic Optimization Algorithms''. Chapter 5 proposes an approach for simultaneous management and control of a PEMFC operating current and stack temperature through presenting an article entitled ''Efficiency Enhancement of an Open Cathode Fuel Cell through a Systemic Management''. Moreover, the integration of the developed bases in this thesis into the design of an EMS is coped with by representing an article entitled ''Efficiency Upgrade of Hybrid Fuel Cell Vehicles' Energy Management Strategies by Online Systemic Management of Fuel Cell''. Finally, the conclusion is drawn

in Chapter 6 with a detailed description of the future steps concerning the further improvement of this work.

Chapter 2 - The significance of performance drifts and thermal management consideration in energy management strategy design

2.1 Introduction

The presented literature survey in the previous chapter illustrated that there is indeed a gap concerning the online characteristics estimation and systemic management of a PEMFC stack while designing an EMS for a FCHEV. In fact, the energetic performance of a PEMFC depends on these factors. Therefore, ignoring them, while developing an EMS, could lead to sub-optimal performances. In this regard, this chapter pursues two important objectives.

The first objective is to demonstrate how serious an aged PEMFC can deteriorate the fuel economy of a FCHEV. In fact, the performance, dependability, and fuel economy of FCHEVs are vastly reliant on the design of an EMS which is in turn influenced by the control and state of the health (SOH) of the on-board PEMFC stack. Thus, many studies have been done on how to optimally distribute the power among the drivetrain components. However, PEMFCs experience irreversible degradation in terms of power delivery as they age, and therefore the performance of the FCHEV will be negatively impacted even with an optimal EMS. The rate of PEMFC aging is dictated by several factors including operating and environmental conditions. Therefore, it stands to reason to consider the effect of PEMFC degradation over the performance of an EMS.

The second objective is to show the amount of hydrogen consumption decline due to the inclusion of temperature dimension (systemic management) into developing a strategy. Indeed, an overriding factor for improving the performance of a FCHEV is to adopt a systemic standpoint for controlling the PEMFC stack. The present-day EMSs typically determine the required current from the PEMFC to meet the requested power by the driver. However, a specific level of power can be supplied by different combinations of operating parameters, such as current, temperature, pressure, and so forth. Having a systemic viewpoint towards PEMFC stack opens up a unique opportunity to efficiently supply the power by finding the right combination as more degrees of freedom are accessible. To this end, the effect of PEMFC thermal management on the vehicle performance is studied by formulating an EMS which determines the cooling fan duty cycle as well as the required current from the PEMFC stack.

The effectiveness of the targets of this chapter is elucidated through presenting an article entitled "Investigating the Impact of Aging and Thermal Management of a Fuel Cell System in Energy Management Strategies". Before presenting the paper, the employed methodology is explained. Subsequently, the main results are briefly discussed. The paper, which includes the details of the proposed work, is then presented. Finally, a conclusion is given.

2.2 Article 1: Investigating the Impact of Aging and Thermal Management of a Fuel Cell System in Energy Management Strategies

Journal: Applied Energy (Elsevier) (https://www.journals.elsevier.com/applied-energy)

Authors: M. Kandidayeni, A. Macias, L. Boulon, and S. Kelouwani.

Submission date: 29/Nov/2019 (Under review)

2.2.1   Methodology

EMS of a FCHEV is, by itself, a delicate problem which needs the reference solution from an optimal control method with multiple states, control inputs, limits, and disturbances. Considering the fact that dynamic programming is one of the optimal control approaches that can guarantee global optimality regardless of problem complexity level, it is used for the purpose of this paper, as shown in Figure 2.1.
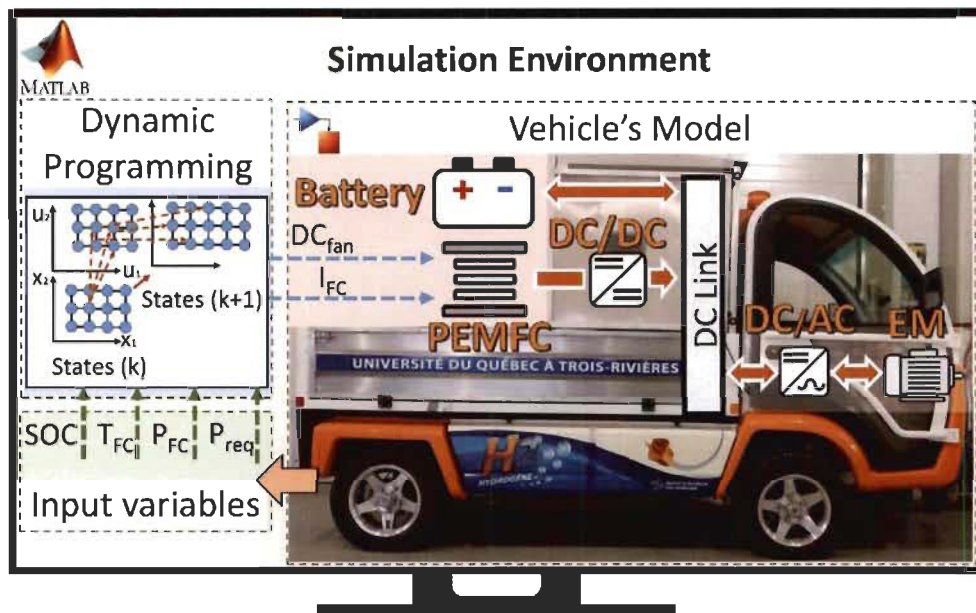
Figure 2.1   The utilized simulator for formulating a multi-dimensional DP.

As previously started, this chapter investigates the impact of two significant aspects, namely FC degradation phenomenon and thermal management, over the performance of an EMS in a FCHEV. To do so, firstly, a vehicle model is developed in simulation environment for a FCHEV composed of a FC stack and a battery pack. Subsequently, deterministic dynamic programming (DP) is used to formulate an optimal EMS to minimize the hydrogen consumption while respecting the operating constraints of the power sources. The performance of DP is assessed in two different scenarios.

The first scenario clarifies the effect of FC stack degradation on the performance of vehicle. In this regard, DP determines the required current from the FC stack for two FCs with different levels of degradation while battery state of charge (SOC) and FC power are the states of the system. The first scenario is composed of three cases, namely unidimensional DP (one control variable) for new PEMFC (1D − New FC), unidimensional DP for aged PEMFC (1D − Aged FC), and unidimensional DP with the false input (1D − FI). In 1D − FI case, the obtained optimal control policy of 1D − New FC case is employed while the used PEMFC is the aged one.

The second scenario evaluates the thermal management contribution in improving the hydrogen economy. In this respect, a bidimensional DP is developed for the new PEMFC (2D − New FC). It has two control variables (FC current and cooling fan duty cycle) and three states (battery SOC, FC power, and FC stack temperature). The results of this case study are comparable with 1D − New FC case and illustrate the influence of temperature dimension inclusion over the performance of the vehicle. The bidimensional DP formulation for the aged PEMFC and false input cases has not been repeated to avoid the discussion of similar analyses.

2.2.2   Synopsis of the results analysis

The performance of the formulated EMS based on DP is explored under two driving cycles, namely worldwide harmonized light-duty vehicles test cycles (WLTC_class 2) and West Virginia Interstate Driving Schedule (CYC_WVUINTER). It is worth mentioning that the cooling fan duty factor for the case of unidimensional strategy is kept constant (34%) and only if the temperature reaches 60 °C, the duty cycle switches to 100% to avoid reaching the limiting stack temperature, which is 65 °C. This policy for controlling the cooling fan duty

cycle has been adopted based on the observation of the 500-W Horizon PEMFC operation with its commercial controller.

Figure 2.2 compares the consumed hydrogen, which is the most important factor in this work, for all the previously-discussed cases of scenario 1 and scenario 2. According to this figure, the hydrogen economy decreases as the PEMFC gets aged. By comparing the unidimensional DP of new and aged FC cases, it can be seen that hydrogen consumption increases by 14.7% in WLTC_class 2 and 11.7% in CYC_WVUINTER. Moreover, it is observed if the PEMFC gets aged and the DP policy remains the same ($1D - FI$ case study), the hydrogen consumption increases by 24.8% compared to $1D - New$ FC case and 8.7% compared to $1D - Aged$ FC in WLTC_class 2. In CYC_WVUINTER, $1D - FI$ case study escalates the hydrogen consumption by 20.2% and 7.6% compared to $1D - New$ FC and $1D - Aged$ FC respectively. The obtained results from $1D - FI$ case study shows that the energy management policy should be adapted to the real state of health of the PEMFC stack, otherwise it leads to poor performance of the strategy. Regarding the influence of thermal management incorporation into the EMS formulation, it is seen that the hydrogen consumption declines by 2.91% and 4.1% in WLTC_class 2 and CYC_WVUINTER respectively.

Figure 2.2 Hydrogen consumption a) WLTC_class 2 driving profile, and b) CYC_WVUINTER driving profile.

Investigating the Impact of Aging and Thermal Management of a Fuel Cell System in Energy Management Strategies

M. Kandidayeni [a,b] *, A. Macias [a,b], L. Boulon [a, b], S. Kelouwani [c]

[a] Hydrogen Research Institute, Department of Electrical Engineering and Computer Science, Université du

Québec à Trois-Rivières, Trois-Rivières, Québec, G9A 5H7, Canada

[b] Canada Research Chair in Energy Sources for the Vehicles of the Future

[c] Hydrogen Research Institute, Department of Mechanical Engineering, Université du Québec à Trois-

Rivières, Trois-Rivières, Québec, G9A 5H7, Canada

* Corresponding author.

E-mail address: mohsen.kandi.dayeni@uqtr.ca (M. Kandidayeni).

Abstract

Energetic efficiency of a fuel cell (FC) stack is affected by several factors such as degradation and operating conditions variation. However, most of the existing energy management strategies (EMSs) for a fuel cell hybrid electric vehicle (FCHEV) are based on constant quasi-static models, which are valid in a limited operational range. Moreover, the available strategies solely determine the reference power/current from the FC stack, while FC is a multiphysical system and its efficiency and power delivery are affected by many parameters such as current, temperature, pressure, and so forth. In this regard, this paper investigates the impact of two significant aspects, namely FC degradation phenomenon and thermal management, over the performance of an EMS in a FCHEV. To do so, firstly, a vehicle model is developed in simulation environment for a low-speed FCHEV composed of a FC stack and a battery pack. Subsequently, deterministic dynamic programming (DP) is used to formulate an optimal EMS to minimize the hydrogen consumption while respecting the operating constraints of the power sources. The performance of DP is assessed in two different scenarios. The first scenario clarifies the effect of FC stack degradation on the performance of vehicle. In this regard, DP determines the required current from the FC stack for two FCs with different levels of degradation while battery state of charge (SOC) and FC power are the states of the system. The second scenario evaluates the thermal management contribution in improving the performance. In this respect, a DP with two control variables (FC current and cooling fan duty cycle) and three states (battery SOC, FC power, and FC stack temperature) is developed for the new FC and compared with the considered cases in scenario one. The results of this study indicate that not updating an EMS policy as the PEMFC gets aged can deteriorate the performance of an EMS up to 24.8%. Moreover, the integration of temperature dimension into the EMS can diminish the hydrogen consumption by 4.1%.

Keywords: Bidimensional energy management strategy, dynamic programming, fuel cell hybrid electric vehicle, thermal management.

1. Introduction
1.1. Motivation and challenges

The buildup of carbon dioxide (CO_2) and other greenhouse gases is causing a rise in the average temperature of the climate system, known as global warming [1]. Transportation sector is counted as one of the major contributors to the anthropogenic emission of these gases [2]. Electrification of vehicles through the introduction of hybrid electric and pure electric vehicle technologies has been considered as a potential solution for decarbonization of the conventional vehicles [3]. However, the limitations of these technologies, such as fossil fuel dependency in the former and limited driving autonomy as well as slow recharging rate in the latter, have paved the way for the emergence of other sources such as proton exchange membrane (PEM) fuel cells (FCs) in electrified vehicles [4]. Fuel cell hybrid electric vehicles (FCHEVs), which are still at an initial phase of marketing progress, typically utilize a PEMFC stack as the primary source of power and a battery pack and/or a supercapacitor (SC) as the secondary one [5, 6]. Therefore, the performance of a FCHEV is affected by many interconnected factors due to different nature of powertrain components. An appropriate energy management between power sources can enhance fuel economy and lifetime of the system. The available energy management strategies (EMSs) for FCHEVs can be classified into three types of rule-based, optimization-based, and intelligent-based [7-9]. Rule-based EMSs are typically designed based on heuristic techniques which are not guaranteed to be optimal or perfect, but instead adequate for attaining an immediate purpose [10]. Optimization-based EMSs theoretically offer near-optimal solutions and are also capable of drawing up new guidelines for revising the set of rules and inferential knowledge of the rule-based methods [11]. Optimization-based EMSs fall into two groups of global, optimizing the cost function over a fixed driving cycle, and real-time strategies, defining an instantaneous cost function based on the variables of the system. The former is not suitable for real-time purposes owing to the necessity to know the driving cycle in advance, but nevertheless is highly helpful for defining the optimal policy. Depending on the purpose of the project, dynamic programming (DP) (as an optimal theory-based strategy) [12, 13] and metaheuristic algorithms, such as genetic algorithm (GA) [14], (as near optimal strategies) have been abundantly used for the development of off-line global EMSs. Real-time strategies have been also formulated by using optimal theory-based methods, such as quadratic programming (QP) [15-18], Pontryagin's minimum principle (PMP) [19, 20], and equivalent consumption minimization strategy (ECMS) [21, 22] with respect to the formulation of the cost function. Intelligent-based strategies normally use the car navigation data and the history of motion for recognizing and predicting the driving condition [23, 24]. They can be incorporated into the both of ruled-based and optimization-based strategies to compensate for sensitivities and problems related to the driving condition prediction. Several EMSs based on the discussed categories and their combinations are available in the literature for hybrid vehicles. A brief summary of very recent developed strategies is given in the following paragraph to clearly highlight the contribution of this manuscript.

1.2. Literature survey

A multi-mode fuzzy EMS is proposed in [25] to minimize the hydrogen consumption in a FCHEV where a neural network-based driving condition recognition tool is utilized to select the most suitable mode of the controller. This strategy has reduced hydrogen consumption by 8.89%, compared to a normal fuzzy EMS. In [26], a new configuration composed of three PEMFC stacks and a battery pack is put forward. In this work, a hysteresis EMS is designed to increase the durability of the PEMFC system by utilizing each PEMFC only at a fixed operating point. In [27], a state machine based EMS is suggested for a FC-SC-battery vehicular system to extend the lifetime of the power sources by using them in their desired operational range. Moreover, the output net power of the PEMFC is maximized by regulating the oxygen excess ratio through a PID controller. In [28], a quadratic energy consumption curve of the PEMFC stack is employed in a multi-state ECMS to formulate the power management in a tram. The strategy has led to 2.5% energy consumption reduction compared to a rule-based power following strategy. In [29], an EMS is developed by using adaptive control theory and fuzzy logic control (FLC). The authors recommend updating the values for defining the FLC rules owing to the PEMFC voltage declines due to degradation after a while and under this condition the rule-based values should be reconsidered. In [30], a self-organizing map is developed as the driving condition recognizer tool to select the most suitable mode of a multi-mode FLC and an online PEMFC model

2

is used to estimate the maximum power and efficiency points of the stack which change over time. The output of the FLC is constantly adapted to the real PEMFC state of health (SOH) and the results show an eight-percent improvement in fuel economy compared to a similar strategy without an online model. In [31], a novel degradation model of PEMFC stack is proposed to be combined in the EMS design of a FCHEV. This model is based on wavelet analysis, extreme learning machine, and genetic algorithm and considers the influence of PEMFC load current, relative humidity, temperature, and hydrogen pressure. In [32], an EMS is formulated based on model predictive control and a cost function is proposed inclusive of hydrogen, PEMFC degradation, and battery degradation costs. In [33, 34], two degradation models are proposed for PEMFC and battery and incorporated in the sizing problem of a FCHEV. In [35], an online adaptive ECMS is proposed for a FCHEV powered by PEMFC, battery, and SC. The SOH of PEMFC and battery are traced online by an adaptive filter and the results show that without SOH estimation, the charge sustenance objective of battery cannot be achieved when the power sources go under degradation. A review of health-conscious EMSs for FCHEVs is presented in [36] and it has been concluded that accurate degradation estimation should be integrated into the existing EMSs to enhance the durability of the system.

1.3. Contribution

In the light of the discussed papers, it is clear that the vast majority of the existing studies do not take the degradation of the power sources into account while designing an EMS for a FCHEV. However, recently, some studies have attempted to bring the importance of this inclusion into attention [32-35]. Moreover, the developed EMSs are mainly one dimensional as they just determine the reference current from the PEMFC stack while PEMFC is a multiphysics system and there is an interdependence between its power delivery and operating conditions. Fig. 1 presents the relation of power delivery with operating current and stack temperature in a 500-W PEMFC with two different levels of ageing. As it is observed, stack current and temperature have influence over the drawn power from the stack and the location of maximum power, which is shown by stars, changes noticeably by the time the PEMFC gets degraded. In this respect, the contributions of this work lie into the consideration of two substantial aspects. The first one is inspecting the influence of PEMFC degradation over the performance of an optimal EMS. This is worthwhile since it clarifies the degradation impact of PEMFC, which is a new and expensive technology, over the operation of the vehicle without combining it with the ageing effect of battery pack. The second contribution of this work is the incorporation of PEMFC thermal management into the EMS design. This is vital to be considered as PEMFC is a system and its performance is influenced not only by current but also by temperature and even other operating parameters.
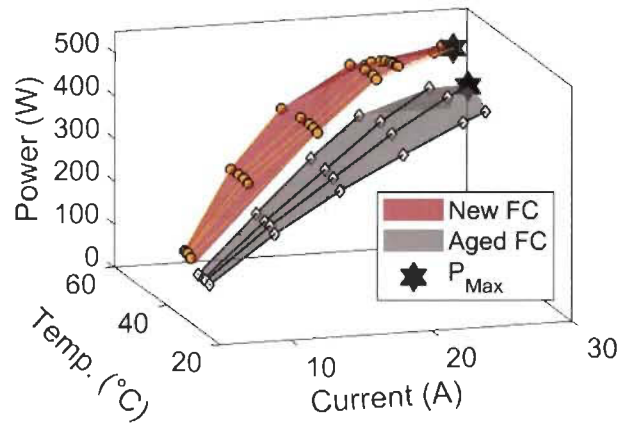
Fig. 1. The experimental characteristics of a PEMFC stack with two different degradation levels.

1.4. Methodology and paper structure

This paper proposes the formulation of a bidimensional EMS (two control variables) based on DP for a FCHEV. The control variables are PEMFC current and stack temperature, which have crucial role in the performance of the stack. The results of the proposed bidimensional strategy are compared with a unidimensional strategy, which only considers the operating current similar to the existing strategies in the literature, under two standard driving cycles. The formulation of DP is done for two cases of new and aged PEMFC stacks to represent the effect of ageing as well as adding the temperature dimension on the operation of the ECHEV.

The remainder of this paper is as follows. Section 2 describes the powertrain modeling of the studied FCHEV along with the characteristics of the employed power sources. Section 3 deals with the development of an optimal EMS based on DP. Section 4 discusses the obtained results of the work, and finally the main conclusions from the performed study are drawn in section 5.

2. Powertrain system modeling

The studied FCHEV in this work is based on a low-speed vehicle called Nemo. The structure of this vehicle is shown in Fig. 2. The electric motor is driven by both of PEMFC stack and battery pack. The PEMFC stack is linked to the DC bus via a DC-DC converter while the battery pack is directly connected to the bus. The vehicle tractive force (F_{tr}), which is required to move the vehicle forward, needs to overcome the slope resistance (F_{sr}), rolling resistance (F_{rr}), aerodynamic drag (F_{ad}), and the acceleration force (F_{acc}). F_{tr} is calculated by sum of the four forces as:

$$\begin{cases} F_{tr} = F_{sr} + F_{rr} + F_{ad} + F_{acc} \\ F_{sr} = M_v \, g \, sin\left(\frac{\alpha\pi}{180°}\right) \\ F_{rr} = -C_f \, M_v \, g \, cos\left(\frac{\alpha\pi}{180°}\right) \\ F_{ad} = 0.5 \, \rho_a \, C_d \, A_f \, v^2(t) \, sgn(v) \text{ where } sgn(v)\begin{cases} 1 \text{ if } v > 0 \\ -1 \text{ if } v < 0 \end{cases} \\ F_{acc} = \delta \, M_v \, a(t) \end{cases} \tag{1}$$

where M_v is the vehicle mass (kg), g is the gravitational acceleration (m/s^2), α is the road angle in degrees, C_f is the rolling friction coefficient, ρ_a is the air density (kg/m^3), C_d is the aerodynamic drag coefficient, A_f is the vehicle frontal area (m^2), $v(t)$ is the vehicle velocity (m/s), δ is the mass factor, and $a(t)$ is vehicle acceleration (m/s^2). Table 1 provides the principal powertrain parameters of this vehicle.
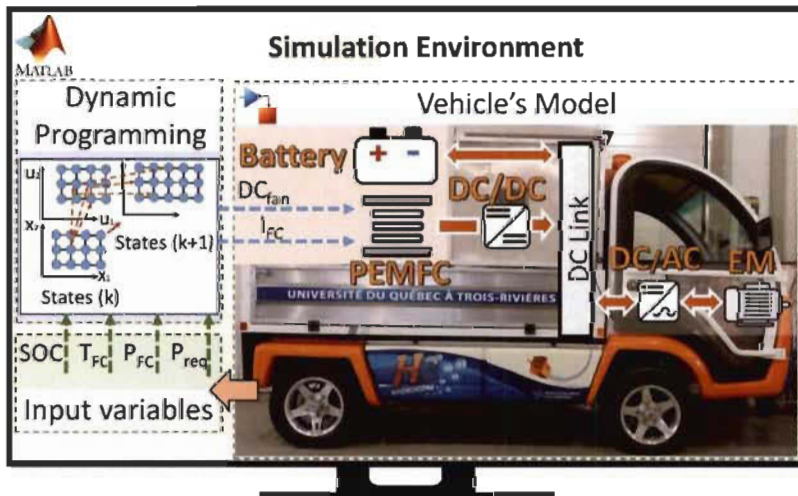
Fig. 2. The simulator for testing the EMS.

Table 1

Parameters of the vehicle

Specification	Parameter	Value
Vehicle's parameters	Rolling resistance	0.015
	Aerodynamic drag	0.42
	Frontal area (m^2)	4
	Density of air (kg/m^3)	1.2
	Mass factor	1.035
	Mass (kg)	896
	Maximum speed (km/h)	40
3-phase induction machine	Power (W)	5690
	Frequency(Hz)	131.1
FC system	Rated power (kW)	4
Battery	voltage (V)	73
	Capacity (Ah)	6

The requested power in the bus (P_{Bus}) by the drive of the induction machine is calculated by:

$$\begin{cases} P_{Bus} = \dfrac{P_{wheel}}{\eta_{EM}\,\eta_t\,\eta_{DC-AC}} \\ P_{wheel} = F_{tr} \times v(t) \end{cases} \tag{2}$$

where P_{wheel} is the required power at wheels, η_t is the transmission efficiency (92%), η_{EM} is the motor average efficiency (90%), and η_{DC-AC} is the inverter efficiency (95%). As shown in Fig. 2, the PEMFC stack and battery pack are connected to the DC bus. Therefore, the relationship of PEMFC power (P_{FC}), battery power (P_{Bat}), and the requested power in the bus can be expressed as:

$$P_{Bus} = P_{FC}\eta_{DC-DC} + P_{Bat} \tag{3}$$

2.1. PEMFC modeling

As the main objectives of this paper are to investigate the effect of degradation and thermal management over the performance of an EMS, the experimental data of two 500-W Horizon PEMFCs with different levels of degradation are employed to form a realistic perception of these effects. The experimental data of this FC are gathered from a developed test bench in Hydrogen Research Institute of Université du Québec à Trois-Rivières (UQTR), as shown in Fig. 3. In this set-up, a Horizon H-500 air breathing PEMFC is connected to a National Instrument CompactRIO through its controller. The PEMFC controller carries out the following tasks:

- Controlling the stack temperature by acting on the blower.
- Opening the hydrogen valve.
- Controlling the purging interval of the purge valve.
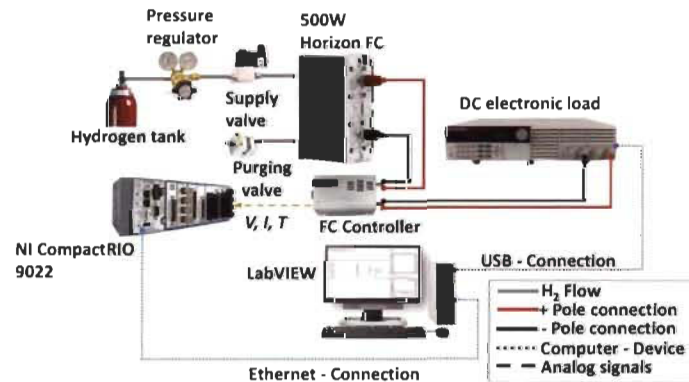
Fig. 3. The developed PEMFC test bench in Hydrogen Research Institute of UQTR

5

The mounted axial fan is responsible for cooling down the stack and supplying the necessary oxygen. The information between the CompactRIO and the PC is transferred by an Ethernet connection every 100 milliseconds. Temperature, current, and voltage of the FC system are recorded and used for the modeling. An 8514 BK Precision DC Electronic Load is used to request load profiles from the PEMFC. Fig. 4 presents the experimental characteristics of the aged and new PEMFCs in terms of power delivery and hydrogen consumption. Fig. 4a shows the relationship of power, temperature, and current for better appreciation of the current and temperature interdependence. From Fig. 4a, it is realized that a specific level of requested power from the PEMFC can be supplied by different combinations of current and temperature. The circle and diamond markers in Fig 4a show the location of optimal current and its corresponded temperature for supplying each power level. Fig. 4b indicates the optimal line of hydrogen consumption for each of the new and aged PEMFCs. The circles and markers correspond to the optimal points of each level shown in Fig. 4a. From this figure, it is observed that there is a noticeable different between the hydrogen consumption of a new and an aged PEMFC. The specifications of this PEMFC are listed in Table 2. According to Table 1, Nemo vehicle requires a 4-kW FC system. Hence, the PEMFC output voltage in the emulator of this work is scaled up after the DC-DC converter to satisfy the requested power in the bus. This emulator utilizes the temperature, current, and pressure as inputs and estimates the voltage of the stack. It is based on a semi-empirical equation, suggested by Mann et al [37], which calculates the stack voltage for a number of cells connected in series.
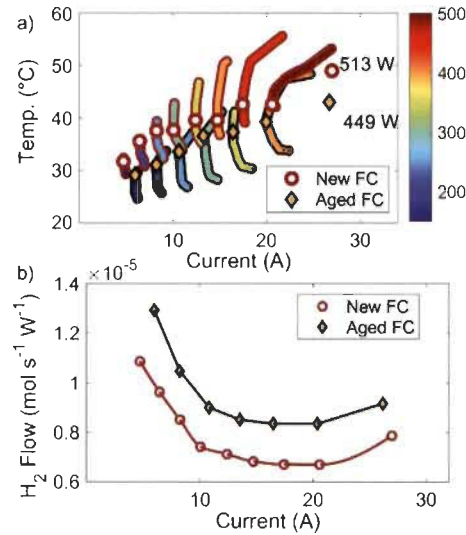
Fig. 4. The experimental characteristics of new and aged PEMFCs, a) temperature-current relationship, and b) Hydrogen flow-current relationship

Table 2

The specifications of the Horizon H-500 PEMFC

PEMFC Technical specification	
Type of FC	PEM
Number of cells	36
Max Current (shutdown)	29 A
Hydrogen pressure	50-60 kPa (0.5-0.6 Bar)
Rated H_2 consumption	7 SLPM
Ambient temperature	5 to 30 °C
Max stack temperature	65 °C
Cooling	Air (integrated cooling fan)

$$V_{FC} = N(E_{Nernst} + V_{act} + V_{ohmic} + V_{con}) \qquad (4)$$
$$E_{Nernst} = 1.229 - 0.85 \times 10^{-3}(T - 298.15) + 4.3085 \times 10^{-5}T[\ln(P_{H2}) + 0.5\ln(P_{O2})] \qquad (5)$$

6

$$\begin{cases} V_{act} = \xi_1 + \xi_2 T + \xi_3 Tln(CO_2) + \xi_4 Tln(i_{FC}) \\ CO_2 = \dfrac{P_{O2}}{5.08 \times 10^{-6} \exp(-498/T)} \end{cases} \tag{6}$$

$$V_{ohmic} = -i_{FC} R_{internal} = -i_{FC}(\zeta_1 + \zeta_2 T + \zeta_3 i_{FC}) \tag{7}$$

$$V_{con} = Bln(1 - \frac{i_{FC}}{i_{FC,max}}) \tag{8}$$

Where V_{FC} is the output voltage (V), N is the number of cells, E_{Nernst} is the reversible cell potential (V), V_{act} is the activation loss (V), V_{ohmic} is the ohmic loss (V), V_{con} is the concentration loss (V), T is the stack temperature (K), P_{H2} is the hydrogen partial pressure in anode side (N m^{-2}), P_{O2} is the oxygen partial pressure in cathode side (N m^{-2}), $\xi_n (n = 1 \dots 4)$ are the semi-empirical coefficients based on fluid mechanics, thermodynamics, and electrochemistry, CO_2 is the oxygen concentration (mol cm^{-3}), i_{FC} is the PEMFC operating current (A), $R_{internal}$ is the internal resistor (Ω), $\zeta_n (n = 1 \dots 3)$ are the parametric coefficients, B is a parametric coefficient (V), i_{FC} is the actual current (A), and $i_{FC,max}$ is the maximum. The stack temperature is calculated based on the energy conservation law [38, 39], where the forced convection equation includes the effect of the blower in the model.

$$m_{st} C_{st} \, dT_{st}/dt = \dot{Q}_{reac} - P_{st} - Q_{Nat} - Q_{Forced} \tag{9}$$

Where m_{st} is stack mass (4.2 kg), C_{st} is specific heat capacity of stack (J/kg K) [39], T_{st} is stack temperature (K), $\dot{Q}_{reac}$ is the released energy from electrochemical reaction (J), P_{st} is the generated electrical power (W), Q_{Nat} is the natural convection (J), and Q_{Forced} is the forced convection (J). The energy generated by electrochemical reaction and the electrical power of the stack are expressed by:

$$\dot{Q}_{reac} = V_{max} \, i_{FC} \, N \tag{10}$$
$$V_{max} = \Delta H / nF \tag{11}$$
$$P_{st} = V_{FC} \, i_{FC} \tag{12}$$

where V_{max} is the maximum voltage obtained by hydrogen high heating value (HHV=1.48V), ΔH is the formation enthalpy, n is the number of electrons per molecule, and F is the Faraday's constant. Convective heat transfer comprises natural and forced convection and is calculated by:

$$Q_{Nat} = h_{Nat} \, A_{Nat}(T_{st} - T_{ca}) \tag{13}$$
$$Q_{Forced} = \alpha \, D_{fan} \, \rho_{air} \, A_{Forced} \, C_p(T_{st} - T_{ca}) \tag{14}$$

where h_{Nat} is the natural heat transfer coefficient (14 W/m^{2}K) [38], A_{Nat} is the total surface area of the 500-W Horizon PEMFC (0.1426 m^2) which has been calculated by the available dimensions in the manual of the device, T_{ca} is the ambient temperature (K), α is an empirical coefficient obtained by experiment, D_{fan} is the fan duty cycle, ρ_{air} is the ambient air density (1.267 kg/m^3), A_{Forced} is the area exposed to the forced convection (0.22m×0.13m×2), and C_p is the air specific heat capacity (1005 J/kg K). Hydrogen flow ($H_{2,flow}$) is calculated by an empirical equation as:

$$H_{2,flow} = a \, i_{FC} + b \, D_{fan} + c \tag{15}$$

where a, b, and c are fitting parameters attained by experimental data and the unit of hydrogen flow is SLPM.

2.2. Battery modeling

A lithium-ion battery pack is employed to assist the PEMFC stack to deliver the requested power from the electric motor side. The specifications of the battery are listed in Table 3. An internal resistance based model is used for modeling the behavior of this battery [40]. Fig. 5 shows the relationship of battery SOC with each of open circuit voltage (U_{bat-OC}), internal resistance (R_{bat}) changes in charge, and internal resistance

7

changes in discharge. The battery current (I_{bat}), bus voltage (U_{bus}), and SOC are determined as:

$$I_{Bat} = \frac{(U_{Bat-OC} - \sqrt{U_{Bat-OC}^2 - 4 \times R_{Bat} \times P_{Bat}})}{2 \times R_{Bat}} \tag{16}$$

$$U_{Bus} = U_{Bat-OC} - I_{Bat} \times R_{Bat} \tag{17}$$

$$SOC(t_f) = SOC(t_0) - \eta_C \frac{\int_{t_0}^{t} I_{Bat} dt}{C_{Bat}} \tag{18}$$

where P_{Bat} is the battery pack power, C_{Bat} is the capacity, and η_C is the coulombic efficiency.

Table 3
The specifications of the employed battery

Specification	Parameter	Value
SAFT Rechargeable lithium-ion battery cell	Maximum current continuous	C/1 A
	Capacity	6 Ah
	Nominal voltage	3.65 V
	No. of cells in series	20
	Cell mass	0.34 kg
	Coulombic efficiency	0.99
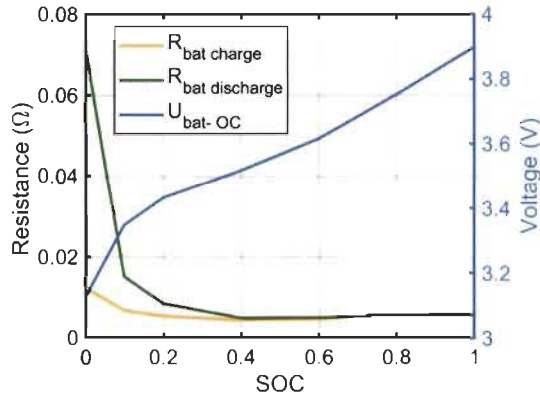
Fig. 5. The relationship of SOC with U_{bat-OC} and R_{bat} per cell.

3. Energy management strategy

The model of a FCHEV can be expressed as a nonlinear state space model. One of the most common methods which focuses on the optimal control of nonlinear, time-variant, constrained, discrete-time approximations of continuous-time dynamic models is deterministic DP. Such DP tools have been already employed successfully in the energy management problem of different HEVs [12, 13, 41]. In this work, the MATLAB function introduced in [12] is utilized to solve the discrete-time optimal-control problem using DP algorithm. The proposed DP here minimizes the hydrogen consumption by determining the optimal trajectories of PEMFC stack current and cooling fan duty cycle. It should be noted that more complex cost functions have not been considered in this study as the main purpose is to clarify the impacts of degradation and temperature dimension consideration in the hydrogen consumption rather than reducing the degradation through time. However, this work paves the way for formulating more complex cost functions in future to reduce both hydrogen consumption and the occurrence of degradation in the PEMFC to the utmost.

The main states of the system are battery SOC and stack temperature. Moreover, the PEMFC power is also considered as a state to be able to prevent sudden and big changes in the drawn power from the stack. It should be noted that according to [42], a dynamic limitation of 50 Ws^{-1}, which means a maximum of 10% of the maximum power per second for rising, and also 30% of the maximum power per second for falling, as

8

suggested in [43], have been considered for the operation of the PEMFC stack. The steady space model equations can be described as:

$$\begin{cases} x_{k+1} = f(x_k, u_k, v_k, a_k, i_k) + x_k \\ x = [SOC, T_{st}, P_{FC,SV}] \\ u = [I_{FC,CV}, D_{fan}] \end{cases} \tag{19}$$

where x_k is the state vector, u_k is the control variable vector, v_k is the vehicle velocity, a_k is the vehivle acceleration, i_k is the gear number, $P_{FC,SV}$ is the PEMFC power as a state variable, and $I_{FC,CV}$ is the state current as a control variable. As the driving cycle is known in advance, the vehicle velocity (v_k), acceleration (a_k) and gear number (i_k) can be included in the model function and as a result the steady space model will be simplified to:

$$x_{k+1} = f(x_k, u_k) + x_k, \quad k = 0,1, \dots N - 1 \tag{20}$$
$$N = \frac{T_F}{T_s} + 1 \tag{21}$$

where T_F is the final time of the driving cycle and T_s is the sampling time. The minimization of the hydrogen consumption is formulated as:

$$J = min \sum_{k=0}^{N-1} H_2(u_k, k) \tag{22}$$

The applied constrains to the control variables are as follows:

$$\begin{cases} I_{FC,min} \le I_{FC,CV}(k) \le I_{FC,max} \\ D_{fan,min} \le D_{fan}(k) \le D_{fan,max} \end{cases} \tag{23}$$

where $I_{FC,min}$ and $I_{FC,max}$ are the minimum and maximum current of the PEMFC stack ($I_{FC,CV} \in [0, 27]$), and $D_{fan,min}$ and $D_{fan,max}$ are the minimum and maximum duty cycle of the cooling fan ($D_{fan} \in [20, 100]$). The constraints on the state variables are defined as:

$$\begin{cases} SOC_{min} \le SOC(k) \le SOC_{max}, & (SOC_{min} = 50\,\%, SOC_{max} = 90\,\%) \\ T_{st,min} \le T_{st}(k) \le T_{st,max}, & (T_{st,min} = 25\,°C, T_{st,max} = 65\,°C) \\ P_{FC,SV,min} \le P_{FC,SV}(k) \le P_{FC,SV,max} & (P_{FC,SV,min} = 0\,W, \ P_{FC,SV,max} = 500\,W) \\ \Delta P_{FC,SV,min} \le \Delta P_{FC,SV}(k) \le \Delta P_{FC,SV,max} & (\Delta P_{FC,SV,min} = -150\,Ws^{-1}, \Delta P_{FC,SV,max} = 50\,Ws^{-1}) \end{cases} \tag{24}$$

4. Results and discussion

The performance of the formulated EMS based on DP is explored under two driving cycles, namely worldwide harmonized light-duty vehicles test cycles (WLTC_class 2) and West Virginia Interstate Driving Schedule (CYC_WVUINTER). Herein, two scenarios are considered to highlight the objectives of the paper. The first scenario is composed of three cases, namely unidimensional DP (one control variable) for new PEMFC (1D − New FC), unidimensional DP for aged PEMFC (1D − Aged FC), and unidimensional DP with the false input (1D − FI). In 1D − FI case, the obtained optimal control policy of 1D − New FC case is employed while the used PEMFC is the aged one. This case study shows the effect of PEMFC degradation on the performance of the optimal EMS. The second scenario investigates the performance of bidimensional strategy (two control variables) for new PEMFC (2D − New FC). The results of this case study are comparable with 1D − New FC case and illustrate the influence of temperature dimension inclusion over the performance of the vehicle. The bidimensional DP formulation for the aged PEMFC and false input cases has not been repeated to avoid the discussion of similar analyses in the paper. It is worth mentioning that the cooling fan duty factor is kept constant (34%) for the case of unidimensional strategy and only if the

temperature reaches 60 °C, the duty cycle switches to 100% to avoid reaching the limiting stack temperature, which is 65 °C. This policy for controlling the cooling fan duty cycle has been adopted based on the observation of the 500-W Horizon PEMFC operation with its controller.

Fig. 6 shows the employed driving cycles and their corresponding requested power curves. According to this figure, WLTC_class 2 contains three driving regimes of low, medium, and high speed. However, CYC_WVUINTER is mainly composed of high driving speed. Fig. 7 illustrates the obtained results from running unidirectional DP for WLTC_class 2 driving cycle in different cases of scenario 1. Fig. 7a presents the scaled-up drawn power signals from the PEMFC for each case study. According to this figure, DP has adopted a specific policy for each of 1D – New FC and 1D – Aged FC case studies, which implies that the
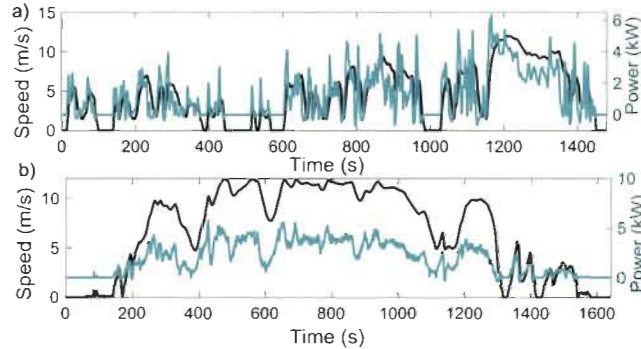
Fig. 6. The utilized driving cycles and the obtained requested power for DP formulation, a) WLTC_class 2, and b) CYC_WVUINTER.

optimal policies of power sharing cannot be the same for an aged and a new PEMFC. Fig. 7b, Fig. 7c, and Fig. 7d present the battery SOC level, the real-scale drawn current from PEMFC, and stack temperature evolution respectively. Comparison of 1D – New FC and 1D – Aged FC case studies show that from 0 to almost 600 s, the SOC descends to around 50% for both strategies. However, from 600 s to almost 1000 s, the strategies show completely different behavior. On the one hand, the unidimensional strategy for the new PEMFC increases the drawn current to a high of 22 A and then it drops to almost 17 A for almost 300 s and then gradually decreases to 0. This variation causes fluctuation in the stack temperature (from 27 °C to almost 40 °C) and battery SOC (from a high of 50% to a low of 80%). The one for the aged PEMFC case, on the other hand, sustains the battery SOC level around 55% by gradually increasing the current and temperature within this interval. From 1000 s to the end, the 1D – Aged FC increases the current to almost 20 A which causes a surge in the stack temperature while the 1D – New FC tries to use less current by discharging the battery and cooling down the stack. Regarding the 1D – FI case study, it demands the same power signal from the PEMFC as 1D – New FC since it uses the same DP policy. However, the PEMFCs' health states are different. Fig. 7b also shows that 1D – FI and 1D – New FC have the same battery SOC variations since they extract the same power from the aged and new PEMFCs respectively. Nonetheless, Fig. 7c illustrates that in 1D – FI case study, the aged PEMFC needs to operate in higher current levels, especially between 700 s to 1000 s, to supply the same power as new PEMFC. The stack temperature is also higher in this period for 1D – FI case.
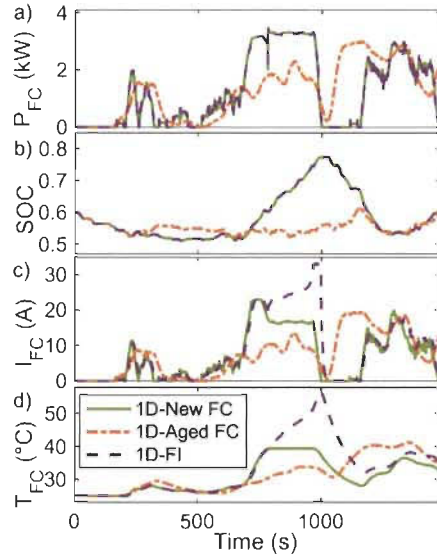
Fig. 7. Unidimensional DP results for WLTC_class 2 driving cycle, a) the drawn power from PEMFC stack (scaled-up signal), b) battery SOC, c) the real scale drawn current from the stacks, and d) the real scale stack temperature evolution.

Fig. 8 represents the results of unidimensional DP for the CYC_WVUINTER driving cycle. Fig. 8a presents the scaled-up power provided by the PEMFC in each scenario and the corresponded battery SOC, stack current, and temperature are shown in Fig. 8b to Fig. 8d respectively. Comparing the 1D − New FC and 1D − Aged FC cases, it is seen that the unidimensional DP for the new FC discharges the battery up to 300 s and after that it turns on the PEMFC to recharge the battery and meet the requested power. However, the unidimensional DP for the aged FC decides to charge the battery to a high of 75% in this interval. From 300 s to almost 1100 s, both strategies increase the drawn current from the PEMFC with slightly different fluctuations to meet the requested power and in both cases the stack temperature rises. From 1100 s to the end, the stack temperature in both cases decreases, and finally, they finish in the same SOC level. With regard to 1D − FI case study, it can be observed that the aged PEMFC requires to work in higher current and temperature levels from almost 400 s to 1400s to supply the requested power and sustain the same battery SOC level as 1D − New FC.

Fig. 9 represents the results of formulating bidimensional DP for the new PEMFC case study under the
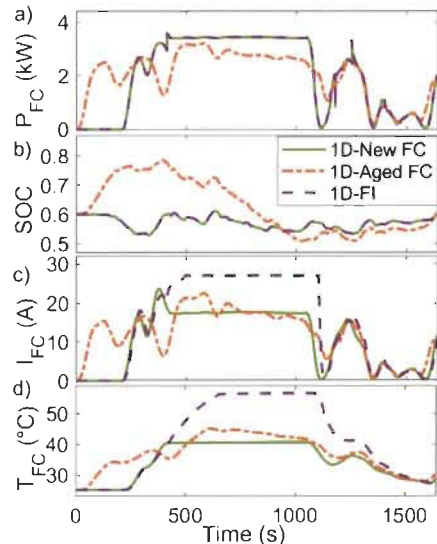
Fig. 8. Unidimensional DP results for CYC_WVUINTER driving cycle, a) the drawn power from PEMFC stack (scaled-up signal), b) battery SOC, c) the real scale drawn current from the stacks, and d) the real scale stack temperature evolution.

11
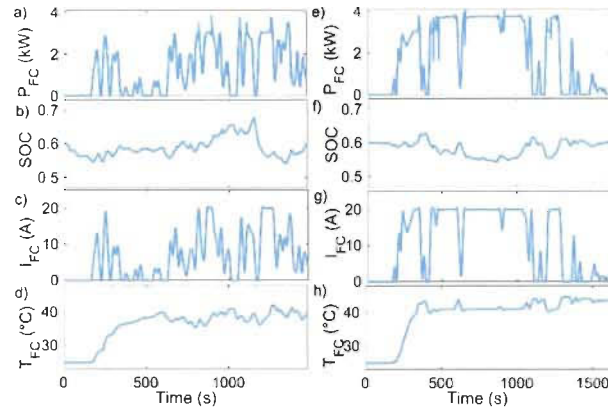
Fig. 9. Bidimensional DP results, WLTC_class 2 driving cycle (a to d) and CYC_WVUINTER driving cycle (e to h). a) and e) The drawn power from PEMFC stacks (scaled-up signal), b) and f) battery SOC, c) and g) the real scale drawn current from the stacks, and d) and h) the real scale stack temperature evolution.

two driving cycles. The comparison of unidimensional and bidimensional DPs indicates that bidimensional DPs have ended up with more variations compared to unidimensional ones. It stems from the fact that in bidimensional cases, each specific level of power can be supplied by different combinations of current and fan duty cycle (which lead to different temperature levels). Therefore, bidimensional DP attempts to choose the combination that leads to the lowest hydrogen consumption. However, there are not many combinations of current and fan duty cycle for the case of unidimensional DP. Regarding the WLTC_class 2 driving cycle, from 0 to almost 600 s, the requested current from the stack is higher than the 1D − New FC (presented in Fig. 6c). This results in warming up the stack to a desired level during this interval for the bidimensional strategy (35 °C to 40 °C) and sustaining the battery SOC level around 60%. From 600 s to almost 1000 s, the bidimensional strategy virtually keeps the stack temperature between 35 °C to 40 °C and SOC level between 60% to 65%. From 1000 s to the end, the bidimensional strategy shows a smooth fluctuation to finish in the same SOC level as initial. Concerning the CYC_WVUINTER driving cycle, it is observed that the bidimensional DP sustains the SOC level around 60% up to 300 s. From 300 s to almost 1100 s, it increases the drawn current from the PEMFC with some oscillations to meet the requested power which in turn increases the stack temperature. From 1100 s to the end, the strategy tries to keep the desired temperature level. Fig. 10 compares the PEMFC current distribution of bidimensional and unidimensional DPs for the new PEMFC. From Fig. 10a, it is seen that both strategies work in various levels as the WLTC_class 2 driving cycle contains several stops and low- speed traffic conditions. However, in case of CYC_WVUINTER driving cycle, the strategies, specifically the bidimensional one, can work more in the efficient current zone which is between 17 A to 21 A according to the presented characteristics in Fig. 4.
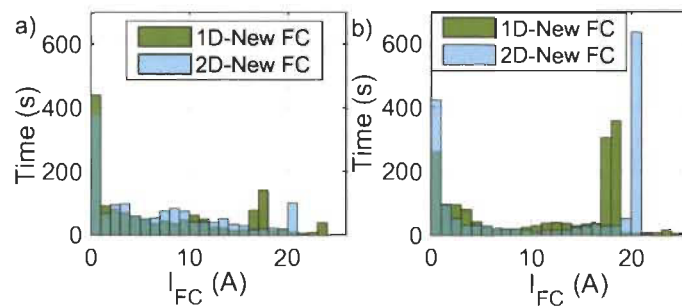
Fig. 10. PEMFC current distribution of bidimensional and unidimensional DPs for: a) WLTC_class 2, and b) CYC_WVUINTER.

Fig. 11 compares the consumed hydrogen, which is the most important factor in this work, for all the previously-discussed cases of scenario 1 and scenario 2. According to this figure, the hydrogen economy decreases as the PEMFC gets aged. By comparing the unidimensional DP of new and aged FC cases, it can

be seen that hydrogen consumption increases by 14.7% in WLTC_class 2 and 11.7% in CYC_WVUINTER. Moreover, it is observed if the PEMFC gets aged and the DP policy remains the same (1D − FI case study), the hydrogen consumption increases by 24.8% compared to 1D − New FC case and 8.7% compared to 1D − Aged FC in WLTC_class 2. In CYC_WVUINTER, 1D − FI case study escalates the hydrogen consumption by 20.2% and 7.6% compared to 1D − New FC and 1D − Aged FC respectively. The obtained results from 1D − FI case study shows that the energy management policy should be adapted to the real state of health of the PEMFC stack, otherwise it leads to poor performance of the strategy. Regarding the influence of thermal management incorporation into the EMS formulation, it is seen that the hydrogen consumption declines by 2.91% and 4.1% in WLTC_class 2 and CYC_WVUINTER respectively.

Fig. 11. Hydrogen consumption a) WLTC_class 2 driving profile, and b) CYC_WVUINTER driving profile

5. Conclusion

This paper focuses attention on the influence assessment of a PEMFC stack degradation and thermal management over the fuel economy of a FCHEV. In this respect, a deterministic DP is formulated in unidimensional and bidimensional ways for a new and an aged PEMFC stack. Similar to the existing EMSs in the literature, the unidimensional DP only determines the required current from the PEMFC stack, while respecting the limitation of the power sources, and the remainder is supplied by the battery pack. However, the bidimensional DP determines the required current and stack temperature of the PEMFC stack to supply the power. Considering this temperature dimension in addition to the current is a new step regarding the EMS design which has escaped the attentions in previous studies. The performance of the formulated EMSs is evaluated under two driving profiles of WLTC_class 2 and CYC_WVUINTER. The analysis of various scenarios indicate that the integration of the temperature dimension can enhance the fuel economy up to 4.1% in new PEMFC case study. Moreover, the ageing of the PEMFC stack can deteriorate the fuel economy up to 14.7% in unidimensional. The final results also indicate that if the policy of energy management for power distribution between PEMFC and battery is not updated as the PEMFC gets aged, it can increase the hydrogen consumption up to 24.8%. Looking forward, future investigations are necessary to validate the kinds of conclusions that can be drawn from the proposed bidimensional EMS of this work by using more complex cost functions including the degradation of PEMFC stack and battery pack. Moreover, as this study shows the potential of a bidimensional EMS in improving the fuel economy of a FCHEV, it is necessary to formulate real-time bidimensional strategies to have more realistic perception in real-world cases.

References

[1]   H. T. Vu, Y. Liu, and D. V. Tran, "Nationalizing a global phenomenon: A study of how the press in 45 countries and territories portrays climate change," *Global Environmental Change,* vol. 58, p. 101942, 2019/09/01/ 2019.

[2]   F. Ülengin, M. Işık, Ş. Ö. Ekici, Ö. Özaydın, Ö. Kabak, and Y. İ. Topçu, "Policy developments for the reduction of climate change impacts by the transportation sector," *Transport Policy,* vol. 61, pp. 36-50, 2018/01/01/ 2018.

[3]   J. Shin, W.-S. Hwang, and H. Choi, "Can hydrogen fuel vehicles be a sustainable alternative on vehicle market?: Comparison of electric and hydrogen fuel cell vehicles," *Technological Forecasting and Social Change,* vol. 143, pp. 239-248, 2019/06/01/ 2019.

13

[4]   C. Acar and I. Dincer, "The potential role of hydrogen as a sustainable transportation fuel to combat global warming," *International Journal of Hydrogen Energy,* 2018/11/23/ 2018, (https://doi.org/10.1016/j.ijhydene.2018.10.149).

[5]   B. Tanç, H. T. Arat, E. Baltacıoğlu, and K. Aydın, "Overview of the next quarter century vision of hydrogen fuel cell electric vehicles," *International Journal of Hydrogen Energy,* vol. 44, pp. 10120-10128, 2019/04/19/ 2019.

[6]   Z. Li, A. Khajepour, and J. Song, "A comprehensive review of the key technologies for pure electric vehicles," *Energy,* vol. 182, pp. 824-839, 2019/06/14/ 2019.

[7]   C. M. Martinez, X. Hu, D. Cao, E. Velenis, B. Gao, and M. Wellers, "Energy Management in Plug-in Hybrid Electric Vehicles: Recent Progress and a Connected Vehicles Perspective," *IEEE Transactions on Vehicular Technology,* vol. 66, pp. 4534-4549, 2017.

[8]   A. M. Ali and D. Söffker, "Towards Optimal Power Management of Hybrid Electric Vehicles in Real-Time: A Review on Methods, Challenges, and State-Of-The-Art Solutions," *Energies,* vol. 11, p. 476, 2018.

[9]   N. Sulaiman, M. A. Hannan, A. Mohamed, P. J. Ker, E. H. Majlan, and W. R. Wan Daud, "Optimization of energy management system for fuel-cell hybrid electric vehicles: Issues and recommendations," *Applied Energy.* vol. 228, pp. 2061-2079, 2018/10/15/ 2018.

[10]   H. Li, A. Ravey, A. N. Diaye, and A. Djerdir, "A Review of Energy Management Strategy for Fuel Cell Hybrid Electric Vehicle," in *2017 IEEE Vehicle Power and Propulsion Conference (VPPC),* 2017, pp. 1-6.

[11]   Y. Huang, H. Wang, A. Khajepour, B. Li, J. Ji, K. Zhao, *et al.,* "A review of power management strategies and component sizing methods for hybrid vehicles," *Renewable and Sustainable Energy Reviews,* vol. 96, pp. 132-144, 2018/11/01/ 2018.

[12]   W. Zhou, L. Yang, Y. Cai, and T. Ying, "Dynamic programming for new energy vehicles based on their work modes Part II: Fuel cell electric vehicles," *Journal of Power Sources,* vol. 407, pp. 92-104, 2018/12/15/ 2018.

[13]   W. Zhou, L. Yang, Y. Cai, and T. Ying, "Dynamic programming for New Energy Vehicles based on their work modes part I: Electric Vehicles and Hybrid Electric Vehicles," *Journal of Power Sources,* vol. 406, pp. 151-166, 2018/12/01/ 2018.

[14]   R. Zhang and J. Tao, "GA-Based Fuzzy Energy Management System for FC/SC-Powered HEV Considering H2Consumption and Load Variation," *IEEE Transactions on Fuzzy Systems,* vol. 26, pp. 1833-1843, 2018.

[15]   Z. Chen, Y. Wu, N. Guo, J. Shen, and R. Xiao, "Energy management for plug-in hybrid electric vehicles based on quadratic programming with optimized engine on-off sequence," in *IECON 2017 - 43rd Annual Conference of the IEEE Industrial Electronics Society,* 2017, pp. 7134-7139.

[16]   Z. Chen, C. C. Mi, R. Xiong, J. Xu, and C. You, "Energy management of a power-split plug-in hybrid electric vehicle based on genetic algorithm and quadratic programming," *Journal of Power Sources,* vol. 248, pp. 416-426, 2014/02/15/ 2014.

[17]   M. Koot, J. T. B. A. Kessels, B. d. Jager, W. P. M. H. Heemels, P. P. J. v. d. Bosch, and M. Steinbuch, "Energy management strategies for vehicular electric power systems," *IEEE Transactions on Vehicular Technology,* vol. 54, pp. 771-782, 2005.

[18]   Y. Liu, J. Li, Z. Chen, D. Qin, and Y. Zhang, "Research on a multi-objective hierarchical prediction energy management strategy for range extended fuel cell vehicles," *Journal of Power Sources,* vol. 429, pp. 55-66, 2019/07/31/ 2019.

[19]   Q. Li, W. Huang, W. Chen, Y. Yan, W. Shang, and M. Li, "Regenerative braking energy recovery strategy based on Pontryagin's minimum principle for fell cell/supercapacitor hybrid locomotive," *International Journal of Hydrogen Energy,* vol. 44, pp. 5454-5461, 2019/02/26/ 2019.

[20]   S. Xie, X. Hu, Z. Xin, and J. Brighton, "Pontryagin's Minimum Principle based model predictive control of energy management for a plug-in hybrid electric bus," *Applied Energy,* vol. 236, pp. 893-905, 2019/02/15/ 2019.

[21]   H. Li, A. Ravey, A. N'Diaye, and A. Djerdir, "A novel equivalent consumption minimization strategy for hybrid electric vehicle powered by fuel cell, battery and supercapacitor," *Journal of Power Sources,* vol. 395, pp. 262-270, 2018/08/15/ 2018.

[22]   W. Zhang, J. Li, L. Xu, and M. Ouyang, "Optimization for a fuel cell/battery/capacity tram with equivalent consumption minimization strategy," *Energy Conversion and Management,* vol. 134, pp. 59-69, 2017/02/15/ 2017.

14

[23]   E. Kamal and L. Adouane, "Intelligent Energy Management Strategy Based on Artificial Neural Fuzzy for Hybrid Vehicle," *IEEE Transactions on Intelligent Vehicles,* vol. 3, pp. 112-125, 2018.

[24]   H. Kazemi, Y. P. Fallah, A. Nix, and S. Wayne, "Predictive AECMS by Utilization of Intelligent Transportation Systems for Hybrid Electric Vehicle Powertrain Control," *IEEE Transactions on Intelligent Vehicles,* vol. 2, pp. 75-84, 2017.

[25]   R. Zhang, J. Tao, and H. Zhou, "Fuzzy Optimal Energy Management for Fuel Cell and Supercapacitor Systems Using Neural Network Based Driving Pattern Recognition," *IEEE Transactions on Fuzzy Systems,* vol. 27, pp. 45-57, 2019.

[26]   H. Zhang, X. Li, X. Liu, and J. Yan, "Enhancing fuel cell durability for fuel cell plug-in hybrid electric vehicles through strategic power management," *Applied Energy,* vol. 241, pp. 483-490, 2019/05/01/ 2019.

[27]   Y. Wang, Z. Sun, and Z. Chen, "Energy management strategy for battery/supercapacitor/fuel cell hybrid source vehicles based on finite state machine," *Applied Energy,* vol. 254, p. 113707, 2019/11/15/ 2019.

[28]   Y. Yan, Q. Li, W. Chen, B. Su, J. Liu, and L. Ma, "Optimal Energy Management and Control in Multimode Equivalent Energy Consumption of Fuel Cell/Supercapacitor of Hybrid Electric Tram," *IEEE Transactions on Industrial Electronics,* vol. 66, pp. 6065-6076, 2019.

[29]   J. Chen, C. Xu, C. Wu, and W. Xu, "Adaptive Fuzzy Logic Control of Fuel-Cell-Battery Hybrid Systems for Electric Vehicles," *IEEE Transactions on Industrial Informatics,* vol. 14, pp. 292-300, 2018.

[30]   M. Kandidayeni, A. O. M. Fernandez, A. Khalatbarisoltani, L. Boulon, S. Kelouwani, and H. Chaoui, "An Online Energy Management Strategy for a Fuel Cell/Battery Vehicle Considering the Driving Pattern and Performance Drift Impacts," *IEEE Transactions on Vehicular Technology,* 2019, (doi: 10.1109/TVT.2019.2936713).

[31]   K. Chen, S. Laghrouche, and A. Djerdir, "Degradation model of proton exchange membrane fuel cell based on a novel hybrid method," *Applied Energy,* vol. 252, p. 113439, 2019/10/15/ 2019.

[32]   X. Hu, C. Zou, X. Tang, T. Liu, and L. Hu, "Cost-optimal energy management of hybrid electric vehicles using fuel cell/battery health-aware predictive control," *IEEE Transactions on Power Electronics,* 2019, (doi: 10.1109/TPEL.2019.2915675).

[33]   Y. Wang, S. J. Moura, S. G. Advani, and A. K. Prasad, "Optimization of powerplant component size on board a fuel cell/battery hybrid bus for fuel economy and system durability," *International Journal of Hydrogen Energy,* vol. 44, pp. 18283-18292, 2019/07/05/ 2019.

[34]   Y. Wang, S. J. Moura, S. G. Advani, and A. K. Prasad, "Power management system for a fuel cell/battery hybrid vehicle incorporating fuel cell and battery degradation," *International Journal of Hydrogen Energy,* vol. 44, pp. 8479-8492, 2019/03/29/ 2019.

[35]   H. Li, A. Ravey, A. N'Diaye, and A. Djerdir, "Online adaptive equivalent consumption minimization strategy for fuel cell hybrid electric vehicle considering power sources degradation," *Energy Conversion and Management,* vol. 192, pp. 133-149, 2019/07/15/ 2019.

[36]   M. Yue, S. Jemei, R. Gouriveau, and N. Zerhouni, "Review on health-conscious energy management strategies for fuel cell hybrid electric vehicles: Degradation models and strategies," *International Journal of Hydrogen Energy,* vol. 44, pp. 6844-6861, 2019/03/08/ 2019.

[37]   R. F. Mann, J. C. Amphlett, M. A. I. Hooper, H. M. Jensen, B. A. Peppley, and P. R. Roberge, "Development and application of a generalised steady-state electrochemical model for a PEM fuel cell," *Journal of Power Sources,* vol. 86, pp. 173-180, 2000/03/01/ 2000.

[38]   K. Ou, W.-W. Yuan, M. Choi, S. Yang, and Y.-B. Kim, "Performance increase for an open-cathode PEM fuel cell with humidity and temperature control," *International Journal of Hydrogen Energy,* vol. 42, pp. 29852-29862, 2017/12/14/ 2017.

[39]   Y.-X. Wang, F.-F. Qin, K. Ou, and Y.-B. Kim, "Temperature Control for a Polymer Electrolyte Membrane Fuel Cell by Using Fuzzy Rule," *IEEE Transactions on Energy Conversion,* vol. 31, pp. 667-675, 2016.

[40]   V. H. Johnson, "Battery performance models in ADVISOR," *Journal of Power Sources,* vol. 110, pp. 321-329, 2002/08/22/ 2002.

[41]   O. Sundstrom and L. Guzzella, "A generic dynamic programming Matlab function," in *2009 IEEE Control Applications. (CCA) & Intelligent Control, (ISIC),* 2009, pp. 1625-1630.

[42]   K. Ettihir, L. Boulon, and K. Agbossou, "Optimization-based energy management strategy for a fuel cell/battery hybrid power system," *Applied Energy,* vol. 163, pp. 142-153, 2016/02/01/ 2016.

[43]   M. Carignano, V. Roda, R. Costa-Castelló, L. Valiño, A. Lozano, and F. Barreras, "Assessment of Energy Management in a Fuel Cell/Battery Hybrid Vehicle," *IEEE Access,* vol. 7, pp. 16110-16122, 2019.

2.3   Conclusion

This chapter focuses attention on the influence assessment of a PEMFC stack degradation and thermal management over the fuel economy of a FCHEV. This evaluation is necessary to ensure that the set objectives of the thesis stand to reason before advancing further to develop an online model and a systemic management for the PEMFC stack.

In this respect, a deterministic DP is formulated in unidimensional and bidimensional ways for a new and an aged PEMFC stack. The unidimensional DP only determines the required current from the PEMFC stack, while respecting the limitation of the power sources. However, the bidimensional DP determines the required current and stack temperature of the PEMFC stack to supply the power. The analysis of various scenarios indicates that the ageing of the PEMFC stack can deteriorate the fuel economy up to 24.8% if the policy of energy management is not updated. Moreover, the integration of the temperature dimension can enhance the fuel economy up to 4.1%.

The obtained results confirm the relevance of the defined final goals of this work. To take things to a further step, next chapter will explore the online modeling of a PEMFC stack to be able to adapt the performance of an EMS to the real state of the stack.

Chapter 3 - Online parameters estimation of proton exchange membrane fuel cells

3.1 Introduction

The primary analysis performed in the previous chapter confirmed that the degradation of a PEMFC stack can lead to a considerable mismanagement in the EMS and increase the hydrogen consumption. In fact, the fluctuation of operating conditions (temperature, pressure, current, etc.) and the ageing phenomenon affect the operational specifications of a PEMFC, such as maximum power, maximum efficiency, and nominal power. For instance, the maximum power of the stack decreases through time owing to the ageing. These specifications have a significant role while designing an EMS for a FCHEV, since the operating range and limitations of the system are determined with respect to them. Normally, PEMFC models are used to extract the discussed characteristics while designing an EMS. However, the mentioned performance drifts have made the design of a comprehensive PEMFC model highly difficult.

In this respect, this chapter aims at suggesting a suitable semi-empirical model and an identification technique to track the real performance of a FC system online by providing a scientific rigor. Semi-empirical models offer an acceptable compromise between complexity and simplicity. They are premised upon the physical relationships which are supported by experimental data and demonstrate the fundamental electrochemical aspects of the PEMFCs (polarization curve). However, they can estimate the characteristics of a PEMFC within a specific operation range, and their parameters require to be returned to work well in a new operation rage. Recursive filters, which are appropriate for applications in which the desired

parameters change over time, appear to be very fit for online parameter estimation of the semi-empirical models.

The process of selecting and developing a suitable model and parameter identification technique regarding the defined objectives of this chapter is explained by presenting an article entitled ''Overview and benchmark analysis of fuel cell parameters estimation for energy management purposes''. The utilized methodology and the summary of the results are discussed first. Afterwards, the paper is presented. This chapter finishes by giving a conclusion of the achieved results.

It should be reminded that an article entitled ''Comparative Analysis of Two Online Identification Algorithms in a Fuel Cell System'' is added in Appendix B. This article mainly introduces two algorithms for identifying linear parameters of a PEMFC model online and has not been placed in this section to keep this chapter coherent and concise.

3.2 Article 2: Overview and benchmark analysis of fuel cell parameters estimation for energy management purposes

Authors: M. Kandidayeni, A. Macias, A. Amamou, L. Boulon, and S. Kelouwani, H. Chaoui

3.2.1 Methodology

This chapter comprehensively reviews PEMFC model parameters estimation methods with a specific view to online identification algorithms, which are considered as the basis of global energy management strategy design, to estimate the linear and nonlinear parameters of a PEMFC model in real time. In this respect, different PEMFC models with different categories and purposes are discussed first. Subsequently, a thorough investigation of PEMFC parameter estimation methods in the literature is conducted in terms of applicability. Three potential algorithms for online applications, Recursive Least Square (RLS), Kalman filter (KF), and extended Kalman filter (EKF), which has escaped the attention in previous works, have been then utilized to identify the parameters of two well-known semi-empirical models in the literature, Squadrito et. al and Amphlett et. al. To the best of our knowledge, this is the first attempt to identify the linear and nonlinear parameters of a PEMFC semi-empirical model online. Regarding the selected models, apart from the fact that they are well-known in the literature, they provide a good opportunity to make a comparison between a multi-input model (Amphlett et. al.) and a single input model (Squadrito et. al.).

It should be noted that the proposed online PEMFC model identification technique of this chapter can be easily integrated into the EMS loop to avoid the mismanagement owing to the performance drifts of the PEMFC stack. The general concept of estimating the parameters of a PEMFC stack online and the procedure to include it into the EMS design is shown in Figure 3.1. From this figure, it can be seen that the parameters of the model are extracted first by using an estimator. Then the updated model is utilized to estimate the present-state polarization and power curves. The required points used in the EMS are extracted from these curves and transferred to the power split strategy. This chapter mainly takes care of the choice

of identification method and PEMFC model, which are the core of the presented scheme. To take an example, the provided basis for online parameter estimation of a PEMFC model in this chapter has been used to design an EMS for a FCHEV in Appendix C. The details of this strategy are presented in an article entitled ''An Online Energy Management Strategy for a Fuel Cell/Battery Vehicle Considering the Driving Pattern and Performance Drift Impacts'' in this appendix. However, this article has not been placed within the context of the thesis to have a better coherence of the work.
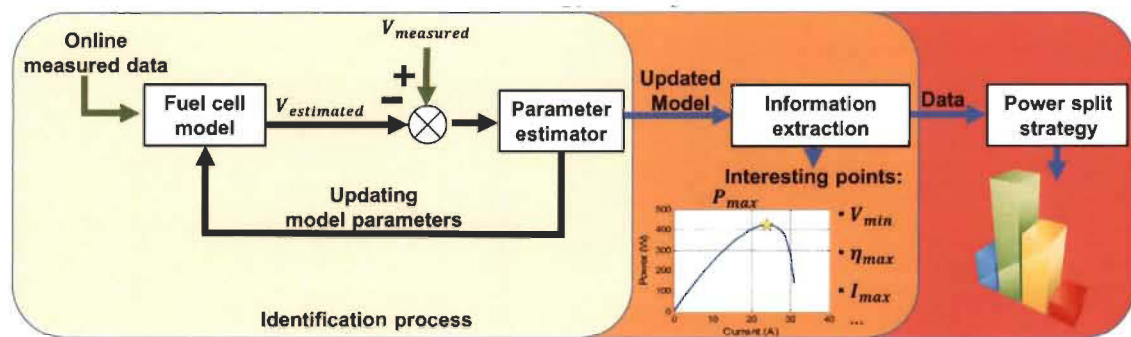
Figure 3.1   PEMFC online parameters estimation and the utilization for EMS design

3.2.2   Synopsis of the results analysis

In the first stage, the accuracy of the selected models and identification algorithms is checked regarding the estimation of the polarization curve. Figure 3.2 provides a comparison of the achieved polarization curves by RLS and Kalman filter for the two PEMFC models. As it is observed, regardless of the identification techniques, the model proposed by Amphlett et. al gives more accurate polarization curves and results than Squadrito et. al model. The difference in the accuracy level of the two models for polarization curve prediction can be attributable to the difference in the consideration of operating conditions in the two models and it sheds light on the positive influence of including temperature and pressure, in addition

to the current, to the PEMFC model. Another worth discussing observation apropos of Figure 3.2 is the performance comparison of the two employed identification algorithms. Looking more closely at the polarization curves implies that in case of Squadrito et. al model, which has four parameters to be estimated, RLS and Kalman filter show to a great extent similar performance. However, in case of Amphlett et. al model, which has eight parameters to be estimated for linear estimation, the Kalman filter seems to outperform RLS to some extent. The increase in the number of parameters, the original difference in the structure of Kalman filter and RLS, and the model uncertainties can all contribute to make the distinction between the performance of the RLS and Kalman filter in this particular application.
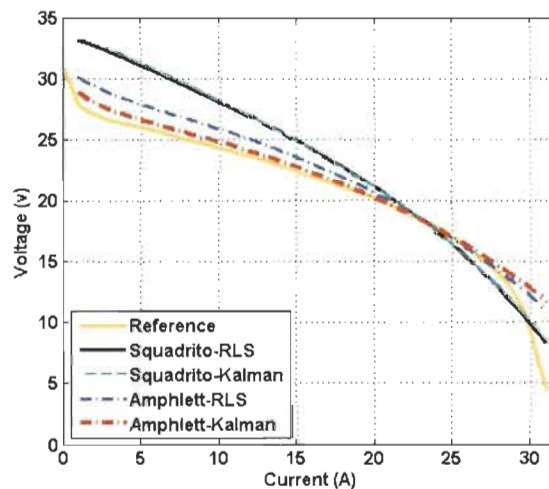
Figure 3.2   Polarization curves comparison for linear cases (R2 values: Squadrito-RLS: 0.7993, Squadrito-Kalman: 0.8440, Amphlett-RLS: 0.9001, Amphlett-Kalman: 0.9215)

In the second stage of the investigation, the linear and nonlinear parameters of Amphlett et. al model are estimated and the results are compared with the linear estimation of the same model. The aim of this analysis is to investigate the influence of maximum current density, which is a nonlinear parameter, in the process of model identification. This parameter is usually considered constant in the other similar works although it changes over time owing

to the effect of degradation and operating conditions. In this case, since the structure in one of the targeted parameters for estimation is nonlinear, RLS and KF cannot be used for identification process and instead of them EKF is tested. According to the presented results in Figure 3.3, EKF is capable of predicting a better polarization and power curves than the Kalman filter. This is very interesting for the ultimate purpose of this work, which is to integrate this online modeling into EMS design. In fact, the maximum power, which is used in the EMS design, is extracted from this curve. This result justifies the importance of considering the maximum current density estimation in the parameter identification process.
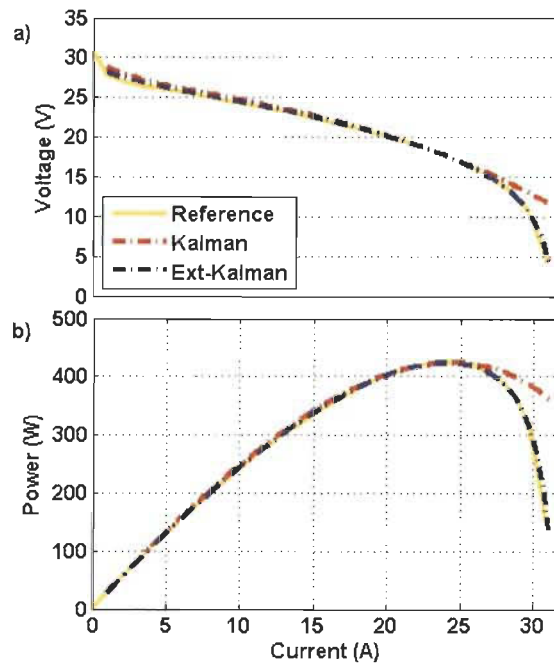
Figure 3.3   Comparison of linear and nonlinear identification cases, a) Polarization curves, b) Power curves (R^2 values: Kalman: 0.9215, Extended Kalman: 0.9984).

Overview and benchmark analysis of fuel cell parameters estimation for energy management purposes

M. Kandidayeni[a,b,:], A. Macias[a,b], A.A. Amamou[a,b], L. Boulon[a,b], S. Kelouwani[c], H. Chaoui[d]

[a] Hydrogen Research Institute, Department of Electrical Engineering and Computer Science, Université du Québec à Trois-Rivières, Trois-Rivières, Québec, G9A 5H7, Canada
[b] Canada Research Chair in Energy Sources for the Vehicles of the Future, Canada
[c] Hydrogen Research Institute, Department of Mechanical Engineering, Université du Québec à Trois-Rivières, Trois-Rivières, Québec, G9A 5H7, Canada
[d] Department of Electronics, Carleton University, Ottawa, Ontario, K1S 5B6, Canada

HIGHLIGHTS

- Thoroughgoing modeling and parameter estimation review of PEMFCs are presented.
- Nonlinear parameter identification is addressed by utilizing extended Kalman filter.
- Good precision of the results is proved via experimental tests.
- Application of this methodology to energy management design is demonstrated.

GRAPHICAL ABSTRACT
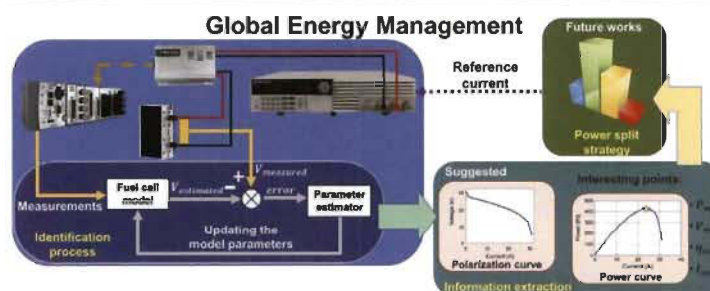
ARTICLE INFO

ABSTRACT

Proton exchange membrane fuel cells (PEMFCs) have become the center of attention for energy conversion in many areas such as automotive industry, where they confront a high dynamic behavior resulting in their characteristics variation. In order to ensure appropriate modeling of PEMFCs, accurate parameters estimation is in demand. However, parameter estimation of PEMFC models is highly challenging due to their multivariate, nonlinear, and complex essence. This paper comprehensively reviews PEMFC models parameters estimation methods with a specific view to online identification algorithms, which are considered as the basis of global energy management strategy design, to estimate the linear and nonlinear parameters of a PEMFC model in real time. In this respect, different PEMFC models with different categories and purposes are discussed first. Subsequently, a thorough investigation of PEMFC parameter estimation methods in the literature is conducted in terms of applicability. Three potential algorithms for online applications, Recursive Least Square (RLS), Kalman filter, and extended Kalman filter (EKF), which has escaped the attention in previous works, have been then utilized to identify the parameters of two well-known semi-empirical models in the literature, Squadrito et al. and Amphlett et al. Ultimately, the achieved results and future challenges are discussed.

1. Introduction

The harmful discharges from the conventional vehicles, running on fossil fuels, play a significant part in the growth of CO_2 emissions. Therefore, the requisite energy of future vehicles should be supplied by cleaner sources [1,2]. Among the various technical solutions, i.e.
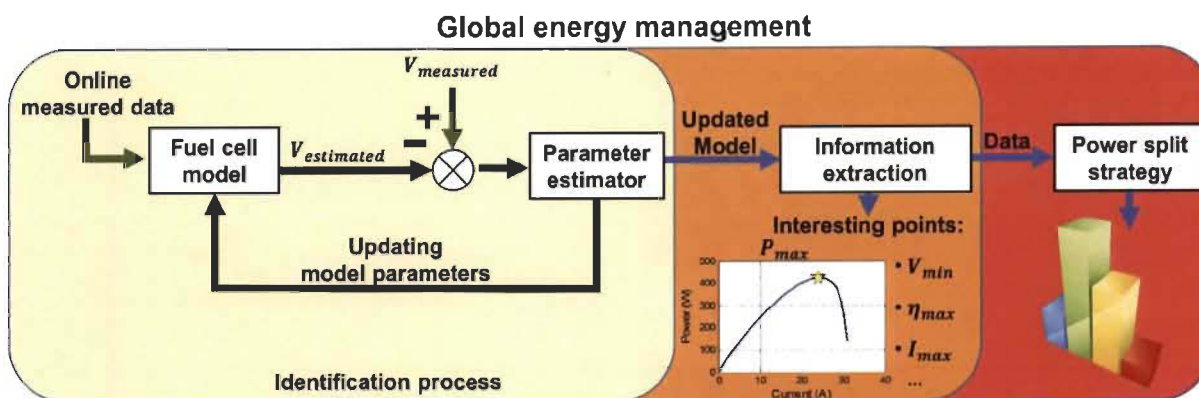
Fig. 1. Global EMS representation.

electric vehicles, hybrid electric vehicles etc., fuel cell vehicle (FCV) is one of the most promising due to no local emissions, high driving range, and very short refuelling duration [3]. FCVs mainly utilize proton exchange membrane fuel cells (PEMFCs) as the prime power source because of their low temperature and pressure operating range as well as their high power density in comparison to other fuel cell types such as carbon dioxide and solid membrane [4]. PEMFCs show satisfactory durability in slow dynamic applications. The intrinsic slow dynamic characteristic of a PEMFC and its incapability in storing extra energy make the utilization of a secondary power source, such as battery, necessary to satisfy the fast dynamic load in some applications like vehicles. Hybridization of the sources creates a multi-source system in which an energy management strategy (EMS) is in demand for splitting the power [5]. The majority of the existed EMSs in the literature, namely rule-based, and optimization-based, are premised on PEMFC models, especially static models [6–8]. In this respect, PEMFC modeling is of vital importance, and a wise selection of the model should be made with regard to the particular goals of the project. However, some factors such as dependency of PEMFC energetic performance on its operating conditions (temperature, pressure, and current), impact of aging and degradation phenomena on its performance, and so forth have made the design of a comprehensive PEMFC model immensely complicated. In this regard, utilization of identification algorithms has been suggested to deal with the problems caused by operating conditions change, degradation and aging by adjusting online the models parameters [9]. It should be noted that the careful selection of identification method is as important as the choice of model since it can complement the model and even compensate for its lack of details and considerations.

This paper provides an extensive review of identification methods for estimating PEMFC models parameters and introduces the suitable ones for EMS purposes. Moreover, an experimental benchmark study that compares three promising online identification techniques by using two renowned PEMFC models is conducted. It should be noted that in this work, online identification refers to the processing of the data in real time, i.e. the data is evaluated immediately after each sample. The remainder of this article is structured as follows:

A general description of the proposed article methodology is presented in section 2. An overview of the existed PEMFC models in the literature along with a broad review of identification algorithms, utilized for PEMFC parameter estimation, is provided in section 3. Section 4 deals with a benchmark study on online identification techniques. Finally, the conclusion is given in section 5.

2. Overall process

In a multi-source system, the operating points of the components can be determined by the EMS in a way to maximize the output power, system efficiency, lifetime, and autonomy. However, determining the operating point in a PEMFC, which is a multiphysics system and its

energetic performances are operating conditions dependent, is very difficult, and the desired operating point constantly moves through the operating space. Regarding the FCVs, it is very interesting to keep PEMFC running at its best power. Nevertheless, the power versus current curve of the PEMFC is moving with temperature and aging. Moreover, comprehensive modeling of a PEMFC, including the effect of degradation and operation points drift, is very difficult, time-consuming, and still a study limitation.

Maximum power or efficiency point tracking (MPPT) could be a good solution for this problem if they were not limited to a single specific objective. Perturbation and observation (P&O) and incremental conductance are MPPT algorithms that vary the current to get the maximum power point from the power curve; this process is known as hill climbing. Those variations increase the hydrogen consumption. These algorithms are sensitive to rapid changes, and they might be trapped in a local maximum [10,11]. Moreover, the implementation of such techniques in PEMFC systems is highly challenging due to different electrochemical, fluidic, and thermal time constants that vary from milliseconds to minutes.

In order to address these issues, the employment of a global energy management, as shown in Fig. 1, is vital to reach a good compromise between energetic efficiency and durability under various operating conditions. The whole process is performed online during the operation of the PEMFC. The global energy management strategy is composed of three steps, namely parameter identification, information extraction, and power split strategy. The main idea is to perform a real time model identification to find the best operating points through an information extraction. Subsequently, the power split strategy can use the provided data from the updated PEMFC model to optimally distribute the power flow. As shown in Fig. 1, the information extraction step, which is maximum power (P_{max}) in this work, is one example out of several possibilities, such as maximum efficiency point (η_{max}), minimum voltage (V_{min}), maximum current (I_{max}), and so forth. This step provides the power split strategy with essential information based on which it can decide how to share the power among the components. It should be noted that this paper mainly takes care of the choice of identification method and PEMFC model, which are the core of the presented global energy management. The parameter estimation of PEMFC models is really challenging due to their complex behavior. Next section provides a broad review of PEMFC modeling and identification techniques. The future works can extend the information extraction step and use such basis to design online power split strategies.

3. Review

3.1. Modeling

Modeling has a significant part to play in the technological evolution of PEMFCs. Several applications, such as automotive industry
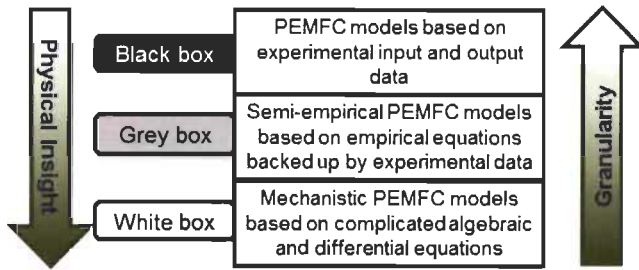
Fig. 2. PEMFC models categories.

[12–14], portable applications [15], distributed generation [15], military [16], etc., and objectives, such as multiphysics modeling, diagnosis, monitoring, energy management, control, etc., can be counted for modeling of PEMFCs. The existed PEMFC models in the literature can be fallen into three categories of white box, black box, and grey box [17–23], as shown in Fig. 2. White box models, known as mechanistic or theoretical models, consist of algebraic and differential equations which are based on thermodynamics, electrochemistry, and fluid mechanics [24–28].

They are designed to investigate various phenomena, such as polarization influences, catalyst employment, water management, and so forth, and have different spatial dimensions. As opposed to the white box models, black box models are obtained by means of observations and do not go through the details of physical relationships inside the PEMFC [29–35]. Since the computational effort of black box models is very low, they are very interesting for online applications like vehicles. However, the uncertainties of such models increase when confronting new operating conditions. Artificial neural networks, fuzzy logic, and their combination are perceived as prevalent approaches in developing PEMFC black box models [36]. Grey box models, known as semi-empirical models, offer an acceptable compromise between complexity and simplicity [37–43]. These models are premised upon the physical relationships which are supported by experimental data and demonstrate the fundamental electrochemical aspects of the PEMFCs (polarization curve). One of the interesting practical applications of grey box PEMFC models is in the area of energy management design. The physical insight provides significant information about polarization curve effects such as cell reversible voltage, activation drop, ohmic loss, and concertation overvoltage, which are highly valuable to investigate the relevance of the outcomes. Table 1 gives a brief summary of the discussed PEMFC models.

In the light of the previously discussed models, grey and black box models seem to be the fittest types for control and energy management purposes. Next section provides a thorough review of the utilized identification methods for parameters estimation of PEMFC models, which are based on grey and black box models.

Table 1
Comparison of PEMFC models.

Features	White box (Mechanistic)	Grey box (Semi-empirical)	Black box
Experimental data dependency	Low	Average	High
Computational time effort	High	Average	Low
Precision	High	Satisfactory	Satisfactory
Granularity	High	Average	Low
Physical insight	High	Satisfactory	Very low
Application area	Cell level understanding, Emulators design, Diagnosis purposes	Energy management, Control, Diagnosis studies	Energy management, Control, Diagnosis studies
Online applicability	Not applicable	OK	OK

3.2. Identification

System identification utilizes a black box or a grey box model to estimate a dynamic system features. Appropriate parameter identification of PEMFC models can strikingly increase the accuracy and compensate for the lack of details. However, the parameter estimation of PEMFC models is really demanding owing to their complicated features. A number of approaches have been reported in the literature to optimize and identify the parameters of a PEMFC model, namely metaheuristic based methods (GA, PSO …) [37–66], Electrochemical impedance spectroscopy (EIS) based methods (Frequency, Nyquist …) [67–72], black box based methods (ANN, SVM …) [73–89], Adaptive filter based methods (RLS, SRUKF …) [90–93], and some other methods such as current change, parametric table etc. [94–100], which fit to none of the categories. Table 2 summarizes the advantages and disadvantages of these methods. It should be noted that all of these methods have different convergence time, i.e. the required time for the algorithm to reach an acceptable value of the identified parameter. This convergence time mainly depends on their implementation and complexity. However, some of them, such as recursive and black box based methods, have been reported to be much faster than the others.

3.2.1. Metaheuristic-based optimization techniques

Numerous manuscripts have proposed metaheuristic-based optimization techniques to identify the linear and nonlinear parameters of an electrochemical PEMFC model without trapping in local optima. Regarding the metaheuristic-based methods, the majority of them [44–66] are amazingly based upon the proposed model by Amphlett et al. [41,43], which is a semi-empirical model and is able to imitate the behavior of the PEMFC to a satisfactory extent. All of these works revolve around the idea of introducing a new optimization algorithm to estimate the physical parameters of the static semi-empirical PEMFC model. Table 3 introduces the range of the identified parameters in the mentioned articles.

It should be noted that the utilized model in these articles describes the polarization curve and is based on the thermodynamic potential of the cell and three voltage drops (activation, ohmic, and concentration). In this respect, the parameters $\xi_n (n = 1…4)$ are related to the activation drop, λ and R_C are related to the ohmic drop, and b, and J_{max} are related to the concentration drop. Table 4 provides data on the type of proposed algorithms and obtained values for the parameters in the mentioned articles.

It should be noted that in Ref. [45] ten parameters of a new semi-empirical model, which is based on [43] with an additional cathode inlet pressure actor, are estimated by an AC-POA, but only its common parameters with other manuscripts is reported in Table 4. The other manuscripts, which are based on optimization algorithms, have worked on the models with more dynamic properties [67–73]. A summary of the methods employed in these papers is given in Table 5.

3.2.2. Electrochemical impedance spectroscopy

Another category of methods, applied in the parameter estimation of PEMFC models, is the works based on EIS technique. EIS is a frequency-based approach, which has been well established in PEMFC filed in recent years. The application of this approach covers a wide range of studies such as temperature and humidity effects, sub-zero condition, catalyst layer, and so on [74]. Taleb et al. have employed EIS method to validate a PEMFC fractional order impedance model, which imparts a good level of physical parameters comprehension. They have used the EIS data for estimating the parameters of the model by means of a frequency identification method based on nonlinear optimization. Subsequently, they have used Taylor series to obtain a third-order transfer function and applied least square and recursive least square methods for parameter estimation of the fractional order model. Their method is applicable in online application although the relationship between the physical parameters and the online identified parameters

Table 2
Identification methods characteristics.

Approach	Advantage	Disadvantage
Metaheuristic based	• Extracting an acceptable model regardless of the number of parameters • Revealing the defects of the device	• High computational burden • No online implementation reported
EIS based	- Suitable for different parts modeling and diagnosis objectives	- Expensive and time-consuming - Parameters are solely valid in the vicinity of the tested points - Ambiguous relation between the estimated and real parameter in fractional models
Black box based	• Accurate output • Online applicability	• No physical interpretation • Demanding training process • Unreliable in new conditions
Recursive filter based	- Matched with semi-empirical models - Providing good internal insight - Appropriate for online applications	- Choice of filter is very sensitive - Challenging Initialization and customization

remains ambiguous [75]. In Ref. [76], a comparative study is conducted for three cases of Dicks-Larminie dynamic model, EIS model, and equivalent circuit model. The parameter estimation is performed with the help of least square and recursive least square methods for the load resistances of the electrical equivalent circuit model and the impedance of Dicks-Larminie and EIS models. It is concluded that both EIS and electrical equivalent circuit model offer better precision than the Dicks-Larminie dynamic model. However, they cannot be applied in vehicular applications due to their level of complexities and computational time. In Ref. [77], the EIS technique is utilized to obtain the impedance model and frequency identification methods are used to estimate the fractional order transfer function impedance model's parameters. In this regard, least square methods, as a time domain approach, estimate the initial values for coefficients of the derivation operators and a nonlinear optimization, as a frequency domain approach, finalizes the values. In Ref. [78], the Nyquist and Bode diagrams, computed from EIS, are used to estimate the PEMFC catalyst layer parameters. In Ref. [79], an equivalent circuit model of PEMFC, which is based on non-integer derivatives for diffusion modeling, is introduced, and its parameters are extracted by means of EIS technique.

3.2.3. Black box based identification

The next group of works are premised upon the black box based identification of PEMFC models. In this regard, some manuscripts are based on artificial neural networks (ANNs) employment [80–84]. Linear regression technique, which uses gradient descent algorithms for updating the parameters, is compared with an ANN approach, which uses Levenberge-Marquardt algorithm for training, to model a 250-W PEMFC for an electric bicycle application in Ref. [80], and is concluded that ANN model benefits from more accuracy as well as convenience in modeling. In Ref. [81], two neural structures of nonlinear auto regressive with exogenous input (NARX) and nonlinear output error (NOE) are utilized to develop a PEMFC stack voltage model and NARX is recommended for real time applications while NOE is suggested for off-line applications. In Ref. [82], radial basis function neural network is utilized to develop a PEMFC metamodel for the data obtained from design of experiment approach. In Ref. [83], Gaussian radial basis function variable ANN is employed to identify the PEMFC model parameters online. In Ref. [84], the capabilities of PSO, for global search, and Levenberg–Marquardt algorithm neural network, for fast

convergence around the global optimum, are combined to obtain a voltage and thermal model for the PEMFC. In Refs. [85,86], nonlinear autoregressive moving average model with exogenous inputs (NARMAX) is employed to obtain a temperature model and a voltage model of PEMFC respectively. In Ref. [85], orthogonal least mean square is used to obtain the parameters of NARMAX temperature model first, then the selection is modified by GA. In Ref. [86], time domain and frequency domain NARMAX model of PEMFC are compared and the time domain is preferred. In Refs. [87,88], support vector machine (SVM) principle is utilized. Mathematical modeling of a laboratory PEMFC air supply system is dealt with by a novel Wiener model identification based on SVM in Ref. [87]. In Ref. [88], SVM is employed to model a PEMFC for real time and monitoring applications. Fuzzy logic control (FLC) principle is utilized in Refs. [89,90], in which an adaptive neuro-fuzzy inference system (ANFIS) is proposed for voltage modeling of PEMFC in high temperature condition, and an adaptive FLC is used for adding the control of gas flow to a PEMFC model respectively. In Ref. [91], a black box approach is compared with a white box one, and it is concluded that the black box model has higher accuracy. In Ref. [92], the Volterra and Wiener model methods are utilized to obtain a linear PEMFC model for vehicular applications. In Ref. [93], the nonlinear black box time series model of [94] and the proposed PEMFC control approach of [95] are combined to follow the optimum operating points of the fuel cell.

3.2.4. Recursive filter based methods

Next category of the articles belongs to the application of recursive filters for estimating the parameters of a PEMFC semi-empirical model. This category, which had escaped the attentions for many years, seems to be very interesting for energy management purposes. As previously mentioned, PEMFC is a very complicated, nonlinear, and multiphysic device, which is not easy to be comprehensively modeled. Furthermore, the performance of the PEMFC is influenced on the one hand by its operating conditions alteration and on the other hand by aging and degradation. All of the mentioned complexity, dependency, and phenomena widen the gap between the performance of a PEMFC model and the real device. Proper tuning of a PEMFC model parameters, by means of parameter identification techniques, can narrow the existed gap in the modeling to a great extent and integrate the influence of different factors into the model. Ettihir et al. have proposed the employment of

Table 3
Boundaries of the parameters.

Parameters	ξ_1	$\xi_2 \times 10^{-3}$	$\xi_3 \times 10^{-5}$	$\xi_4 \times 10^{-4}$	λ	$R_C \times 10^{-4}$ (Ω)	b (V)	J_{max} (Acm^{-2})
Maximum	−0.80	5	9.8	−0.954	24	8	0.5	1.5
Minimum	−1.2	1	3.6	−2.6	10	1	0.0135	0.5

Table 4

Metaheuristic-based algorithms utilized for parameters estimation of the PEMFC model in Refs. [41,43].

Reference	Method	FC power (W)	Parameters							
			ξ_1	$\xi_2 \times 10^{-3}$	$\xi_3 \times 10^{-5}$	$\xi_4 \times 10^{-4}$	λ	$R_C \times 10^{-4}$	b	J_{max}
[44]	ABSO	250	−0.9519	3.0850	7.8	−1.880	23	1	0.02789	0.84478
[45]	AC-POA	250	−0.8997	2.5468	5.4432	−1.3650	14.206	0.8261	0.01	–
[46]	AIS	250	−0.9469	3.0271	7.4944	−1.8845	18.996	6.429	0.02896	0.85279
[47]	ARNA-GA	250	−0.8806	2.9451	8.4438	−1.2883	13.4860	1.0068	0.03167	–
[48]	BIPOA	250	−0.8016	2.6673	8.1288	−1.2713	13.5158	0.8	0.0324	–
[49]	DE	250	−0.9878	2.6167	3.6	−1.5694	24	1	0.0355	–
[50]	HABC	250	−0.8540	2.8498	8.3371	−1.2940	14.2873	1	0.0340	–
[51]	HADE	250	−0.8532	2.8100	8.0920	−1.2870	14.0448	1	0.03353	–
[52]	MPSO	250	−0.944	3.0037	7.4	−1.945	23	1	0.0272	0.85228
[53]	Simple GA	250	−0.8020	2.9521	6	−1.5812	13	2.47	0.0261	–
[54]	STLBO	250	−0.9520	2.9400	7.8000	−1.8800	23	1	0.0328	–
[55]	TLBO-DE	250	−0.8532	2.6432	7.9960	−1.4050	10.0068	1.0498	0.0299	1.15843
[59]	TRADE	SR-12 500	−0.9373	3.465	9.308	−0.954	23.9999	1	0.2375	0.50045
[61]	ADE	BCS 500	−1.0291	3.6	8.2495	−2.600	18.6921	7.9	0.0287	1495.40
		SR-12 500	−0.8955	2.46	3.9074	−0.954	24	1.1	0.2113	753.05
[62]	GWO	BCS 500	−1.018	2.3151	5.24	−1.2815	18.8547	7.5036	0.0136	–
		SR-12 500	−0.9664	2.2833	3.40	−0.954	15.7969	6.6853	0.1804	–
[63]	IGHS	BCS 500	−1.0098	3.3	6.93	−2.59	21.25	7.6	0.0489	1.41915
		SR-12 500	−1.0368	2.9	4.07	−0.954	22.53	2.4	0.2029	0.74453
[65]	Rank	BCS 500	−1.0269	3.2749	6.40	−2.60	22.0226	8	0.0138	1.49985
		SR-12 500	−0.9987	3.2155	7.09	−0.954	23.9999	1	0.1861	0.71224

Table 5

Features of the estimation approaches.

Reference	Method	Parameters and considered areas	Real time applicability
[67]	Hybrid stochastic strategy (PSO + DE)	12 parameters. Activation, Ohmic, Concentration	No
[68]	PSO	5 parameters. Activation, Ohmic	No
[69]	Evolution strategy	22 parameters. Activation, Ohmic, Concentration, Thermal model	No
[70]	Quantum-based optimization	3 parameters. Activation, Ohmic, Concentration	Yes
[71]	Hybrid optimization (PSO + Big Bang-Big Crunch)	7 parameters. Activation, Ohmic, Concentration	No
[72]	PSO and DE	5 parameters. Activation, Ohmic, Concentration	No
[73]	PSO	8 parameters. Activation, Ohmic, Concentration	No

adaptive recursive least square (RLS) in Refs. [96–98], and square root unscented Kalman filter (SRUKF) in Ref. [99], to estimate the parameters of a semi-empirical model, proposed by Squadrito et al. [42]. They have concluded that the classical power split approaches may result in mismanagement due to the fact that they are not capable of tracing the performances alteration arising from aging and operating condition variations. Their proposed adaptive EMS can meet the power demand while sustaining the battery state of charge. Moreover, it is able to track real behavior of the PEMFC and to request a relevant power. It should be noted that the selected model in these works is solely a function of PEMFC operating current, and they have proposed the extension of their work by adding more operating parameters such as temperature and pressure.

3.2.5. Other methods

There are some other methods that have been utilized in the PEMFC model identification. In Ref. [100], a parametric table, obtained from experimental test, is utilized to optimize the operating conditions of a one-dimensional analytical model. Although the proposed method of this work has shown interesting results, the process of obtaining such data to form a map seems to be highly time-consuming. In Refs. [101,102], two online methods for PEMFC model identification are proposed based on data-driven schemes to be used in model predictive control and adaptive control respectively. However, both of the suggested methods require data storage and high memory capacity for identifying the parameters online. In Ref. [103], least square methods are employed to fit the parameters of three models, Amphlett [43], Larminie-Dicks [4] and Chamberlin-Kim [4], and the obtained models have been compared regarding their levels of accuracy. In Ref. [104], current change technique is proposed to estimate the parameters of an equivalent circuit PEMFC model, in which waveform measurement analysis of current change tests is employed for parameter extraction. In Ref. [105], static and dynamic modeling of PEMFC based on data measurement is introduced, in which a simple Matlab curve fitting method is utilized for the identification of static model parameters, and Pspice Optimizer is used for the dynamic one. In Ref. [20], a dynamic model of PEMFC is developed in the gPROMS modeling environment, and the parameters are extracted based on experimental data. In Ref. [106], nonlinear least squares based on Lagrangian approach is developed to estimate the parameters of a one-dimensional PEMFC model.

3.3. Synopsis of the modeling and identification review

In the light of the discussed sections, it can be inferred that the recursive filter based methods appear to be very fit for online applications and energy management purposes. This is partly due to the fact that the semi-empirical PEMFC models, which increase the internal comprehension about the device, are used with these approaches and partly due to the fact that they are suitable for applications in which the desired parameters change over time. However, special attention should be paid to the choice of filter and its design, in terms of initialization and customization, to achieve satisfactory outcomes. It should be noted that the thing which makes the recursive based methods more preferable than black box based methods in this work is that the former easily enables one to investigate the relevance of the results (physical meaning), and it also makes the power and efficiency curve plots really convenient (polarization curve).
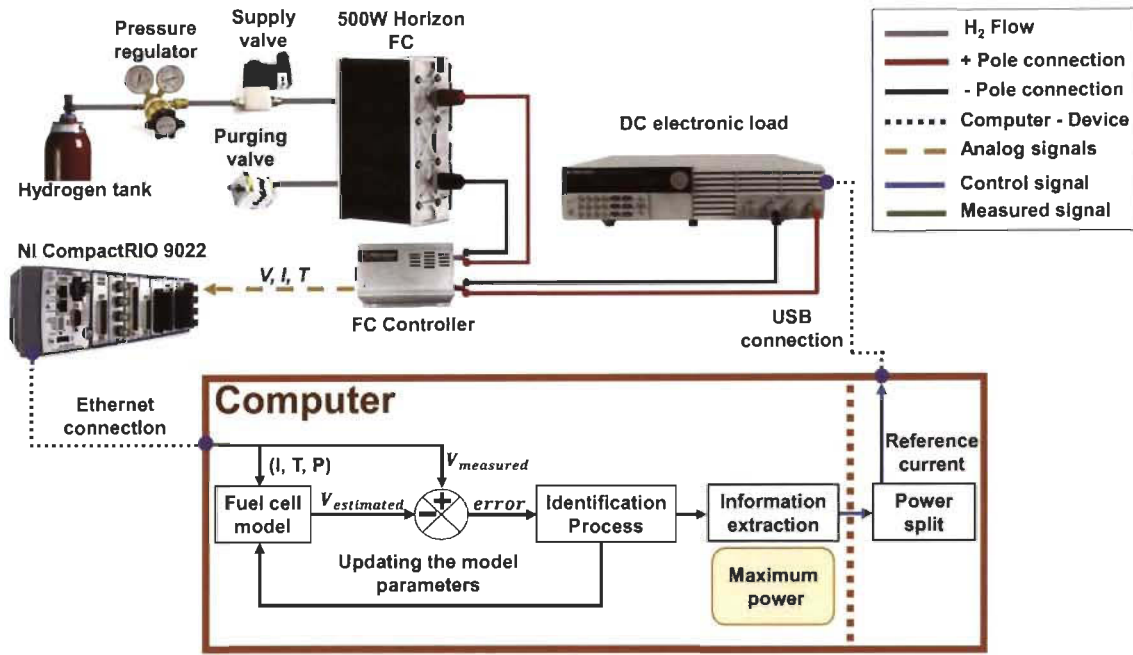
Fig. 3. Test bench and intended methodology representation.

4. Benchmark study

Unlike the aforementioned techniques, this paper presents a comparative study of online recursive methods with the purpose of facilitating the energy management design. To do so, extended Kalman filter (EKF) is suggested for the process of parameter identification. To the best of our knowledge, this is the first attempt to identify the linear and nonlinear parameters of a PEMFC semi-empirical model online. As discussed in the preceding section, the recursive filter based methods are highly appropriate for online applications and global energy management designs. In this respect, three potential recursive filters (RLS, Kalman filter, and EKF) are utilized to identify the parameters of two famous semi-empirical models, in the literature, in this section. Apart from the fact that the selected PEMFC models are well-known in the literature, they provide a good opportunity to make a comparison between a multi-input model (Amphlett et al.) and a single input model (Squadrito et al.). Fig. 3 represents the experimental test bench utilized for testing the PEMFC models as well as identification algorithms in this work. Regarding the test bench, it should be noted that a 500-W air breathing Horizon PEMFC, described in Table 6, is connected to a National Instrument CompactRIO through its controller. A programmable DC electronic load is used to ask some load profiles from the PEMFC. According to the manufacturer, the difference between the atmospheric pressure in the cathode side and the pressure of the PEMFC in the anode side should be adjusted to about 50.6 kPa. The pressure in the anode

Table 6
PEMFC characteristics.

PEMFC Technical specification	
Type of FC	PEM
Number of cells	36
Active area	52 cm^2
Rated Power	500 W
Rated performance	22 V @ 23.5 A
Max Current	42 A
Hydrogen pressure	50-60 kPa (0.5–0.6 Bar)
Rated H$_2$ consumption	7 l/min
Ambient temperature	5 to 30 °C
Max stack temperature	65 °C
Cooling	Air (integrated cooling fan)

side is set to 55.7 kPa. The measured data (temperature, voltage, current) from the real PEMFC is transferred to the PC, by means of the CompactRIO, to be used in the selected model for identification process. Concerning the energy management, it is worth reminding that this paper only deals with the implementation of the models and algorithms to pave the way towards designing an EMS. As an example of information extraction, the real maximum power of the PEMFC is obtained at each moment, in this work. Therefore, a power split strategy can be easily added to this work in future to benefit from a global energy management.

4.1. PEMFC models introduction

The general formulation of the electrochemical PEMFC model proposed by Amphlett et al. [41,43], which is for a number of cells connected in series, is as follows. This model takes several operating conditions into account, as it is seen in (1–5) and opens up a good opportunity to compare the effect of linear and nonlinear parameter identification due to its structure in the concentration loss calculation.

$$V_{FC} = N\left(E_{Nernst} + V_{act} + V_{ohmic} + V_{con}\right) \tag{1}$$

$$E_{Nernst} = 1.229 - 0.85 \times 10^{-3}(T - 298.15) + 4.3085 \\ \times 10^{-5}T\left[\ln(P_{H2}) + 0.5\ln(P_{O2})\right] \tag{2}$$

$$\begin{cases} V_{act} = \xi_1 + \xi_2 T + \xi_3 T\ln(CO_2) + \xi_4 T\ln(i) \\ CO_2 = \dfrac{P_{O2}}{5.08 \times 10^6 \exp(-498/T)} \end{cases} \tag{3}$$

$$V_{ohmic} = -iR_{internal} = -i(\zeta_1 + \zeta_2 T + \zeta_3 i) \tag{4}$$

$$V_{con} = B\ln\left(1 - \frac{J}{J_{max}}\right) \tag{5}$$

Where V_{FC} is the output voltage (V), N is the number of cells, E_{Nernst} is the reversible cell potential (V), V_{act} is the activation loss (V), V_{ohmic} is the ohmic loss (V), V_{con} is the concentration loss (V), T is the stack temperature (K), P_{H2} is the hydrogen partial pressure in anode side (N m^{-2}), P_{O2} is the oxygen partial pressure in cathode side (N m^{-2}), $\xi_n (n = 1...4)$ are the semi-empirical coefficients based on fluid mechanics, thermodynamics, and electrochemistry, CO_2 is the oxygen concentration (mol cm^{-3}), i is the PEMFC operating current (A), $R_{internal}$

Table 7
Targeted parameters for estimation.

Algorithm	PEMFC model	Parameters vector
RLS and Kalman filter	Amphlett et al.	$[\xi_1,\ \xi_2,\ \xi_3,\ \xi_4,\ \zeta_1,\ \zeta_2,\ \zeta_3,\ B]$
RLS and Kalman filter	Squadrito et al.	$[V_O,\ b,\ R_{internal},\ \alpha]$
EKF	Amphlett et al.	$[\xi_1,\ \xi_2,\ \xi_3,\ \xi_4,\ \zeta_1,\ \zeta_2,\ \zeta_3,\ B,\ J_{max}]$

Table 8
Current levels and PEMFC stack temperature during ohmic measurement.

Current (A)	Temperature (K)
3	297.55
6	297.95
9	299.55
12	300.45
15	301.95
18	304.15
21	306.35
24	309.95
26	312.15

is the internal resistor (Ω), $\zeta_n (n = 1...3)$ are the parametric coefficients, B is a parametric coefficient (V), J is the actual current density (A cm^{-2}), and J_{max} is the maximum current density (A cm^{-2}).

It should be noted that the utilized ohmic loss calculation is based on the formula introduced in Ref. [43] rather than [41], because it is a more general formula, which can be used for different commercial fuel cells like Horizon, and more importantly it does not need any specific data like thickness and active area of membrane, which are only available for a limited number of fuel cells. The electrochemical PEMFC model suggested by Squadrito et al. [42] is presented below.

$$V_{FC} = N\left[V_O - b\ log\,(J) - R_{internal}\,J + \alpha J^{\sigma}\ \ln(1 - \beta J)\right] \tag{6}$$

Where N is the number of cells, V_{FC} is output voltage (V), V_O is the reversible cell potential (V), b is the Tafel slope, J is actual current density (A cm^{-2}), $R_{internal}$ is cell resistance (Ω), α is a semi-empirical parameter related to the diffusion mechanism, σ (between 1 and 4) is a dimensionless number which is related to the water flooding phenomena, and β is the inverse of the limiting current density (cm^2 A^{-1}). Table 7 presents the parameters to be identified by the recursive algorithms. Indeed, the increased number of parameters bring more accuracy about at the cost of increasing the computational time. However, the utilized methods in this paper have no problem in this regard due to the fact that the identifiable parameters are linear in structure, except in one case which is dealt with EKF. It should be noted that the parameter J_{max}, which is not linear in the structure and assumed to be constant in most of the previous articles, is estimated online by EKF to draw an analogy between the linear and nonlinear parameters estimation methods. This parameter changes over time due to the influence of degradation and is highly sensitive regarding voltage and polarization curve estimation, as reported in Ref. [107].

4.1.1. Resistor measurement

So as to check the appropriateness of the parameter identification process and relevance of the obtained values with the physical meaning, some clues about the real values of the device are required. Regarding the Amphlett et al. model, the range of all the parameters is available according to the reported values in Table 3. However, as explained in the previous section, the employed resistor formulation in this paper is different with the demonstrated resistor parameters of Table 3 due to the fact that specific information about membrane type of the 500-W commercial air-breathing Horizon fuel cell is not accessible. Thus, in this paper, the current interrupt method, which is a well-known electrochemical technique [108–111], is used to measure the evolution of resistor with respect to the temperature and current. This measurement clarifies the range of the resistor for the whole stack and is a helpful tool to check the accuracy of the achieved results by both PEMFC models. The effectiveness of utilizing current interrupt method for measuring the ohmic resistor has been already proved in Ref. [111]. The principle behind the current interrupt method is that ohmic losses fade almost immediately after current interruption, and activation losses decrease to the open circuit voltage at a strikingly slower pace. Thus, rapid acquisition of the measured voltage is essential for splitting the ohmic from activation loss. The advantages of current interrupt method to other electrochemical techniques is that data analysis is highly straightforward. However, one of the difficulty of this method is the determination of the exact point in which the voltage jumps and a fast oscilloscope is in demand to solve this issue. In this paper, the

procedure for performing the current interrupt test is strictly according to [111]. Table 8 presents the various stack temperature and currents while conducting the test. It should be noted that the stack has been given enough time to achieve a stable temperature at each current level before conducting the current interrupt measurement, and all the measurements have been performed for the forced convection condition.

Fig. 4 indicates the result of resistor measurement. Fig. 4a shows the evolution of the PEMFC resistor with respect to the increase of current, and Fig. 4b presents the temperature related evolution. These results are obtained from the conducted current interrupt test. The main purpose of conducting current interrupt test is to realize the variation range in the value of resistor for the employed 500-W PEMFC and utilize this range as a tool to check the evolution of the resistor in the PEMFC model.

4.2. Recursive filters

As previously mentioned, the parameters of a PEMFC model are time-varying since the device is affected by degradation and operating conditions. The focus of this section is to introduce three recursive algorithms. These algorithms are utilized for online identification of the parameters, and they are independent of saving data because they benefit from recursive structures, in which new measurement data can be analyzed as they arrive. RLS and Kalman filter are utilized to estimate the parameters, which are linear in the structure, while EKF is utilized to estimate linear and nonlinear parameters.

4.2.1. Recursive least square

RLS algorithm is premised upon the concept of minimizing the error related to input signal. RLS gives excellent performance when operating in time varying conditions. The enhanced performance is achieved at the cost of increased computational cost and some stability problems. The structure of the employed RLS in this work is as follows:

$$\theta(t) = \theta(t - 1) + k(t)e(t) \tag{7}$$

$$k(t) = \frac{\Gamma(t)^{-1}p(t - 1)\phi(t)}{(1 + \Gamma(t)^{-1}\phi^T(t)p(t - 1)\phi(t))} \tag{8}$$

$$p(t) = \Gamma(t)^{-1}p(t - 1) - \Gamma(t)^{-1}k(t)\phi^T(t)p(t - 1) + bI \tag{9}$$

$$\begin{cases} \Gamma(t) = \Psi - \dfrac{1 - \Psi}{\phi^T(t)p(t - 1)\phi(t)}; & if\ \phi^T(t)p(t - 1)\phi(t) > 0 \\ \Gamma(t) = 1; & if\ \phi^T(t)p(t - 1)\phi(t) = 0 \end{cases} \tag{10}$$

$$e(t) = u(t) - \phi^T(t)\theta(t - 1) \tag{11}$$

Where t denotes discrete time, $\theta(t)$ is the parameter vector, $k(t)$ is the gain vector, $e(t)$ is the error, $\Gamma(t)$ is the directional forgetting factor, $\phi(t)$ is the regression vector, $p(t)$ is the covariance matrix, b is a nonnegative scalar, which increases covariance matrix and prevents estimation faults due to big changes, I is the identity matrix, Ψ is the forgetting factor ($0 < \Psi < 1$), and $u(t)$ is the measured output, which is obtained
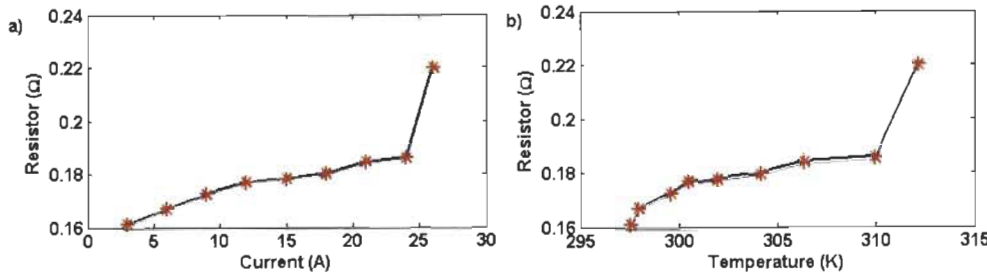
from the test bench. The parameters vector of each model ($\theta(t)$) has been already shown in Table 7 and the corresponded regression vector of each model is defined as below.

$$\phi(t) = \left[1, \; T, \; Tln(CO_2), \; Tln(i), \; -i, \; -iT, \; -i^2, \right.$$

$$\left. ln\left(1 - \frac{J}{J_{max}}\right)\right] \text{(Amphlett et al. model)} \tag{12}$$

$$\phi(t) = [1, \; log(J), \; -J, \; J^\sigma \; ln(1 - \beta J)] \text{(Squadrito et al. model)} \tag{13}$$

4.2.2. Kalman filter

Kalman filter is considered as an optimal estimator and it can conclude the parameters of interest from imprecise and uncertain observations. This filter estimates the current state variables firstly and then updates them when the next measurement is received. The structure of Kalman filter is as follows:

$$\begin{cases} x(t+1) = F(t+1|t)x(t) + w(t) \\ y(t) = H(t)x(t) + v(t) \end{cases} \text{(State–space model)} \tag{14}$$

$$\hat{x}(t) = F(t|t-1)\hat{x}(t-1) \text{(State estimate propagation)} \tag{15}$$

$$P(t) = F(t|t-1)P(t-1)F^T(t|t-1)$$
$$+ Q(t-1) \text{(Error covariance propagation)} \tag{16}$$

$$G(t) = P(t)H^T(t)[H(t)P(t)H^T(t) + R(t)]^{-1} \text{(Kalman gain matrix)} \tag{17}$$

$$\hat{x}(t) = \hat{x}(t) + G(t)(y(t) - H(t)\hat{x}(t)) \text{(State estimate update)} \tag{18}$$

$$P(t) = (I - G(t)H(t))P(t) \text{(Error covariance update)} \tag{19}$$

Where t is the discrete time, $x(t)$ is the state vector, which is unknown and here it can be called parameters vector as well, $\hat{x}(t)$ is the estimate of the state vector, $\hat{x}(t)$ denotes priori estimate of the state vector, $F(t+1|t)$ is the transition matrix, which takes the state vector from time t to time $t+1$, $w(t)$ is the process noise, $y(t)$ is the output, $H(t)$ is the measurement matrix, $v(t)$ is the measurement noise, $P(t)$ is the error covariance matrix, $Q(t)$ is the process noise covariance matrix, $G(t)$ is the Kalman gain, $R(t)$ is the measurement noise covariance matrix, and I is the identity matrix. It should be noted that the state vector is exactly like the parameter vectors shown in Table 7, the measurement matrix is the same as (12) and (13), and the transition matrix is assumed to be an identity matrix.

4.2.3. Extended Kalman filter

The EKF is the nonlinear version of the Kalman filter which linearizes the state space model at each time instant with respect to the latest state estimate. The structure of the EKF is defined as follows:

$$\begin{cases} x(t+1) = f(t, x(t)) + w(t) \\ y(t) = h(t, x(t)) + v(t) \end{cases} \text{(State–space model)} \tag{20}$$

$$F(t+1|t) = \frac{\partial f(t, x)}{\partial x}\bigg|_{x=x(t)} \tag{21}$$

$$H(t) = \frac{\partial h(t, x)}{\partial x}\bigg|_{x=x(t)} \tag{22}$$

$$\hat{x}(t) = f(t, \hat{x}(t-1)) \text{(State estimate propagation)} \tag{23}$$

$$P(t) = F(t|t-1)P(t-1)F^T(t|t-1)$$
$$+ Q(t-1) \text{(Error covariance propagation)} \tag{24}$$

$$G(t) = P(t)H^T(t)[H(t)P(t)H^T(t) + R(t)]^{-1} \text{(Kalman gain matrix)} \tag{25}$$

$$\hat{x}(t) = \hat{x}(t) + G(t)y(t) - h(t, \hat{x}(t)) \text{(State estimate update)} \tag{26}$$

$$P(t) = (I - G(t)H(t))P(t) \text{(Error covariance update)} \tag{27}$$

Where, $f(t, x(t))$ is a nonlinear transition matrix function, and $h(t, x(t))$ is a nonlinear measurement matrix function. The state vector is already presented in Table 7 for EKF. It should be noted that in this work, the $f(t, x(t))$ is not nonlinear and it is assumed to be an identity matrix. However, $h(t, x(t))$ is a nonlinear function and its derivation is as below.

$$\begin{cases} V_{FC}(t) = N\left[\xi_1 + \xi_2 T + \xi_3 Tln(CO_2) + \xi_4 Tln(i) - i(\zeta_1 + \zeta_2 T + \zeta_3 i) \right. \\ \qquad\qquad \left. + Bln\left(1 - \frac{J}{J_{max}}\right)\right] \\ x(t) = [\xi_1, \; \xi_2, \; \xi_3, \; \xi_4, \; \zeta_1, \; \zeta_2, \; \zeta_3, \; B, \; J_{max}] \\ H(t) = \frac{\partial h(t, x)}{\partial x} = \left[1, \; T, \; Tln(CO_2), \; Tln(i), \; -i, \; -iT, \; -i^2, \right. \\ ln\left(1 - \frac{J}{J_{max}}\right), \; \frac{BJ}{J_{max}(J_{max} - J)}\right] \end{cases} \tag{28}$$

4.3. Results and discussion

The obtained results from the performed comparative study is presented in this section. All the mentioned algorithms and PEMFC models, introduced in the previous section, are tested on the presented test bench in Fig. 4 to assess the performance of the proposed methodology, in terms of estimating the behavior of the real PEMFC to be used in EMS designs. In the first stage of the analysis, RLS and Kalman filter algorithms are utilized to estimate the demonstrated parameters in Table 7 for both of the models. This analysis enables one to form a primary opinion about the accuracy of the models. The entire estimated parameters are linear at this stage. Further analyses are performed in the first stage to compare the results of RLS and Kalman filter. In the second stage of the investigation, the linear and nonlinear parameters of Amphlett et al. model are estimated, and the results are compared with the linear estimation of the same model. The aim of this analysis is to investigate the influence of J_{max}, which is a nonlinear parameter, in the process of model identification. This parameter is usually considered constant in the other similar works although it changes over time owing to the effect of degradation and operating conditions.

Fig. 5a represents the employed current profile to conduct the test. This current profile varies between the minimum and maximum
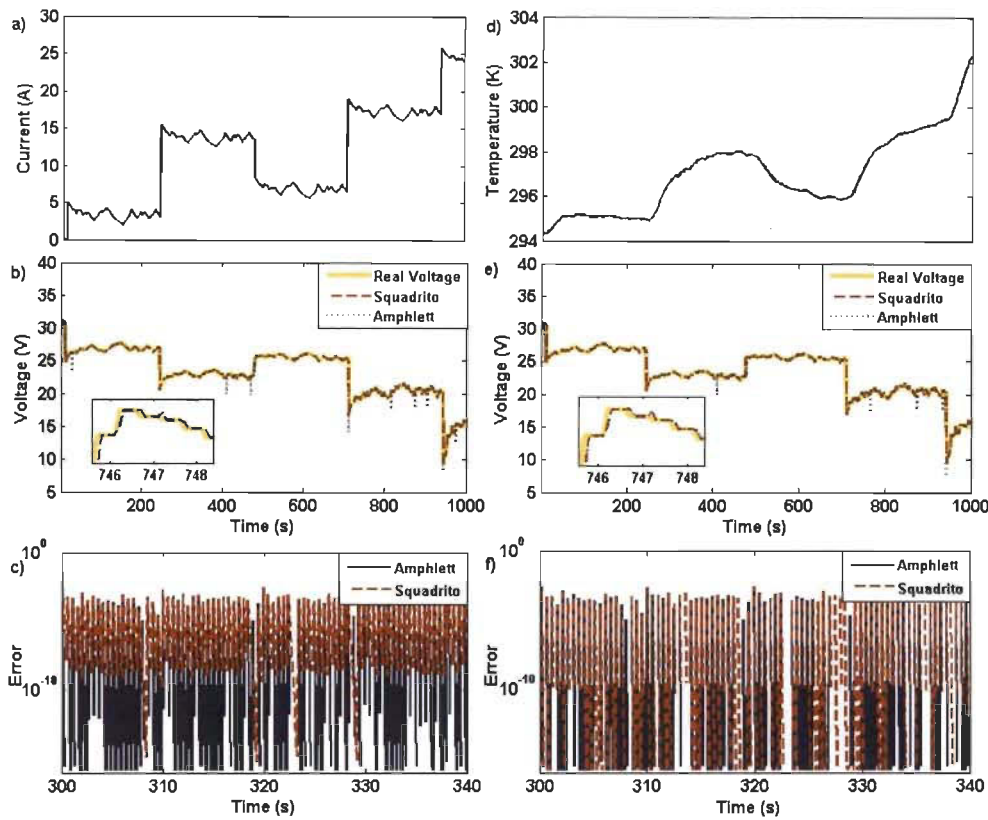
Fig. 5. Accuracy comparison of the two PEMFC models with RLS and Kalman filter algorithms, (a) the employed current profile, (b) voltage estimation by RLS, (c) RLS relative error ($|V_{measured} - V_{estimated}|/|V_{estimated}|$), (d) temperature evolution due to current profile, (e) voltage estimation by Kalman filter, (f) Kalman filter relative error.

operating current of the utilized 500-W Horizon PEMFC. Fig. 5d shows the corresponded temperature evolution to the current profile. The current profile is applied to the PEMFC system and the output voltage of the real PEMFC is recorded. The current and temperature data as well as the regulated pressure are concurrently sent to the PEMFC model and the output voltage of the model is calculated after estimation of the parameters by the identification methods. It should be noted that the whole explained process happens online. The estimated output voltage of the two introduced PEMFC models is compared with the real PEMFC voltage in Fig. 5b in which the parameters are identified by means of RLS algorithm, and this estimation seems to be satisfactory for both models. The relative error estimation of the output voltage by RLS, shown in Fig. 5c, also confirms that the both PEMFC models demonstrate acceptable voltage approximation. The same test, regarding voltage estimation and relative error, has been done for Kalman filter, as shown in Fig. 5e and f, respectively. It is observed that both of the models and algorithms are able to estimate the output voltage with almost the same accuracy, and that is why further analyses regarding the performance comparison of models and algorithms are required as hereinafter provided.

Fig. 6 provides a comparison of the achieved polarization curves by RLS and Kalman filter for the both discussed PEMFC models. As it is observed in Fig. 6, regardless of the identification techniques, the obtained polarization curves by Squadrito et al. model are noticeably different with the reference polarization curve, which belongs to the real PEMFC. This difference infers that the model proposed by Amphlett et al. gives more accurate polarization curves and results than Squadrito et al. model. It also shows that only accurate voltage estimation does not guaranty that the model benefits from enough precision because the physical relevance of the results should be investigated through the polarization curves. Moreover, when an identification technique is utilized, it tries to minimize the voltage estimation error for one single point irrespective of how the parameters fluctuate or the system behaves. Thus, the employment of another tool like a polarization curve seems to be vital for the process of PEMFC model parameters
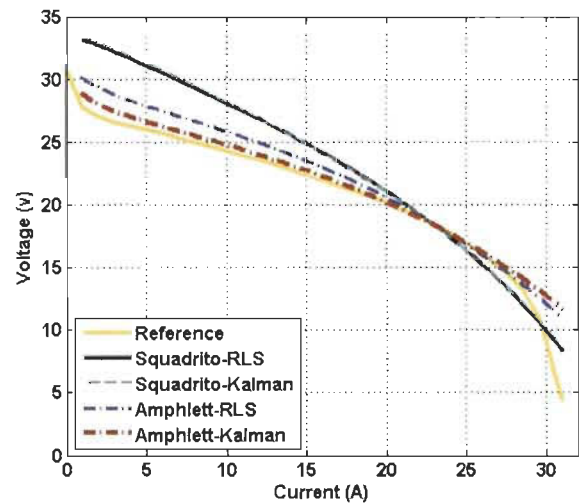
Fig. 6. Polarization curves comparison for linear cases (R^2 values: Squadrito-RLS: 0.7993, Squadrito-Kalman: 0.8440, Amphlett-RLS: 0.9001, Amphlett-Kalman: 0.9215).

identification. The difference in the accuracy level of the two models for polarization curve prediction can be attributable to the difference in the consideration of operating conditions in the two models, and it sheds light on the positive influence of including temperature and pressure, in addition to the current, to the PEMFC model. Another worth discussing observation apropos of Fig. 6 is the performance comparison of the two employed identification algorithms. Looking more closely at the polarization curves implies that in the case of using Squadrito et al. model, which has four parameters to be estimated, RLS and Kalman filter show to a great extent similar performances. However, in the case of Amphlett et al. model, which has eight parameters to be estimated for linear estimation, the Kalman filter seems to outperform RLS to some extent. The increase in the number of parameters, the original difference in the structure of Kalman filter and RLS, and the model

Fig. 7. Comparison of linear and nonlinear identification cases, a) Polarization curves, b) Power curves (R^2 values: Kalman: 0.9215, Extended Kalman: 0.9984).

Table 9
Average values of the activation and concentration parameters.

Method	ξ_1	$\xi_2 \times 10^{-3}$	$\xi_3 \times 10^{-5}$	$\xi_4 \times 10^{-4}$	B	J_{max}
RLS	−0.9950	2.1285	2.1881	−1.2379	0.4970	1.2381
Kalman	−0.9950	2.1228	2.1264	−1.1337	0.4970	1.2381
EKF	−0.9950	2.1300	2.1423	−0.9785	0.0130	1.6250

uncertainties can all contribute to make the distinction between the performance of the RLS and Kalman filter in this particular application. It should be noted that the R-squared value, which indicates how well the observed outcomes are replicated by the model, are reported in the caption of Fig. 6 for all the combinations to clarify the amount of error.

Fig. 7 presents the results concerning the effectiveness investigation of estimating the nonlinear parameter, J_{max}, in addition to the other parameters for the Amphlett et al. model. In this case, since the structure in one of the targeted parameters for estimation is nonlinear, RLS and Kalman filter cannot be used for identification process and instead of them EKF is tested. Fig. 7a compares the obtained polarization curve by EKF with Kalman filter. As it can be seen in this figure, EKF is capable of predicting a better polarization curve than the Kalman filter and its polarization curve is closer to the reference. Fig. 7b shows the corresponded power curve to each polarization curve. As is clear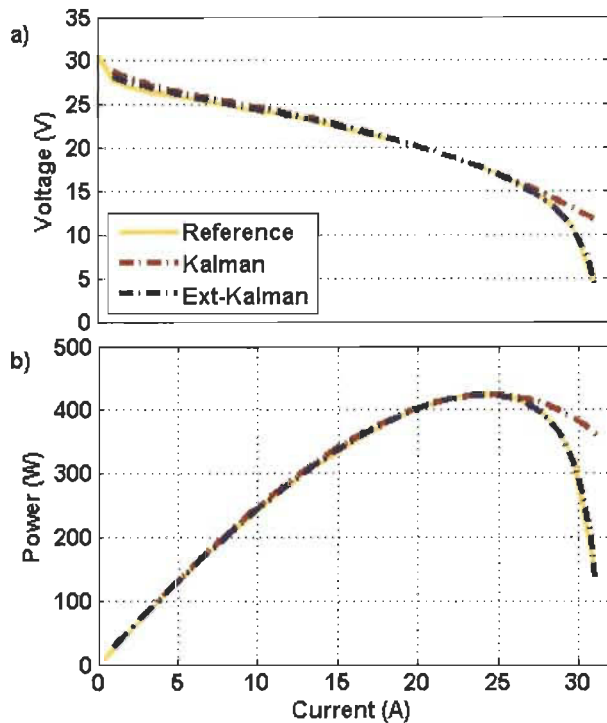 in this figure, there is a clear relationship between the starting point of concentration region and maximum power of the PEMFC. Obtaining this maximum power can be considered as an example of the information extraction step as shown in Fig. 4, and it can be easily integrated into a power split strategy for a global energy management design of FCVs.

Fig. 8 represents the resistor evolution of the Amphlett et al. model with different identification methods. As is seen in this figure, the estimated resistors by all the identification methods are almost in the same range as the conducted current interrupt test, shown in Fig. 4, although the results of EKF and Kalman filter are more accurate than RLS. It should be reminded that so far it has been observed that
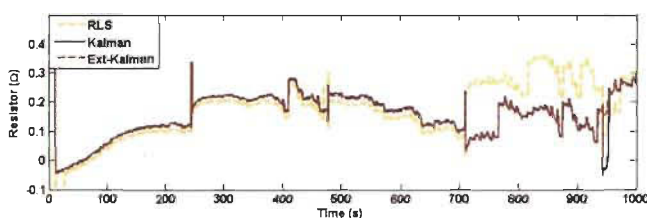
employment of the suggested identification techniques results in not only precise voltage estimation but also accurate polarization curve and resistor. To put the finishing touches to the validation of the relevance of the achieved results to the physical meaning of the PEMFC, the average values of the activation and concentration related parameters of the Amphlett et al. model are reported in Table 9 for all of the three identification algorithms. It should be noted that these parameters are not constant and constantly evolve over time. However, their evolution range is almost in the same range as Table 3.

4.4. Synopsis of the benchmark study

The benchmark study is composed of a two-stage analysis. In the first stage, the linear case comes under scrutiny, in which the performance of RLS and Kalman filter is examined for each of the models. It is inferred from the first stage of analysis that Amphlett et al. model relatively outperforms Squadrito et al. model. Concerning RLS and Kalman filter, it is observed that both of them give similar performances for Squadrito et al. model. However, Kalman filter performs to some extent better than RLS for the case of Amphlett et al. model. In the second stage, the performance of EKF for identifying linear and nonlinear parameters of the superior model in the first stage is investigated and compared with the results of the superior identification technique in the first stage. It is observed that EKF is capable of improving the estimation process to a certain extent. It should be noted that in the estimation process the accuracy of voltage estimation, polarization curve prediction, and resistor evolution is considered as the means of validation.

5. Conclusion

A thorough review of necessary steps from modeling to employing identification techniques for online energy management design of FCVs is carried out in this paper. In this respect, firstly, PEMFC modeling approaches are investigated in which semi-empirical models are singled out as one the most suitable models for online purposes. Secondly, PEMFC parameter identification methods, related to the last five years, are discussed and one of the categories which is highly appropriate for real time energy management design is selected for further analysis. Finally, an in-depth comparative study of three potential parameter identification techniques, RLS, Kalman filter, and EKF, is conducted by utilizing two renowned semi-empirical PEMFC models. The obtained results of the benchmark study indicate that in case of linear analysis, the integration of Kalman filter with the suggested model by Amphlett et al., which is a multi-input model, has a superior performance compared to other combinations. More importantly, it is observed that the proposed nonlinear identification method of this work, by means of EKF and Amphlett et al. model, results in the most precise polarization curve estimation for the utilized PEMFC.

The results of this paper suggest the following directions for future researches:

- Integrating the introduced model and identification technique into the energy management design of a FCV, since this work has paved the way in this direction.
- Integrating a thermal model in addition to the introduced voltage model of PEMFC to increase the accuracy of polarization curve

Fig. 8. Resistor evolution obtained by Amphlett et al. model.

prediction.

Acknowledgements

Nomenclature

ABSO	Artificial Bee Swarm Algorithm
AC-POA	Aging and Challenging P Systems Based Optimization Algorithm
ADE	Adaptive Differential Evolution
AIS	Artificial Immune System-Based
ANFIS	Adaptive neuro-fuzzy inference system
ANN	Artificial neural network
ARNA-GA	Adaptive RNA Genetic Algorithm
BIPOA	Bio-Inspired P Systems Based Optimization Algorithm
BMO	Bird Mating Optimizer
DE	Differential Evolution
EIS	Electrochemical impedance spectroscopy
EKF	Extended Kalman filter
EMS	Energy Management Strategy
FCV	Fuel Cell Vehicle
FLC	Fuzzy logic control
GA	Genetic Algorithm
GGHS	Grouping-Based Global Harmony Search
GWO	Grey Wolf Optimizer
HABC	Hybrid Artificial Bee Colony
HADE	Hybrid Adaptive Differential Evolution
IGHS	Innovative Global Harmony Search
MPPT	Maximum power point tracking
MPSO	Modified Particle Swarm Optimization
NARMAX	Nonlinear autoregressive moving average model with exogenous inputs
NARX	Nonlinear auto regressive with exogenous input
NOE	Nonlinear output error
PEMFC	Proton exchange membrane fuel cell
P&O	Perturbation and observation
PSO	Particle Swarm Optimization
Rank-MADE	Improved Multi-Strategy Adaptive Differential Evolution
RLS	Recursive least square
SOA	Seeker Optimization Algorithm
SRUKF	Square root unscented Kalman filter
STLBO	Simplified Teaching-Learning Based Optimization
SVM	Support vector machine
TLBO-DE	Teaching Learning Based Optimization-Differential Evolution
TRADE	Transferred adaptive differential evolution

Symbols

V_{FC}	Output voltage (V)
N	Number of cells
E_{Nernst}	Reversible cell potential (V)
V_{act}	Activation loss (V)
V_{ohmic}	Ohmic loss (V)
V_{con}	Concentration loss (V)
P_{max}	Maximum power (W)
η_{max}	Maximum efficiency point (%)
V_{min}	Minimum voltage (V)
I_{max}	Maximum current (A)
T	Stack temperature (K)
P_{H2}	Hydrogen partial pressure in anode side (kPa)
P_{O2}	Oxygen partial pressure in cathode side (kPa)
CO_2	Oxygen concentration (mol cm^{-3})

i	PEMFC operating current (A)
$R_{internal}$	Internal resistor (Ω)
B	Concentration loss related parametric coefficient (V)
J	Actual current density (A cm^{-2})
J_{max}	Maximum current density (A cm^{-2})
V_O	Reversible cell potential (V)
b	Tafel slope
t	Discrete time
$k(t)$	Kalman gain
$e(t)$	Error
$p(t)$	Covariance matrix
c	Nonnegative scalar
I	Identity matrix
$u(t)$	Measured output
$x(t)$	State vector
$\hat{x}(t)$	Estimate of the state vector
$\hat{x}(t)$	A priori estimate of the state vector
$F(t+1|t)$	Transition matrix
$w(t)$	Process noise
R_C	Contact resistance to electron conduction
$y(t)$	Output
$H(t)$	Measurement matrix
$v(t)$	Measurement noise
$P(t)$	Error covariance matrix
$Q(t)$	Process noise covariance matrix
$G(t)$	Kalman gain
$R(t)$	Measurement noise covariance matrix
$f(t, x(t))$	Nonlinear transition matrix function
$h(t, x(t))$	Nonlinear measurement matrix function

Greek symbols

$\xi_n (n = 1...4)$	Activation loss related semi-empirical coefficients
$\xi_n (n = 1...3)$	Ohmic loss related parametric coefficients
α	Semi-empirical parameter related to the diffusion mechanism
σ	Dimensionless number related to the water flooding phenomena
β	Inverse of the limiting current density (cm^2 A^{-1})
$\theta(t)$	Parameter vector
$\Gamma(t)$	Directional forgetting factor
$\phi(t)$	Regression vector
Ψ	Forgetting factor
λ	Water content of the membrane

References

[1] Z. Zoundi, CO2 emissions, renewable energy and the Environmental Kuznets Curve, a panel cointegration approach, Renew. Sustain. Energy Rev. 72 (2017) 1067–1075.

[2] D. Karamanev, V. Pupkevich, K. Penev, V. Glibin, J. Gohil, V. Vajihinejad, Biological conversion of hydrogen to electricity for energy storage, Energy 129 (2017) 237–245.

[3] H.S. Das, C.W. Tan, A.H.M. Yatim, Fuel cell hybrid electric vehicles: a review on power conditioning units and topologies, Renew. Sustain. Energy Rev. 76 (2017) 268–291.

[4] J. Larminie, A. Dicks, J. Larminie, A. Dicks, Introduction, Fuel Cell Systems Explained, John Wiley & Sons, Ltd., 2013, pp. 1–24.

[5] N. Sulaiman, M.A. Hannan, A. Mohamed, E.H. Majlan, W.R. Wan Daud, A review on energy management system for fuel cell hybrid electric vehicle: issues and challenges, Renew. Sustain. Energy Rev. 52 (2015) 802–814.

[6] L. Xu, J. Li, M. Ouyang, Energy flow modeling and real-time control design basing on mean values for maximizing driving mileage of a fuel cell bus, Int. J. Hydrogen Energy 40 (2015) 15052–15066.

[7] J. Bernard, S. Delprat, T.M. Guerra, F.N. Büchi, Fuel efficient power management strategy for fuel cell hybrid powertrains, Contr. Eng. Pract. 18 (2010) 408–417.

[8] D. Feroldi, M. Serra, J. Riera, Energy management strategies based on efficiency map for fuel cell hybrid vehicles, J. Power Sources 190 (2009) 387–401.

[9] K. Ettihir, L. Boulon, K. Agbossou, On-line proton exchange membrane fuel cell identification based on a rls algorithm, 5th International Conference on Fundamentals & Development of Fuel Cells (FDFC 2013), 2013.

[10] M. Seyedmahmoudian, A. Mohamadi, S. Kumary, A.M.T. Oo, A. Stojcevski, A comparative study on procedure and state of the art of conventional maximum power point tracking techniques for photovoltaic system, Int. J. Comput. Electr.

Eng. 6 (2014) 402–414.

[11] D. Sera, T. Kerekes, R. Teodorescu, F. Blaabjerg, Improved MPPT algorithms for rapidly changing environmental conditions, 2006 12th International Power Electronics and Motion Control Conference, 2006, pp. 1614–1619.

[12] F. Nandjou, J.P. Poirot-Crouvezier, M. Chandesris, J.F. Blachot, C. Bonnaud, Y. Bultel, Impact of heat and water management on proton exchange membrane fuel cells degradation in automotive application, J. Power Sources 326 (2016) 182–192.

[13] F. Martel, Y. Dubé, S. Kelouwani, J. Jaguemont, K. Agbossou, Long-term assessment of economic plug-in hybrid electric vehicle battery lifetime degradation management through near optimal fuel cell load sharing, J. Power Sources 318 (2016) 270–282.

[14] L. Boulon, K. Agbossou, D. Hissel, P. Sicard, A. Bouscayrol, M.-C. Péra, A macroscopic PEM fuel cell model including water phenomena for vehicle simulation, Renew. Energy 46 (2012) 81–91.

[15] T. Wilberforce, A. Alaswad, A. Palumbo, M. Dassisti, A.G. Olabi, Advances in stationary and portable fuel cell applications, Int. J. Hydrogen Energy 41 (2016) 16509–16522.

[16] GM, US Navy partner on fuel cell powered underwater vehicles, Fuel Cell. Bull. 2016 (2016) 4.

[17] T. Jahnke, G. Futter, A. Latz, T. Malkow, G. Papakonstantinou, G. Tsotridis, et al., Performance and degradation of proton exchange membrane fuel cells: state of the art in modeling from atomistic to system scale, J. Power Sources 304 (2016) 207–233.

[18] E. Lechartier, E. Laffly, M.-C. Péra, R. Gouriveau, D. Hissel, N. Zerhouni, Proton exchange membrane fuel cell behavioral model suitable for prognostics, Int. J. Hydrogen Energy 40 (2015) 8384–8397.

[19] R. Petrone, Z. Zheng, D. Hissel, M.C. Péra, C. Pianese, M. Sorrentino, et al., A review on model-based diagnosis methodologies for PEMFCs, Int. J. Hydrogen Energy 38 (2013) 7077–7091.

[20] C. Ziogou, S. Voutetakis, S. Papadopoulou, M.C. Georgiadis, Modeling, simulation and experimental validation of a PEM fuel cell system, Comput. Chem. Eng. 35 (2011) 1886–1900.

[21] A.A. Shah, K.H. Luo, T.R. Ralph, F.C. Walsh, Recent trends and developments in polymer electrolyte membrane fuel cell modelling, Electrochim. Acta 56 (2011) 3731–3757.

[22] D. Cheddie, N. Munroe, Review and comparison of approaches to proton exchange membrane fuel cell modeling, J. Power Sources 147 (2005) 72–84.

[23] A. Biyikoglu, Review of proton exchange membrane fuel cell models, Int. J. Hydrogen Energy 30 (2005) 1181–1212.

[24] A.D. Le, B. Zhou, A generalized numerical model for liquid water in a proton exchange membrane fuel cell with interdigitated design, J. Power Sources 193 (2009) 665–683.

[25] A.D. Le, B. Zhou, A general model of proton exchange membrane fuel cell, J. Power Sources 182 (2008) 197–222.

[26] V. Mishra, F. Yang, R. Pitchumani, Analysis and design of PEM fuel cells, J. Power Sources 141 (2005) 47–64.

[27] T. Berning, D.M. Lu, N. Djilali, Three-dimensional computational analysis of transport phenomena in a PEM fuel cell, J. Power Sources 106 (2002) 284–294.

[28] J.J. Baschuk, X. Li, Modelling of polymer electrolyte membrane fuel cells with variable degrees of water flooding, J. Power Sources 86 (2000) 181–196.

[29] A. Kheirandish, F. Motlagh, N. Shafiabady, M. Dahari, A. Khairi Abdul Wahab, Dynamic fuzzy cognitive network approach for modelling and control of PEM fuel cell for power electric bicycle system, Appl. Energy 202 (2017) 20–31.

[30] I.-S. Han, S.-K. Park, C.-B. Chung, Modeling and operation optimization of a proton exchange membrane fuel cell system for maximum efficiency, Energy Convers. Manag. 113 (2016) 52–65.

[31] M. Esfandyari, M.A. Fanaei, R. Gheshlaghi, M.A. Mahdavi, Neural network and neuro-fuzzy modeling to investigate the power density and Columbic efficiency of microbial fuel cell, J. Taiwan Inst. Chem. Eng. 58 (2016) 84–91.

[32] M. Shao, X.-J. Zhu, H.-F. Cao, H.-F. Shen, An artificial neural network ensemble method for fault diagnosis of proton exchange membrane fuel cell system, Energy 67 (2014) 268–275.

[33] A. Maghsoodi, E. Afshari, H. Ahmadikia, Optimization of geometric parameters for design a high-performance ejector in the proton exchange membrane fuel cell system using artificial neural network and genetic algorithm, Appl. Therm. Eng. 71 (2014) 410–418.

[34] J. Lobato, P. Cañizares, M.A. Rodrigo, C.-G. Piuleac, S. Curteanu, J.J. Linares, Direct and inverse neural networks modelling applied to study the influence on the gas diffusion layer properties on PBI-based PEM fuel cells, Int. J. Hydrogen Energy 35 (2010) 7889–7897.

[35] S. Jemei, D. Hissel, M.C. Pera, J.M. Kauffmann, Black-box modeling of proton exchange membrane fuel cell generators, IEEE 2002 28th Annual Conference of the Industrial Electronics Society, IECON 02, vol. 2, 2002, pp. 1474–1478.

[36] S. Tao, Y. Si-jia, C. Guang-yi, Z. Xin-jian, Modelling and control PEMFC using fuzzy neural networks, J. Zhejiang Univ. Sci. A 6 (2005) 1084–1089.

[37] M.A.R.S. Al-Baghdadi, Modelling of proton exchange membrane fuel cell performance based on semi-empirical equations, Renew. Energy 30 (2005) 1587–1599.

[38] C.N. Maxoulis, D.N. Tsinoglou, G.C. Koltsakis, Modeling of automotive fuel cell operation in driving cycles, Energy Convers. Manag. 45 (2004) 559–573.

[39] L. Pisani, G. Murgia, M. Valentini, B. D'Aguanno, A new semi-empirical approach to performance curves of polymer electrolyte fuel cells, J. Power Sources 108 (2002) 192–203.

[40] G. Maggio, V. Recupero, L. Pino, Modeling polymer electrolyte fuel cells: an innovative approach, J. Power Sources 101 (2001) 275–286.

[41] R.F. Mann, J.C. Amphlett, M.A.I. Hooper, H.M. Jensen, B.A. Peppley,

P.R. Roberge, Development and application of a generalised steady-state electrochemical model for a PEM fuel cell, J. Power Sources 86 (2000) 173–180.

[42] G. Squadrito, G. Maggio, E. Passalacqua, F. Lufrano, A. Patti, An empirical equation for polymer electrolyte fuel cell (PEFC) behaviour, J. Appl. Electrochem. 29 (1999) 1449–1455.

[43] J.C. Amphlett, R.M. Baumert, R.F. Mann, B.A. Peppley, P.R. Roberge, T.J. Harris, Performance modeling of the Ballard Mark IV solid polymer electrolyte fuel cell: II. Empirical model development, J. Electrochem. Soc. 142 (1995) 9–15.

[44] A. Askarzadeh, A. Rezazadeh, A new artificial bee swarm algorithm for optimization of proton exchange membrane fuel cell model parameters, J. Zhejiang Univ. Sci. C 12 (2011) 638–646.

[45] S. Yang, R. Chellali, X. Lu, L. Li, C. Bo, Modeling and optimization for proton exchange membrane fuel cell stack using aging and challenging P systems based optimization algorithm, 109 (2016) 569–577.

[46] A. Askarzadeh, A. Rezazadeh, Artificial immune system-based parameter extraction of proton exchange membrane fuel cell, Int. J. Electr. Power Energy Syst. 33 (2011) 933–938.

[47] L. Zhang, N. Wang, An adaptive RNA genetic algorithm for modeling of proton exchange membrane fuel cells, Int. J. Hydrogen Energy 38 (2013) 219–228.

[48] S. Yang, N. Wang, A novel P systems based optimization algorithm for parameter estimation of proton exchange membrane fuel cell model, Int. J. Hydrogen Energy 37 (2012) 8465–8476.

[49] U.K. Chakraborty, T.E. Abbott, S.K. Das, PEM fuel cell modeling using differential evolution, Energy 40 (2012) 387–399.

[50] W. Zhang, N. Wang, S. Yang, Hybrid artificial bee colony algorithm for parameter estimation of proton exchange membrane fuel cell, Int. J. Hydrogen Energy 38 (2013) 5796–5806.

[51] Z. Sun, N. Wang, Y. Bi, D. Srinivasan, Parameter identification of PEMFC model based on hybrid adaptive differential evolution algorithm, Energy 90 (2015) 1334–1341.

[52] A. Askarzadeh, A. Rezazadeh, Optimization of PEMFC model parameters with a modified particle swarm optimization, Int. J. Energy Res. 35 (2011) 1258–1265.

[53] K. Priya, T. Sudhakar Babu, K. Balasubramanian, K. Sathish Kumar, N. Rajasekar, A novel approach for fuel cell parameter estimation using simple Genetic Algorithm, Sustain. Energy Technol. Assess. 12 (2015) 46–52.

[54] Q. Niu, H. Zhang, K. Li, An improved TLBO with elite strategy for parameters identification of PEM fuel cell and solar cell models, Int. J. Hydrogen Energy 39 (2014) 3837–3854.

[55] O.E. Turgut, M.T. Coban, Optimal proton exchange membrane fuel cell modelling based on hybrid Teaching Learning Based Optimization – Differential Evolution algorithm, Ain Shams Eng. J. 7 (2016) 347–360.

[56] N. Rajasekar, B. Jacob, K. Balasubramanian, K. Priya, K. Sangeetha, T. Sudhakar Babu, Comparative study of PEM fuel cell parameter extraction using Genetic Algorithm, Ain Shams Eng. J. 6 (2015) 1187–1194.

[57] B.H. Juan, Q.Z. Dong, X.S. Yuan, L.B. Yang, S. Liang, Research on PEMFC fractional model based on an improved genetic algorithm, 2015 34th Chinese Control Conference (CCC), 2015, pp. 2028–2032.

[58] A. Askarzadeh, A. Rezazadeh, A new heuristic optimization algorithm for modeling of proton exchange membrane fuel cell: bird mating optimizer, Int. J. Energy Res. 37 (2013) 1196–1204.

[59] W. Gong, X. Yan, X. Liu, Z. Cai, Parameter extraction of different fuel cell models with transferred adaptive differential evolution, Energy 86 (2015) 139–151.

[60] C. Dai, W. Chen, Z. Cheng, Q. Li, Z. Jiang, J. Jia, Seeker optimization algorithm for global optimization: a case study on optimal modelling of proton exchange membrane fuel cell (PEMFC), J. Electr. Power Energy Syst. 33 (2011) 369–376.

[61] J. Cheng, G. Zhang, Parameter fitting of PEMFC models based on adaptive differential evolution, Int. J. Electr. Power Energy Syst. 62 (2014) 189–198.

[62] M. Ali, M.A. El-Hameed, M.A. Farahat, Effective parameters' identification for polymer electrolyte membrane fuel cell models using Grey Wolf optimizer, Renew. Energy 111 (01 Oct 2017) 455–462.

[63] A. Askarzadeh, A. Rezazadeh, An innovative global harmony search algorithm for parameter identification of a PEM fuel cell model, IEEE Trans. Ind. Electron. 59 (2012) 3473–3480.

[64] A. Askarzadeh, A. Rezazadeh, A grouping-based global harmony search algorithm for modeling of proton exchange membrane fuel cell, Int. J. Hydrogen Energy 36 (2011) 5047–5053.

[65] W. Gong, Z. Cai, Parameter optimization of PEMFC model with improved multi-strategy adaptive differential evolution, Eng. Appl. Artif. Intell. 27 (2014) 28–40.

[66] R. Chibante, D. Campos, An experimentally optimized PEM fuel cell model using PSO algorithm, 2010 IEEE International Symposium on Industrial Electronics, 2010, pp. 2281–2285.

[67] M. Guarnieri, E. Negro, V. Di Noto, P. Alotto, A selective hybrid stochastic strategy for fuel-cell multi-parameter identification, J. Power Sources 332 (2016) 249–264.

[68] R. Salim, M. Nabag, H. Noura, A. Fardoun, The parameter identification of the Nexa 1.2 kW PEMFCs model using particle swarm optimization, Renew. Energy 82 (2015) 26–34.

[69] C. Restrepo, T. Konjedic, A. Garces, J. Calvente, R. Giral, Identification of a proton-exchange membrane fuel Cell's model parameters by means of an evolution strategy, IEEE Trans. Ind. Inf. 11 (2015) 548–559.

[70] A.K. Al-Othman, N.A. Ahmed, F.S. Al-Fares, M.E. AlSharidah, Parameter identification of PEM fuel cell using quantum-based optimization method, Arabian J. Sci. Eng. 40 (2015) 2619–2628.

[71] M. Sedighizadeh, M.M. Mahmoodi, M. Soltanian, Parameter identification of proton exchange membrane fuel cell using a Hybrid Big Bang-Big Crunch optimization, 2014 5th Conference on Thermal Power Plants (CTPP), 2014, pp. 35–39.

[72] P. Alotto, M. Guarnieri, Stochastic methods for parameter estimation of

multiphysics models of fuel cells, IEEE Trans. Magn. 50 (2014) 701–704.

[73] Q. Li, W. Chen, Y. Wang, S. Liu, J. Jia, Parameter identification for PEM fuel-cell mechanism model based on effective informed adaptive particle swarm optimization. IEEE Trans. Ind. Electron. 58 (2011) 2410–2419.

[74] S.M. Rezaei Niya, M. Hoorfar, Study of proton exchange membrane fuel cells using electrochemical impedance spectroscopy technique – a review, J. Power Sources 240 (2013) 281–293.

[75] M.A. Taleb, O. Béthoux, E. Godoy, Identification of a PEMFC fractional order model, Int. J. Hydrogen Energy 42 (2017) 1499–1509.

[76] A. Saadi, M. Becherif, D. Hissel, H.S. Ramadan, Dynamic modeling and experimental analysis of PEMFCs: a comparative study, Int. J. Hydrogen Energy 42 (2017) 1544–1557.

[77] M.A. Taleb, E. Godoy, O. Bethoux, Frequential identification of a proton exchange membrane fuel cell (PEMFC) fractional order model, IECON 2014-40th Annual Conference of the IEEE Industrial Electronics Society, 2014, pp. 5647–5653.

[78] M. Kheirmand, A. Asnafi, Analytic parameter identification of proton exchange membrane fuel cell catalyst layer using electrochemical impedance spectroscopy, Int. J. Hydrogen Energy 36 (2011) 13266–13271.

[79] M.U. Iftikhar, D. Riu, F. Druart, S. Rosini, Y. Bultel, N. Retière, Dynamic modeling of proton exchange membrane fuel cell using non-integer derivatives, J. Power Sources 160 (2006) 1170–1182.

[80] A. Kheirandish, F. Motlagh, N. Shafiabady, M. Dahari, Dynamic modelling of PEM fuel cell of power electric bicycle system, Int. J. Hydrogen Energy 41 (2016) 9585–9594.

[81] F. d. C. Lopes, E.H. Watanabe, L.G.B. Rolim, Analysis of the time-varying behavior of a PEM fuel cell stack and dynamical modeling by recurrent neural networks, 2013 Brazilian Power Electronics Conference, 2013, pp. 601–608.

[82] S.-J. Cheng, J.-M. Miao, S.-J. Wu, Use of metamodeling optimal approach promotes the performance of proton exchange membrane fuel cell (PEMFC), Appl. Energy 105 (2013) 161–169.

[83] P. Li, J. Chen, T. Cai, G. Liu, P. Li, On-line identification of fuel cell model with variable neural network, Proceedings of the 29th Chinese Control Conference, 2010, pp. 1417–1421.

[84] P. Hu, G.-Y. Cao, X.-J. Zhu, J. Li, Modeling of a proton exchange membrane fuel cell based on the hybrid particle swarm optimization with Levenberg–Marquardt neural network, Simulat. Model. Pract. Theor. 18 (2010) 574–588.

[85] L.P. Fagundes, H.J. Avelar, F.D. Fagundes, M. J. d. Cunha, F. Vincenzi, Improvements in identification of fuel cell temperature model, 2015 IEEE 13th Brazilian Power Electronics Conference and 1st Southern Power Electronics Conference (COBEP/SPEC), 2015, pp. 1–5.

[86] S.-J. Cheng, J.-J. Liu, Nonlinear modeling and identification of proton exchange membrane fuel cell (PEMFC), Int. J. Hydrogen Energy 40 (2015) 9452–9461.

[87] D. Feroldi, J.C. Gomez, V. Roda, Identification of PEM fuel cells based on support vector regression and orthonormal bases, 2016 IEEE International Symposium on Intelligent Control (ISIC), 2016. pp. 1–6.

[88] Z.-D. Zhong, X.-J. Zhu, G.-Y. Cao, Modeling a PEMFC by a support vector machine, J. Power Sources 160 (2006) 293–298.

[89] K.K. Justesen, S.J. Andreasen, S.L. Sahlin, Modeling of a HTPEM fuel cell using adaptive neuro-fuzzy inference systems, Int. J. Hydrogen Energy 40 (2015) 16814–16819.

[90] N.E. Benchouia, A. Derghal, B. Mahmah, B. Madi, L. Khochemane, E. Hadjadj Aoul, An adaptive fuzzy logic controller (AFLC) for PEMFC fuel cell, Int. J. Hydrogen Energy 40 (2015) 13806–13819.

[91] V. Boscaino, R. Rizzo, R. Miceli, G. Ricco Galluzzo, G. Capponi, Comparison of models of fuel cells based on experimental data for the design of power electronics

systems, IET Renew. Power Gener. 9 (2015) 660–668.

[92] J.P. Torreglosa, F. Jurado, P. García, L.M. Fernández, PEM fuel cell modeling using system identification methods for urban transportation applications, Int. J. Hydrogen Energy 36 (2011) 7628–7640.

[93] R.N. Methekar, S.C. Patwardhan, R.D. Gudi, V. Prasad, Adaptive peak seeking control of a proton exchange membrane fuel cell, J. Process Contr. 20 (2010) 73–82.

[94] W. Bamberger, R. Isermann, Adaptive on-line steady-state optimization of slow dynamic processes, Automatica 14 (1978) 223–230.

[95] P.S. Bedi, R.N. Methekar, S.C. Patwardhan, V. Prasad, R.D. Gudi, Nonlinear internal model control of PEM fuel cell, IFAC Proc. Vol. 40 (2007) 101–106.

[96] K. Ettihir, L. Boulon, K. Agbossou, Energy management strategy for a fuel cell hybrid vehicle based on maximum efficiency and maximum power identification, IET Electr. Syst. Transp. 6 (2016) 261–268.

[97] K. Ettihir, L. Boulon, K. Agbossou, Optimization-based energy management strategy for a fuel cell/battery hybrid power system, Appl. Energy 163 (2016) 142–153.

[98] K. Ettihir, L. Boulon, M. Becherif, K. Agbossou, H.S. Ramadan, Online identification of semi-empirical model parameters for PEMFCs, Int. J. Hydrogen Energy 39 (2014) 21165–21176.

[99] K. Ettihir, M. Higuita Cano, L. Boulon, K. Agbossou, Design of an adaptive EMS for fuel cell vehicles, Int. J. Hydrogen Energy 42 (2017) 1481–1489.

[100] J.A. Salva, A. Iranzo, F. Rosa, E. Tapia, E. Lopez, F. Isorna, Optimization of a PEM fuel cell operating conditions: obtaining the maximum performance polarization curve, Int. J. Hydrogen Energy 41 (2016) 19713–19723.

[101] C. Hähnel, V. Aul, J. Horn, Online identification of an electric PEMFC model for power control by NMPC, 2015 20th International Conference on Methods and Models in Automation and Robotics (MMAR), 2015, pp. 133–138.

[102] S. Kelouwani, K. Adegnon, K. Agbossou, Y. Dube, Online system identification and adaptive control for PEM fuel cell maximum efficiency tracking, IEEE Trans. Energy Convers. 27 (2012) 580–592.

[103] A. Saadi, M. Becherif, A. Aboubou, M.Y. Ayad, Comparison of proton exchange membrane fuel cell static models, Renew. Energy 56 (2013) 64–71.

[104] W.-Y. Chang, Estimating equivalent circuit parameters of proton exchange membrane fuel cell using the current change method, Int. J. Electr. Power Energy Syst. 53 (2013) 584–591.

[105] V. Boscaino, R. Miceli, G. Capponi, MATLAB-based simulator of a 5 kW fuel cell for power electronics design, Int. J. Hydrogen Energy 38 (2013) 7924–7934.

[106] B. Carnes, N. Djilali, Systematic parameter estimation for PEM fuel cell models, J. Power Sources 144 (2005) 83–93.

[107] J.M. Correa, F.A. Farret, V.A. Popov, M.G. Simoes, Sensitivity analysis of the modeling parameters used in Simulation of proton exchange membrane fuel cells, IEEE Trans. Energy Convers. 20 (2005) 211–218.

[108] A. Husar, S. Strahl, J. Riera, Experimental characterization methodology for the identification of voltage losses of PEMFC: applied to an open cathode stack, Int. J. Hydrogen Energy 37 (2012) 7309–7315.

[109] J. Wu, X. Yuan, H. Wang, M. Blanco, J. Martin, J. Zhang, Diagnostic tools in PEM fuel cell research: Part I Electrochemical techniques, Int. J. Hydrogen Energy 33 (2008) 1735–1746.

[110] K.R. Cooper, M. Smith, Electrical test methods for on-line fuel cell ohmic resistance measurement, J. Power Sources 160 (2006) 1088–1095.

[111] T. Mennola, M. Mikkola, M. Noponen, T. Hottinen, P. Lund, Measurement of ohmic voltage losses in individual cells of a PEMFC stack, J. Power Sources 112 (2002) 261–272.

3.3 Conclusion

As one of the objectives of this thesis is to deal with the uncertainties arising from the performance drifts of a PEMFC stack while designing an EMS, this chapter mainly investigates a suitable model and an online identification technique for estimating the present-state characteristics of the stack.

In this respect, a thorough review of necessary steps from modeling to employing identification techniques for online energy management design of FCHEVs is carried out in this chapter. An in-depth comparative study of three potential parameter identification techniques, RLS, Kalman filter, and EKF, is conducted by utilizing two renowned semi-empirical PEMFC models. The obtained results of the benchmark study indicate that in case of linear analysis, the integration of Kalman filter with the suggested model by Amphlett et. al, which is a multi-input model, has a superior performance compared to other combinations. More importantly, it is observed that the proposed nonlinear identification method of this work, by means of EKF and Amphlett et. al model, results in the most precise polarization curve estimation for the utilized PEMFC.

The obtained results from this chapter confirm the effectiveness of the studied online modeling procedure. However, as mentioned in the presented paper, the customization and initialization of the recursive filters have an important role in their accuracy. In this regard, next chapter will focus on the preparation of these filters for achieving precise estimations.

Chapter 4 - Customization of recursive filters for PEMFC online parameters estimation

4.1 Introduction

The conducted benchmark problem in Chapter 3 revealed that the recursive filters are very suitable for online parameters estimation of a PEMFC stack and KF was selected as one of the most appropriate filters in this regard. However, one issue that has not been discussed is the initialization of the PEMFC model parameters and customization of the KF variables. Inappropriate initialization of the model parameters might lead to misinterpretation of the physical phenomena. Moreover, it can increase the necessary time to obtain high quality prediction of the characteristics of the interest. On the other hand, the improper customization of process and measurement noise covariance matrices can decrease the accuracy of the FC output voltage estimation. Furthermore, once these matrices are disorganized, they keep being disorganized and will never be updated in KF process. This disorganization might prevent the KF from having its best performance

In this respect, this chapter aims at proposing a method for initializing the previously-discussed model parameters and recursive filters. One of the most common methods to perform this initialization and customization is to tune the necessary parameters offline by metaheuristic optimization algorithms before employing KF or other recursive filters in the online parameter's estimation process. Metaheuristic optimization algorithms have been the focus of many studies due to their robustness, flexibility, and parallel computing for extracting the linear and nonlinear parameters of a PEMFC model. These methods are utilized as an alternative to conventional derivative-based techniques.

So far, no optimization algorithm has been proved to be the most proper and accordingly there is always this necessity to evaluate the performance of any newly developed optimization methods for exploring the optimal solution of a specific problem under attention. In this regard, this chapter first goes through the details of tuning the parameters of a PEMFC model offline using metaheuristic algorithms by presenting an article entitled ''Benchmark of Proton Exchange Membrane Fuel Cell Parameters Extraction with Metaheuristic Optimization Algorithms''. This article proposes a trustworthy optimization algorithm for the offline initialization and customization. Subsequently, the effect of initializing the parameters of the PEMFC model and KF variables in the online estimation process is thoroughly investigated by using the selected algorithm in the article. Finally, a conclusion is given.

4.2 Article 3: Benchmark of proton exchange membrane fuel cell parameters extraction with metaheuristic optimization algorithms

Authors: M. Kandidayeni, A. Macias, A. Khalatbarisoltani, L. Boulon, and S. Kelouwani

4.2.1 Methodology

This chapter utilizes three algorithms, namely shuffled frog-leaping algorithm (SFLA), firefly optimization algorithm (FOA), and imperialist competitive algorithm (ICA) for the PEMFC model calibration. In this regard, firstly, the algorithms are employed to find the parameters of a benchmark PEMFC model by minimizing the sum of squared errors (SSE) between the measured and estimated voltage for two available case studies in the literature. After conducting 100 independent runs, the algorithms are compared in terms of the best and the worst SSEs, the variance, and standard deviation. The most performant algorithm in terms of precision and repeatability is selected based on these analyses and, finally, it will be used to calibrate the model for a new case study (Horizon 500-W PEMFC) with variable temperature. Figure 4.1 represents the general process of utilizing an optimization algorithm for the parameter extraction of a PEMFC.
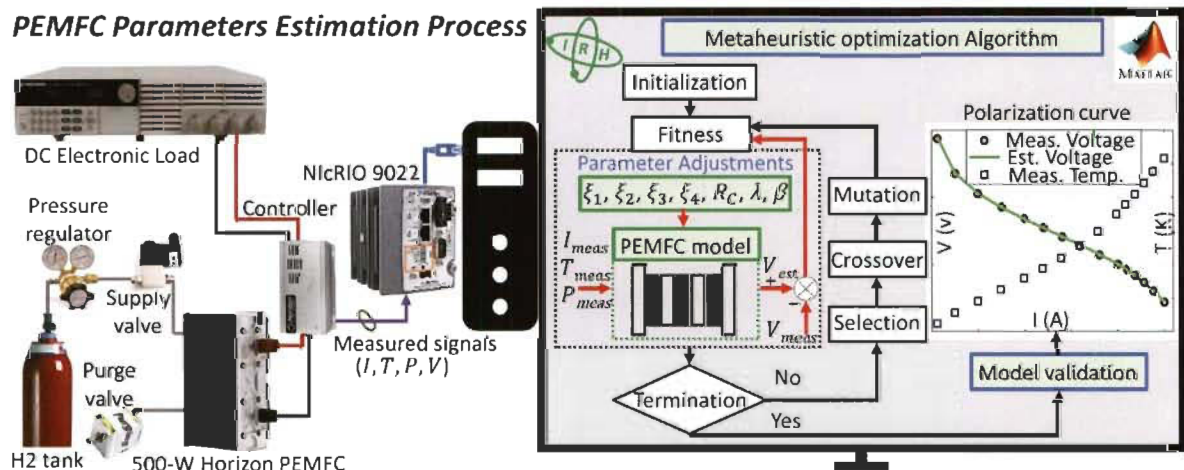

Figure 4.1   The process of PEMFC model parameters estimation and validation by using metaheuristic optimization algorithms.

4.2.2 Synopsis of the results analysis

The results obtained from the first two case studies indicate that SFLA marginally outperforms ICA and FOA regarding the best SSE while it performs 20% and twofold better than other algorithms concerning the worst SSE. Furthermore, the obtained variance and standard deviation by SFLA are much less than the other algorithms showing the precision and repeatability of this algorithm. It should be noted that the performance of the three optimization algorithms of this paper has been compared to other available optimizers in the literature and realized that the slap swarm optimizer (SSO) performs batter than ICA and FOA while SFLA has the best performance among all of them. In this respect, SFLA algorithm is selected to be used for the optimization of the 500-W Horizon PEMFC, which is a new case study introduced in this work. It should be noted that this selection has been made based on the defined comparison criteria and utilized controlling parameters and it does not mean that the other two introduced algorithms are not suitable for parameters estimation of a PEMFC model. In fact, all the three algorithms are able to predict the PEMFC polarization curve with good accuracy. However, SFLA shows more robustness than the others do in the investigated cases.

Regarding the third case study, the data have been collected from an experimental test bench developed in Hydrogen Research Institute of University of Quebec in Trois-Rivieres. Figure 4.2a shows the obtained results by the SFLA to extract the parameters of the PEMFC model for predicting the polarization curve. The minimization trend of the fitness function is represented in Figure 4.2b. It can be seen that the stable value is achieved after almost 10 iterations. The comparison of the estimated and reference curve v shows the satisfying performance of SFLA.
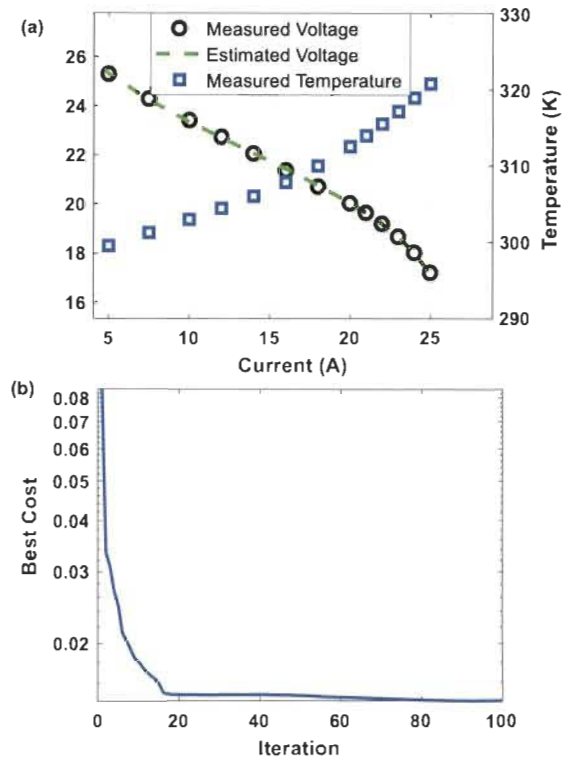
Figure 4.2   500-W Horizon PEMFC case study: a) estimated polarization curve by SFLA, b) fitness function (SSE) minimization trend comparison

Contents lists available at ScienceDirect

Energy

journal homepage: www.elsevier.com/locate/energy

Benchmark of proton exchange membrane fuel cell parameters extraction with metaheuristic optimization algorithms

M. Kandidayeni [a, b, ﹡], A. Macias [a, b], A. Khalatbarisoltani [a, b], L. Boulon [a, b], S. Kelouwani [c]

[a] Hydrogen Research Institute, Department of Electrical Engineering and Computer Science, Université du Québec à Trois-Rivières, Trois-Rivières, Québec, G9A 5H7, Canada
[b] Canada Research Chair in Energy Sources for the Vehicles of the Future, Canada
[c] Hydrogen Research Institute, Department of Mechanical Engineering, Université du Québec à Trois-Rivières, Trois-Rivières, Québec, G9A 5H7, Canada

A R T I C L E   I N F O

A B S T R A C T

Proton exchange membrane fuel cell (PEMFC) models are multivariate with different nonlinear elements which should be identified accurately to assure dependable modeling. Metaheuristic algorithms are perfect candidates for this purpose since they do an informed search for finding the parameters. This paper utilizes three algorithms, namely shuffled frog-leaping algorithm (SFLA), firefly optimization algorithm (FOA), and imperialist competitive algorithm (ICA) for the PEMFC model calibration. In this regard, firstly, the algorithms are employed to find the parameters of a benchmark PEMFC model by minimizing the sum of squared errors (SSE) between the measured and estimated voltage for two available case studies in the literature. After conducting 100 independent runs, the algorithms are compared in terms of the best and the worst SSEs, the variance, and standard deviation. This comparison indicates that SFLA marginally outperforms ICA and FOA regarding the best SSE in both cases while it performs 20% and twofold better than other algorithms concerning the worst SSE. Furthermore, the obtained variance and standard deviation by SFLA are much less than the other algorithms showing the precision and repeatability of this method. Finally, SFLA is used to calibrate the model for a new case study (Horizon 500-W PEMFC) with variable temperature.

© 2019 Elsevier Ltd. All rights reserved.

1. Introduction

Exhaustion of fossil fuels, owing to the growth of energy consumption, and the gained public insights into environmental protection have turned the attentions of both individual and governmental sectors to alternative sources of energy [1]. As a result, many researchers have been engrossed by greener energy sources such as wind, solar, waves, and so forth [2]. The major problems with the stated sources are their unforeseeable nature and reliance on climate conditions. These pitfalls, on the other hand, have marked the paramount need of energy storage. Hydrogen, which is the trending topic nowadays, can operate as an energy storage medium to efficiently store renewable energy until an energy conversion device turns it into electricity [3]. Fuel cell

(FC) is one of the most significant conversion devices, which usually produces electricity through a chemical reaction between hydrogen and oxygen. Among different kinds of FCs, proton exchange membrane FC (PEMFC) has been used in a number of areas such as automotive, on-site generation, and portable electronic devices because of its low operating temperature, high power density, and solid electrolyte [4,5].

One of the key issues in the technical maturity of PEMFCs is their mathematical modeling. Modeling can disclose more details about the operation of this device resulting in a better appreciation of the performance enhancement [6,7]. One of the most important challenges through the process of modeling a PEMFC is the precise estimation of its characteristics [8]. This difficulty is mainly owing to the fact that PEMFC is a multiphysics system and its parameters are strictly related to the operating conditions [9—11]. Although there are many approaches for the PEMFC modeling, such as mechanistic and black-box [12], mathematical modeling based on semi-empirical equations have been given a lot of attentions due to their capabilities to mimic the behavior of this device in variant operating conditions [13]. Unlike the mechanistic models, which

﹡ Corresponding author. Hydrogen Research Institute, Department of Electrical Engineering and Computer Science, Université du Québec à Trois-Rivières, Trois-Rivières, Québec, G9A 5H7, Canada.
E-mail address: mohsen.kandi.dayeni@uqtr.ca (M. Kandidayeni).

offer deep apprehension of the underlying phenomena, and black box models, which provide shallow insight into heat and mass phenomena, semi-empirical models attempt to illuminate the electrochemical behavior of a FC by imitating the polarization curve [14]. So far, several semi-empirical models have been proposed to predict the polarization curve [15,16]. Among them, the model introduced by Amphlett et al. [17], which is a semi-empirical model supported by a mechanistic background, has been used in many studies and its parameters estimation has become a benchmark problem in this field [18]. A number of similar suggested models in the literature can result in a satisfactory prediction for a particular FC system. However, few of them have had these wide applications. The topical issue related to this model and modeling approach is the inaccessibility of the exact parameters. Hence, the proper calibration of model parameters has a vital role in achieving accurate output. Several methods, such as artificial neural networks, adaptive filters, and experimental electrochemical approaches, have been used for modeling and parameter extraction of PEMFCs as described completely in Ref. [19]. Among them, metaheuristic optimization algorithms have been the focus of many studies for offline identification due to their robustness, flexibility, and parallel computing for extracting the linear and nonlinear parameters of a PEMFC model [20–22]. These methods are utilized as an alternative to conventional derivative-based techniques. They are quite appropriate for global searches due to their potential at exploration and discovering promising domains in the defined search space at a particular time. The majority of the metaheuristic optimization techniques are nature-inspired. Although they offer near optimal rather than optimal solutions, they do not need the cost function derivatives and/or constraints and employ deterministic rules to solve nonlinear and nonconvex problems [23]. Another worth noting applicability of parameter extraction by metaheuristic algorithms is that the obtained set of parameters by these algorithms can be used as initial values for online adaptive filter based parameter identification to enhance the performance of the filter [19,24]. This stems from the fact that the performance of adaptive filters is very sensitive to the initialization stage, and they do not have the same exploration capability as metaheuristic algorithms to find the suitable parameters [25]. A comprehensive review of the utilized optimization algorithms in the parameter estimation of semi-empirical PEMFC models can be found in Ref. [26]. Table 1 lists some of the recently utilized algorithms along with the PEMFC case studies.

The literature study evidently demonstrates the application and significance of metaheuristic algorithms in the PEMFC parameter estimation problem. So far, no optimization algorithm has been proved to be the most proper and accordingly there is always this necessity to evaluate the performance of any newly developed optimization methods for exploring the optimal solution of a specific problem under attention.

This paper aims at investigating the performance of three metaheuristic algorithms, namely shuffled frog-leaping algorithm (SFLA), firefly optimization algorithm (FOA), and imperialist competitive algorithm (ICA), in the parameters estimation benchmark of the PEMFC model proposed by Amphlett et al. These algorithms have been used in several engineering problems. However, to the best of the authors' knowledge, this is the first attempt to identify the parameters of a FC system by means of the mentioned algorithms. Herein, the stated algorithms are exploited to estimate the Amphlett's model parameters for the experimental data of NedStack PS6 (6 kW), and BCS 500-W PEM generator, which are available in the literature, and Horizon 500-W open cathode PEMFC, which is accessible on a developed test bench for this work. The performance of the algorithms has been compared with one another for a defined fitness function over 100 independent runs to

investigate the accuracy and probability of repeating the satisfying solution. It should be noted that the introduced algorithms performance has been also compared with very recent used optimizers in PEMFC modeling, such as SSO, GHO, and GWO, for the common case studies.

The remainder of this paper is structured as follows. A general description of the benchmark PEFMC modeling problem is provided in section 2. The explanation of algorithms is presented in section 3. Section 4 deals with the investigation of the obtained results regarding the comparison of the algorithms and the PEMFC case studies. Finally, the conclusion is given in section 5.

2. Mathematical PEMFC stack modeling

The steady-state behavior of the PEMFC has been modeled by means of an electrochemical model proposed by Amphlett et al. in Refs. [17,44]. In this model, the output voltage of the PEMFC (V_{FC}) is considered as the sum of cell reversible voltage (E_{Nernst}) and three voltage losses, namely activation (V_{Act}), ohmic (V_{Ohmic}), and concentration (V_{Con}). This model is for a number of cells (N_{cell}) connected in series and considers the same behavior for all the cells. The general formulation of the utilized electrochemical model is as follows:

$$V_{FC} = N_{cell}(E_{Nernst} - V_{Act} - V_{Ohmic} - V_{Con}) \tag{1}$$

where the Nernst equation, which calculates the thermodynamic potential, is formulated based on [28,44]:

$$E_{Nernst} = 1.229 - 0.85 \times 10^{-3}(T_{stack} - 298.15) + 4.3085$$
$$\times 10^{-5}T_{stack}[\ln(P_{H2}) + 0.5\ln(P_{O2})] \tag{2}$$

where T_{stack} is the stack temperature (K), P_{H2} is the hydrogen partial pressure in anode side (atm), and P_{O2} is the oxygen partial pressure in cathode side (atm).

The reactant partial pressures in the inlet flow channels will vary with the humidification level of the inlet streams, and the consumption rates of oxygen and hydrogen [17,44]. Under such basis, if the utilized reactants are air and Hydrogen, which is the case in this work and the majority of the utilized PEMFC systems, P_{O2} can be calculated as [27–29,33,34,38]:

$$P_{O2} = P_C - \left(RH_C P_{H_2O}^{sat}\right) - \frac{0.79}{0.21}P_{O2} \, exp\left(\frac{0.291(I_{FC}/A)}{T_{stack}^{0.832}}\right) \text{ (air and } H_2) \tag{3}$$

If the reactants are Oxygen and Hydrogen, then P_{O2} is obtained as [27–29,33,34,38]:

$$P_{O2} = RH_C \, P_{H_2O}^{sat} \left[\left(exp\left(\frac{4.192(I_{FC}/A)}{T_{stack}^{1.334}}\right) \times \frac{RH_C \, P_{H_2O}^{sat}}{P_C} \right)^{-1} \right.$$
$$\left. - 1 \right] \text{ (O}_2 \text{ and } H_2) \tag{4}$$

In both cases, the P_{H2} is given by Refs. [27–29,33,34,38]:

$$P_{H2} = 0.5 \, RH_a P_{H_2O}^{sat} \left[\left(exp\left(\frac{1.635(I_{FC}/A)}{T_{stack}^{1.334}}\right) \times \frac{RH_C P_{H_2O}^{sat}}{P_a} \right)^{-1} - 1 \right] \tag{5}$$

where RH_C and RH_a are relative humidity of vapor in electrodes, P_C and P_a are the cathode and anode inlet partial pressures (atm), I_{FC} is

Table 1
The studied metaheuristic algorithms for PEMFC parameters extraction.

Optimization Algorithm	Case study	Year	Reference
Eagle strategy	A PEMFC stack [27]	2019	[28]
Cuckoo search algorithm with explosion operator (CS-EO)	A PEMFC stack [27]	2019	[29]
	SR-12 500 W		
	Ballard Mark V (1 cell)		
	BCS 500 W		
Slap swarm optimizer (SSO)	NedStack PS6	2018	[30]
	BCS 500 W		
Grasshopper optimization (GHO)	Ballard Mark V (1 cell)	2018	[31]
	SR-12 500 W		
	250-W PEMFC		
Grey wolf optimizer (GWO)	250-W PEMFC	2017	[32]
	Ballard V 5 kW		
	SR-12 500 W		
	BCS 500 W		
	Temasek 1 kW		
Aging and challenging P systems based optimization algorithm (AC-POA)	250-W PEMFC	2016	[33]
Hybrid teaching learning based optimization – differential evolution (TLBO—DE)	250-W PEMFC	2016	[34]
Generalized reduced gradient (GRG)	A single cell	2016	[35]
Hybrid adaptive differential evolution algorithm (HADE)	250-W PEMFC	2015	[36]
Evolutionary strategy	1.2-kW Nexa	2015	[37]
Genetic algorithm (GA)	250-W PEMFC	2015	[38,39]
Transferred adaptive differential evolution (TRADE)	Ballard V 5 kW	2015	[40]
	SR-12 500 W		
	BCS 500 W		
	Temasek 1 kW		
	WNS-FC		
Simplified teaching-learning based optimization algorithm (STLBO)	250-W PEMFC	2014	[41]
Multi-strategy adaptive differential evolution (rank-Made)	Ballard V 5 kW	2014	[42]
	SR-12 500 W		
	BCS 500 W		
	Temasek 1 kW		
	WNS-FC		
Adaptive differential evolution algorithm (ADE)	Ballard V 5 kW	2014	[43]
	SR-12 500 W		
	BCS 500 W		

the PEMFC operating current (A), A is the active area of the membrane (cm^2), and $P_{H_2O}^{sat}$ is the saturation water pressure (atm). The saturation vapor pressure at the FC operating temperature can be defined as [27,45]:

$$log_{10}\left(P_{H_2O}^{sat}\right) = 2.95 \times 10^{-2}(T_{stack} - 273.15) - 9.18$$
$$\times 10^{-5}(T_{stack} - 273.15)^2 + 1.44 \times 10^{-7}(T_{stack} - 273.15)^3$$
$$- 2.18$$

(6)

The activation loss is the overpotential required to activate the electrodes. This loss is dominant in low current density region and is calculated by:

$$\begin{cases} V_{Act} = -[\xi_1 + \xi_2 T_{stack} + \xi_3 T_{stack} \ln(Co_2) + \xi_4 T_{stack} ln(I_{FC})] \\ Co_2 = \left(Po_2/5.08\right) \times 10^6 exp\left(-498/T_{stack}\right) \end{cases}$$

(7)

where Co_2 is the oxygen concentration (mol cm^{-3}), and $\xi_k(k = 1...4)$ are the semi-empirical coefficients based on theoretical equations with kinetic, thermodynamic, and electrochemical foundations [17]. These parameters have been already defined in the literature [17,44,46] by solving the Butler-Volmer equation, which is a thermodynamics relation based on transfer coefficient, exchange current density, universal gas constant, Faraday constant, and number of electrons transferred due to reaction, etc., for both of

anode and cathode reaction sides. The ohmic voltage drop, which is the consequence of resistance to the electrons transfer through the collecting plates and carbon electrodes and the resistance to the protons transfer through the solid membrane, is calculated by a general expression based on the equivalent resistance of the membrane [44]:

$$\begin{cases} V_{Ohmic} = I_{FC}(R_m + R_C) \\ R_m = \rho_m\, l/A \\ \rho_m = \dfrac{181.6\left[1 + 0.03(J) + 0.062\left(T_{stack}/303\right)^2 (J)^{2.5}\right]}{[\lambda - 0.643 - 3(J)]exp\left(4.18\left(\dfrac{T_{stack} - 303}{T_{stack}}\right)\right)} \end{cases}$$

(8)

where R_m is the membrane resistance (Ω), R_C is the equivalent contact resistance to electron conduction (Ω), ρ_m is the resistivity of the membrane ($\Omega.cm$), l is the membrane thickness, J is the actual current density (A cm^{-2}), and λ is an adjustable parameter related to the water content of the membrane. R_C is usually considered as constant. However, λ is an adaptable parameter related to the membrane and its preparation process. It is a function of relative humidity and stoichiometry relation of the anode gas. As reported in Refs. [28,36,38,40,41,47], its value ranges from 10 to 23 where lower values signify high relative humidity ratio and higher values indicate oversaturated conditions.

The concentration voltage drop is indeed due to the mass transport which influences the concentrations of hydrogen and

oxygen and, as a result, reduces the partial pressure of these gases. Oxygen and hydrogen pressures drop relies on the electrical current and the physical characteristics of the system. To determine an equation for this drop, a maximum current density is defined based on which the current density cannot surpass this limit since the fuel cannot be provided at a higher rate. V_{Con} is determined by:

$$V_{Con} = - \beta \ln \left(J_{max} - J_{/J_{max}} \right) \tag{9}$$

where β is a parametric coefficient (V) that depends on the cell and its operation state [48], and J_{max} is the maximum current density. The parameters which need to be extracted in the discussed steady-state model are listed in Table 2. This table also clarifies the maximum and minimum range of each parameter.

3. Metaheuristic optimization algorithms

Constrained optimization is a vital part of most of the engineering and industrial problems [49]. In this type of problem, the mathematical optimization is defined by different kinds of constraints which modify the form of the search space. The metaheuristic optimization techniques are usually used to find global or near-global answers in such problems. In this work, SFLA, ICA, and FOA algorithms are used in PEMFC parameter extraction. This is a new application for these algorithms. They have shown satisfactory performance in other engineering problems. Therefore, it is worthwhile to use them in PEMFC modeling, which is a highly nonlinear problem. The performance of these algorithms is assessed based on a defined fitness function for 100 independent runs to show their robustness.

3.1. Fitness function definition

The optimization problem is normally defined by introducing a fitness function as the objective of minimization, the decision variables as the targeted parameters of estimation, and the search space formed by the upper and lower limits of each decision variable. The optimization algorithms use the fitness function to direct the population towards better solutions. The main goal of the fitness function definition, based on which all the algorithms are compared, is to extract the steady-state model parameters by minimizing the sum of squared errors (SSE) between the output voltage of each PEMFC stack and the estimated voltage by the model. The main reason for defining such fitness function is that it is commonly used in the literature [26] and makes the results of this work comparable to the existing optimizers in other manuscripts. This fitness function can be formulated by:

$$\begin{cases} \begin{pmatrix} \mathbf{min} \\ steady - state \\ params. \end{pmatrix} \sum_{i=1}^{N} \left(V_{FC.meas}(i) - V_{FC.est}(i) \right)^2 \\ \xi_{k, min} \leq \xi_k \leq \xi_{k, max}(k = 1 \ldots 4) \\ R_{C, min} \leq R_C \leq R_{C.max} \\ \lambda_{min} \leq \lambda \leq \lambda_{max} \\ \beta_{min} \leq \beta \leq \beta_{max} \end{cases} \tag{10}$$

where $V_{FC.meas}$ is the measured output voltage, $V_{FC.est}$ is the estimated output voltage by the model, and N is the number of sample data. The suitability of the estimated parameters value is scrutinized by testing the described PEMFC models in MATLAB software. It should be noted that selecting appropriate initial values for the parameters has a significant role in the quality of the estimation process. In this work, the fitness function is exposed to practical inequality constraints defined by the upper and lower bounds.

3.2. Shuffled frog-leaping algorithm

SFLA is considered as a memetic metaheuristic method put forward to find a global optimal answer by conducting an informed search [50]. It integrates the virtue of particle swarm optimization local search into the idea of combining the information from parallel local searches to a global solution. The population in SFLA is composed of a number of frogs/solutions, which are divided into some subsets known as memeplexes. Each memeplexe is the representative of a group of frogs performing a local search. Each individual frog inside of a memeplexe has an idea affected by the ideas of other individuals. This idea is improved through a memetic evolution. After a specific number of steps, ideas are shared among the memeplexes by means of a shuffling process. The process of shuffling as well as the local search are sustained until the expected convergence criteria are satisfied. Fig. 1 shows the flowchart of the SFLA. According to this flowchart, an initial population is first generated randomly (P) within the search space. In multidimensional problems, each frog i is defined by S variables as $X_i = (x_{i1}, x_{i2}, \ldots, x_{iS})$. The frogs are then put in a descending order with respect to their achieved fitness values. After that the whole population is partitioned into m memeplexes, where each one includes n frogs ($P = m \times n$). Each frog is placed into its corresponded memeplex, i.e. the first frog in the first memeplex, the second frog in the second memeplex, and the mth frog in the mth memeplex. The frog $m + 1$ is sent back to the first memeplex again, and this continues until each frog finds a place in each memeplex. Inside each memeplex, the individual frogs with the best X_b, worst X_w, and global best X_g finesses are determined and only the one with the worst fitness is improved as follows:

Table 2
Range of targeted parameters for estimation.

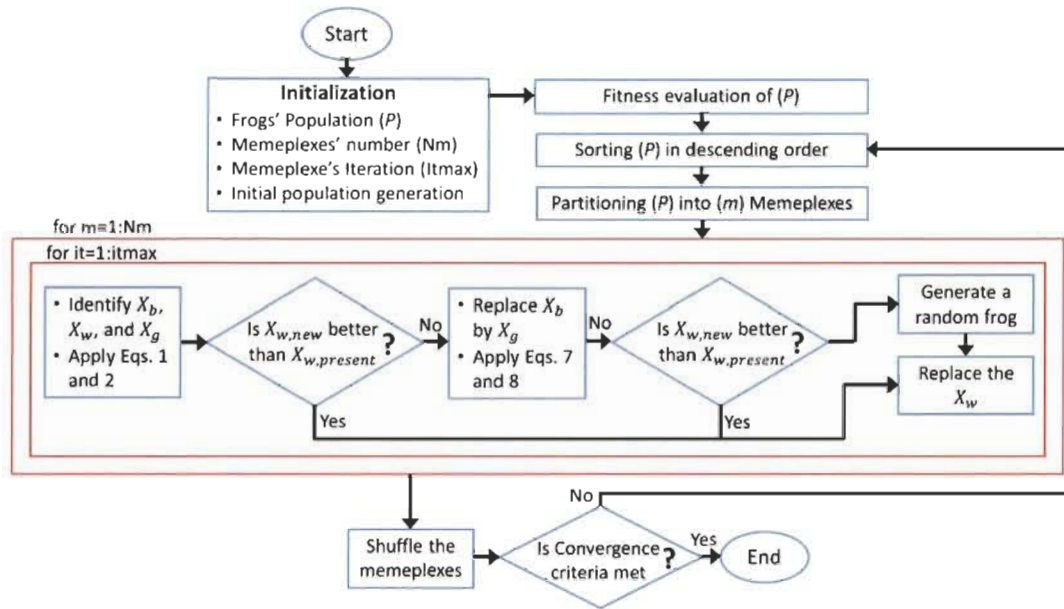| Model	Parameters	Minimum	Maximum	Reference
Semi-empirical	ξ_1	−1.1997	−0.8532	[28–30,32,34,36,38,40,41]
	$\xi_2 \times 10^{-3}$	1	5	
	$\xi_3 \times 10^{-5}$	3.6	9.8	
	$\xi_4 \times 10^{-5}$	−26	−9.54	
	$R_C (\Omega) \times 10^{-4}$	1	8	
	λ	10	23	
	β (V)	0.0136	0.5	

Fig. 1. SFLA flowchart.

$$D_i = randn(X_b - X_w) \tag{11}$$

$$X_{w,new} = X_{w,present} + D_i(-D_{max} \leq D_i \leq D_{max}) \tag{12}$$

where D_i is the frog position change, rnd is a random number between 0 and 1, $X_{w,new}$ is the new position of the frog with the worst fitness inside the feasible space, $X_{w,present}$ is the current position of the frog with the worst fitness, and D_{max} is the maximum possible variation in the position of a frog. It should be noted that if the formulated evolution results in a better solution, it replaces the worst solution. Otherwise, equations (11) and (12) are repeated for the case that X_b is replaced by X_g. In case of observing no improvement in the solution after trying the two mentioned scenarios, a new random solution is generated instead of the frog with the worst solution. The calculation is then continued for a particular number of iterations. The principal parameters of the SFLA are the population or the number of frogs, number of memeplexes, and maximum iteration for each memeplexe.

3.3. Imperialist competitive algorithm

ICA is an imperialistic inspired method which has been successfully implemented in different engineering problems [51,52].

The flowchart of this algorithm is shown in Fig. 2. This algorithm commences by generating some random solutions, known as countries containing the optimization problem variables ($p_1, p_2, ..., p_{N_{var}}$), in the search space. N_{var} is the dimension of the problem. The initial countries are then divided into two classes of imperialist and colony according to their power which is determined by the defined cost function of the optimization problem.

$$Country = [p_1, p_2, ..., p_{N_{var}}] \tag{13}$$

$$Cost = f(p_1, p_2, ..., p_{N_{var}}) \tag{14}$$

The primary empires are established by distributing the colonies among the imperialists. The colonies are divided among the imperialists proportionally by:

$$C_n = c_n - \max\{c_i\} \tag{15}$$

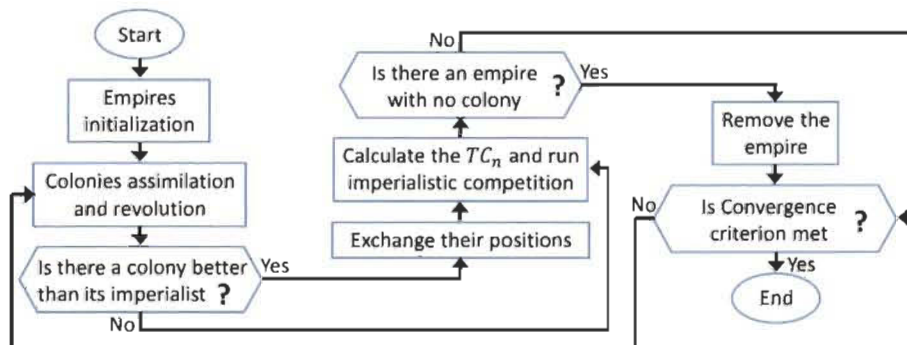$$p_n = \left| C_n / \sum_{i=1}^{N_{imp}} C_i \right| \tag{16}$$

Fig. 2. ICA flowchart.

$$NC_n = round\{p_n N_{col}\} \tag{17}$$

where c_n and C_n are the nth imperialist cost and normalized cost respectively, p_n is the normalized power of each imperialist, N_{imp} is the number of imperialists, NC_n is the nth empire initial number of colonies chosen randomly, and N_{col} is the number of colonies. The empires then go thorough assimilation and revolution processes in which colonies move towards the states of the imperialists with random characteristics. If a colony reaches a better position than its corresponding imperialist (considering the cost function), they exchange positions. The movement of colonies and total power of an empire can be formulated by:

$$\{x\}_{new} = \{x\}_{old} + U(0, \sigma \times d) \times \{V_1\} \tag{18}$$

$$\theta = U(-\gamma, +\gamma) \tag{19}$$

$$TC_n = f_{cost}^{(imp,n)} + \psi\left(\sum_{i=1}^{NC_n} f_{cost}^{(col,i)} \Big/ NC_n\right) \tag{20}$$

where σ is a parameter greater than one, d is the distance between colony and imperialist, $\{V_1\}$ is a vector with unity length, θ is a random number with uniform distribution added to the direction of movement to enhance the searching around the imperialist, γ is a parameter that modifies the deviation from the original direction, TC_n is the total cost of the nth empire, and ψ is a positive number less than one. The values of 2, 0.1, and 0.1 have been found to be good for σ, γ, and ψ respectively. The imperialistic competition slowly decreases the power of weaker empires and increases the power of more powerful ones by choosing the weakest colony of the weakest empire and giving it to the empire with the most possession probability (P_n). When an empire loses all its colonies, it will be eliminated. The normalized total cost and the possession probability of each empire are given by:

$$NTC_n = TC_n - max(TC_i) \tag{21}$$

$$P_n = \left|NTC_n \Big/ \sum_{i=1}^{N_{imp}} NTC_i\right| \tag{22}$$

3.4. Firefly optimization algorithm

FOA is a metaheuristic algorithm premised on the social behavior of fireflies for attracting mates [53]. FOA is based on three fundamental presumptions. First, all the fireflies are perceived as unisex and try to approach the brighter ones until the whole population is compared. Second, the attraction of the fireflies is associated with the potency of their flash signals. This means that in case of having the choice for moving towards two fireflies, the brighter one is preferred. It should be noted that the brightness declines as the distance increases. Third, brightness intensity of a firefly is calculated by the value of the optimization problem fitness function. The FOA can be mathematically presented by the following equations:

$$\omega(r) = \omega_0 \exp(-\kappa r^m), m \geq 1 \tag{23}$$

$$r_{ij} = \sqrt{\sum_{k=1}^{d}\left(x_{i,k} - x_{j,k}\right)^2} \tag{24}$$

$$x_i = x_i + \omega_0 \exp\left(-\kappa r_{ij}^2\right)\left(x_j - x_i\right) + \alpha\,(randn - 1/2) \tag{25}$$

where $\omega(r)$ is the attractiveness, r is the distance between two fireflies, ω_0 is the initial attractiveness when r is zero, κ is a fixed light absorption factor, d is the dimension of the problem, x_i and x_j are the positions of two i and j fireflies, α is a value between zero and one, and $randn$ is a random number generator uniformly and distributed between [0, 1]. Fig. 3 presents the flowchart of the FOA.

4. Results and discussion

This section presents the achieved results from different parts of the manuscript. First, the results related to the available PEMFC case studies in the literature are investigated, and the algorithms are compared. Subsequently, the data related to the proposed case study of this work, which is a 500-W Horizon PEMFC, is presented along with the description of the utilized test bench for recording the measured data. Finally, the estimation quality of the open cathode PEMFC is studied. It should be noted that the controlling parameters used for each algorithm are listed in Table 3. These parameters have been obtained based on the introduced reference papers and trials and errors over several runs. These algorithms might show better or worse performance by changing the controlling parameters and that is why they are clarified in Table 3. Another worth noting aspect is that since the metaheuristic techniques intrinsically have high level of randomness, 100 independent runs are done for each algorithm and the best result is then chosen out of these tries. The robustness of the algorithms is investigated by means of some statistical factors, such as variance and standard deviation of the defined fitness function. Moreover, the point-by-point measured data, which are the input of the algorithms, are reported for all the case studies.

4.1. Case study 1 (NedSstack PS6)

This case study belongs to a NedSstack PS6 PEMFC stack with the rated power of 6 kW. The operating data of this PEMFC system can be found in Ref. [30], and its characteristics are as follows: $N_{cell} = 65$, $P_{H2} = 1$ atm, $P_{O2} = 1$ atm, $T_{stack} = 343$ K, $A = 240$ cm^2, $l = 178$ μm, and $J_{max} = 0.918$ A cm^{-2}. The maximum operating current of this PEMFC is 225 A. Table 4 indicates the obtained values for each targeted parameter after implementing the algorithms for parameter extraction process. This table also shows the best fitness value attained by each algorithm, which corresponds to the reported estimated parameters. The obtained best solutions by the
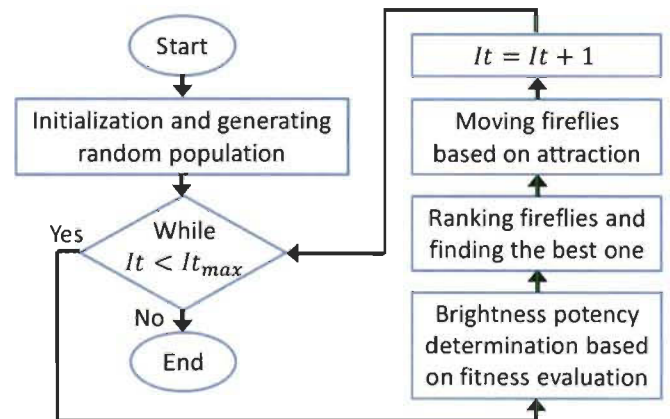

Fig. 3. FOA flowchart.

Table 3
Controlling parameters of the utilized algorithms.

SFLA		ICA		FOA	
Parameter	Value	Parameter	Value	Parameter	Value
Maximum iteration	100	Maximum iteration	100	Maximum iteration	100
Frog population	50	Number of countries	50	Number of fireflies	50
Number of Memeplexes	5	Number of imperialists	10	Light Absorption Coefficient	1
Memes in Memeplexes	10	Assimilation coefficient	2	Attraction coefficient base value	2
Memetic evolutions	10	Revolution probability	0.1	Mutation coefficient	0.2

Table 4
The estimated parameters along with the best fitness value.

Parameter	SFLA	ICA	FOA	SSO [30]	GHO [31]	GA [31]
ξ_1	−1.023071	−1.034322	−1.035664	−0.9719	−1.1997	−1.1997
$\xi_2 \times 10^{-3}$	3.4760	3.3202	2.9502	3.3487	3.5505	3.4172
$\xi_3 \times 10^{-5}$	7.7883354	6.4420795	3.7669451	7.9111	4.6144	3.6000
$\xi_4 \times 10^{-5}$	−9.540000	−9.540000	−9.540000	−9.5435	−9.5400	−9.5400
$R_C\ (\Omega) \times 10^{-4}$	1.62	1.65	1.622	1.000	1.005	1.376
λ	15.03229	15.09701	15.029691	13.0000	13.0092	13.0000
β (V)	0.013600	0.013600	0.0136000	0.0534	0.0579	0.0359
Best fitness (SSE)	2.167055	2.168339	2.167091	2.18067	2.18586	2.4089

introduced algorithms in this work shows that they have considerable accuracy in terms of extracting the parameters of this PEMFC system. The estimated polarization curve of the NedSstack PS6 PEMFC stack by SFLA algorithm is shown in Fig. 4a. SFLA has reached the best fitness value, which is the minimum SSE between measured and predicted voltage. It is worth mentioning that the point-by-point current-voltage values obtained by all of the three algorithms are also reported in Table A1 in the appendix section. The fitness function convergence trend for different algorithms is presented in Fig. 4b. With regard to this figure, the fitness value minimization trend has become almost stable after 20 iterations by all the algorithms.

4.2. Case study 2 (BCS 500-W)

The second case study of this manuscript investigates the polarization behavior of the BCS 500-W PEMFC stack produced by the American Company BCS Technologies. The characteristics of this FC, which have been collected from Ref. [32], are as follows: $N_{cell} = 32$, $P_{H2} = 1$ atm, $P_{O2} = 0.2075$ atm, $T_{stack} = 333$ K, $A = 64$ cm^2, $l = 178$ μm, and $J_{max} = 0.469$ A cm^{-2}. The maximum operating current of this system is 30.016 A. Table 5 presents the estimated parameters and the best fitness achieved for BCS 500-W PEMFC stack by different algorithms. According to Table 5, the utilized algorithms have successfully extracted the suitable parameters for this case study. Moreover, compared to the available optimizers in the literature, some improvement in the minimum value of the defined fitness function can be observed. Table 5 also shows that SFLA has obtained the minimum value in terms of the defined fitness function. Fig. 5a presents the estimated polarization curve by SFLA. The point-by-point current-voltage values achieved by all of the optimization methods are also reported in Table A2 in the appendix. Fig. 5b compares the minimization tend of different algorithms. As it is seen, ICA and SFLA converges faster than the FOA.

4.3. Algorithm selection

In fact, all the three utilized algorithms in this manuscript have already shown a great potential for solving different engineering problems. So far, it has been observed that these algorithms are able to improve the defined best fitness value of this work (SSE between the measured and estimated voltage) compared to other available optimizers in the literature. Realized by the performed comparative study of the standard form of these algorithms in this work, it can be stated that ICA and FOA algorithms are more prone to premature convergence than SFLA, as shown in Figs. 4b and 5b. This is mainly due to the fact that SFLA combines the merits of genetic-based memetic and social behavior-based algorithms. It executes
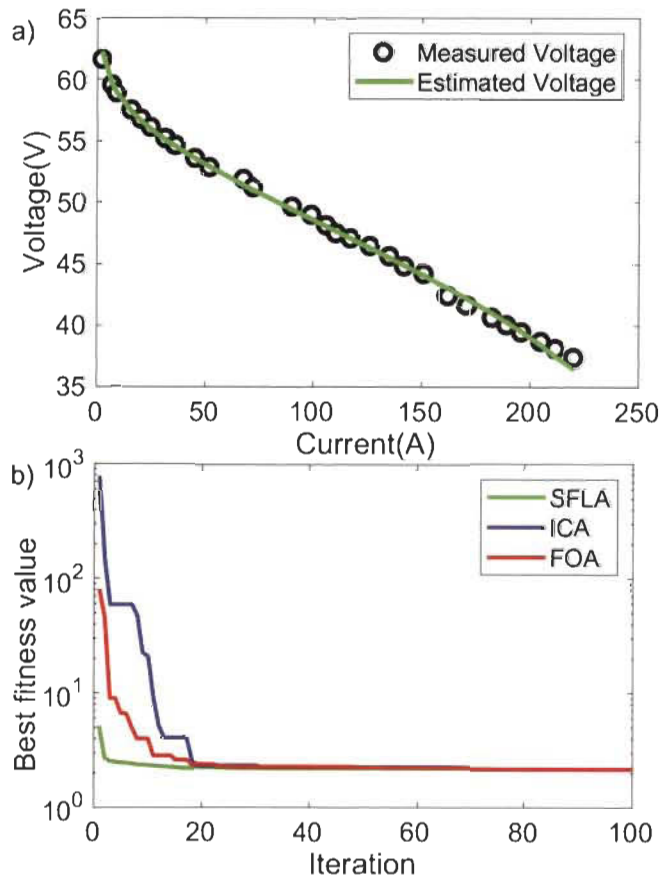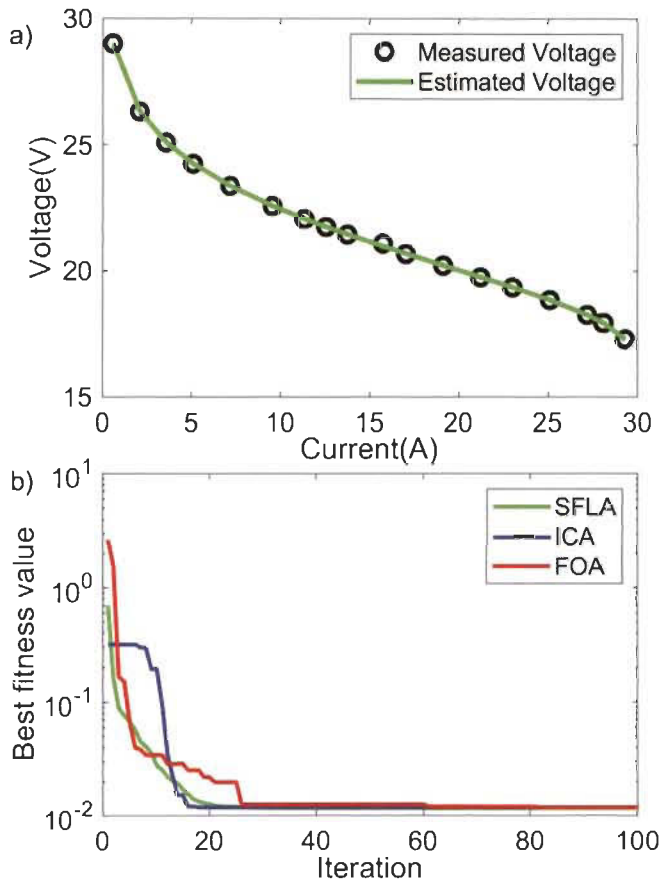

Fig. 4. NedSstack PS6 PEMFC case study: a) estimated polarization curve by SFLA, b) fitness function (SSE) minimization trend comparison.

Table 5
The identified parameters and the corresponded fitness value.

Parameter	SFLA	ICA	FOA	SSO [30]	DEM [30]	GWO [32]
ξ_1	−0.965740	−0.908643	−0.992829	−0.8532	−0.948	−1.0180
$\xi_2 \times 10^{-3}$	3.080	2.4798	2.621	4.8115	4.8115	2.3115
$\xi_3 \times 10^{-5}$	7.223600	4.4583194	3.746368	9.4334	7.6000	5.2400
$\xi_4 \times 10^{-5}$	−19.3	−19.3	−19.3	−19.205	−19.300	−12.815
$R_C\ (\Omega) \times 10^{-4}$	1.00	2.46	1.00	3.499	3.000	7.504
λ	20.88622	22.66264	21.101126	23	23	18.8547
β (V)	0.016126	0.016238	0.016269	0.01589	0.0160	0.0136
Best fitness	0.011697	0.011856	0.011819	0.01219	0.01299	7.1889

Fig. 5. BCS 500-W PEMFC case study: a) estimated polarization curve by SFLA, b) fitness function (SSE) minimization trend comparison.

concurrently an independent local search inside each memeplex, and the entire frogs are then shuffled and reorganized into new memeplexes after a predefined number of local iterations to ensure global exploration. Concerning the FOA, one of the reasons for its premature convergence is the dependency of the updates on the current performance and not having a knowledge of the preceding best solutions. To alleviate this drawback, a new updating strategy can be formulated for FOA in future and the random and attraction movement parameters can be modified. Regarding the ICA, its performance can be improved by paying more attentions to the tuning parameters, which are more critical than the ones in other optimizers, especially the deviation parameter of the assimilation process. This parameter has a direct impact on achieving a balance between local and global explorations.

Another noteworthy aspect is that the performance of these algorithms is based on randomness and the sole best fitness value (SSE) in one of the runs cannot assure the acceptable performance

of the optimization algorithm. As mentioned earlier, the listed values in Tables 4 and 5 belong to the best solution found out of 100 independent runs, and there is no guarantee that the algorithms can repeat the same results. In this regard, some statistical measures, namely best, worst, variance, and standard deviation, are calculated by using the obtained best fitness values through each of the independent runs to show the robustness and probability of finding the optimal answer by the algorithms. These statistical factors are listed in Table 6. Variance value shows how far a set of numbers are from their mean value and in this case the lesser the variance the better. Standard deviation also specifies the scattering of the data and a low value for this measure means the data tends to be closer to the average of the set. Table 6 includes the results of the mentioned statistical measures for SSO algorithm, in addition to SFLA, FOA, and ICA. This is because SSO has already shown a very good performance from itself over 100 independent runs. Moreover, the required data for calculating all the measures for this algorithm are available in Ref. [30]. According to Table 6, SFLA has achieved the lowest value in terms of variance and standard deviation compared to other algorithms. However, neither ICA nor FOA could achieve a better result than SSO. This superior performance of SFLA justifies the previously discussed advantages of this algorithm regarding the simultaneous local and global exploration. In this respect, SFLA algorithm is selected to be used for the optimization of the 500-W Horizon PEMFC, which is a new case study introduced in this work. It should be noted that this selection has been made based on the defined comparison criteria and utilized controlling parameters and it does not mean that the other two introduced algorithms are not suitable for parameters estimation of a PEMFC model. In fact, all the three algorithms are able to predict the PEMFC polarization curve with good accuracy. However, SFLA has shown more robustness than the others in the investigated cases.

### 4.4. Case study 3 (500-W Horizon PEMFC)

The last case study of this work, which is the main focus of this manuscript, is for an open cathode 500-W Horizon PEMFC. In order to collect justifiable experimental data and provide the required measurements for extracting the PEMFC model parameters, an experimental set-up has been developed as explained in details in section 4.4.1. Moreover, the obtained results regarding the performance verification of the SFLA algorithm as well as the tuned semi-empirical model are presented in section 4.4.2.

4.4.1. Materials and methods

The required data for the proposed new case study has been recorded from a developed test bench, shown in Fig. 6, in Hydrogen Research Institute of Université du Québec à Trois-Rivières with a standard protocol. This test bench is used to test and validate the SFLA algorithm and the extracted PEMFC model. The set-up is mainly composed of a Horizon open-cathode PEMFC with a rated power of 500 W. The PEMFC characteristics, gathered from Ref. [54]

Table 6
Statistical measures comparison.

Case study	Computed factor	SFLA	ICA	FOA	SSO [30]
1	Best	2.167055	2.168339	2.167091	2.18067
	Worst	2.167598	2.518191	2.614219	2.25060
	Variance	1.06829×10^{-8}	0.005940	0.016838	4.131×10^{-4}
	Standard deviation	1.03358×10^{-4}	0.077072	0.129763	0.0203
2	Best	0.011697	0.011856	0.011819	0.01219
	Worst	0.011698	0.034665	0.030233	0.01520
	Variance	2.53971×10^{-15}	3.43806×10^{-5}	1.74131×10^{-5}	7.588×10^{-7}
	Standard deviation	5.03955×10^{-8}	0.005863	0.004172	8.711×10^{-4}
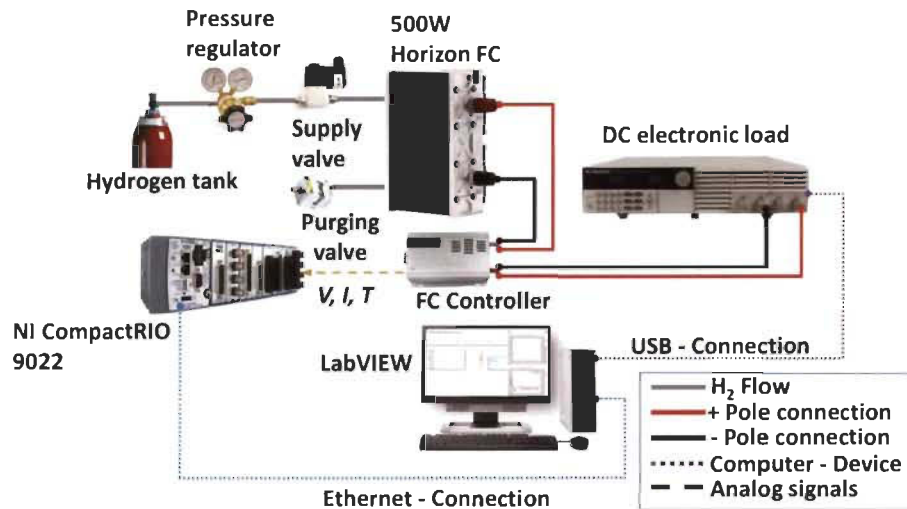
Fig. 6. The developed test bench in Hydrogen Research Institute.

and the manufacture manual, are presented in Table 7. This PEMFC is self-humidified, air-cooled, and known as open-cathode or air breathing. It has two axial fans to provide the cathode with air and to cool down the stack. The flow rate of air supplied to the cathode side is controlled by the duty cycle of the fan which is strongly reliant on the requested power from the PEMFC and the stack temperature. In the anode side, the PEMFC is equipped with an inlet and an outlet valve. The inlet valve is utilized to feed the PEMFC with dry hydrogen. The hydrogen flow rate changes between 0 and 11.67×10^{-2} Ls^{-1} depending on the drawn power from the stack. The outlet valve is responsible for purging the accumulated water and nitrogen every 10 s for a duration of 10 ms to refill the anode with fresh hydrogen during the PEMFC operation. The exhaust flow

of hydrogen after the purge rests on the difference of pressure between the environment (1 atm) and the anode side (1.48 atm as suggested by the manufacturer). Furthermore, the pressure difference between the anode and the cathode sides must not surpass 0.493 atm to prevent the membrane from being damaged. The control of the purge valve, fan speed, and hydrogen valve are performed through the PEMFC controller, and the acquisition of data (temperature, current, and voltage) are done by an embedded computer (National Instrument CompactRIO 9022). A programmable load manufactured by BK Precision with a maximum power of 1200 W is connected to the PEMFC in order to request different power profiles form the stack. The communication between the CompactRIO and the PC is via Ethernet connection every 100 ms. The measured data (temperature, current, and voltage) from the real PEMFC is transferred to the PC by means of the CompactRIO and is used in the PEMFC model verification process.

It should be noted that in this new case study the temperature is variable as opposed to other available case studies in the literature. The voltage-current curve of this PEMFC has been obtained by drawing a fixed current from the FC and measuring its output voltage. By slowly stepping up the load, the FC voltage response can be seen and recorded. After each increase in the current level, 15–25 min have been allowed to the FC to reach equilibrium. As opposed to the other two case studies in which the temperature is constant, this FC system reaches one stable temperature for each current level. It means that for each current level, there is one corresponded voltage and temperature measurement. All the tests have been conducted in a stable environment in the test center of Hydrogen Research Institute to maintain the conditions. Another point which needs to be mentioned is that the actual rated power of the utilized PEMFC in this work is 430 W with a maximum current

Table 7
The characteristics of the Horizon 500-W open cathode PEMFC.

Technical specification	
Type of FC	PEM
Rated Power	500 W
Rated performance	22 V @ 23.5 A
Max Current	42 A
Rated H2consumption	7 SLPM
Ambient temperature	5 to 30 °C
Max stack temperature	65 °C
Cooling	Air (integrated cooling fan)
Reactants	Hydrogen and Air
N_{cell}	36
P_{H2}	0.55 atm
P_{O2}	1 atm
A	52 cm^2
l	25 μm
J_{max}	0.446 A cm^{-2}

Table 8
The identified parameters and the obtained fitness value for 500-W Horizon PEMFC.

Parameter	Estimated value by SFLA
ξ_1	−0.853200
$\xi_2 \times 10^{-3}$	2.522
$\xi_3 \times 10^{-5}$	7.843743
$\xi_4 \times 10^{-5}$	−16.3
R_C (Ω) $\times 10^{-4}$	7.999
λ	13
β (V)	0.048869
Best fitness	0.015622

of 25 A. In fact, the rated power of this PEMFC has decreased over time due to degradation.

4.4.2. Experimental results

Table 8 presents the identified values for each unknown parameter after using the SFLA for parameter extraction. This table also shows the best fitness value achieved by using the identified parameters.

The polarization characteristics of the 500-W Horizon PEMFC stack are reported point by point in Table 9 and shown in Fig. 7a. The minimization trend of the fitness function is represented in Fig. 7b. It can be seen that the stable value is achieved after almost 10 iterations.
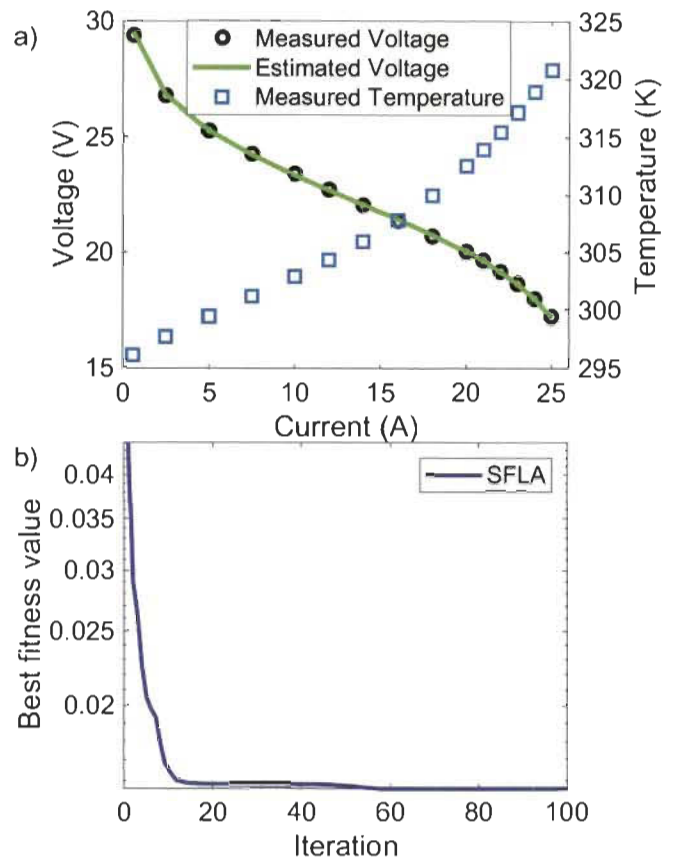
In order to assess the probability of achiving a satisfactory fitness values, the previous defined statistical measures are calculated for this new case study. Fig. 8 presents the histogram of the obtained best fitness value over 100 independent runs. The statistical measures are also reported in this figure to clarify the histogram plot. As it can be seen in this histogram, the frequency of obtaining the best fitness value is strikingly high by SFLA ensuring the reliablity of this metaheuristic algorithm. Fig. 9 presents the simulated performance analysis of the 500-W Horizon PEMFC over various partial pressures of hydrogen in the anode side (P_{H2}). Since this FC is an open cathode PEMFC, the pressure in the cathode side (P_{O2}) is always 1 atm. As is obsereved in Fig. 9, regulating the pressure under 0.55 atm can result in less output power by the PEMFC. While setting a value more than 0.55 atm can increse the output power to some extent.

To further evaluate the performance of the tuned PEMFC model by the SFLA algorithm, the presented current profile in Fig. 10a has been applied to the Horizon PEMFC on the developed test bench and its stack temperature and voltage signals have been recorded. Subsequently, the same current profile has been imposed to the

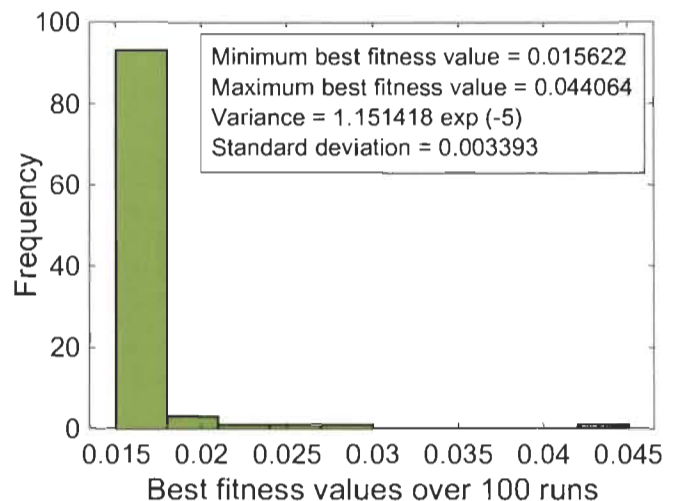**Fig. 7.** 500-W Horizon PEMFC case study: a) estimated polarization curve by SFLA, b) fitness function (SSE) minimization trend comparison.

PEMFC model and its voltage estimation is compared with the measured one in Fig. 10b. According to this figure, the tuned PEMFC model is able to imitate the output voltage of the real PEMFC satisfactorily. It should be noted that the PEMFC model is fed with the measured temperature, shown in Fig. 10a, to predict the output voltage.

Table 9
The steady-state characteristics of the 500-W Horizon PEMFC.

Current (A)	$V_{FC.meas}$ (V)	$V_{FC.est}$ (SFLA)	|Residual|	Temperature (K)
0.6	29.370000	29.514760	0.144759	296.200000
2.5	26.777390	26.813765	0.036374	297.810917
5	25.290250	25.287802	0.002448	299.520062
7.5	24.281859	24.235411	0.046448	301.227449
10	23.418000	23.356632	0.061367	302.950000
12	22.739103	22.709020	0.030083	304.404279
14	22.058523	22.078801	0.020277	306.006926
16	21.386148	21.442688	0.056540	307.842680
18	20.721728	20.775549	0.053821	309.994399
20	20.026000	20.041864	0.015864	312.532000
21	19.636350	19.632033	0.004317	313.961094
22	19.191807	19.176821	0.014986	315.501399
23	18.663630	18.653590	0.010040	317.153087
24	18.015227	18.020263	0.005036	318.913454
25	17.201250	17.182838	0.018412	320.776562

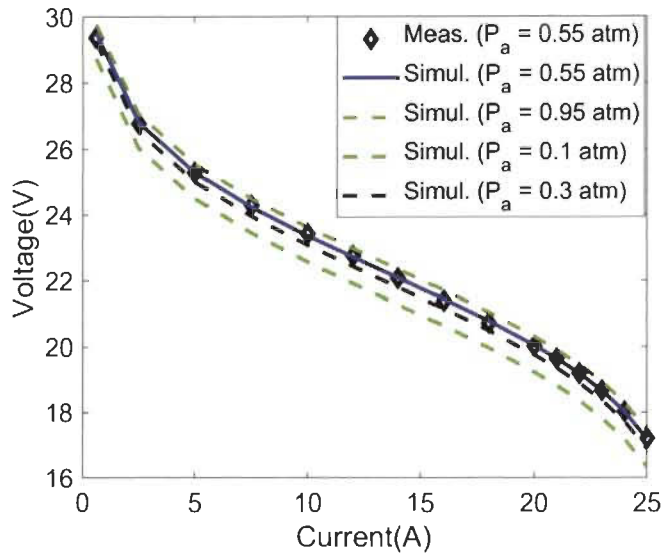**Fig. 8.** The histogram analysis of SFLA.

Fig. 9. Polarization behavior analysis in different partial pressures of hydrogen.

5. Conclusion

This paper investigates the performance of three metaheuristic optimization algorithms, namely SFLA, ICA, and FOA, in a PEMFC parameter extraction problem. In this regard, the performance comparison of the algorithms is performed by using the SSE between the measured and estimated PEMFC voltage as the fitness function for two available case studies in the literature over 100 independent runs. Subsequently, the precision of the algorithms is judged based on their achieved best fitness value, worst fitness value, variance, and standard deviation. Finally, the selected algorithm from the comparison step is used to identify the parameters of the PEMFC model for a new case study, a 500-W Horizon PEMFC, provided by this work. This new case study is an open cathode

Fig. 10. Performance validation of the tuned PEMFC model for the Horizon 500-W PEMFC case study: a) the current profile applied to the real PEMFC and the corresponding measured temperature, and b) the comparison of the estimated and measured voltage.

PEMFC and has variable temperature as opposed to the other existing case studies in the literature. The final results of this work indicate that with regard to the best SSE, SFLA slightly outperforms ICA and FOA in both case studies. However, the obtained worst SSEs show that SFLA performs 20% better than ICA and two times better than FOA in the first and second case studies. Moreover, the attained variance and standard deviation of SFLA are noticeably less than the other algorithms which are the justification of accuracy and repeatability of this method. The results of this paper open up the following avenues for future researches:

- Utilizing the selected optimization algorithm of this work in dynamic PEMFC model calibration.
- Investigating the performance of new optimization algorithms by using the provided case study of this research.
- Using the proposed metaheuristic optimization algorithms for a more complete PEMFC model including hydrogen consumption prediction.

Acknowledgements

Nomenclature

Variables

V_{FC}	Output voltage of the PEMFC, V
E_{Nernst}	Sum of cell reversible voltage, V
V_{Act}	Activation voltage, V
V_{Ohmic}	Ohmic voltage, V
V_{Con}	Concentration voltage, V
N_{cell}	Number of cells
T_{stack}	Stack temperature, K
P_{H2}	Hydrogen partial pressure in anode side, atm
P_{O2}	Oxygen partial pressure in cathode side, atm
RH_C	Relative humidity of vapor in the cathode, %
RH_a	Relative humidity of vapor in the anode, %
P_C	Cathode inlet pressures, atm
P_a	Anode inlet pressures, atm
I_{FC}	FC operating current, A
A	Active area of the membrane, cm^2
$P_{H_2O}^{sat}$	Saturation water pressure, atm
ξ_k	Semi-empirical coefficients
Co_2	Oxygen concentration, mol cm^{-3}
R_m	Membrane resistance, Ω
R_C	Equivalent contact resistance to electron conduction, Ω
ρ_m	Resistivity of the membrane, Ω cm
l	Membrane thickness, cm
J	Actual current density, A cm^{-2}
λ	Adaptable parameter related to the water content of the membrane
β	Parametric coefficient
J_{max}	Maximum current density, A cm^{-2}
$V_{FC,meas}$	Measured output voltage, V
$V_{FC,est}$	Estimated output voltage by the model, V
N	Number of sample data
P	Initial population
X_i	Individual frog solution
m	Memplexe
n	Number of frog per memplex
X_b	Best frog solution
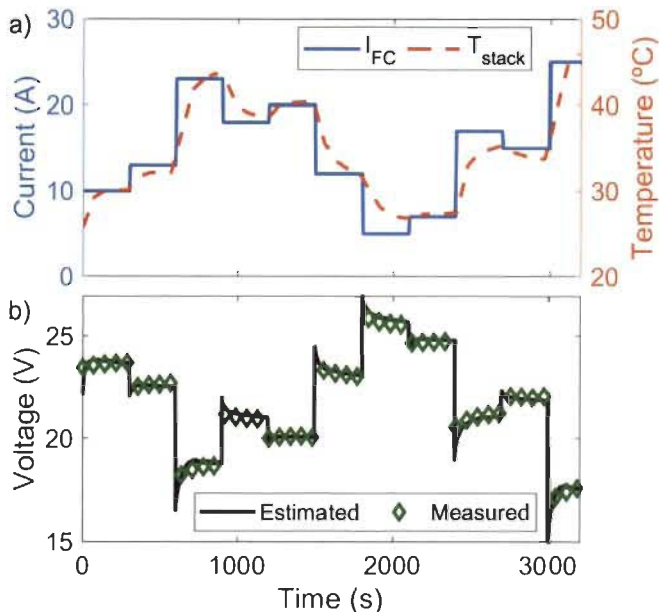
X_w	Worst frog solution
X_g	Global best frog solution
D_i	Frog position change
$X_{w,new}$	New position of the frog with the worst fitness
$X_{w,present}$	Current position of the frog
D_{max}	Maximum possible variation in the position of a frog
$p_{N_{var}}$	Countries containing the optimization problem variables
N_{var}	Dimension of the problem
C_n	Nth imperialist normalized cost
c_n	Nth imperialist cost
p_n	Normalized power of each imperialist
N_{imp}	Number of imperialists
NC_n	Nth empire initial number of colonies
N_{col}	Number of colonies
σ	Tuning parameter of ICA
d	Distance between colony and imperialist
$\{V_1\}$	Vector with unity length
θ	Random number with uniform distribution
γ	Ratio of deviation from the original direction
TC_n	Total cost of the nth empire
ψ	Empirical forgetting factor of ICA
P_n	Possession probability
$\omega(r)$	Attractiveness
r	Distance between two fireflies
ω_0	Initial attractiveness
κ	Fixed light absorption facto
d	Dimension of the problem
x_i	Positions of i firefly
α	Tuning parameter of FOA

Abbreviations

SFLA	Shuffled Frog-Leaping Algorithm
FOA	Firefly Optimization Algorithm
ICA	Imperialist Competitive Algorithm
SSE	Sum Square Error
PEMFC	proton exchange membrane fuel cell
FC	Fuel Cell
CS-EO	Cuckoo search algorithm with explosion operator
SSO	Slap swarm optimizer
GHO	Grasshopper optimization
GWO	Grey wolf optimizer
AC-POA	Aging and challenging P systems based optimization algorithm
TLBO−DE	Hybrid teaching learning based optimization − differential evolution
GRG	Generalized reduced gradient
HADE	Hybrid adaptive differential evolution
GA	Genetic algorithm
TRADE	Transferred adaptive differential evolution
STLBO	Simplified teaching-learning based optimization
ADE	Adaptive differential evolution
DEM	dynamic electrochemical model

Appendix

Figure A1 and Figure A2 present the measured and estimated polarization curves for NedSstack PS6 and BCS 500-W respectively. Moreover, Table A1 and Table A2 provide the point-by-point data regarding the current-voltage characteristics of the NedSstack PS6 and BCS 500-W respectively in different scenarios.
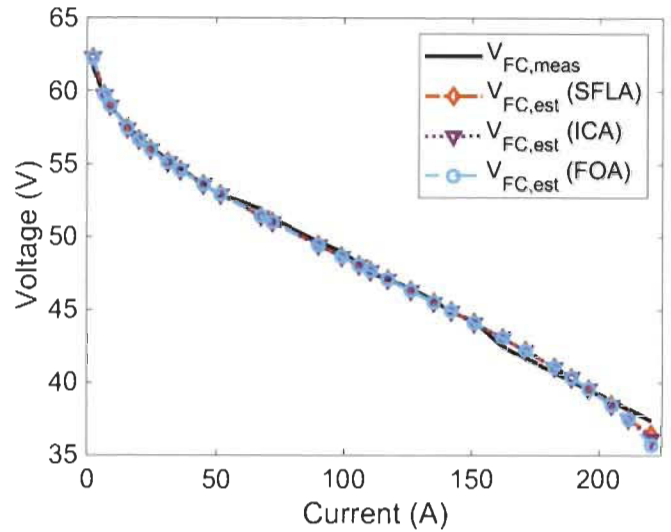

Fig. A.1. Estimated polarization curves by different algorithms in case study 1 (NedSstack PS6).
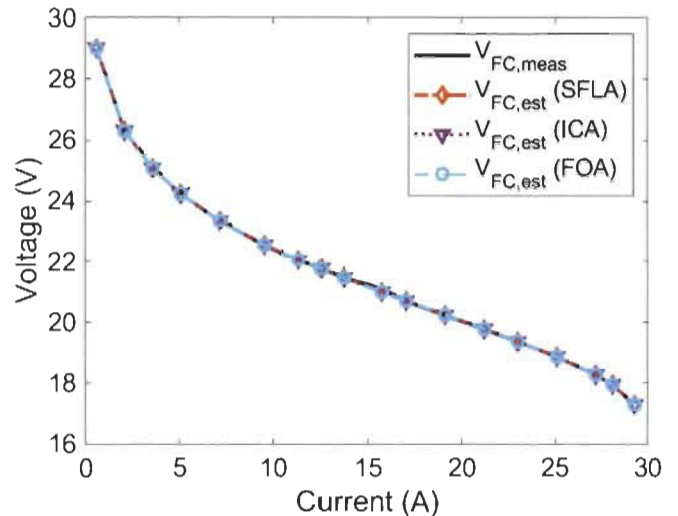

Fig. A.2. Estimated polarization curves by different algorithms in case study 2 (BCS 500-W).

Table A.1 Estimated voltage for each current level (case study 1)

Current (A)	$V_{FC,meas}$ (V)	$V_{FC,est}$ (SFLA)	$V_{FC,est}$ (ICA)	$V_{FC,est}$ (FOA)
2.25	61.64	62.274793	62.266538	62.274723
6.75	59.57	59.702854	59.694581	59.702843
9	58.94	58.972628	58.964351	58.972646
15.75	57.54	57.424395	57.416125	57.424500
20.25	56.8	56.648715	56.640467	56.648877
24.75	56.13	55.978682	55.970471	55.978901
31.5	55.23	55.096910	55.088779	55.097213
36	54.66	54.564243	54.556183	54.564601
45	53.61	53.585377	53.577508	53.585843
51.75	52.86	52.903552	52.895867	52.904098
67.5	51.91	51.418171	51.411066	51.418897
72	51.22	51.011656	51.004757	51.012432
90	49.66	49.428950	49.423070	49.429917
99	49	48.651772	48.646526	48.652829
105.8	48.15	48.066470	48.061764	48.067594
110.3	47.52	47.679019	47.674699	47.680184
117	47.1	47.100754	47.097055	47.101981
126	46.48	46.318935	46.316158	46.320241
135	45.66	45.528012	45.526266	45.529393

(continued)

Current (A)	$V_{FC,meas}$ (V)	$V_{FC,est}$ (SFLA)	$V_{FC,est}$ (ICA)	$V_{FC,est}$ (FOA)
141.8	44.85	44.922139	44.921248	44.923573
150.8	44.24	44.106073	44.106419	44.107573
162	42.45	43.061514	43.063578	43.063089
171	41.66	42.191767	42.195365	42.193396
182.3	40.68	41.047602	41.053336	41.049291
189	40.09	40.331979	40.339095	40.333698
195.8	39.51	39.565790	39.574404	39.567536
204.8	38.73	38.457496	38.468245	38.459271
211.5	38.15	37.507940	37.520399	37.509734
220.5	37.38	36.442502	36.142308	35.725957

Table A.2 Estimated voltage for each current level (case study 2)

Current (A)	$V_{FC,meas}$ (V)	$V_{FC,est}$ (SFLA)	$V_{FC,est}$ (ICA)	$V_{FC,est}$ (FOA)
0.60	29	28.997223	29.001417	28.993084
2.10	26.31	26.305937	26.307798	26.301435
3.58	25.09	25.093555	25.094224	25.089256
5.08	24.25	24.254620	24.254447	24.250678
7.17	23.37	23.375416	23.374433	23.372080
9.55	22.57	22.584615	22.583084	22.582041
11.35	22.06	22.071327	22.069605	22.069350
12.54	21.75	21.758463	21.756711	21.756882
13.73	21.45	21.461262	21.459553	21.460072
15.73	21.09	20.987741	20.986259	20.987190
17.02	20.68	20.694509	20.693271	20.694346
19.11	20.22	20.230985	20.230291	20.231390
21.20	19.76	19.770943	19.770945	19.771789
23	19.36	19.366024	19.366701	19.367081
25.08	18.86	18.866466	18.867889	18.867407
27.17	18.27	18.274720	18.276501	18.274690
28.06	17.95	17.953310	17.954837	17.952238
29.26	17.30	17.292877	17.292559	17.288378

References

[1] Jha SK, Puppala H. Prospects of renewable energy sources in India: prioritization of alternative sources in terms of Energy Index. Energy 2017;127: 116–27. 2017/05/15/.

[2] Al-Nassar WK, Neelamani S, Al-Salem KA, Al-Dashti HA. Feasibility of offshore wind energy as an alternative source for the state of Kuwait. Energy 2019;169:783–96. 2019/02/15/.

[3] Karamanev D, Pupkevich V, Penev K, Glibin V, Gohil J, Vajihinejad V. Biological conversion of hydrogen to electricity for energy storage. Energy 2017;129: 237–45. 2017/06/15/.

[4] Uzunoglu M, Alam MS. 33 - fuel-cell systems for transportations A2 - rashid. Muhammad H. In: Power electronics handbook. fourth ed. Butterworth-Heinemann; 2018. p. 1091–112.

[5] Soltani AK, Kandidayeni M, Boulon L, St-Pierre DL. Modular energy systems in vehicular applications. Energy Procedia 2019;162:14–23. 2019/04/01/.

[6] Blal M, Benatiallah A, NeÇaibia A, Lachtar S, Sahouane N, Belasri A. Contribution and investigation to compare models parameters of (PEMFC), comprehensives review of fuel cell models and their degradation. Energy 2019;168:182–99. 2019/02/01/.

[7] Chavan SL, Talange DB. Modeling and performance evaluation of PEM fuel cell by controlling its input parameters. Energy 2017;138:437–45. 2017/11/01/.

[8] Macias A, Kandidayeni M, Boulon L, Chaoui H. A novel online energy management strategy for multi fuel cell systems. In: 2018 IEEE international conference on industrial technology (ICIT); 2018. p. 2043–8.

[9] Kandidayeni M, Macias A, Amamou AA, Boulon L, Kelouwani S. Comparative analysis of two online identification algorithms in a fuel cell system. Fuel Cells 2018;18:347–58.

[10] Amamou A, Kandidayeni M, Boulon L, Kelouwani S. Real time adaptive efficient cold start strategy for proton exchange membrane fuel cells. Appl Energy 2018;216:21–30. 2018/04/15/.

[11] Kandidayeni M, Macias A, Boulon L, Kelouwani S. Optimized fuzzy thermal management of an open cathode fuel cell system. In: 2018 IEEE vehicle power and propulsion conference. VPPC); 2018. p. 1–6.

[12] Petrone R, Zheng Z, Hissel D, Pera MC, Pianese C, Sorrentino M, et al. A review on model-based diagnosis methodologies for PEMFCs. Int J Hydrogen Energy 2013;38:7077–91. 2013/06/10/.

[13] Etthir K, Boulon L, Becherif M, Agbossou K, Ramadan HS. Online identification of semi-empirical model parameters for PEMFCs. Int J Hydrogen Energy 2014;39:21165–76. 2014/12/12/.

[14] Wu J, Yuan XZ, Wang H, Blanco M, Martin JJ, Zhang J. Diagnostic tools in PEM fuel cell research: Part I Electrochemical techniques. Int J Hydrogen Energy 2008;33:1735–46. 2008/03/01/.

[15] Saadi A, Becherif M, Aboubou A, Ayad MY. Comparison of proton exchange membrane fuel cell static models. Renew Energy 2013;56:64–71. 2013/08/01/.

[16] Boulon L, Hissel D, Bouscayrol A, Pera M. From modeling to control of a PEM fuel cell using energetic macroscopic representation. IEEE Trans Ind Electron 2010;57:1882–91.

[17] Amphlett JC, Baumert RM, Mann RF, Peppley BA, Roberge PR, Harris TJ. Performance modeling of the Ballard Mark IV solid polymer electrolyte fuel cell. 1: mechanistic model development. J Electrochem Soc 1995:1–8. Medium: X; Size.

[18] Soltani M, Mohammad Taghi Bathaee S. Development of an empirical dynamic model for a Nexa PEM fuel cell power module. Energy Convers Manag 2010;51:2492–500. 2010/12/01/.

[19] Kandidayeni M, Macias A, Amamou AA, Boulon L, Kelouwani S, Chaoui H. Overview and benchmark analysis of fuel cell parameters estimation for energy management purposes. J Power Sources 2018;380:92–104. 2018/03/15/.

[20] Yang S, Wang N. A novel P systems based optimization algorithm for parameter estimation of proton exchange membrane fuel cell model. Int J Hydrogen Energy 2012;37:8465–76.

[21] Chakraborty UK, Abbott TE, Das SK. PEM fuel cell modeling using differential evolution. Energy 2012;40:387–99.

[22] Askarzadeh A, Rezazadeh A. An innovative global harmony search algorithm for parameter identification of a PEM fuel cell model. IEEE Trans Ind Electron 2012;59:3473–80.

[23] Sadollah A, Choi Y, Kim JH. Metaheuristic optimization algorithms for approximate solutions to ordinary differential equations. In: 2015 IEEE congress on evolutionary computation (CEC); 2015. p. 792–8.

[24] Tripathi S, Ikbal MA. Optimization of LMS algorithm for adaptive filtering using global optimization techniques. Int J Comput Appl 2015;132: 0975–8887.

[25] Zhao S, Huang B. On initialization of the Kalman filter. In: 2017 6th international symposium on advanced control of industrial processes. AdCONIP); 2017. p. 565–70.

[26] Priya K, Sathishkumar K, Rajasekar N. A comprehensive review on parameter estimation techniques for Proton Exchange Membrane fuel cell modelling. Renew Sustain Energy Rev 2018;93:121–44. 2018/10/01/.

[27] Mo Z-J, Zhu X-J, Wei L-Y, Cao G-Y. Parameter optimization for a PEMFC model with a hybrid genetic algorithm. Int J Energy Res 2006;30:585–97.

[28] Xu S, Wang Y, Wang Z. Parameter estimation of proton exchange membrane fuel cells using eagle strategy based on JAYA algorithm and Nelder-Mead simplex method. Energy 2019;173:457–67. 2019/04/15/.

[29] Chen Y, Wang N. Cuckoo search algorithm with explosion operator for modeling proton exchange membrane fuel cells. Int J Hydrogen Energy 2019;44:3075–87. 2019/01/28/.

[30] El-Fergany AA. Extracting optimal parameters of PEM fuel cells using Salp Swarm Optimizer. Renew Energy 2018;119:641–8.

[31] El-Fergany AA. Electrical characterisation of proton exchange membrane fuel cells stack using grasshopper optimiser. IET Renew Power Gener 2018;12: 9–17.

[32] Ali M, El-Hameed MA, Farahat MA. Effective parameters' identification for polymer electrolyte membrane fuel cell models using grey wolf optimizer. Renew Energy 2017;111:455–62. 2017/10/01/.

[33] Yang S, Chellali R, Lu X, Li L, Bo C. Modeling and optimization for proton exchange membrane fuel cell stack using aging and challenging P systems based optimization algorithm. Energy 2016;109:569–77.

[34] Turgut OE, Coban MT. Optimal proton exchange membrane fuel cell modelling based on hybrid Teaching Learning Based Optimization – differential Evolution algorithm. Ain Shams Engineering Journal 2016;7:347–60.

[35] Geem ZW, Noh JS. Parameter estimation for a proton exchange membrane fuel cell model using GRG technique. Fuel Cells 2016;16:640–5.

[36] Sun Z, Wang N, Bi Y, Srinivasan D. Parameter identification of PEMFC model based on hybrid adaptive differential evolution algorithm. Energy 2015;90: 1334–41.

[37] Restrepo C, Konjedic T, Garces A, Calvente J, Giral R. Identification of a proton-exchange membrane fuel cell's model parameters by means of an evolution strategy. IEEE Transactions on Industrial Informatics 2015;11:548–59.

[38] Rajasekar N, Jacob B, Balasubramanian K, Priya K, Sangeetha K, Sudhakar Babu T. Comparative study of PEM fuel cell parameter extraction using Genetic Algorithm. Ain Shams Engineering Journal 2015;6:1187–94.

[39] Priya K, Sudhakar Babu T, Balasubramanian K, Sathish Kumar K, Rajasekar N. A novel approach for fuel cell parameter estimation using simple Genetic Algorithm. Sustainable Energy Technologies and Assessments 2015;12: 46–52.

[40] Gong W, Yan X, Liu X, Cai Z. Parameter extraction of different fuel cell models with transferred adaptive differential evolution. Energy 2015;86:139–51.

[41] Niu Q, Zhang H, Li K. An improved TLBO with elite strategy for parameters identification of PEM fuel cell and solar cell models. Int J Hydrogen Energy 2014;39:3837–54.

[42] Gong W, Cai Z. Parameter optimization of PEMFC model with improved multi-strategy adaptive differential evolution. Eng Appl Artif Intell 2014;27:28–40.

[43] Cheng J, Zhang G. Parameter fitting of PEMFC models based on adaptive

differential evolution. Int J Electr Power Energy Syst 2014;62:189–98.

[44] Mann RF, Amphlett JC, Hooper MAI, Jensen HM, Peppley BA, Roberge PR. Development and application of a generalised steady-state electrochemical model for a PEM fuel cell. J Power Sources 2000;86:173–80. 2000/03/01/.

[45] Nguyen TV, White RE. A water and heat management model for proton-exchange-membrane fuel cells. J Electrochem Soc 1993;140:2178–86. August 1, 1993.

[46] Niya SMR, Hoorfar M. Determination of activation losses in proton exchange membrane fuel cells. 2014. V001T06A002.

[47] Khan MJ, Iqbal MT. Modelling and analysis of electro-chemical, thermal, and reactant flow dynamics for a PEM fuel cell system. Fuel Cells 2005;5:463–75.

[48] Correa JM, Farret FA, Canha LN, Simoes MG. An electrochemical-based fuel-cell model suitable for electrical engineering automation approach. IEEE Trans Ind Electron 2004;51:1103–12.

[49] Garg H. A hybrid PSO-GA algorithm for constrained optimization problems. Appl Math Comput 2016;274:292–305. 2016/02/01/.

[50] Eusuff M, Lansey K, Pasha F. Shuffled frog-leaping algorithm: a memetic meta-heuristic for discrete optimization. Eng Optim 2006;38:129–54. 2006/03/01.

[51] Fathy A, Rezk H. Parameter estimation of photovoltaic system using imperialist competitive algorithm. Renew Energy 2017;111:307–20. 2017/10/01/.

[52] Atashpaz-Gargari E, Lucas C. Imperialist competitive algorithm: an algorithm for optimization inspired by imperialistic competition. In: 2007 IEEE congress on evolutionary computation; 2007. p. 4661–7.

[53] Yang X-S. Chapter 8 - firefly algorithms. In: Nature-inspired optimization algorithms. Oxford: Elsevier; 2014. p. 111–27.

[54] SALEH IMM, ALI R, ZHANG H. Simplified mathematical model of proton exchange membrane fuel cell based on horizon fuel cell stack. Journal of Modern Power Systems and Clean Energy October 01 2016;4:668–79.

Contents lists available at ScienceDirect

Energy

journal homepage: www.elsevier.com/locate/energy

Corrigendum

Corrigendum to "Benchmark of proton exchange membrane fuel cell parameters extraction with metaheuristic optimization algorithms" [Energy 183 (2019) 912–925]

M. Kandidayeni [a, b, *], A. Macias [a, b], A. Khalatbarisoltani [a, b], L. Boulon [a, b], S. Kelouwani [c]

[a] Hydrogen Research Institute, Department of Electrical Engineering and Computer Science, Université du Québec à Trois-Rivières, Trois-Rivières, Québec, G9A 5H7, Canada
[b] Canada Research Chair in Energy Sources for the Vehicles of the Future, Canada
[c] Hydrogen Research Institute, Department of Mechanical Engineering, Université du Québec à Trois-Rivières, Trois-Rivières, Québec, G9A 5H7, Canada

The authors regret that the manuscript contains a typographical error in Eq. (7). The correct form of this equation is:

$$\begin{cases} V_{Act} = -[\xi_1 + \xi_2 \, T_{stack} + \xi_3 \, T_{stack} \, \ln(Co_2) + \xi_4 \, T_{stack} \, \ln(I_{FC})] \\ Co_2 = \dfrac{Po_2}{5.08 \times 10^6 \, \exp\left(-498/T_{stack}\right)} \end{cases}$$

(7)

Moreover, there had been a typographical error in the code of the previous version of the paper for the values of maximum current (I_{max}) and active area (A) to calculate J_{max}. The reported value for J_{max} in Table 7 should be changed to:

$$J_{max} = \frac{I_{max}}{A} = \frac{27 \, A}{52 \, cm^2} = 0.51923 \, A \, cm^{-2}$$

The reported I_{max} in the first line of page 921 should be changed to 27 A. Due to this typographical error, the authors needed to update the parameters in Table 8 and Table 9 and as a result replot Figs. 7–10. It should be noted that the mentioned typographical errors have not changed the conclusion or the discussion of the paper results. The only reason that the authors have updated all the data is to make this work reproducible for the researchers who want to use the provided data in their research projects. The authors would like to apologise for any inconvenience caused. Hereinafter, the updated tables and figures are presented.

Table 7 The characteristics of the Horizon 500-W open cathode PEMFC.

Technical specification	
Type of FC	PEM
Rated Power	500 W
Rated performance	22 V @ 23.5 A

(*continued*)

Technical specification	
Max Current (brand new)	42 A
Rated H2consumption	7 SLPM
Ambient temperature	5 to 30 °C
Max stack temperature	65 °C
Cooling	Air (integrated cooling fan)
Reactants	Hydrogen and Air
N_{cell}	36
P_{H2}	0.55 atm
P_{O2}	1 atm
A	52 cm^2
l	25 μm
Actual J_{max}	0.51923 A cm^{-2}

Table 8: The identified parameters and the obtained fitness value for 500-W Horizon PEMFC.

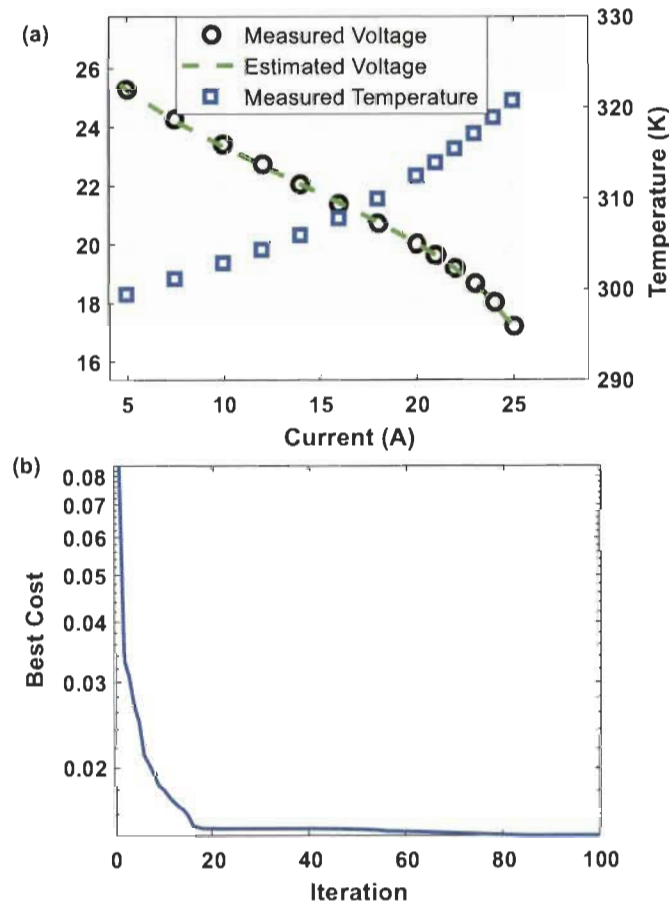| Parameter	Estimated value by SFLA
ξ_1	−0.8532
$\xi_2 \times 10^{-3}$	2.698
$\xi_3 \times 10^{-5}$	9.136174
$\xi_4 \times 10^{-5}$	−16.1
$R_C (\Omega) \times 10^{-4}$	7.999
λ	13
β (V)	0.048504
Best fitness	0.01444

Fig. 7: 500-W Horizon PEMFC case study: a) estimated polarization curve by SFLA, b) fitness function (SSE) minimization trend comparison.

Table 9: The steady-state characteristics of the 500-W Horizon PEMFC.

Current (A)	$V_{FC\,meas}$ (V)	$V_{FC.est}$ (SFLA)	|Residual|	Temperature (K)
0.6	29.370000	29.4951	0.125191	296.200000
2.5	26.777390	26.8104	0.033025	297.810917
5	25.290250	25.2894	0.000774	299.520062
7.5	24.281859	24.2381	0.043659	301.227449
10	23.418000	23.3590	0.058951	302.950000
12	22.739103	22.7106	0.028503	304.404279
14	22.058523	22.0792	0.020775	306.006926
16	21.386148	21.4420	0.055883	307.842680
18	20.721728	20.7738	0.052142	309.994399
20	20.026000	20.0395	0.013585	312.532000
21	19.636350	19.6297	0.006596	313.961094
22	19.191807	19.1748	0.016932	315.501399
23	18.663630	18.6524	0.011152	317.153087
24	18.015227	18.0208	0.005577	318.913454
25	17.201250	17.1865	0.014695	320.776562

Fig. 10: Performance validation of the tuned PEMFC model for the Horizon 500-W PEMFC case study: a) the current profile applied to the real PEMFC and the corresponding measured temperature, and b) the comparison of the estimated and measured voltage.

Minimum best fitness value = 0.0144
Maximum best fitness value = 0.0185
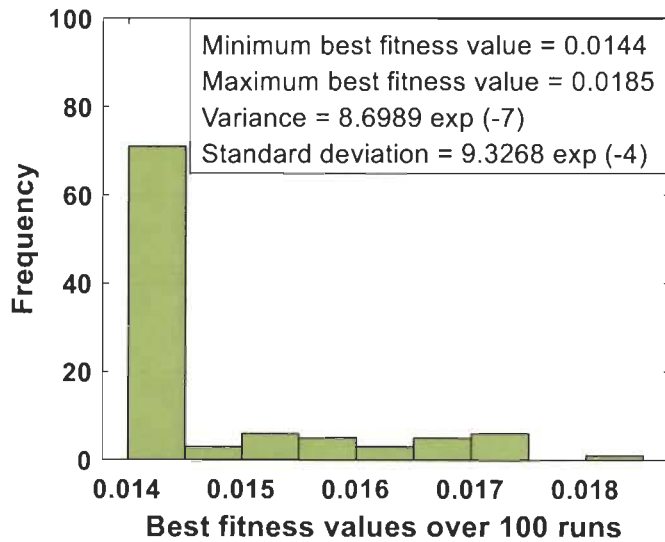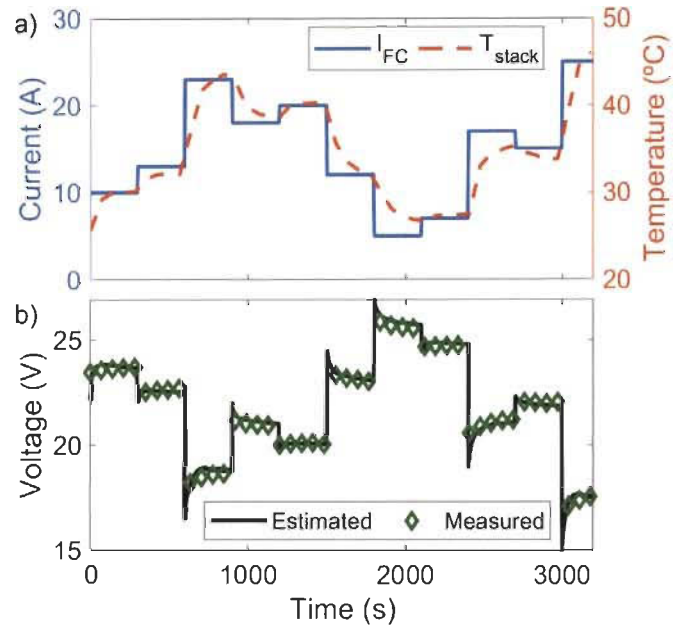Variance = 8.6989 exp (-7)
Standard deviation = 9.3268 exp (-4)

Fig. 8: The histogram analysis of SFLA.
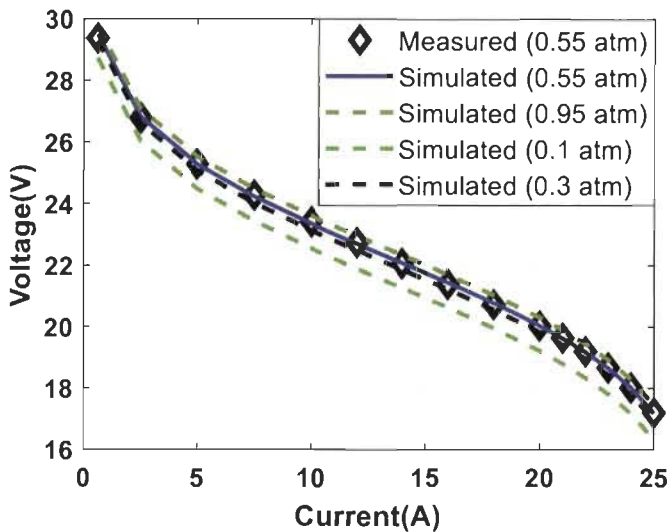
Fig. 9: Polarization behaviour analysis in different partial pressures of hydrogen.

4.3 **Enhancing the Performance of Kalman Filter for Online Identification of a Fuel Cell Semi-Empirical Model**

Earlier in this thesis, it was shown that KF is a powerful tool for parameter estimation of a semi-empirical PEMFC model. However, special attentions need to be paid to the initialization of this filter before its implementation in such a problem. The principal purpose of this section is to use the selected metaheuristic optimization algorithm in Article 3 (SFLA) for tuning the initial parameters of the PEMFC model as well as KF variables for online estimation of the PEMFC characteristics.

4.3.1 Methodology

This section proposes the employment of a new metaheuristic optimization technique, SFLA, for the initialization and customization of KF in the online parameter identification of a FC semi-empirical model. To do so, firstly, the SFLA is used offline to find the right initial values for the parameters of the semi-empirical model proposed by Amphlett et al. using the available data regarding the polarization curve of the FC system. Subsequently, the metaheuristic technique tunes the covariance matrices of KF (R and Q), while utilizing the obtained initial values in the first step. Finally, the tuned KF is used online to deal with the uncertainties and update the parameters of the FC model. Since the tuning process of KF is performed once before its implementation in the real FC system, the online identification will not be affected by the computational time of the optimization process. The tuning process is composed of finding a set of parameters for the PEMFC semi-empirical model and initializing the covariance matrices of the KF. After initializing the KF offline, it is used online to keep track of performance drifts in the PEMFC system. Figure 4.3 represents the

overall picture of the explained tuning procedure as well as the online model identification of the FC system.
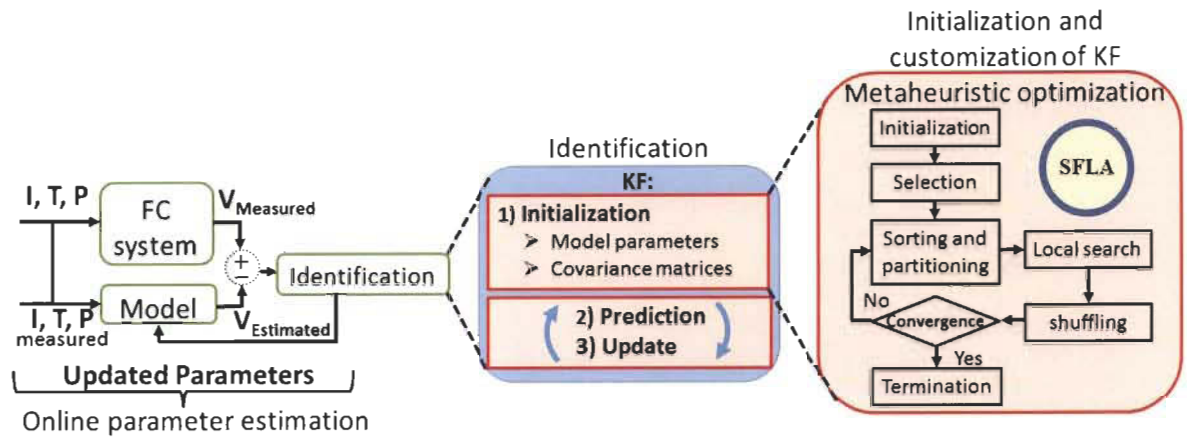

Figure 4.3   The tuning process of KF for online PEMFC parameters estimation.

4.3.2   *Synopsis of the results analysis*

To show the effectiveness of the proposed tuning process for online parameter estimation of a FC system, some simulations based on experimental data are performed and explained in this section. The polarization curve experimental data used in this section are the same as the ones in Article 3. Therefore, to avoid the repetition of the figures, the polarization curve and the optimization trend for finding the initial values of the PEMFC model are not shown here and they are available in Article 3.

After finding the initial values for the PEMFC model parameters, another optimization is performed to determine the suitable values for covariance matrices. Figure 4.4 represents the improvement trend of the MSE objective function for finding the right values for Q and R matrices of KF. As it can be observed, the MSE value has decreased from almost 5.7904e-05 to 4.3246e-05. Although this value is small, it approximately represents 25% improvement compared to the case that R and Q are assumed as 1.
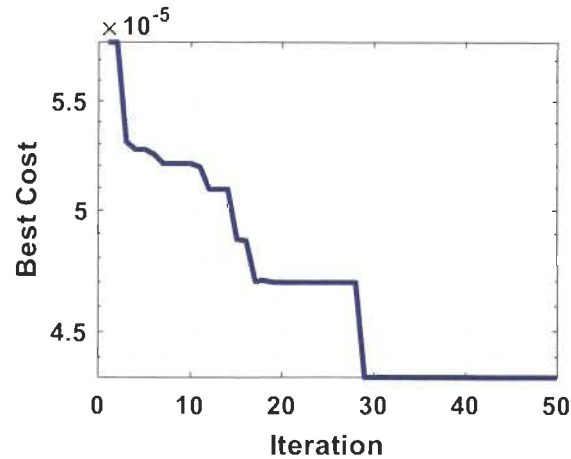
Figure 4.4   MSE objective function minimization trend for funding Q and R matrices.

The obtained initial values for the PEMFC model parameters and KF variables are listed in Table 1 along with the imposed inequality constraints. The presented current profile in Figure 4.5a has been imposed to the 500-W Horizon PEMFC and its corresponded temperature and voltage have been measured and recorded to verify the performance of KF in online parameter extraction of the described semi-empirical PEMFC model. The temperature variation of the PEMFC stack is also shown in Figure 4.5a. Figure 4.5b compares the estimated voltage online by the KF with the measured voltage of the PEMFC. From Figure 4.5b, it is clear that the estimation has a good quality. Figure 4.5c and Figure 4.5d represent the estimated polarization curves and power curves of the PEMFC for two cases of initial parameters based on the datasheet information and the obtained optimal initial conditions by SFLA. As is seen, the optimal initial condition leads to more accurate results specially in activation and concentration zones. Moreover, accurate characteristics estimation is achieved quicker and more conveniently when starting with the appropriate initialization. This can be very interesting in applications that the fast prediction of the maximum power is needed such as PEMFC cold-start up.

Table 4-1   The obtained parameters after the tuning process

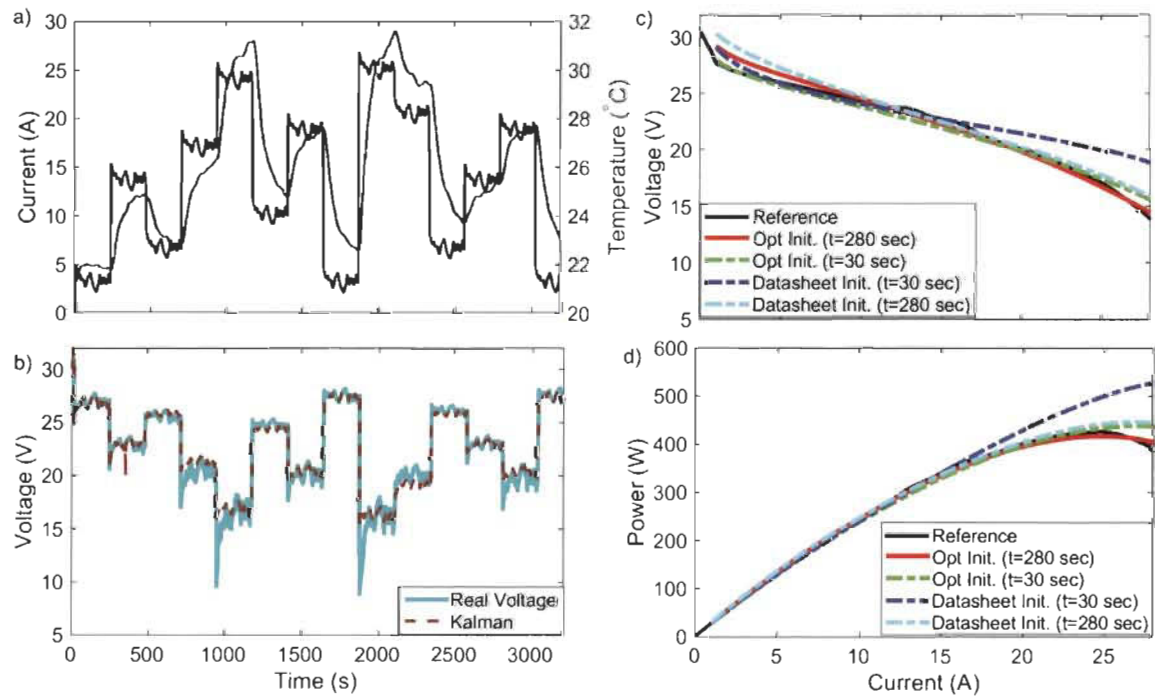| Optimization process	Obtained value	Minimum value	Maximum value
First optimization	$\xi_1 = -1.1316$	-1.2	-0.80
	$\xi_2 = 2.603e\text{-}3$	1e-3	5e-3
	$\xi_3 = 5.859e\text{-}5$	3.6e-3	9.8e-3
	$\xi_4 = -9.04e\text{-}5$	-2.6e-4	-0.954e-4
	$R_{internal} = 0.18$	0.16	0.22
	$B = 0.155$	0.0135	0.5
Second optimization	$Q = 0.00536$	1e-15	100
	$R = 84.38112$	1e-15	100

Figure 4.5   a) Current profile and stack temperature variation, b) Voltage estimation by KF, c) Polarization curve estimation, d) Power curve estimation.

4.4   Conclusion

This chapter puts forward the employment of an optimization algorithm for initialization of the KF to estimate the parameters of a PEMFC stack online.

In this respect, firstly, a benchmark study of different metaheuristic algorithms is performed for three different case studies. As a result, SFLA is selected as a trustworthy algorithm for the parameters extraction of a PEMFC model. Secondly, SFLA is used for the the initialization of KF is in two steps of finding the right primary values for the targeted PEMFC model, and tuining the values of R and Q covariance matrices. The final results of this work confirm that a good initilaization can improve the estimation quality in terms of speed and precision. In fact, finding the appropriate initial values for the PEMFC model parameters of interest leads to estimating better characteristics curves in a shorter time and tuning of the covariance matrices enhances the estimation accuracy to a certain level. The focus of this chapter has been mainly in the parameter extraction in the ambient temperature. However, the outcomes seem to be very interesting in applications where a fast performant identification is required. In this regards, future works should focus on the utilization of such strategy for performanig the adaptive cold start-up of the PEMFC stack.

The results of this chapter confirm the practicality of the developed online model and the suggested initialization approach. Next chapter will discuss the design of a systemic management strategy for the PEMFC stack and, as an example, put forward two EMSs which use the systemic management and the online modeling for upgrading the efficiency of the system.

Chapter 5 - Systemic management of a fuel cell system and its inclusion into a real-time energy management strategy design

5.1 Introduction

To reach the ultimate goal of the thesis, which is having an EMS considering the online modeling and systemic management of the PEMFC stack, this chapter proposes a PEMFC systemic management of current and temperature in the first place. Subsequently, this systemic management is integrated into the design of a real-time EMS to assess the fuel economy improvement.

The proposed systemic management aims at delivering the requested power with high efficiency. In fact, the output power of the PEMFC is dependent on different operating points such as temperature, current, and pressure. By regarding the PEMFC as a system, the mentioned operating points can come under control. In each power level, a reference value for the temperature and current can be assigned to acquire the optimal efficiency, by the assumption of having a constant pressure. This reference value is like an equilibrium point in which all the influential operating conditions are stable. A specific level of demanded power can be supplied by different combinations of these operating conditions and how to go towards selecting the right combination for having an efficient performance is the main goal of the proposed systemic management. Unlike the other similar works, the proposed approach capitalizes on the usage of both thermal management strategy and current control to meet the requested power from the system by the minimum fuel consumption.

Regarding the EMS integration, the main objective is to put forward a new EMS for boosting the energetic efficiency of a FCHEV based on performing an online systemic management of the PEMFC system. One important aspect that has escaped the attention of many researchers in the domain of EMS design for FCHEVs is adopting a systemic approach towards the management of the PEMFC stack while developing a strategy. The existing EMSs normally define the required current/power from the PEMFC stack. Nonetheless, the integration of the systemic management of PEMFC stack (current and temperature) into the design of an EMS leads to the determination of two or more reference signals by the EMS. This strategy capitalizes on the concurrent regulation of power and temperature which have very different dynamic behavior.

Hereinafter in this chapter, the development of a concurrent temperature and current management scheme is done first thorough the presentation of an article entitled ''Efficiency Enhancement of an Open Cathode Fuel Cell through a Systemic Management''. Subsequently, the integration of the proposed systemic management into the formulation of an online EMS is dealt with in an article entitled ''Efficiency Upgrade of Hybrid Fuel Cell Vehicles' Energy Management Strategies by Online Systemic Management of Fuel Cell''. Finally, a conclusion is drawn.

5.1 Article 4: Efficiency Enhancement of an Open Cathode Fuel Cell through a Systemic Management

Authors: M. Kandidayeni, A. Macias, L. Boulon, and S. Kelouwani

Journal: IEEE Transactions on Vehicular Technology (published)

Publication date: 28/September/2019 (Doi: 10.1109/TVT.2019.2944996)

5.1.1 Methodology

This paper presents a methodology to formulate a systemic management for an open cathode PEMFC. To do so, two important stages of management, to determine the reference signals, and control, to reach them, are required. In the proposed systemic management, depending on the requested power level, a reference temperature is extracted through a generated 3D power map which enables the supply of the power with the lowest current. The lower the current level, the lower the hydrogen consumption. This map is obtained through experimental data and its functionality is to relate the requested power form the PEMFC to its operating temperature and current. Subsequently, a temperature controller is used to reach the assigned reference temperature, while the current of the PEMFC is controlled by a PI controller. The temperature control is formulated by an optimized fuzzy logic scheme to reach the determined reference temperature by acting on the cooling fan of the PEMFC system, whilst the current is being regulated by its controller. The inputs of the fuzzy controller are the PEMFC current and temperature error and the sole output is the duty factor of the fan. The proposed methodology is tested on an experimental test bench to be better evaluated in a real condition. The general structure of the temperature and current control is presented in Figure 5.1. As it is seen, in a hybrid system, the PEMFC deals with supplying the average power and the dynamic part is left to the battery pack or other energy storage systems. For each requested power level from the PEMFC system, a specific reference temperature (T_{ref}) is set through the power map. This T_{ref} is imposed to a FLC which acts on the cooling fan to reach it. However, the temperature regulation is a slow dynamic process, contrary to the current control which is very fast. In this regard, while the FLC is trying to regulate the temperature, a PI power controller is used to give the PEMFC system enough

relaxation time for efficient supply of the power by gaining the T_{ref} which corresponds to the minimum current. As the FLC increases or decreases the temperature to reach the set point, depending on the initial stack temperature, the PI controller regulates the PEMFC current in a way to track the requested power.
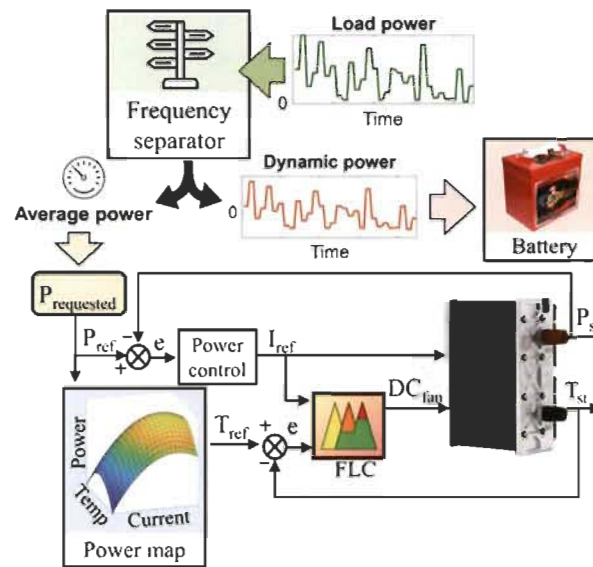

Figure 5.1 Configuration of the systemic temperature and current management and control.

5.1.2   *Synopsis of the results analyses*

Two assessment tests are designed to show the efficiency of the proposed systemic management. The first test deals with supplying a constant power profile, and the second test copes with variable power profile. In each stage, the performance of the proposed approach is compared with the commercial controller from manufacturer.

The obtained results of supplying a constant power of 380 W shows that by using the proposed thermal scheme, a lower current level is required to meet the demanded power, compared to the manufacturer controller. It is worth noting that achieving the same level of

power by using different current levels in this test highlights the importance of the thermal management. The commercial controller tends to keep the stack temperature at a higher level than the proposed approach. This higher temperature can result in a dryer membrane and less available oxygen for reaction. Moreover, the proposed systemic control consumes less hydrogen (4.47 SLPM) for providing the requested constant power profile as opposed to the manufacturer controller (5.35 SLPM).

The second test, which belongs to a variable power profile, contains various high and low levels and indicates more clearly the performance of the proposed thermal strategy in different conditions. The outcomes of this test indicate that both of controllers are able to provide the demanded power. However, the temperature evolution of the PEMFC stack by each of the controllers is different. The required current levels for supplying the power are also different. Both of the controllers tend to use the same current in low power levels. However, in high power levels, the proposed strategy uses less current to meet the power. The effect of using a lower current level to satisfy the requested power can be embraced by checking the hydrogen consumption.

The comparison of the total hydrogen consumption of the discussed constant and variable power profiles for the case of commercial controller and the proposed systemic strategy are shown in Figure 5.2. From this figure, the proposed strategy of this work is able to decrease the hydrogen consumption of the PEMFC system by 16% and 13% for the case of constant and variable power profiles respectively.
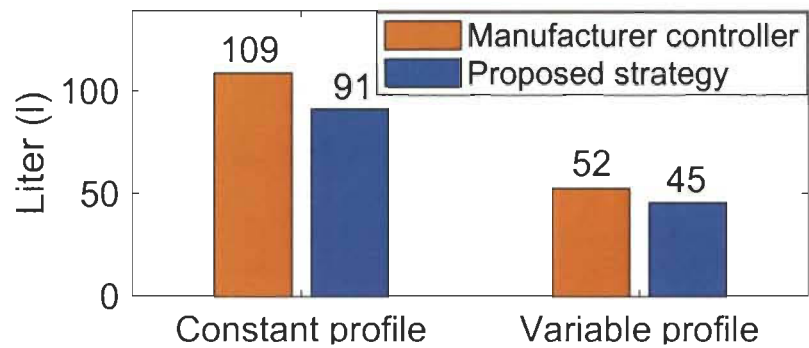
Figure 5.2 Hydrogen consumption comparison of the PEMFC system for different

scenarios.

Efficiency Enhancement of an Open Cathode Fuel Cell Through a Systemic Management

Mohsen Kandidayeni, *Student Member, IEEE*, Alvaro Macias F., *Student Member, IEEE*,
Loïc Boulon, *Senior Member, IEEE*, and Sousso Kelouwani, *Senior Member, IEEE*

Abstract—This paper addresses the design of a systemic management to improve the energetic efficiency of an open cathode proton exchange membrane fuel cell (PEMFC) in a hybrid system. Unlike the other similar works, the proposed approach capitalizes on the usage of both thermal management strategy and current control to meet the requested power from the system by the minimum fuel consumption. To do so, firstly, an experimentally based 3D mapping is performed to relate the requested power form the PEMFC to its operating temperature and current. Secondly, the reference temperature which leads to gaining the demanded power by the minimum current level is determined to minimize the hydrogen consumption. Finally, the temperature control is formulated by an optimized fuzzy logic scheme to reach the determined reference temperature by acting on the cooling fan of the PEMFC system, whilst the current is being regulated by its controller. The inputs of the fuzzy controller are the PEMFC current and temperature error and the sole output is the duty factor of the fan. The proposed methodology is tested on an experimental test bench to be better evaluated in a real condition. The obtained results from the proposed systemic management indicate promising enhancement of the system efficiency compared to a commercial controller. The proposed method of this work is extendable and applicable in fuel cell hybrid electric vehicles.

Index Terms—Fuel cell efficiency improvement, fuzzy logic control, optimization, power mapping, systemic management, thermal management strategy.

I. INTRODUCTION

PROTON exchange membrane fuel cell (PEMFC) is perceived as a promising technology for green and efficient generation of power in stationary and transportation applications [1]. In the literature, the performance of a PEMFC has been improved by concentrating on two principles of membrane electrode assembly design and system design. The first one

includes modifying the material and structural properties of the gas diffusion layer, cathode catalyst layer, and membrane to operate in the existence of liquid water [2]–[4]. The second one involves proper flow field design of channels, which can upgrade the performance in a passive manner by, for instance, balancing the cooling fan effects and air flow for reaching complete reactions at the cathode leading also to a better water balance. Moreover, it includes operating condition control, anode water removal, and electro-osmotic pumping [5], [6]. The output power of the PEMFC is dependent on different operating points such as temperature, current, and pressure [7]–[9]. Regarding the PEMFC as a system provides several degrees of freedom in terms of supplying the power due to the fact that the mentioned operating points, which are influential in the performance of the PEMFC, can come under control in this way. A specific level of demanded power can be supplied by different combinations of these operating conditions and how to go towards selecting the right combination for having an efficient performance is the goal of this work. The temperature of a PEMFC stack has an impact on the electrochemical, thermodynamics, electro-kinetics, transport, and water distribution processes, which jointly dictate system efficiency and long-term durability [10]. This is significant in all sorts of PEMFCs and operating modes, but is chiefly relevant to air-breathing/cooled PEMFCs where the input air is responsible for both reactant and cooling the system [11]. The increase of the fan speed enhances the reactant supply, decreases the temperature (depending on the ambient temperature), and may also lead to a dry membrane (depending on the air humidity). The combination of these three effects can result in various impacts on power and hydrogen consumption which are difficult to highlight with an analytical model. The proton exchange membrane and the ionomer in the porous catalyst layers of this type of PEMFC need the presence of a particular amount of water to ensure satisfactory protonic conductivity. The water content in the ionomer of the membrane and catalyst layers is deeply affected by the operating temperature of the stack. The dynamics of water absorption of the ionomer and the diffusion of water across the membrane are both dependent on the stack temperature as discussed in [12], [13]. In fact, the temperature influence over the water transport in the catalyst layers is primarily premised on the absorption and desorption of water in the ionomer as well as the condensation and evaporation in the pores. As discussed in [14], the active area of membrane is directly affected by the water content in the catalyst layer. If the catalyst layer becomes dry

owing to the water drain from its pores, less protons arrive at the active sites for the electrochemical reaction with the reactant gases and the electrons. This phenomenon in turn diminishes the PEMFC performance [15]. In this respect, the optimal management of temperature is critical in open cathode PEMFCs to avoid the occurrence of the discussed phenomena and enhance the efficiency of the system. In each power level, a reference value for the temperature and current can be assigned to acquire the optimal efficiency, by the assumption of having a constant pressure. This reference value is like an equilibrium point in which all the influential operating conditions are stable. Another important factor which particularly influences the performance of an open cathode PEMFC is the cooling fan operation which has a vital role in the occurrence of drying and flooding and also electrochemical reactions [16].

Several researches have been conducted on the temperature regulation of a PEMFC system. Many of these studies have used PID controllers for thermal management. The temperature behavior of a closed-cathode PEMFC equipped with liquid cooling is controlled through a feedback PID control in [17], and a PI controller in [18], [19]. A standard PID controller along with an ON/OFF switch are used for thermal management in a 3-kW water-cooled PEMFC in [20]. A state feedback control [21] is compared in simulation with a model reference adaptive control in terms of regulating the temperature of a closed-cathode PEMFC and concluded that the second method shows more robustness in [22]. In [23], [24], two controllers based on active disturbance rejection are proposed to regulate the temperature of a closed-cathode and an open-cathode PEMFC respectively. Both of these controllers have shown successful performance in simulation. In [25], a 500-W open-cathode PEMFC model is studied in which the temperature is controlled by an on-off strategy.

Literature consideration indicates that most of the discussed papers are fundamentally premised on simulation and furthermore, very few works have focused on open cathode PEMFCs. In [26], [27], the performance of two fuzzy logic controllers (FLCs) have been compared with PID controllers on an experimental test bench regarding the temperature regulation of a 2000-W and a 100-W open cathode PEMFC respectively. The authors have shown that the PID controllers cause large temperature overshoot in different operating conditions compared to the FLC. Two reasons can be given to explain the overshoot problem. First, PID controllers work well for a limited operating range. Second, their adjustment is dependent on the accuracy of the model, which is an ongoing research domain in the PEMFC area. Therefore, FLC seems to be a good choice since it shows better flexibility in a wide range of operation while working with not very accurate models.

Another worth reminding aspect is that very few works have tried to propose a methodology to create a link between the temperature control and the operating point tracking of a PEMFC, such as maximum power and efficiency points. These operating conditions are abundantly used in vehicular applications [28]–[30], and they are only conceivable in particular stable operating temperature. In [31], a simple single-input single-output FLC is used to control the temperature for finding the maximum efficiency point of an open cathode PEMFC. In the majority
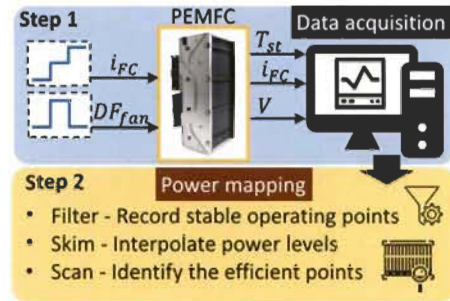

Fig. 1. Experimental procedure for generating the power map.

of the existent maximum operating point tracking methods, from perturb and observe and step size methods [32], [33] to identification techniques coupled with an optimization method [34]–[38], the PEMFC has been considered as just a component in which the only reference signal (control variable) is the operating current by assuming constant temperature and/or pressure. However, PEMFC is a system, and several local controls should be defined over this system to reach the desired condition.

This paper presents a methodology to formulate a systemic management for an open cathode PEMFC. The main contribution of this work is to simultaneously control temperature and current with the goal of supplying the requested power from the PEMFC system with a high level of efficiency. To do so, two important stages of management, to determine the reference signals, and control, to reach them, are required. In the proposed systemic management, depending on the requested power level, a reference temperature is extracted through a generated 3D power map which enables the supply of the power with the lowest current. The lower the current level, the lower the hydrogen consumption. Subsequently, an optimized FLC is used to reach the assigned reference temperature, while the current of the PEMFC is controlled by a PI controller. In contrast to [26], [27] in which the FLCs have been adjusted by many trials and errors, the utilized FLC is tuned by a hybrid optimization algorithm in this paper. The FLC is first tested on a PEMFC model before implementation on the test bench. The remainder of this manuscript is organized as follows:

Section II deals with the process of obtaining the power map. Determining the reference operating point is dealt with in Section III. Section IV describes the formulation of the optimized fuzzy controller. The results are discussed in Section V, and finally the conclusion is given in Section VI.

II. 3D POWER MAPPING

This section puts forward an experimental framework to determine the output power of a PEMFC by considering the influence of operating current, temperature, and cooling fan duty factor while the air pressure is constant in this set-up. To do so, two steps of data collection, and power map generation are required as shown in Fig. 1. Initially, some tests need to be conducted on the open cathode PEMFC to analyze the influence of operating current and duty factor over the stack temperature. The presented test bench in Fig. 2 is used to perform all the experiments in this work.
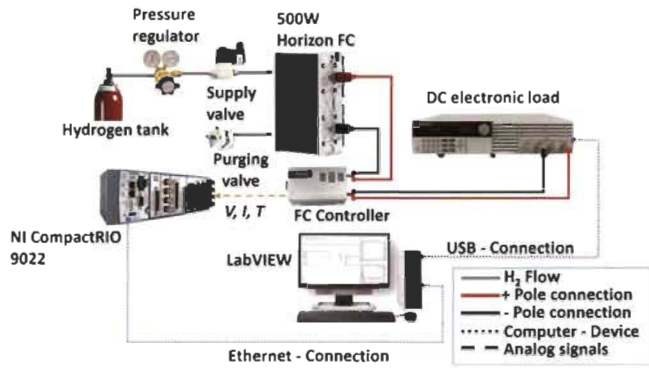
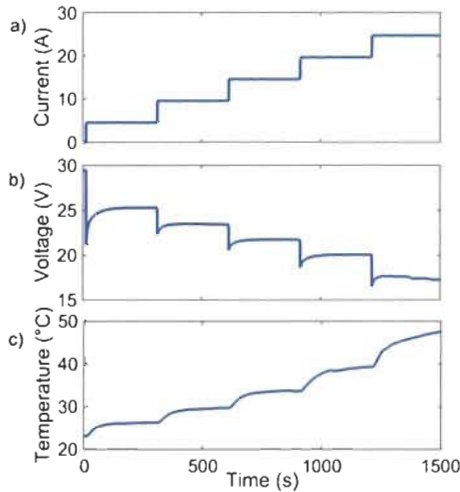Fig. 2.   The developed test bench in Hydrogen Research Institute.

Fig. 3.   Ramp-up current profile (a) and its corresponding recorded voltage (b) and temperature (c).

Fig. 4.   Influence of operating current and fan duty factor over the stack temperature.

Fig. 5.   Generated power map from experimental data.

The utilized fuel cell system in this set-up is the commercially available 500-W PEMFC with 36 cells from Horizon Fuel Cell Technologies. This open-cathode PEMFC is self-humidified and air- cooled. It has two axial cooling fans straightly connected to the housing, which decrease the temperature of the stack by forced convection and in the same time provides oxygen to the cathode. As it is seen, the open-cathode PEMFC is connected to a National Instrument CompactRIO through a controller. A DC electronic load is utilized to request current profiles from the PEMFC. According to the manual of the system, the difference between the atmospheric pressure in the cathode side and the pressure of the PEMFC in the anode side should be 50.6 kPa. The pressure in the anode side is set to 55.7 kPa. The temperature and voltage of the real PEMFC are measured and transferred to the PC with the help of CompactRIO to be used in the control process. The PC and CompactRIO communicate by means of an Ethernet connection every 100 milliseconds. It is worth mentioning that the proposed methodology of this work is expandable to other PEMFC types with higher or lower power rates due to its data-driven foundation.

To acquire the necessary data for power mapping, a ramp-up current profile, as shown in Fig. 3(a), is applied to the PEMFC system in five different fan duty factors, namely 0.25, 0.34, 0.5,
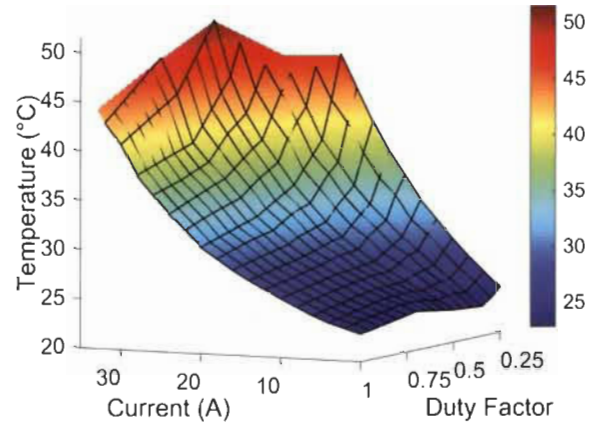
0.7, and 1. At each level of fan duty factor, the test is continued until the maximum power of the PEMFC is achieved, and the voltage drop due to the concentration loss is observed. After completing the test, the recorded stable points of the PEMFC stack (current, voltage, and temperature), as shown in Fig. 3, are used to plot the map. Since the chosen current and fan duty factors contain the minimum and maximum levels, the acquired map covers almost all the operating conditions.

Fig. 4 characterizes the influence of cooling fan and current on the stack temperature of the PEMFC. This figure has been generated by using the collected data from the conducted experiments. Fig. 5 presents the obtained power map from the experimental measurements. This power map is used to determine the reference temperature for the systemic management process.

III. REFERENCE OPERATING POINT DETERMINATION

As shown in Fig. 5, a given power can be reached by using several operating points like temperature and current. So, a degree of freedom remains. In this work, current and temperature are considered as the main variables and the objective is to meet a requested power while minimizing the hydrogen consumption of the system. Fig. 6, which has been obtained by doing some experiments on the real PEMFC, indicates two important interdependences. First, the relation of hydrogen consumption
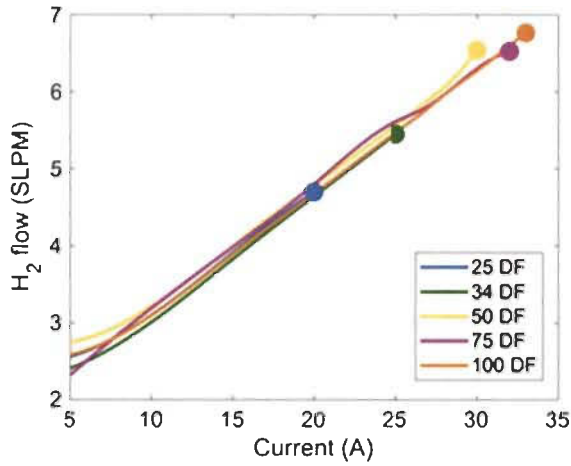
Fig. 6. Effect of current and cooling fan duty factor on the hydrogen consumption and operating range of the stack.
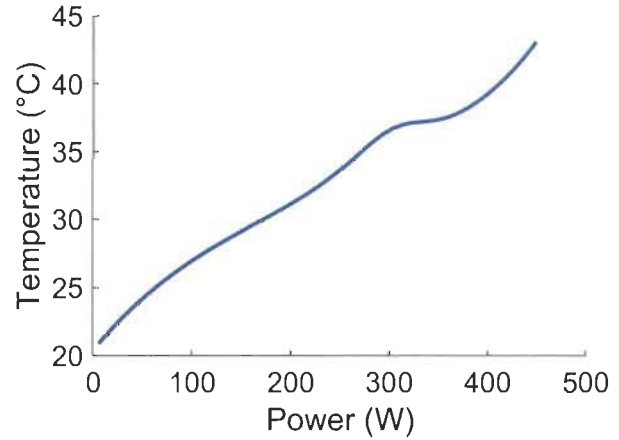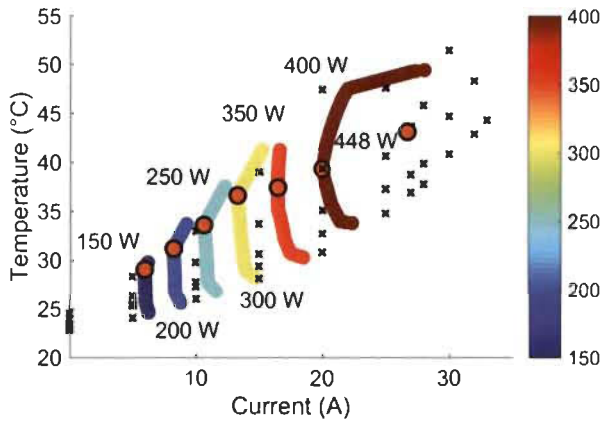

Fig. 8. Power versus optimal temperature.

Fig. 7. 2D demonstration of PEMFC power map for different levels of temperature and current.
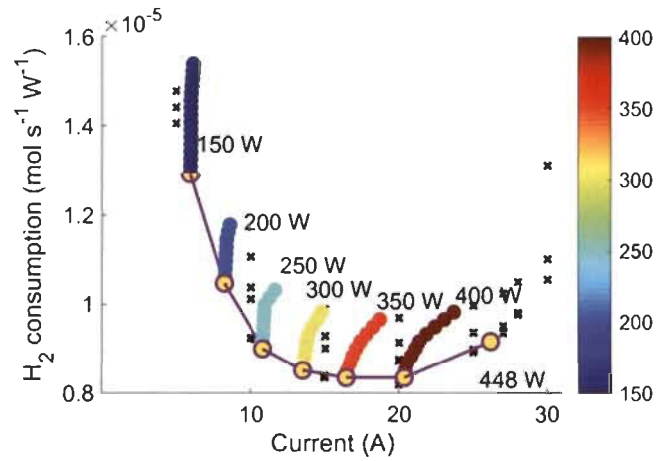

Fig. 9. Hydrogen consumption and required current for each specific power level.

with respect to the operating current and fan duty factor, and second, the influence of the fan duty factor over the operating range of the PEMFC stack in terms of current. As is seen in this figure, hydrogen consumption is significantly dependent on the operating current of the stack rather than the fan duty factor. However, fan duty factor plays an important role in determining the range of the stack operating current where lower duty factors lead to limited operating ranges and higher duty factors extend the range of stack operation.

The behavior of the hydrogen molar flow (f_{H2}) can be estimated by (1) [39]:

$$f_{H2} = a\, i_{fc} + b\, DF_{fan} + c \qquad (1)$$

where i_{fc} is the PEMFC operating current (A) and DF_{fan} is the cooling fan duty factor.

Fig. 7 represents the 2D power map attained through the explained methodology by doing interpolation. For each power, the best operating point (temperature and current) in terms of H2 consumption is highlighted by a circle. These points lead to an optimal path to reach the requested power by minimizing the H2 consumption. The presented power map belongs to the fuel

cell system, which means that the auxiliary power consumptions such as valves and the fan have been subtracted from the stack power. This map also shows that a specific function can be generated to relate the power and optimal temperature. This relation is represented in Fig. 8 and is used to determine the reference temperature of the controller to match the requested power and the minimal hydrogen consumption. Providing such experimental basis guaranties that the controller leads to a high efficiency region at each specific power level.

Fig. 9 confirms that each selected optimal point, presented in the power map of Fig. 7, corresponds to the minimum hydrogen consumption and mathematically the interpolated lines in each power level can be considered as a convex problem which has only one minimum. It should be noted that one of the advantages of the proposed method for determining the reference temperature is that it is easily updatable with respect to the performance drifts of the PEMFC stack arising from the ambient conditions variation and even ageing phenomenon. In this respect, the map can be easily updated by recording some stable points (current, voltage, and temperature) from different operation zones of the PEMFC stack and using them for generating a new map with the commonly used least square approaches.
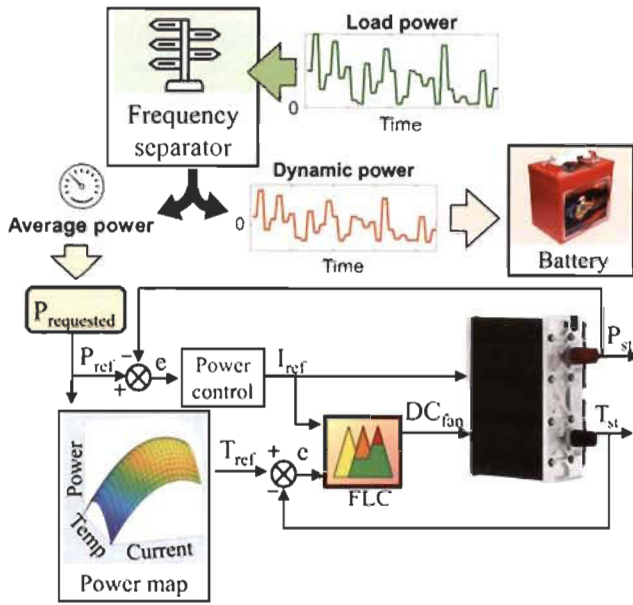
Fig. 10.   Configuration of the systemic temperature and current management and control.

e \ I_{ref}	Low	Medium	High
Hot	Very Fast	Very Fast	Very Fast
Warm	Average	Fast	Very Fast
Normal	Slow	Slow	Fast
Cold	Very Fast	Slow	Slow
Very Cold	Very Fast	Very Fast	Slow

Fig. 11.   PEMFC system model.

IV.   TEMPERATURE AND CURRENT CONTROL

The general structure of the temperature and current control is presented in Fig. 10. As it is seen, in a hybrid system, the PEMFC deals with supplying the average power and the dynamic part is left to the battery pack or other energy storage systems. For each requested power level from the PEMFC system, a specific T_{ref} is set through the obtained 2D power map. This T_{ref} is imposed to a FLC which acts on the cooling fan to reach it. However, the temperature regulation is a slow dynamic process, contrary to the current control which is very fast. In this regard, while the FLC is trying to regulate the temperature, a PI power controller is used to give the PEMFC system enough relaxation time for efficient supply of the power by gaining the T_{ref} which corresponds to the minimum current. As the FLC increases or decreases the temperature to reach the set point, depending on the initial stack temperature, the PI controller regulates the PEMFC current in a way to track the requested power.

The explained FLC for temperature regulation of the PEMFC uses the temperature error and the reference current of the PEMFC as inputs and determines the fan duty factor as the output. The obtained fan duty factor from the FLC is sent to the real PEMFC to warm up or cool down the system. The temperature error is the difference between the stack temperature and the reference temperature obtained from the explained power map. The reference current signal, which strikingly influences the PEMFC stack performance, is determined by a PI controller. The input of the PI controller is the error between the requested power from PEMFC and the supplied power by PEMFC, and the output is the current, which will be the input of the fuzzy controller. Using this PI regulator ensures that the requested power is met. The characteristics of the FLC are as follows: inference engine is AND (minimum operator), diffuzication is
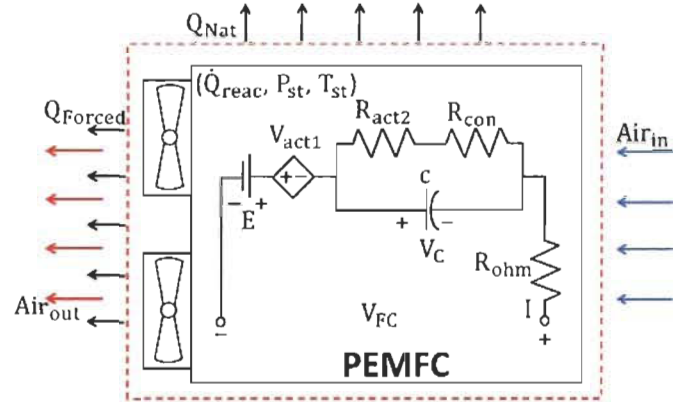
centroid, and fuzzy system type is Mamdani. Table I specifies the fuzzy reasoning rules.

A.   Fuzzy Optimization

Since the distribution of input membership functions (MFs) has been considered as consistent over the universe of discourse, the FLC might not perform optimally over various operating conditions of the PEMFC. In this regard, instead of conducting several trials to define the boundaries of the input MFs, they are tuned by means of a hybrid optimization algorithm composed of particle swarm optimization and genetic algorithm (PSO-GA). However, before going through the optimization process, a PEMFC model, capable of imitating the real-behavior of the stack, is needed to be used in the tuning process of the FLC parameters. This is due to the fact that utilizing the real PEMFC stack for performing the optimization process damages its state of health. Hereinafter, firstly, the employed PEMFC model for the optimization process is described. Subsequently, the utilized PSO-GA algorithm and its controlling parameters are explained in details.

1) PEMFC Stack Model: In this work, a model made up of an electrochemical and a thermal sub-model is employed to imitate the behavior of an open cathode PEMFC. The utilized model, which is shown in Fig. 11, is able to mimic the PEMFC behavior in steady-state and low-dynamic conditions.

a)   Electrochemical Model: The electrochemical model is based on the Amphlett *et al.* model which has been justified in several studies [34], [35]. This model, which is shown in Fig. 11

in the form of an electrical circuit, includes the polarization effects. The charge double layer phenomenon has been added to this model based on [40], [41]. The output voltage of the PEMFC, which is for a number of cells connected in series, is obtained by:

$$V_{FC} = N\left(E_{Nernst} + V_{act1} + V_C + V_{ohmic}\right) \quad (2)$$

where V_{FC} is the output voltage (V), N is the number of cells, E_{Nernst} is the reversible cell potential (V), V_C is the double-layer charging effect, V_{ohmic} is the ohmic loss (V), and V_{act} is the activation loss (V). Activation loss is composed of a drop related to the PEMFC internal temperature (V_{act1}) and a drop related to the both current and temperature of the stack (V_{act2}). The reversible cell potential is calculated by:

$$E_{Nernst} = 1.229 - 0.85 \times 10^{-3}\left(T_{st} - 298.15\right) + 4.3085$$
$$\times 10^{-5}T_{st}\left[\ln\left(P_{H2}\right) + 0.5\ln\left(P_{O2}\right)\right] \quad (3)$$

where T_{st} is the stack temperature (K), P_{H2} is the hydrogen partial pressure in anode side (N m^{-2}), and P_{O2} is the oxygen partial pressure in cathode side (N m^{-2}). The activation loss is given by:

$$\begin{cases} V_{act} = -[V_{act1} + V_{act2}] \\ V_{act1} = -\left[\xi_1 + \xi_2 T_{st} + \xi_3 T_{st}\ln\left(CO_2\right)\right] \\ V_{act2} = -\left[\xi_4 T_{st}\ln\left(i\right)\right] \\ CO_2 = P_{O2}/5.08 \times 10^6\exp\left(-498/T_{st}\right) \end{cases} \quad (4)$$

where $\xi_k (k = 1\ldots 4)$ are the semi-empirical coefficients based on fluid mechanics, thermodynamics, and electrochemistry, CO_2 is the oxygen concentration (mol cm^{-3}), and i is the PEMFC operating current (A). The double-layer charging effect is formulated by:

$$\begin{cases} V_C = (i - cdV/dt)\left(R_{act2} + R_{con}\right) \\ R_{act2} = V_{act2}/i \\ R_{con} = V_{con}/i = \left(Bln\left(1 - J/J_{max}\right)/i\right) \end{cases} \quad (5)$$

where c is the equivalent capacitor due to the double-layer charging effect (F), which is in order of several Farads because of porous electrodes of the PEMFC, B is a parametric coefficient (V), J is the actual current density (A cm^{-2}), J_{max} is the maximum current density (A cm^{-2}), and V_{con} is the concentration loss (V). The ohmic overvoltage can be described by:

$$V_{ohmic} = -iR_{internal} = -i\left(\zeta_1 + \zeta_2 T_{st} + \zeta_3 i\right) \quad (6)$$

where $R_{internal}$ is the internal resistor (Ω), and $\zeta_k(k = 1\ldots 3)$ are the parametric coefficients.

b) Thermal Model: The thermal behavior of the open cathode PEMFC is modeled by means of energy conservation equations for a lumped system, as introduced in [26], [27]. According to the energy conservation law, the energy balance for describing the temperature dynamic of the PEMFC can be given by:

$$m_{st}C_{st}dT_{st}/dt = \dot{Q}_{reac} - P_{st} - Q_{Nat} - Q_{Forced} \quad (7)$$

where m_{st} is stack mass (4.2 kg), C_{st} is specific heat capacity of stack (J/kg K) [27], T_{st} is stack temperature (K), $\dot{Q}_{reac}$ is

TABLE II
PEMFC MODEL PARAMETERS

Model	Parameter	Value	Reference for min. and max. limits
Electrochemical	ξ_1	-1.29	[34, 41]
	ξ_2	3.2042×10^{-3}	
	ξ_3	2.60×10^{-5}	
	ξ_4	-1.50×10^{-6}	
	c (F)	6.107	
	B (V)	0.3513	
	ζ_1	0.00375	
	ζ_2	1×10^{-6}	
	ζ_3	-0.00027	
Thermal	C_{st} (J/kg K)	1241	[26, 27]
	α	0.8653	

the released energy from electrochemical reaction (J), P_{st} is the generated electrical power (W), Q_{Nat} is the natural convection (J), and Q_{Forced} is the forced convection (J). The obtained energy form electrochemical reaction and the produced electrical power of the stack can be presented by:

$$\dot{Q}_{reac} = V_{max}i\,N \quad (8)$$
$$V_{max} = \Delta H/nF \quad (9)$$
$$P_{st} = V_{FC}\,i \quad (10)$$

where V_{max} is the maximum voltage obtained by hydrogen low heating value (1.23 V) or hydrogen high heating value (1.48 V), ΔH is the formation enthalpy, n is the number of electrons per molecule, and F is the Faraday's constant. The convective heat transfer, which is composed of natural and forced convection, can be formulated by:

$$Q_{Nat} = h_{Nat}A_{Nat}\left(T_{st} - T_{ca}\right) \quad (11)$$
$$Q_{Forced} = \alpha D_{fan}\rho_{air}A_{Forced}C_p\left(T_{st} - T_{ca}\right) \quad (12)$$

where h_{Nat} is the natural heat transfer coefficient (14 W/m^{2}K) [26], A_{Nat} is the total surface area of the 500-W Horizon PEMFC (0.1426 m^2) which has been calculated by the available dimensions in the manual of the device, T_{ca} is the ambient temperature (K), α is an empirical coefficient obtained by experiment, D_{fan} is the fan duty factor, ρ_{air} is the ambient air density 1.267 kg/m^3, A_{Forced} is the area exposed to the forced convection (0.22 m × 0.13 m × 2), and C_p is the air specific heat capacity 1005 J/kg K. The parameters which need to be tuned in the discussed electrochemical and thermal sub-models are listed in Table II. The values of these parameters have been obtained by GA from the Global Optimization Toolbox of Matlab using the measured experimental voltage, temperature, and current of the PEMFC.

To assess the capability of the developed PEMFC model in imitating the behavior of a 500-W Horizon PEMFC, the presented current profile in Fig. 12(a) has been applied to the model and the emulation results are compared with the measurements. Fig. 12(b) and Fig. 12(c) represent the voltage and temperature estimations respectively. As is seen in Fig. 12, the model is able to predict the PEMFC behavior with a satisfactory precision.

2) PSO-GA Optimization Process: GA and PSO are two well-known metaheuristic algorithms which have been used to
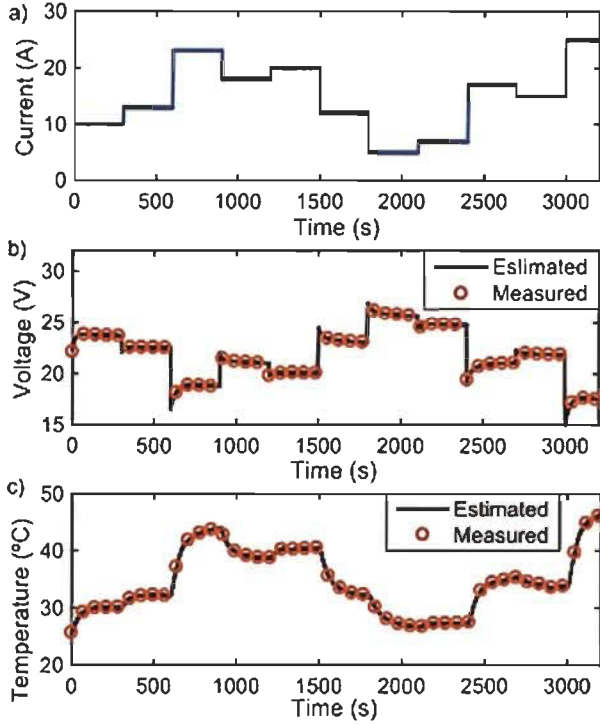
Fig. 12. Verification of the PEMFC model, (a) the utilized current profile, (b) voltage prediction, and (c) temperature prediction.

Fig. 13. Flowchart of the PSO-GA algorithm.

resolve a number of different engineering problems. The main reason for using hybrid PSO-GA optimization method is to combine their merits. By employing the genetic operators in the structure of PSO, the exploration and exploitation capabilities can be enhanced to some extent. In GA, the information of an individual will be forgotten in case it is not chosen, as opposed to PSO which has memory. On the other hand, PSO might use the resources for weak individuals since it does not have a selection operator. Hence the primary intention to develop PSO-GA is to integrate the social behavior of PSO into the search potential of GA [42]. The flowchart of the utilized PSO-GA algorithm is shown in Fig. 13. As is seen in this figure, first, the optimization problem should be defined by introducing a fitness function as the objective of minimization, the decision variables which are the targeted parameters for estimation, and the search space which is formed by describing the upper and lower limits of each decision variable. In this work, the constructing parameters of the input MFs are considered as the decision variables. To direct the population towards better solutions, a fitness function is required. Regarding the temperature FLC, the main goal is to reach the assigned reference temperature by the power map. In this respect, the integral time-weighted absolute error (ITAE), described in (13), is used as a fitness function for adjusting the parameters of the FLC MFs. The ITAE based tuning leads to much quicker settling time compared to other measures such as integral squared error and integral absolute error.

$$\min_{(\text{Decision variables})} \int_{1}^{N} t \, |T_{ref} - T_{st}| \, dt \qquad (13)$$

TABLE III
PSO-GA PARAMETERS DEFINITION

PSO-GA operators	Definition	Quantity
$Iter_{Max}$	Maximum iteration	100
$Subiter_{PSO}$	Maximum PSO subiteration	10
$Subiter_{GA}$	Maximum GA subiteration	10
N_{Pop}	Number of population (particles)	500
C	Constriction factor	0.729
$CO_{pct.}$	Crossover percentage	0.8
$Mu_{pct.}$	Mutation percentage	0.2

where t is time (s), T_{ref} is the reference temperature, and T_{st} is the PEMFC stack temperature. It should be noted that the optimization process of the FLC is performed on the explained PEMFC model since it can damage the real PEMFC. The optimized FLC is then implemented on the test bench to control the real PEMFC.

After defining the optimization problem, the operating parameters of the PSO-GA optimization algorithm should be defined according to Table III. Then the problem goes to the main loop of the optimization and the PSO and GA operators try to find the near optimal answer. In this work, separate iterations are introduced for PSO and GA operators inside the main loop to provide more control over them. The PSO algorithm updates the velocity and position of each particle by:

$$\begin{cases} v_i^{n+1} = C \left[v_i^n + \alpha_1 r_1 \left(p_{best_i} - p_i^n \right) + \alpha_2 r_2 \left(g_{best} - p_i^n \right) \right] \\ p_i^{n+1} = p_i^n + v_i^{n+1} \end{cases}$$

$$(14)$$
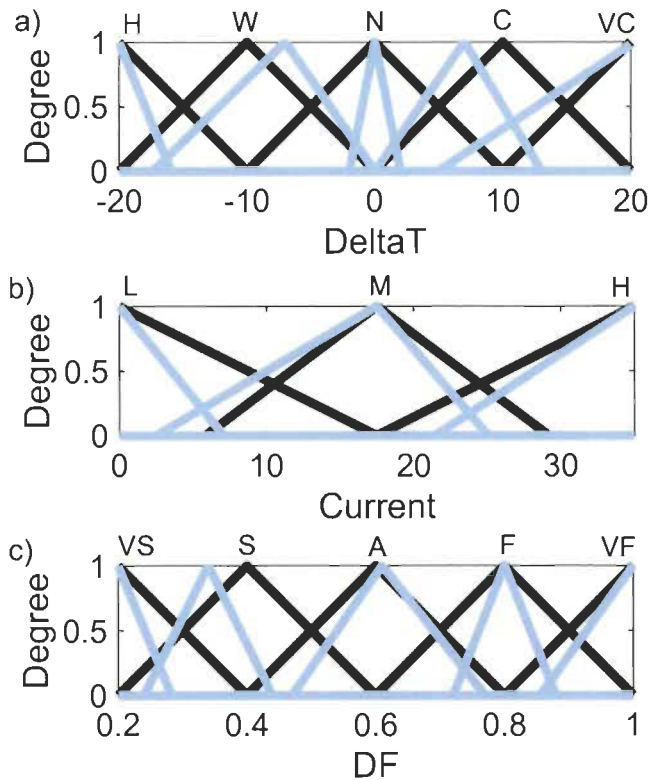
Fig. 14.   Input and output MFs before and after tuning.

Fig. 15.   Optimization results of the FLC tuning, (a) the employed current profile for the tuning process, (b) the minimization trend of the objective function, and (c) the test of the optimized FLC for reaching the reference temperature.

where v_i^{n+1} is the velocity of particle i at iteration $n + 1$, C is the constriction factor, which ensures the balance between exploration and exploitation of the particles [43], α_1 and α_2 are the weighing factors, r_1 and r_2 are two random numbers between 0 and 1, p_i^n is the position of particle i at iteration n, $pbest_i$ is the best position of particle i, and $gbest$ is the best position of the swarm. The constriction factor can be formulated by:

$$\begin{cases} C = 2/ \left| 2 - \varphi - \sqrt{\varphi^2 - 4\varphi} \right| \\ \varphi = \alpha_1 + \alpha_2 \end{cases} \quad (15)$$

It is worth mentioning that the value of φ should be kept between 4.1 and 4.2 by choosing 2.05 for α_1 and α_2 to acquire quality solutions [44].

Fig. 14 represents the input and output MFs of the designed temperature FLC before and after optimization process. The total number of decision variables are 27. Since the optimization process is performed once, the computational time is not a concern.

Fig. 15 represents the results of the tuned FLC performance after the optimization process. The optimization process has been conducted for the indicated current profile in Fig. 15(a) by using the explained PEMFC model. The reference temperature for each operating current level of Fig. 15(a) has been obtained from the extracted map of the PEMFC shown in Fig. 7. According to Fig. 15(b), the best fitness value of the fitness function levels off after almost 25 iterations and the mean value of the fitness reaches the best value after about 85 iterations. Fig. 15(c) represents that the tuned FLC can reach the determined referenced temperature in an acceptable time. Moreover, the behavior of the

cooling fan duty factor, which causes this temperature evolution, is shown in Fig. 15(c).

V. EXPERIMENT AND RESULTS ANALYSIS

Two assessment tests are designed to show the efficiency of the proposed systemic management. The first test deals with supplying a constant power profile, and the second test copes with variable power profile. In each stage, the performance of the proposed approach is compared with the commercial controller from manufacturer. Fig. 16 represents the stabilization process of the PEMFC system for supplying a constant power of 380 W. From Fig. 16(a), it is observed that by using the proposed thermal scheme, a lower current level is required to meet the demanded power, compared to the manufacturer controller. It is worth noting that achieving the same level of power by using different current levels in this test highlights the importance of the thermal management. According to Fig. 16(b), the manufacturer controller tends to keep the stack temperature at a higher level than the proposed approach. This higher temperature can result in a dryer membrane and less available oxygen for reaction. Moreover, the proposed systemic control consumes less hydrogen (4.47 SLPM) for providing the requested constant power profile as opposed to the manufacturer controller (5.35 SLPM).

Fig. 16. Corresponded current (a), and temperature (b) for supplying a 380-W constant power.

Fig. 17. Variable power profile test (a) along with its corresponded temperature (b), current (c), and H₂ consumption (d).

Fig. 18. Hydrogen consumption comparison of the PEMFC system for different scenarios.

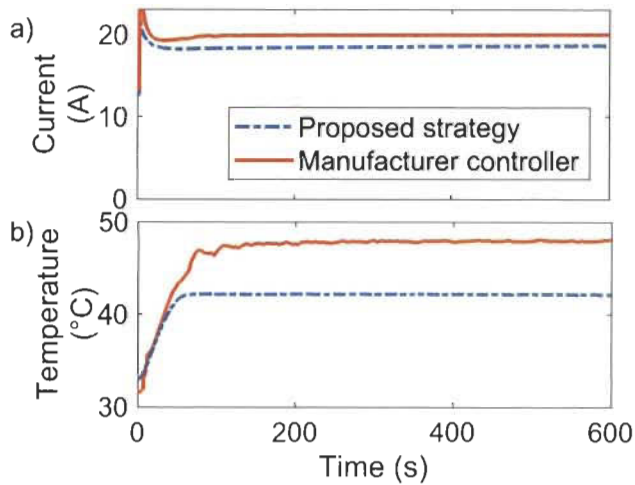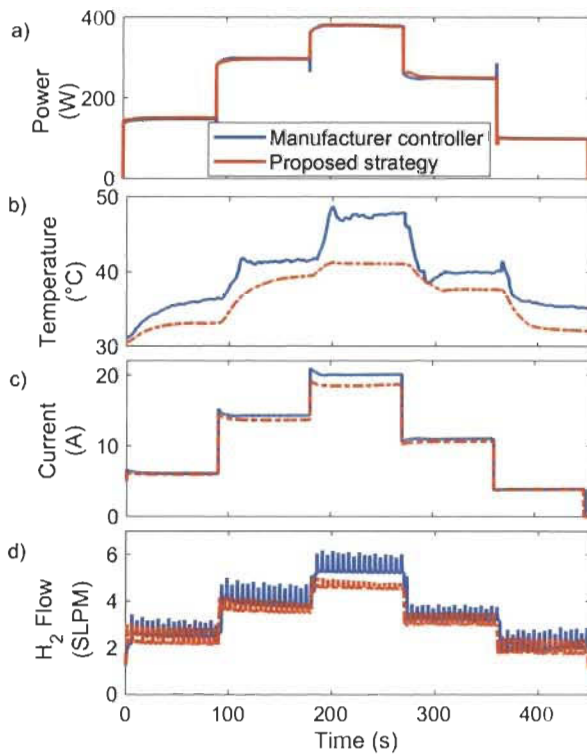The second test, which belongs to a variable power profile, is shown in Fig. 17. This low dynamic profile contains various high and low levels and indicates more clearly the performance of the proposed thermal strategy in different conditions.

Fig. 17(a) indicates that both of controllers are able to provide the demanded power. However, the temperature evolution of the PEMFC stack by each of the controllers is different as represented in Fig. 17(b). The required current levels for supplying the power are also different, as shown in Fig. 17(c). Both of the controllers tend to use the same current in low power levels. However, in high power levels, the proposed strategy
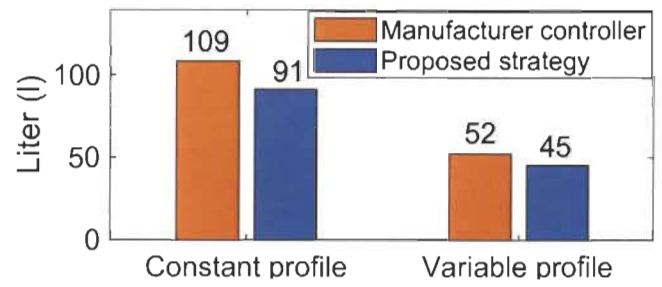
uses less current to meet the power. The effect of using a lower current level to satisfy the requested power can be embraced by checking the hydrogen consumption, which is represented in Fig. 17(d). It is observed that the hydrogen consumption achieved by utilizing the proposed FLC controller is lower than the manufacturer controller, specifically in high-power regions. Looking more carefully at Fig. 17, it can be seen that although the drawn current from the stack is almost the same in low-current regions (Fig. 17(c)), the hydrogen consumption is different. This is mainly due to the fact that the temperature levels are clearly different (Fig. 17(b)) in low-current regions. It is worth noting that this difference in temperature levels implies that the duty factor of the fan, which is responsible both for cooling the system and providing the necessary oxygen for the reactions, is also variable. Moreover, this result justifies the presented behavior of the open cathode PEMFC in Fig. 7 of the paper where the current levels are remarkably near to the minimum current while the temperature level changes more distinctly in low-power region.

Fig. 18 represents the comparison of the total hydrogen consumption of the discussed constant and variable power profiles for the case of manufacturer controller and the proposed systemic strategy. According to this figure, the proposed strategy of this work is able to decrease the hydrogen consumption of the PEMFC system by 13% and 16% for the case of constant and variable power profiles respectively.

VI. CONCLUSION

In this manuscript, a systemic management strategy is proposed to enhance the efficiency of an open cathode PEMFC system in different requested power levels. This strategy focuses on the usage of 3D mapping to determine the reference temperature of the control scheme. In this respect, a number of experiments are conducted to get a 3D power map for various stack temperatures and currents. This power map provides an efficient path based on the stack temperature and the current level of the PEMFC system and determines the reference temperature for each particular demanded power level from the system. Finally, an optimized FLC is used to achieve the defined reference temperature as the current of the PEMFC is being controlled by a PI controller. The obtained results from the conducted experiments highlight the satisfying performance of the proposed methodology by improving the system efficiency up to 13% and 16% for constant and variable power profiles respectively.

While this manuscript has demonstrated the potential of the suggested systemic management strategy, some opportunities for extending the scope of this paper remain as follows:

- Integrating the proposed methodology into the design of an energy management strategy for a fuel cell hybrid electric vehicle.
- Integrating an online system identification method to update the 3D power map to adapt to the performance drifts of the PEMFC system.
- Carrying out an ageing study of the PEMFC while using the suggested current and temperature control.

REFERENCES

[1] J. Snoussi, S. B. Elghali, M. Benbouzid, and M. F. Mimouni, "Optimal sizing of energy storage systems using frequency-separation-based energy management for fuel cell hybrid electric vehicles," *IEEE Trans. Veh. Technol.*, vol. 67, no. 10, pp. 9337–9346, Oct. 2018.

[2] H. Pei *et al.*, "Performance improvement in a proton exchange membrane fuel cell with separated coolant flow channels in the anode and cathode," *Energy Convers. Manage.*, vol. 187, pp. 76–82, 2019.

[3] D. K. Shin, D. G. Kang, J. H. Yoo, and M. S. Kim, "Study on the performance improvement of polymer electrolyte membrane fuel cell with inclined channel shape," *Electrochimica Acta*, vol. 320, p. 134630, Oct. 2019.

[4] O. S. Ijaodola *et al.*, "Energy efficiency improvements by investigating the water flooding management on proton exchange membrane fuel cell (PEMFC)," *Energy*, vol. 179, pp. 246–267, 2019.

[5] M. Pourabdollah, B. Egardt, N. Murgovski, and A. Grauers, "Convex optimization methods for powertrain sizing of electrified vehicles by using different levels of modeling details," *IEEE Trans. Veh. Technol.*, vol. 67, no. 3, pp. 1881–1893, Mar. 2018.

[6] F. Odeim, J. Roes, and A. Heinzel, "Power management optimization of a fuel cell/battery/supercapacitor hybrid system for transit bus applications," *IEEE Trans. Veh. Technol.*, vol. 65, no. 7, pp. 5783–5788, Jul. 2016.

[7] H. Chen, B. Liu, T. Zhang, and P. Pei, "Influencing sensitivities of critical operating parameters on PEMFC output performance and gas distribution quality under different electrical load conditions," *Appl. Energy*, vol. 255, 2019, Art. no. 113849.

[8] G. Zhang and K. Jiao, "Multi-phase models for water and thermal management of proton exchange membrane fuel cell: A review," *J. Power Sources*, vol. 391, pp. 120–133, 2018.

[9] J. Chen, Z. Liu, F. Wang, Q. Ouyang, and H. Su, "Optimal oxygen excess ratio control for PEM fuel cells," *IEEE Trans. Control Syst. Technol.*, vol. 26, no. 5, pp. 1711–1721, Sep. 2018.

[10] L. Huang, J. Chen, Z. Liu, and M. Becherif, "Adaptive thermal control for PEMFC systems with guaranteed performance," *Int. J. Hydrogen Energy*, vol. 43, pp. 11550–11558, Jun. 2018.

[11] L. Yin, Q. Li, T. Wang, L. Liu, and W. Chen, "Real-time thermal management of open-cathode PEMFC system based on maximum efficiency control strategy," *Asian J. Control*, vol. 21, pp. 1796–1810, 2019.

[12] S. Strahl and R. Costa-Castelló, "Temperature control of open-cathode PEM fuel cells," *IFAC-PapersOnLine*, vol. 50, pp. 11088–11093, 2017.

[13] S. Strahl, A. Husar, P. Puleston, and J. Riera, "Performance improvement by temperature control of an open-cathode PEM fuel cell system," *Fuel Cells*, vol. 14, pp. 466–478, 2014.

[14] Y. Nagai *et al.*, "Improving water management in fuel cells through microporous layer modifications: Fast operando tomographic imaging of liquid water," *J. Power Sources*, vol. 435, 2019, Art. no. 226809.

[15] G. Dotelli, R. Ferrero, P. G. Stampino, S. Latorrata, and S. Toscani, "PEM fuel cell drying and flooding diagnosis with signals injected by a power converter," *IEEE Trans. Instrum. Meas.*, vol. 64, no. 8, pp. 2064–2071, Aug. 2015.

[16] L. Sun, G. Li, Q. S. Hua, and Y. Jin, "A hybrid paradigm combining model-based and data-driven methods for proton exchange membrane fuel cell stack cooling control," *Renewable Energy*, vol. 147, pp. 1642–1652, 2019.

[17] V. Liso, M. P. Nielsen, S. K. Kær, and H. H. Mortensen, "Thermal modeling and temperature control of a PEM fuel cell system for forklift applications," *Int. J. Hydrogen Energy*, vol. 39, pp. 8410–8420, 2014.

[18] D. O'Keefe, M. Y. El-Sharkh, J. C. Telotte, and S. Palanki, "Temperature dynamics and control of a water-cooled fuel cell stack," *J. Power Sources*, vol. 256, pp. 470–478, 2014.

[19] A. Fly and R. H. Thring, "Temperature regulation in an evaporatively cooled proton exchange membrane fuel cell stack," *Int. J. Hydrogen Energy*, vol. 40, pp. 11976–11982, 2015.

[20] Y. Saygili, I. Eroglu, and S. Kincal, "Model based temperature controller development for water cooled PEM fuel cell systems," *Int. J. Hydrogen Energy*, vol. 40, pp. 615–622, 2015.

[21] J. Han, J. Park, and S. Yu, "Control strategy of cooling system for the optimization of parasitic power of automotive fuel cell system," *Int. J. Hydrogen Energy*, vol. 40, pp. 13549–13557, 2015.

[22] J. Han, S. Yu, and S. Yi, "Advanced thermal management of automotive fuel cells using a model reference adaptive control algorithm," *Int. J. Hydrogen Energy*, vol. 42, pp. 4328–4341, 2017.

[23] D. Li, C. Li, Z. Gao, and Q. Jin, "On active disturbance rejection in temperature regulation of the proton exchange membrane fuel cells," *J. Power Sources*, vol. 283, pp. 452–463, 2015.

[24] N. Lotfi, H. Zomorodi, and R. G. Landers, "Active disturbance rejection control for voltage stabilization in open-cathode fuel cells through temperature regulation," *Control Eng. Pract.*, vol. 56, pp. 92–100, 2016.

[25] Y. Devrim, H. Devrim, and I. Eroglu, "Development of 500 W PEM fuel cell stack for portable power generators," *Int. J. Hydrogen Energy*, vol. 40, pp. 7707–7719, 2015.

[26] K. Ou, W.-W. Yuan, M. Choi, S. Yang, and Y.-B. Kim, "Performance increase for an open-cathode PEM fuel cell with humidity and temperature control," *Int. J. Hydrogen Energy*, vol. 42, pp. 29852–29862, 2017.

[27] Y.-X. Wang, F.-F. Qin, K. Ou, and Y.-B. Kim, "Temperature control for a polymer electrolyte membrane fuel cell by using fuzzy rule," *IEEE Trans. Energy Convers.*, vol. 31, no. 2, pp. 667–675, Jun. 2016.

[28] Q. Li, T. Wang, C. Dai, W. Chen, and L. Ma, "Power management strategy based on adaptive droop control for a fuel cell-battery-supercapacitor hybrid tramway," *IEEE Trans. Veh. Technol.*, vol. 67, no. 7, pp. 5658–5670, Jul. 2018.

[29] Y. Han, Q. Li, T. Wang, W. Chen, and L. Ma, "Multisource coordination energy management strategy based on SOC consensus for a PEMFC–Battery–supercapacitor hybrid tramway," *IEEE Trans. Veh. Technol.*, vol. 67, no. 1, pp. 296–305, Jan. 2018.

[30] S. Ziaeinejad, Y. Sangsefidi, and A. Mehrizi-Sani, "Fuel cell-based auxiliary power unit: EMS, sizing, and current estimator-based controller," *IEEE Trans. Veh. Technol.*, vol. 65, no. 6, pp. 4826–4835, Jun. 2016.

[31] M. Higuita Cano, M. I. A. Mousli, S. Kelouwani, K. Agbossou, M. Hammoudi, and Y. Dubé, "Improving a free air breathing proton exchange membrane fuel cell through the maximum efficiency point tracking method," *J. Power Sources*, vol. 345, pp. 264–274, 2017.

[32] N. Karami, L. E. Khoury, G. Khoury, and N. Moubayed, "Comparative study between P&O and incremental conductance for fuel cell MPPT," in *Proc. Int. Conf. Renewable Energies Developing Countries*, 2014, pp. 17–22.

[33] P.-Y. Chen, K.-N. Yu, H.-T. Yau, J.-T. Li, and C.-K. Liao, "A novel variable step size fractional order incremental conductance algorithm to maximize power tracking of fuel cells," *Appl. Math. Model.*, vol. 45, pp. 1067–1075, 2017.

[34] M. Kandidayeni, A. Macias, A. A. Amamou, L. Boulon, S. Kelouwani, and H. Chaoui, "Overview and benchmark analysis of fuel cell parameters estimation for energy management purposes," *J. Power Sources*, vol. 380, pp. 92–104, 2018.

[35] M. Kandidayeni, A. Macias, A. A. Amamou, L. Boulon, and S. Kelouwani, "Comparative analysis of two online identification algorithms in a fuel cell system," vol. 18, no. 3, pp. 347–358, 2018.

[36] S. Ahmadi, S. Abdi, and M. Kakavand, "Maximum power point tracking of a proton exchange membrane fuel cell system using PSO-PID controller," *Int. J. Hydrogen Energy*, vol. 42, pp. 20430–20443, 2017.

[37] K. Ettihir, L. Boulon, and K. Agbossou, "Optimization-based energy management strategy for a fuel cell/battery hybrid power system," *Appl. Energy*, vol. 163, pp. 142–153, 2016.

[38] K. Ettihir, L. Boulon, M. Becherif, K. Agbossou, and H. S. Ramadan, "Online identification of semi-empirical model parameters for PEMFCs," *Int. J. Hydrogen Energy*, vol. 39, pp. 21165–21176, 2014.

[39] A. Macias, "Online identification for energy management of multi-stack systems," M.S. Thesis, Université du Québec à Trois-Rivières, Trois-Rivières, QC, Canada, 2018.

[40] C. Restrepo, T. Konjedic, A. Garces, J. Calvente, and R. Giral, "Identification of a Proton-Exchange membrane fuel cell's model parameters by means of an evolution strategy," *IEEE Trans. Ind. Inform.*, vol. 11, no. 2, pp. 548–559, Apr. 2015.

[41] C. Wang, M. H. Nehrir, and S. R. Shaw, "Dynamic models and model validation for PEM fuel cells using electrical circuits," *IEEE Trans. Energy Convers.*, vol. 20, no. 2, pp. 442–451, Jun. 2005.

[42] H. Garg, "A hybrid PSO-GA algorithm for constrained optimization problems," *Appl. Math. Comput.*, vol. 274, pp. 292–305, 2016.

[43] M. Clerc and J. Kennedy, "The particle swarm - explosion, stability, and convergence in a multidimensional complex space," *IEEE Trans. Evol. Comput.*, vol. 6, no. 1, pp. 58–73, Feb. 2002.

[44] G. Abbas, J. Gu, U. Farooq, M. U. Asad, and M. El-Hawary, "Solution of an economic dispatch problem through particle swarm optimization: A detailed survey - Part I," *IEEE Access*, vol. 5, pp. 15105–15141, 2017.

Loïc Boulon (M'10–SM'16) received the master's degree in electrical and automatic control engineering from the University of Lille, Lille, France, in 2006, and the Ph.D. degree in electrical engineering from University of Franche-Comté, Besançon, in France. Since 2010, he is a Professor with the Université du Québec à Trois-Rivières, Trois-Rivières, QC, Canada, and he works at the Hydrogen Research Institute as a Full Professor since 2016. His work deals with modeling, control and energy management of multiphysics systems. His research interests include hybrid electric vehicles, energy and power sources (especially battery in cold weather operation), and fuel cell systems. He has published more than 100 scientific papers in peer-reviewed international journals and international conferences. Prof. Boulon, in 2015, was a General Chair of the IEEE-Vehicular Power and Propulsion Conference in Montréal, QC, Canada. He is with VP-Motor Vehicles of the IEEE Vehicular Technology Society and is the holder of the Canada Research Chair in energy sources for the vehicles of the future.

Mohsen Kandidayeni (S'18) received the master's degree in mechatronics from Arak University, Arak, Iran, in 2014. He is currently working toward the Ph.D. degree with Université du Québec à Trois-Rivières, Trois-Rivières, QC, Canada, in energy-related topics such as hybrid electric vehicles, fuel cell systems, energy management, multiphysics systems, modeling and control. His research interests are in the area of renewable energy, fuel cell, transportation, intelligent transport systems, vehicular systems control, hybrid electric and electric vehicles.

Sousso Kelouwani (M'00–SM'17) received the B.S. and M.Sc.A. degrees from the Université du Québec à Trois-Rivières (UQTR), Trois-Rivières, QC, Canada, in 2000 and 2002, respectively, and the Ph.D. degree in automation and systems from École Polytechnique de Montréal, Montréal, QC, Canada, in 2010, all in electrical engineering. He is the holder of the Industrial Research Chair DIVEL in Intelligent Navigation of Autonomous Industrial Vehicles. He is currently a Full Professor of mechatronics with the Department of Mechanical Engineering, since 2018. Before starting his doctoral studies, he worked in research and development in the field of cell phone application optimization for Cilys 53, Inc., from 2002 to 2005 and Openwave, Inc., from 2005 to 2006. He is holder of three patents in the United States, his research interests include on the optimization of energy systems for vehicular applications, advanced driving assistance techniques, eco-energy navigation of autonomous vehicles, hybridization of energy sources for vehicles with low ecological impact (battery, fuel cell, hydrogen generator, etc.) in harsh weather conditions. In 2017, he was the recipient of the Environment Award of the Grand Prix for Excellence in Transport from the Quebec Transportation Association (AQTr) for the development of a hydrogen range extender based on a hydrogen generator for electric vehicles. He was also a recipient of the Canada Governor General's Gold Medal in 2000. Moreover, he has worked with several Canadian transportation companies to develop intelligent, energy-efficient, and driverless vehicles.

Alvaro Macias F. (M'17) was born in Mexico City, in 1992. He received the B.S. degree in mechatronics engineering in 2015 from Tecnológico de Monterrey, Guadalajara, Mexico, and the M.S. degree in electrical engineering in 2018 from Université du Québec à Trois-Rivières, Trois-Rivières, QC, Canada, where he is currently working toward the Ph.D. degree in electrical engineering. From 2015 to 2016, he worked as a Research and Development with the Centro de Investigación y de Estudios Avanzados del Instituto Politécnico Nacional, Mexico. His current research interest includes the development of energy management strategies for fuel cell systems, passive and active system configuration, and fuel cell modeling.

5.2 Article 5: Efficiency Upgrade of Hybrid Fuel Cell Vehicles' Energy Management Strategies by Online Systemic Management of Fuel Cell

Authors: M. Kandidayeni, A. Macias, L. Boulon, and S. Kelouwani

5.2.1 Methodology

This paper suggests an approach for enhancing the energetic efficiency of a FCHEV based on an online systemic management of the PEMFC stack. In this regard, firstly, an online systemic management scheme is developed to guarantee the supply of the requested power from the stack with the highest efficiency. This scheme is based on an updatable 3D map which relates the requested power form the stack to its optimal operating temperature and current levels. The map is generated by a semi-empirical voltage model and a polynomial thermal model being updated by KF and least square methods respectively. Secondly, two EMSs, namely QP and bounded load following strategy (BLFS), are developed to distribute the power between the FCS and battery in a low-speed FCHEV. The constraints of the EMSs, such as FCS maximum efficiency and maximum power, are constantly updated by the utilized online model to embrace the performance drifts of the stack due to degradation and operating conditions variation. Finally, the effect of integrating the developed FCS systemic management into the design of EMSs is experimentally scrutinized. The process of EMS integration into the systemic management of the PEMFC stack is shown in Figure 6.2.
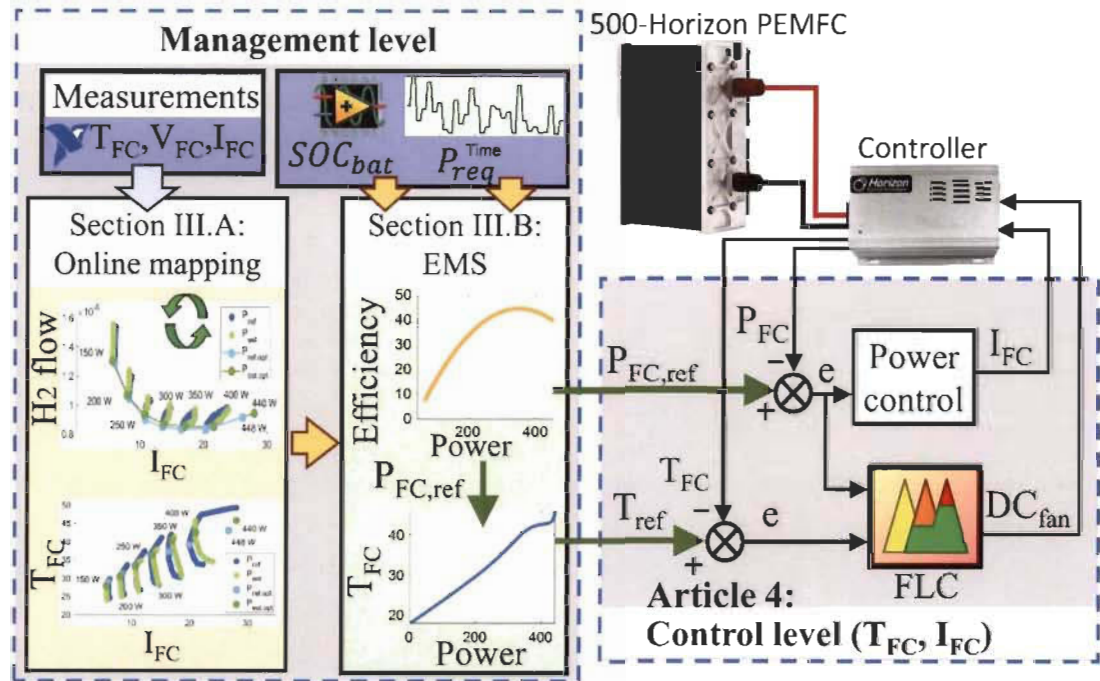
Figure 5.3 The process of EMS integration into systemic management and control of

the PEMFC stack.

To show the effect of online systemic management incorporation into the EMS design,

five scenarios, namely the proposed EMSs based on systemic management and the updated

map (QP_{Sys-Up} and $BLFS_{Sys-Up}$), the proposed EMSs using commercial controller and the

updated map (QP_{Com-Up} and $BLFS_{Com-Up}$), and QP using commercial controller and an

outdated map ($QP_{Com-Out}$) are taken into consideration under two driving cycles, worldwide

harmonized light-duty vehicles test cycles (WLTC_class 3) and West Virginia Interstate

Driving Schedule (CYC_WVUINTER).

In QP_{Sys-Up} and $BLFS_{Sys-Up}$ case studies, the proposed systemic management uses the

estimated PEMFC characteristics shown in Figs. 12 and 13 to determine the right current and

temperature combinations for supplying the reference power imposed by the EMS to the

PEMFC system. In fact, the reference temperature is determined by the optimal power-

versus-temperature line and after that FLC controls the cooling fan to reach the reference

temperature. In QP_{Com-Up} and $BLFS_{Com-Up}$ case studies, the imposed power by the EMS is supplied by the PEMFC using the commercial fan controller of the PEMFC stack and the updated characteristics. The comparison of QP_{Sys-Up} and $BLFS_{Sys-Up}$ with QP_{Com-Up} and $BLFS_{Com-Up}$ case studies illustrates the effect of including systemic management in the EMS design which is one of the main objectives of this manuscript. QP_{Com_Out} case study supplies the power by using the commercial fan controller and outdated characteristics of the PEMFC stack. The outdated map belongs to the presented PEMFC in its BOL in Fig. 1a. By using this map, the EMS is fed by false inputs because the characteristics map is different with the utilized PEMFC on the HIL set-up. The comparison of QP_{Com-Up} and $QP_{Com-Out}$ illuminates the importance of online updating in the performance of the vehicle.

5.2.2   Synopsis of the results analyses

Figure 5.4 indicates the hydrogen consumption of the PEMFC stack as well as the influence of initial and final battery SOC over the performance of the studied cases. In this regard, each test is repeated five times starting with different initial SOCs (60%, 65%, 70%, 75%, and 80%). Subsequently, the difference between initial and final SOC (ΔSOC) versus the hydrogen consumption is plotted. Form this figure, it is clear that under both driving cycles, regardless of the initial and final battery SOC, the QP_{Sys-Up} achievs the lowest and the QP_{Com_Out} reaches the highest hydrogen consumption. Comparing QP_{Sys-Up} and QP_{Com-Up} shows that hydrogen consumption has decreased up to 3.7% and 2.6% in Figure 5.4a and Figure 5.4b respectively due to the integration of the proposed systemic management. Moreover, comparison of QP_{Com-Up} and QP_{Com_Out} shows that ignorance of adaptation to the PEMFC health state has increased hydrogen consumption up to 3.2% and

6.6% in Figure 5.4a and Figure 5.4b respectively. Regarding the BLFS, inclusion of the systemic management has declined the hydrogen consumption up to 3.4% in Figure 5.4c and 3% in Figure 5.4d.
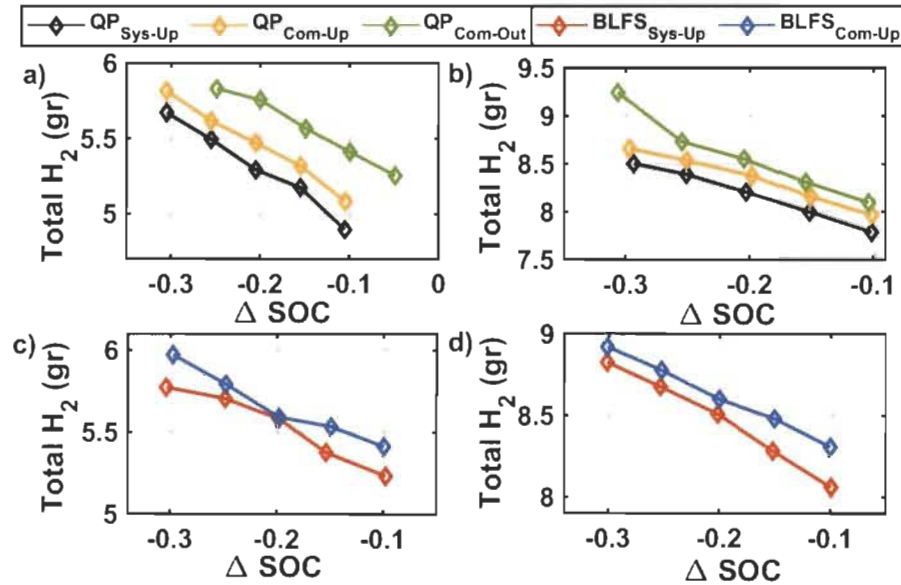

Figure 5.4   Hydrogen consumption for various initial Battery SOCs, a) and c) WLTC_class 3, b) and d) CYC_WVUINTER.

Efficiency Upgrade of Hybrid Fuel Cell Vehicles' Energy Management Strategies by Online Systemic Management of Fuel Cell

Mohsen Kandidayeni, *Student Member, IEEE*, Alvaro Macias, *Student Member, IEEE*, Loïc Boulon, *Senior Member, IEEE*, and Sousso Kelouwani, *Senior Member, IEEE*

Abstract—This paper puts forward an approach for boosting the efficiency of energy management strategies (EMSs) in fuel cell hybrid electric vehicles (FCHEVs) using an online systemic management of the fuel cell system (FCS). Unlike other similar works which solely determine the requested current from the FCS, this work capitalizes on simultaneous regulation of current and temperature, which have different dynamic behavior. In this regard, firstly, an online systemic management scheme is developed to guarantee the supply of the requested power from the stack with the highest efficiency. This scheme is based on an updatable 3D map which relates the requested power from the stack to its optimal temperature and current. Secondly, two different EMSs are used to distribute the power between the FCS and battery. The EMSs' constraints are constantly updated by the online model to embrace the stack performance drifts owing to degradation and operating conditions variation. Finally, the effect of integrating the developed online systemic management into the EMSs' design is experimentally scrutinized under two standard driving cycles and indicated that up to 3.7% efficiency enhancement can be reached by employing such a systemic approach. Moreover, FCS health adaptation unawareness can increase the hydrogen consumption up to 6.6%.

Index Terms—Online parameter estimation, optimal energy management strategy, proton exchange membrane fuel cell, systemic management, thermal control.

NOMENCLATURE

$\hat{P}_{FC}$	fuel cell estimated power (W)
$\hat{T}_{FC}$	fuel cell estimated stable temperature (°C)
$\dot{n}_{cons}^{O_2}$	consumed oxygen in the reaction (mol/s)
$\dot{n}_{in}^{O_2}$	supplied oxygen to PEMFC (mol/s)
$\Delta P_{Fall,k}$	negative PEMFC power change (W)
ΔP_{Rise}	positive PEMFC power change (W)

CO_2	oxygen concentration (mol/cm^3)
C_{bat}	battery capacity (Ah)
DC_{Fan}	cooling fan duty cycle
E_{Nernst}	reversible cell potential (V)
I_{FC}	fuel cell current (A)
I_{Valve}	current of the Hydrogen valve (A)
I_{bat}	battery current (A)
I_{max}	fuel cell maximum current (A)
$MAPE_{P_{FC}}$	fuel cell power mean absolute percentage error
M_{air}	air molar mass (kg/mol)
N_{cell}	number of cells
P_{Bat}	battery power (W)
P_{FC}	fuel cell stack power (W)
P_{FC-Sys}	PEMFC system power (W)
P_{Fan}	consumed power by cooling fan (W)
P_{H2}	hydrogen pressure in anode side (Pa)
P_{O2}	oxygen partial pressure in cathode side (Pa)
P_{Valve}	consumed power by hydrogen valve (W)
P_{bat}	battery pack power (W)
P_{req}	requested power (W)
Q_{air}	air flow (m^3/s)
$RMSE_{T_{FC}}$	stack temperature root-mean-square error
R_{bat-ch}	internal resistance during charging (Ω)
$R_{bat-dch}$	internal resistance during discharging (Ω)
$R_{internal}$	fuel cell internal resistor (Ω)
S_{O_2}	oxygen stoichiometry
$Slew_{rate,fall}$	falling dynamic limitation (W/s)
$Slew_{rate,rise}$	rising dynamic limitation (W/s)
T_{FC}	stack temperature (°C)
T_{FC}	stack temperature (°C)
T_{amb}	ambient temperature (°C)
U_{bat-OC}	open circuit voltage (V)
U_{bus}	bus voltage (V)
V_{FC}	stack voltage (V)
V_{Valve}	voltage of the Hydrogen valve (V)
V_{act}	activation loss (V)
V_{con}	concentration loss (V)
V_{ohmic}	ohmic loss (V)
a_n	fitting parameters ($n = 1,2,3$)
c_n	empirical coefficients ($n = 1 \dots 3$)
f_{H2}	hydrogen flow (SLPM)
p_n	fitting parameters ($n = 1 \dots 6$)
t_0	initial step time (s)
t_f	final step time (s)
α_n	fitting parameters ($n = 0,1,2$)

ζ_n	parametric coefficients ($n = 1 \dots 3$)
η_{DC-DC}	DC-DC converter efficiency
η_{FC-Sys}	efficiency of the PEMFC system
ξ_n	semi-empirical coefficients ($n = 1 \dots 4$)
ρ_{air}	air density (kg/m^3)
Δt	time interval (s)
B	parametric coefficient
CVE	cross-validation error
F	Faraday constant (sA/mol)
LHV	hydrogen low heating value (J/mol)
N	number of data points
SOC	state of charge
t	total time of driving cycle (s)

I. INTRODUCTION

A. Literature survey

FUEL cell hybrid electric vehicles (FCHEVs) normally employ a proton exchange membrane (PEM) fuel cell (FC) stack, as the main power source, and a battery pack or/and a supercapacitor (SC), as the secondary power source [1]. The specific characteristics of each source, in terms of power delivery and efficiency, make the design of an energy management strategy (EMS) vital for having an efficient power distribution [2]. The existing EMSs in the literature can be divided into three categories of rule-based, optimization-based, and intelligent-based [3]. Several strategies based on these categories and their combinations are available in the literature. In [4], a multi-mode fuzzy logic controller (FLC) is used to perform the power distribution in a FCHEV. The modes of the FLC are determined by a multi-layer perceptron neural network using the historical velocity window, and the rule base is optimized by a genetic algorithm. This strategy has improved the fuel economy by 8.89%, compared to a single-mode FLC. In [5], a multi-state (i.e., coasting, braking, and station parking) equivalent consumption minimization strategy (ECMS) is formulated by quadratic programming (QP) for a tram. This EMS has led to 2.5% energy consumption decline compared to a rule-based power following EMS. In [6], a convex optimization is proposed to minimize the energy cost by optimizing the control decisions and the cost of power sources. This study shows that appropriate estimation of the PEMFC rated power can decrease the hydrogen cost up to 61%. In [7], a heuristic method called bounded load following strategy (BLFS) is suggested for a FC-battery vehicle. The PEMFC power is bounded between two limits according to the efficiency curve of the stack. The boundaries of this strategy are refined with respect to the optimal trajectory obtained by dynamic programming. In [8], the suggested strategy has two phases of optimal policy generation for a long trip, using a distribution optimization algorithm, and revising the EMS considering the actual traffic conditions in short-term time steps. In [9], an adaptive controller based on tuning the FLC parameters for different loads is proposed. The authors state that the PEMFC voltage declines after a while due to degradation. Under this condition, the rule-based values should be reconsidered.

B. Necessity of online mapping

Performance of a FC system is influenced by several factors, such as ambient operating conditions, stack temperature, operating current, degradation phenomenon, and so forth. The variation of these factors can lead to the change of PEMFC stack power delivery capability which is very important in the design of an EMS. For instance, Fig. 1 indicates the output power of a 500-W PEMFC with respect to its operating current and stack temperature in two different conditions. The data have been obtained from experimental tests in Hydrogen Research Institute of University of Quebec in Trois-Rivières. Fig. 1a presents the characteristics of a new PEMFC stack, which is in its beginning of life (BOL) and an old stack which is in its end of life (EOL) after reaching a 20% decrease in the maximum rated power. Fig. 1b shows the characteristics of a 500-W stack in two different seasons with different ambient temperatures (27°C in Summer and 20°C in Winter). The stars show the location of maximum power (MP) which changes in each case. Therefore, the online updating of the map seems to be necessary to embrace these impacts on the operation of the stack and provide the requested power from the FCS by the best possible combination of current and temperature. Some considerable efforts have been made to prevent the EMS malfunction owing to these performance drifts by adding a degradation model to the system. In [10], FC degradation is quantified by a simplified electrochemical model and integrated into the cost function of an optimal control-based EMS for a hybrid FC bus to extend the PEMFC lifetime. In [11], an online adaptive ECMS is proposed for a FC-battery-SC powertrain, where the degradation of the PEMFC is considered by the variation of resistance and maximum current density using a first-order polynomial function. The authors show that the battery charge sustenance constraint cannot be satisfied as the PEMFC and battery degrade. In [12], a model predictive control framework is proposed for a FCHEV. The PEMFC degradation is also taken into account using some experimental degradation rates for high, low, and transitional loads. However, degradation and ageing mechanisms are very complex to be modeled. Moreover, the operating conditions which are not included in the PEMFC model, such as humidity and ambient temperature, can also change the maximum efficiency (ME) and MP ranges of the stack that are normally among the utilized constraints while designing an EMS.
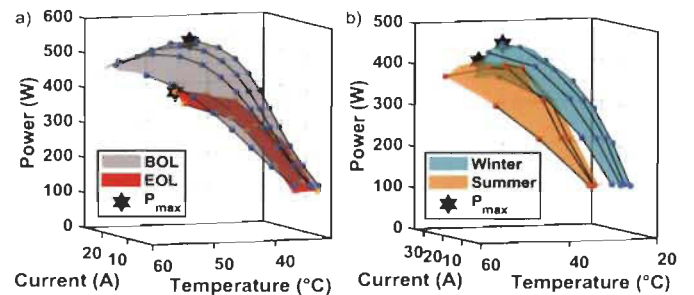

Fig. 1. The variation of characteristics in a PEMFC stack, a) lifetime variation, b) seasonal variation.

To evade the mentioned issues about PEMFC modeling, two approaches of extremum seeking and online identification of PEMFC model parameters have come under attention. The former is based on seeking an optimal operating point by means of a periodic perturbation signal in real-time [13, 14]. Such strategies are of interest mostly due to their straightforward implementation. When concurrent identification of several operating points is required in online applications, the optimization function is changed, and an optimization algorithm is used to search for MP and ME points. Regarding online identification, recursive filters are used for tuning the PEMFC parameters through time. The necessary characteristics are then extracted from the updated model. In [15], the authors employ RLS for updating a single-input PEMF model while designing an EMS for a FCHEV. They indicate that the classical strategies are not very efficient when there are performance drifts in the FC system.

C. Contributions

One important aspect that has escaped the attention of many researchers in the domain of EMS for FCHEVs is adopting a systemic approach towards the management of the PEMFC stack while developing a strategy. In the literature, current and temperature are typically regarded as independent control variables. Nonetheless, PEMFC is a multi-physical system with strong dynamic interactions between current and temperature. Regarding the PEMFC as a system provides several degrees of freedom in terms of power supply [16]. A specific requested power from the PEMFC can be supplied by different combinations of current and temperature to improve the efficiency [17]. Several methods have been proposed concerning the thermal/current management of a PEMFC stack. For instance, in [18], a ten-percent power increase is achieved by controlling the PEMFC stack temperature and input hydrogen humidity level using a FLC and a bubble humidifier respectively. In [19], an approach based on electrochemical impedance spectroscopy is proposed where the current of lowest resistance is used to determine the optimum air flow rate and current density considering the influence of the temperature. In [20], a FLC is suggested to regulate the stack temperature of an open cathode PEMFC by acting on the cooling fan speed. However, to the best of the authors' knowledge, the integration of a simultaneous current and temperature management into the design of an EMS has not been considered before. In this respect, first, an online systemic management scheme is put forward to guarantee the supply of the requested power from the PEMFC stack with the highest efficiency and embrace the effect of performance drifts in this system. Subsequently, two EMSs, namely QP and BLFS, are developed to distribute the power between sources while respecting the limitations of the system. Finally, the effect of including the proposed PEMFC systemic management in the EMSs' design is scrutinized by performing experimental validations in a hardware-in-the-loop (HIL) set-up. As mentioned earlier, the main contribution of this work lies in the efficiency upgrade of the two mentioned EMSs by utilizing the put forward concurrent current and temperature

systemic management scheme.

D. Paper organization

Section II describes the utilized vehicle characteristics along with the designed HIL platform. The development of the proposed online current and temperature management as well as the EMS is discussed in Section III. Section IV presents the obtained results from the considered scenarios, and the conclusion along with some remarks is given in section V.

II. FUEL CELL HYBRID ELECTRIC VEHICLE SYSTEM

The system utilized in this manuscript is based on a low-speed FCHEV, called Nemo. The powertrain of this vehicle is composed of a 3-phase induction machine, a PEMFC stack, and a battery pack. The power sources are connected in series and the PEMFC acts as a range extender [21]. More details about the specifications of this vehicle are available in [22]. For the purpose of this work, a HIL platform is developed to assess the performance of the EMS. As shown in Fig. 2, a Horizon H-500 PEMFC is used as the real component of this platform and the rest are mathematical models. The specifications of this PEMFC are presented in Table I. This open-cathode PEMFC system is self-humidified and air-cooled. It includes two fans attached to the FC stack housing to supply the cooling and process air. The hydrogen supply subsystem consists of a hydrogen tank, a manual forward pressure regulator, a hydrogen supply valve, a hydrogen purging valve, and a mass flowmeter. The pressure regulator keeps the pressure of hydrogen between 0.5 and 0.6 Bar. In the anode side, the PEMFC is equipped with 2 valves.
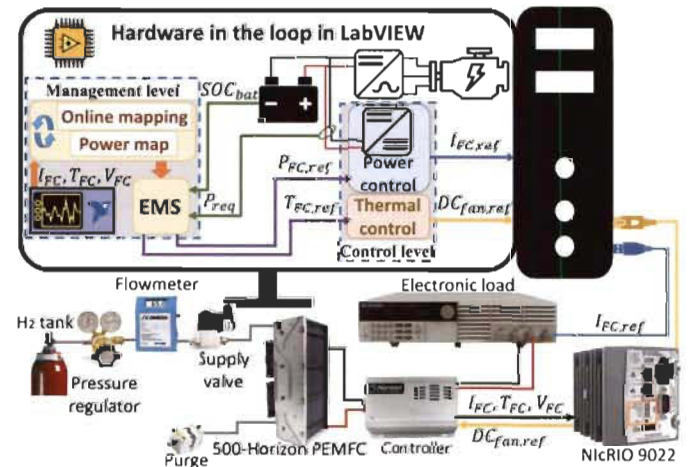
Fig. 2. The developed HIL platform for evaluating an EMS.

TABLE I
SPECIFICATIONS OF THE HORIZON H-500 FC

PEMFC Technical specifications	
Number of cells	36
Max Current (shutdown)	42 A
Hydrogen pressure	0.5-0.6 Bar
Cathode pressure	1 Bar
Ambient temperature	5 to 30 °C
Max stack temperature	65 °C
Hydrogen purity	99.999% dry H_2
Size	130 × 220 × 122 mm
Cooling	Air (integrated cooling fan)

The hydrogen inlet valve allows feeding the PEMFC with dry hydrogen. The hydrogen flow rate changes from 0 to 7 l/min with respect to the drawn power from the stack. Hydrogen flow is measured by an OMEGA flowmeter (FMA-A2309) calibrated for hydrogen gas. It utilizes a capillary type thermal technology to directly measure mass flow and does not require any temperature, pressure, or square root corrections. The purge valve acts as the anode outlet and dispels the excess water and hydrogen from the PEMFC flow channels. In this work, cycling purging is performed to recurrently remove accumulated water, hydrogen and nitrogen. As advised by the manufacturer, the PEMFC is purged every 10 s for a duration of 100 ms in order to refill the anode volume with fresh hydrogen. The hydrogen exhaust flow during the purge depends on the pressure difference between the environment and the anode side. After each purge, if the performance is increased around 10%, the pressure of hydrogen is increased a little bit as it is an indication of flooding (as suggested by the manufacturer). This pressure increase helps pushing the extra water out. In addition, the pressure difference between the anode and the cathode must not exceed 0.5 bar to avoid membrane damages. The PEMFC is linked to a National Instrument CompactRIO (NI cRIO-9022) via its controller which regulates the axial fan as well as the input/output valves. This embedded real-time controller has been combined with a compatible CompactRIO Chassis to include integrated C series I/O module slots. The communication between CompactRIO and the PC, where the LabVIEW software is available, is done by an Ethernet connection. The data between the CompactRIO and the PC are transferred every 100 ms. Current, temperature, and voltage of the PEMFC stack are recorded for updating the model. An 8514 BK Precision DC Electronic Load demands a load profile, imposed by the DC-DC converter, from the PEMFC stack. Since Nemo vehicle has a 4-kW PEMFC stack, the output voltage of the 500-W PEMFC is scaled up after the converter in the HIL platform. The performed tests in this work have been conducted in the ambient temperature and humidity levels of 20 °C and 60 % respectively.

A battery internal resistance model is employed to imitate the behavior of a 6 Ah lithium-ion battery module from Saft Company [23], available in the database of ADVISOR software. In this work, the battery pack is only composed of 20 cells in series. Fig. 3 shows the relationship of battery cell SOC with each of open circuit voltage (U_{bat-OC}), internal resistance during charging (R_{bat-ch}), and internal resistance during discharging ($R_{bat-dch}$).

The battery current (I_{bat}), bus voltage (U_{bus}), and SOC are calculated by:

If $P_{bat} > 0$ (discharge):
$$\begin{cases} I_{bat} = \frac{(U_{bat-OC}(SOC) - \sqrt{U_{bat-OC}(SOC)^2 - 4 \times R_{bat-dch}(SOC) \times P_{bat}}}{2 \times R_{bat-dch}(SOC)} \\ U_{bus} = U_{bat-OC}(SOC) - I_{bat} \times R_{bat-dch}(SOC) \\ SOC(t_f) = SOC(t_0) - \frac{\int_{t_0}^{t_f} I_{bat}dt}{C_{bat}} \end{cases} \quad (1)$$
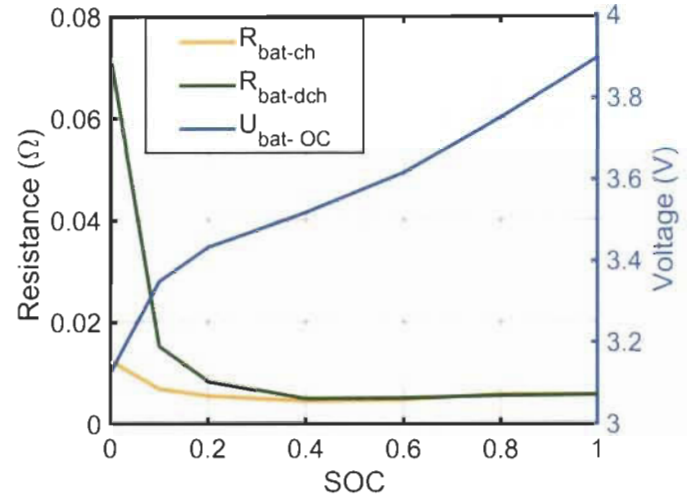

Fig. 3. SOC relationship with open circuit voltage and internal resistance per cell.

If $P_{bat} < 0$ (charge):
$$\begin{cases} I_{bat} = \frac{(U_{bat-OC}(SOC) - \sqrt{U_{bat-OC}(SOC)^2 - 4 \times R_{bat-ch}(SOC) \times P_{bat}}}{2 \times R_{bat-ch}(SOC)} \\ U_{bus} = U_{bat-OC}(SOC) - I_{bat} \times R_{bat-ch}(SOC) \\ SOC(t_f) = SOC(t_0) - \eta_C \frac{\int_{t_0}^{t_f} I_{bat}dt}{C_{bat}} \end{cases} \quad (2)$$

where P_{bat} is the battery pack power, C_{bat} is the capacity, and η_C is the coulombic efficiency only during charge (0.98) [24]. The PEMFC stack is linked to the DC bus through a DC-DC converter. This converter is modeled by using a smoothing inductor and a boost chopper as explained in [25].

III. ONLINE SYSTEMIC MANAGEMENT STRATEGY

Temperature of a PEMFC stack has an impact on the electrochemical, thermodynamics, electro-kinetics, transport, and water distribution processes, which jointly dictate system efficiency and long-term durability [26]. It is favorable to sustain control over the stack temperature to reach homogeneous distribution. Hence, temperature and indeed its spatial variation should be considered alongside the commonly considered operating conditions, such as current and voltage, while characterizing the PEMFC stack performance and searching for optimum operating points. This is significant in all the PEMFCs and operating modes but is chiefly relevant to the air-cooled PEMFCs in which the input air is responsible for both of reaction and cooling the system [27].

In an open cathode PEMFC, the airflow related to the minimum cooling fan duty cycle can ensure a high oxygen stoichiometry ratio at the rated power of the PEMFC stack [19, 28]. Therefore, the principal impact on the performance is made by the changes in the stack temperature rather than the oxygen supply. Regarding the utilized open cathode PEMFC in this manuscript, the cathode stoichiometry is calculated by [28]:

$$S_{O_2} = \dot{n}_{in}^{O_2} \Big/ \dot{n}_{cons}^{O_2} = 0.21 \left(\rho_{air} Q_{air} \Big/ M_{air} \right) \Big/ N_{cell} \frac{I}{4F} \qquad (3)$$

where S_{O_2} is the oxygen stoichiometry, $\dot{n}_{in}^{O_2}$ is the amount of oxygen supplied to the PEMFC, $\dot{n}_{cons}^{O_2}$ is the consumed oxygen in the electrochemical reaction, ρ_{air} is the air density, Q_{air} is the air flow, M_{air} is the air molar mass, N_{cell} is the number of cells, and F is the Faraday constant. In (3), the only unknown parameter is the airflow (Q_{air}), which is calculated according to the presented experimental measurements in Fig. 4.
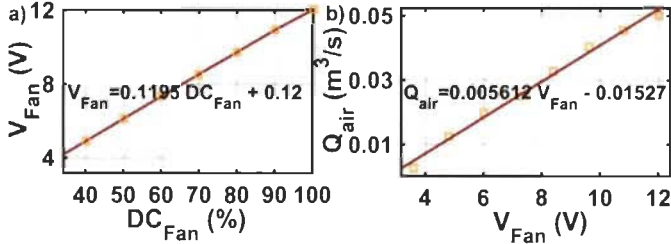

Fig. 4. Cooling fan characteristics, a) fan voltage with respect to duty cycle, and b) air flow with respect to fan voltage.

According to (3) and Fig. 4, even at the minimum duty cycle of the fan (34%), a stoichiometry of around 29 is obtained at the rated power of the PEMFC (448W @ 27A). Such a high oxygen stoichiometry is not unusual for air-cooled open-cathode systems according to the literature [19, 28].

General configuration of the proposed online systemic strategy is shown in Fig. 5. This strategy is based on the proposed work in [16] and has two operating levels of management and control. The management level is responsible for dictating the reference signals to the controllers, and the control level deals with reaching them. In [16], the management level comprised a static 3D power map generated by experimental data. It would determine the reference signal of the temperature controller (FLC) while the reference power of the power controller was assumed to be known. However, such a map is efficient only in a limited operating range as the PEMFC characteristics change through time.

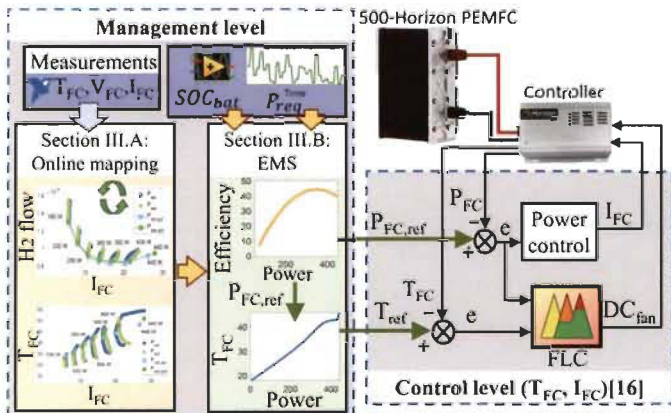In this work, an online PEMFC model is employed to update the key characteristics of the stack, such as power and

efficiency curves, from time to time. The extracted characteristics have two vital roles in this strategy. First, determining a dependable reference signal for the temperature controller through an optimal temperature-versus-power path. Second, providing the EMS with the updated ME and MP points which are utilized to ascertain the requested power from the PEMFC stack. The requested power from the PEMFC stack is indeed the reference signal of the power controller shown in Fig. 5. The two appointed reference signals are then sent to the controllers to be reached. The details about the design and performance of the control level are available in [16]. This work mainly focuses on the online updating of the map and its integration into an EMS.

A. Online mapping

1) Process explanation:

The general process of online mapping in this study is shown in Fig. 6. The core of this process is a semi-empirical PEMFC voltage model which takes the current (I_{FC}), hydrogen partial pressure (P_{H2}), and stack temperature (T_{FC}) as the inputs and estimates the stack voltage (V_{FC}). The hydrogen partial pressure is assumed constant in this work. As discussed in [16], stack temperature mainly depends on the current and cooling fan duty cycle, and it can be represented by a smooth surface. In this respect, a polynomial function is used to create a relationship between the inputs, which are operating current and fan duty cycle, and the output, which is the stack temperature. Indeed, this function provides the stable temperature for each current level with respect to the utilized fan duty cycle. The operating current and its corresponding stable temperature are then used as the inputs of the semi-empirical voltage model, and as a result, the voltage and power curves of the PEMFC are obtained. This map is static and will be used by the EMS for updating the set ME and MP points. The parameters of the voltage model are updated by Kalman filter (KF) using the measured signals from the real PEMFC. As opposed to the semi-empirical model, the polynomial function is updated online by a batch of stable temperature points using a typical least squares method [29]. It should be noted that in the beginning of the process, first, the parameters of the voltage model are updated as it can be done very fast by using the measured data from the real PEMFC. Subsequently, the thermal model is updated when enough measured stable temperature points are captured. Afterwards, the models are updated from time to time.
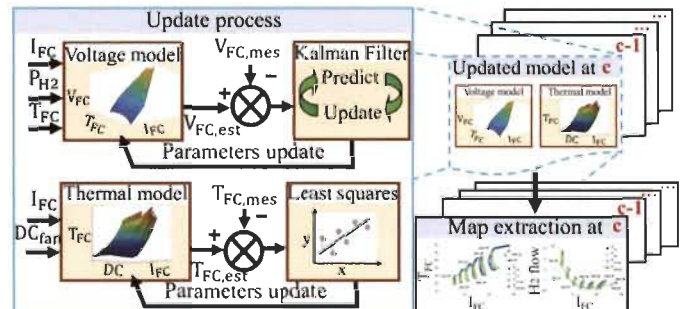

Fig. 5. The systemic current and temperature management and control structure.

Fig. 6. The process of online mapping.

2) Voltage model:

The utilized semi-empirical model estimates the stack voltage for a number of cells connected in series.

$$V_{FC} = N_{cell}(E_{Nernst} + V_{act} + V_{ohmic} + V_{con}) \tag{4}$$

$$E_{Nernst} = 1.229 - 0.85 \times 10^{-3}(T_{FC} - 298.15) + 4.3085 \times 10^{-5} T_{FC}[\ln(P_{H2}) + 0.5\ln(P_{O2})] \tag{5}$$

$$\begin{cases} V_{act} = \xi_1 + \xi_2 T_{FC} + \xi_3 T_{FC} \ln(CO_2) + \xi_4 T_{FC} \ln(I_{FC}) \\ CO_2 = \dfrac{P_{O2}}{5.08 \times 10^{-6} \exp(-498/T_{FC})} \end{cases} \tag{6}$$

$$V_{ohmic} = -I_{FC} R_{internal} = -I_{FC}(\zeta_1 + \zeta_2 T_{FC} + \zeta_3 I_{FC}) \tag{7}$$

$$V_{con} = B\ln(1 - \frac{I_{FC}}{I_{max}}) \tag{8}$$

Where V_{FC} is the stack output voltage (V), N_{cell} is the number of cells, E_{Nernst} is the reversible cell potential (V), V_{act} is the activation loss (V), V_{ohmic} is the ohmic loss (V), V_{con} is the concentration loss (V), T_{FC} is the stack temperature (K), P_{H2} is the hydrogen partial pressure in anode side (N m^{-2}), P_{O2} is the oxygen partial pressure in cathode side (N m^{-2}), $\xi_n (n = 1 \dots 4)$ are the semi-empirical coefficients based on fluid mechanics, thermodynamics, and electrochemistry, CO_2 is the oxygen concentration (mol cm^{-3}), I_{FC} is the PEMFC operating current (A), $R_{internal}$ is the internal resistor (Ω), $\zeta_n (n = 1 \dots 3)$ are the parametric coefficients, B is a parametric coefficient (V), and I_{max} is the maximum current (A). The explanation of KF integration into this semi-empirical model for parameters estimation is considered redundant in this work as it has been already discussed in [22]. The targeted parameters for estimation in the voltage model vary through time. However, their initial values before the online estimation by KF are: ξ_1=-0.995, ξ_2=2.1228×10^{-3}, ξ_3=2.1264×10^{-5}, ξ_4=-1.1337×10^{-4}, ζ_1=-0.024, ζ_2=7.60×10^{-5}, ζ_3=-1.06×10^{-3}, B=0.4970. The power of the PEMFC system (P_{FC-Sys}) is obtained by subtracting the power of the PEMFC stack (P_{FC}) from the consumed power by the cooling fan (P_{Fan}) and hydrogen valve (P_{Valve}). Fig. 7 shows the consumed power by the cooling fan at each duty cycle obtained by measuring the voltage and current of the fan in different duty cycles (34% to 100%). The power consumed by the purge valve is not noticeable as it has a fixed cyclic purging (every 10 s for duration of 100 ms) and has not been considered in this work.

$$P_{FC-Sys} = P_{FC} - P_{Fan} - P_{Valve} \tag{9}$$

$$P_{FC} = V_{FC} \times I_{FC} \tag{10}$$

$$P_{Fan} = c_1 DC_{Fan}^2 + c_2 DC_{Fan} + c_3 \tag{11}$$

$$P_{Valve} = V_{Valve} \times I_{Valve} \tag{12}$$

Where c_1, c_2, and c_3 are empirical coefficients obtained by fitting a single-variable quadratic polynomial function to the measured data shown in Fig. 7 ($c_1 = 0.001365$, $c_2 = 0.1139$, and $c_3 = -0.9946$), V_{Valve} is the voltage of the Hydrogen valve (12 V), and I_{Valve} is the current of the Hydrogen valve (0.72 A). The power consumption of the hydrogen valve is constant since it is normally open when the PEMFC starts operating.

Hydrogen flow is a function of current and duty cycle and is
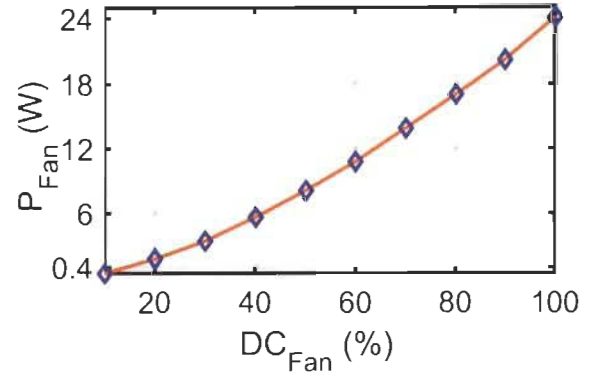
Fig. 7. The 500-W Horizon PEMFC Cooling fan power consumption respecting the duty cycle.

estimated by an empirical equation proposed in [16].

$$f_{H2} = a_1 I_{FC} + a_2 \frac{DC_{Fan}}{100} + a_3 \tag{13}$$

Where f_{H2} is the hydrogen flow (SLPM), and a_n ($n = 1,2,3$) are the fitting parameters obtained by the experimental data ($a_1 = 0.1539$, $a_2 = $ -0.05308, $a_3 = 1.657$). Finally, the efficiency of the PEMFC system is calculated by:

$$\eta_{FC-Sys} = \frac{P_{FC-Sys}}{\frac{f_{H2}}{22.4 \times 60} \times LHV} \tag{14}$$

where LHV is the low heating value of hydrogen (241800 J/mol), and $1/22.4 \times 60$ is the conversion factor from SLPM to mol/s.

3) Thermal model:

As mentioned earlier, the temperature behavior with respect to current and fan duty cycle can be modeled by a polynomial function. Fig. 8 shows the influence of cooling fan and operating current over the stack temperature of the PEMFC.
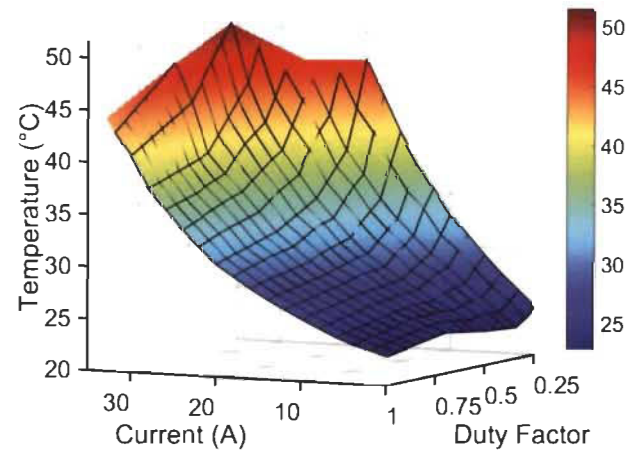
Fig. 8. Influence of operating current and fan duty factor over the stack temperature.

This figure has been generated by applying a ramp-up current profile to the PEMFC system in five different fan duty factors, namely 0.25, 0.34, 0.5, 0.7, and 1. At each duty factor, the test is continued until the maximum power of the PEMFC

is achieved, and the voltage drop due to the concentration loss is observed. It should be noted that while testing the EMS, the minimum fan duty cycle is set to 34% (not 25%) as it is the minimum level defined by the manufacturer to have a good chemical reaction in all the power ranges. To select a suitable degree for the polynomial-based temperature model, K-fold cross validation is used [30]. Fig. 9 shows the cross-validation error (CVE) for the five-fold data set of this manuscript based on which a proper function should be selected for estimating the stable temperature. The CVE is calculated by:

$$CVE = \frac{1}{m}\sum_{i=1}^{m} RMSE_{T_{FC}i} \tag{15}$$

$$RMSE_{T_{FC}} = \sqrt{\frac{\sum_{1}^{N}(T_{FC}-\hat{T}_{FC})^2}{N}} \tag{16}$$

where m is the number of subsets, which is 5 herein, $RMSE_{T_{FC}}$ is the stack temperature root-mean-square error of each subset, N is the number of data points inside each subset, T_{FC} is the measured stable temperature, and $\hat{T}_{FC}$ is the estimated stable temperature by the polynomial function. The CVE has been calculated for several polynomial degrees, as shown in Fig. 9. Apart from overfitting and underfitting problems, it is also significant to avoid increasing the number of parameters since this function will be updated online by least squares method. From Fig. 9, it seems that a third-degree function with respect to the operating current has an acceptable performance as it has achieved a low CVE. According to Fig. 9, the temperature model is given by:

$$T_{FC}(DC_{Fan}, I_{FC}) = T_{amb} + p1\,DC_{Fan} + p2\,I_{FC} + \\ p3\,DC_{Fan}\,I_{FC} + p4\,I_{FC}^2 + p5\,DC_{Fan}\,I_{FC}^2 + p6\,I_{FC}^3 \tag{17}$$

where T_{FC} is the stack temperature, T_{amb} is the ambient temperature (20 °C), DC_{Fan} is the duty cycle of the fan, I_{FC} is the operating current of the PEMFC stack, and $p_n(n = 1 \dots 6)$ are the unknown parameters estimated by least squares method when enough measured data are obtained. The values of these empirical parameters after the first estimation are: $p1$=0.0322, $p2$=1.7112, $p3$=-0.0259, $p4$=0.0117, $p5$=0.0006, and $p6$=-0.001. Fig. 10 indicates the investigation for finding the minimum required time to get stable points for updating the parameters of the temperature model (Fig. 10a) and the number of points needed to do the first estimation (Fig. 10b). Since the final objective of the PEMFC model is to extract the power map, the utilized error in Fig. 10 is the mean absolute percentage error of the estimated PEMFC power ($MAPE_{P_{FC}}$),
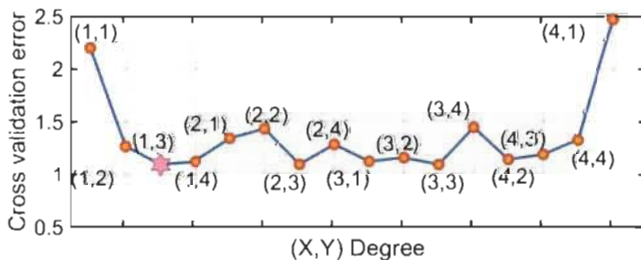

Fig. 9. Evaluation of different polynomial degrees based on CVE.
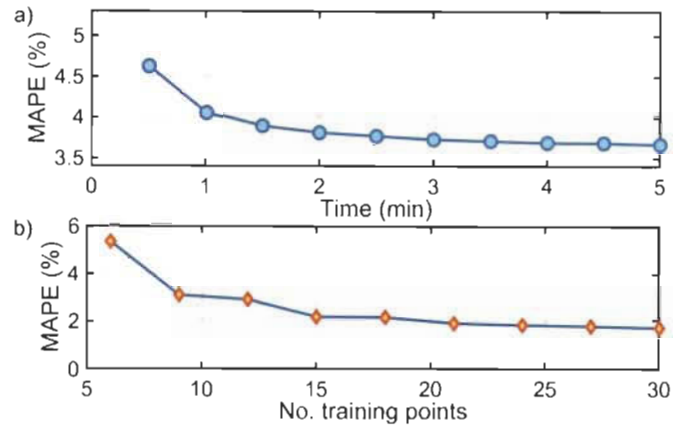
Fig. 10. The required time (a) and data points (b) for updating the parameters of the temperature model.

calculated by (18). That means, first, the stable temperature is estimated by the polynomial function, and after that it is sent to the voltage model to predict the output power of the stack.

$$MAPE_{P_{FC}} = \frac{100\%}{N}\sum_{1}^{N}\left|\frac{P_{FC}-\hat{P}_{FC}}{P_{FC}}\right| \tag{18}$$

Where P_{FC} is the estimated power by using the measured temperature, and $\hat{P}_{FC}$ is the estimated power by using the estimated temperature. From Fig. 10a, it can be stated that the extracted parameters at 2 minutes have an acceptable precision ($MAPE_{P_{FC}} = 3.77\%$) as the decline trend of the error becomes less than 1% after this step. In other words, the error does not decrease considerably after 2 minutes. Moreover, Fig. 10b shows that by having nine measurements, an acceptable estimation can be conducted. As the application of this work will be in FCHEVs which have an energy storage system, it is possible to reach the stable temperature points from PEMFC. Moreover, the primary estimations can be done by recording points in even less than one minute and then the accuracy can be increased by getting more stable points through time.

4) Validation phase:
An experimental test has been conducted to evaluate the extraction quality of the power map and other characteristics by using the above-discussed online modeling approach. Fig. 11a presents the applied current profile to the PEMFC stack and Fig. 11b shows the utilized cooling fan duty cycle profile as well as the corresponding stack temperature. The current profile and the measured temperature are sent to the electrochemical model, and the estimated voltage by the PEMFC model is then presented in Fig. 11c. According to this figure, the voltage estimation by the model has a satisfactory quality. It should be noted that the parameters of the semi-empirical model are tuned by KF. The measured stable temperature data as a result of applying the current and the cooling fan duty cycle profiles, shown in Fig. 11, are employed to extract the optimal power line of the stack with respect to current and temperature.

Fig. 12 represents the estimated and measured power line of the utilized PEMFC stack. As is seen in this figure, several combinations of current and temperature can lead to the same power level. In each power line, the intersection of minimum

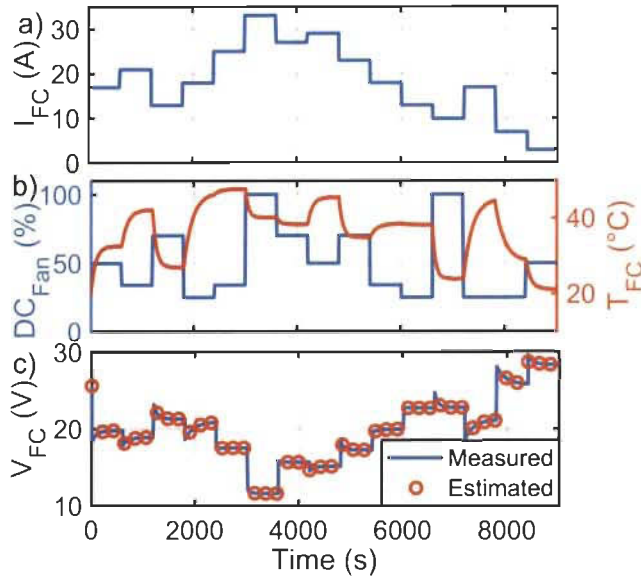Fig. 11. Current profile (a), cooling fan duty cycle profile and its corresponding stack temperature (b), and the voltage estimation (c).

current and its corresponding temperature is shown with a circle where connecting all the circles leads to an optimal power line. The reference power line has been obtained by conducting several tests since it needs a wide range of data. However, the estimated power line has been attained by the model using the minimum time and data points, as discussed earlier. Fig. 13 shows the corresponding hydrogen consumption of each power line. From this figure, it is seen
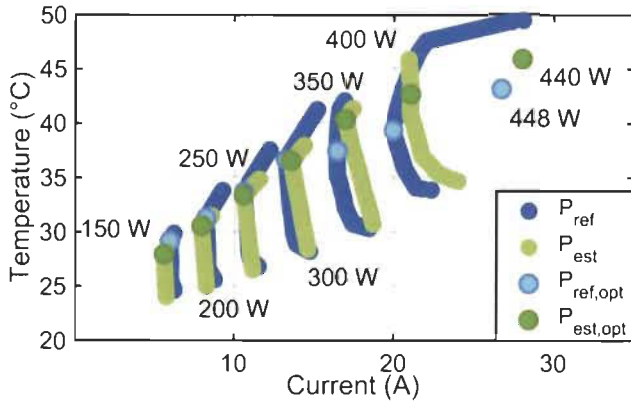

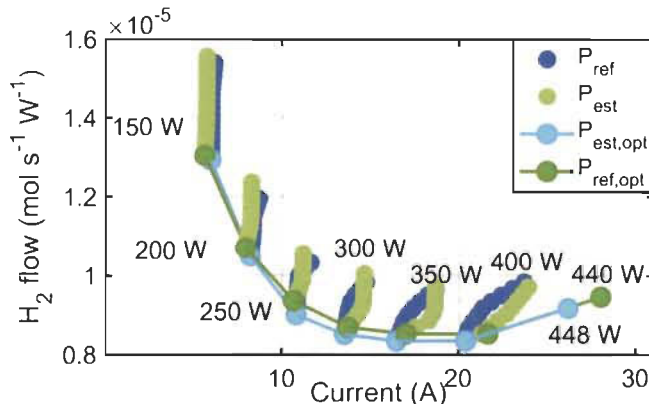Fig. 12. Optimal power line with respect to current and temperature.

Fig. 13. Optimal power line with respect to current and H2 flow.

that each circled optimal point in the estimated power line is equivalent to the minimum hydrogen consumption, implying that the lower the current, the lower the hydrogen flow. Moreover, the interpolated lines in each power level can be mathematically considered as a convex problem which has only one minimum.

B. Energy management strategies

The provided basis in this work regarding online systemic management can be conveniently integrated into most of the existing EMSs in the literature. An EMS or power split strategy, regardless of its type, is expected to determine the reference power from the PEMFC stack. Then, the proposed systemic management is mainly responsible for supplying this reference power by selecting the best combination of PEMFC current and temperature. As the selection of current and temperature comes from an updated experimental map, the supply of the PEMFC reference power, determined by the EMS, is guaranteed with the highest efficiency level. In this section, two EMSs will be discussed to be upgraded by the proposed online systemic management.

1) Quadratic programming-based strategy:

The requested power (P_{req}) from the electric motor side is supplied by both of PEMFC system and battery pack. Therefore, the fuel economy of an FCHEV relies on how the requested power is distributed between these two sources. Herein, the objective of the EMS is to find an online optimal power split trajectory which maximizes PEMFC efficiency while respecting the constraints of the system.

$$P_{req} = \eta_{DC-DC}P_{FC-Sys} + P_{Bat} \qquad (19)$$

Where P_{Bat} is the battery power and η_{DC-DC} is the DC-DC converter efficiency (90%). According to Fig. 14, which has been extracted from the explained online mapping section, the process of maximizing the PEMFC system efficiency can be formulated by a quadratic function as:

$$\max \left(\sum_{k=1}^{n} \alpha_2(k) P_{FC-Sys}^2 + \alpha_1(k)P_{FC-Sys}(k) + \alpha_0(k) \right) \quad (20)$$

$$n = \frac{t}{\Delta t}, n\epsilon\mathbb{N} \qquad (21)$$

where the total time of driving cycle (t) is discretized to n time points with respect to the time interval (Δt). The defined cost function in (20) can be solved by the classical QP method as it is convex in the bounded power ranges shown in Fig. 14. Each cross marker in Fig. 14 represents the location of one measured point in terms of power and efficiency. Each measured point has also a specific current and duty cycle. The estimated curve shows that the highest level for the efficiency curve has been selected.

However, to keep the power sources operation within an admissible range, the following constraints are considered:

$$SOC_{min} \leq SOC_k \leq SOC_{max} \qquad (22)$$
$$P_{FC,min} \leq P_{FC,k} \leq P_{FC,max} \qquad (23)$$
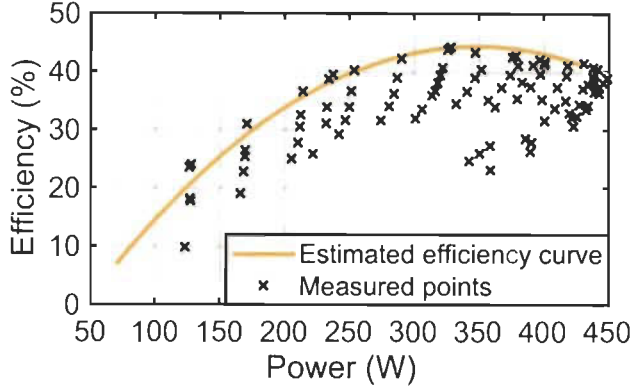$$\Delta P_{Rise,k} - Slew_{rate,rise} \leq 0 \qquad (24)$$

Fig. 14. Relationship between PEMFC system efficiency and power.

$$\Delta P_{Fall,k} - Slew_{rate,fall} \leq 0 \tag{25}$$

where the battery SOC should be kept between 50% (SOC_{min}) and 90% (SOC_{max}), $P_{FC,min}$ is zero, $P_{FC,max}$ is determined by the online model, $\Delta P_{Rise,k}$ is the positive PEMFC power change, $Slew_{rate,rise}$ is the rising dynamic limitation, $\Delta P_{Fall,k}$ is the negative PEMFC power change, and $Slew_{rate,fall}$ is the falling dynamic limitation. According to [15], a dynamic limitation of 50 Ws^{-1}, which means a maximum of 10% of the maximum power per second for rising, and also 30% of the maximum power per second for falling, as suggested in [7], have been considered for the operation of the PEMFC stack. The proposed strategy avoids operation in the open-circuit voltage (OCV) of the PEMFC. When the requested power from the PEMFC decreases to zero, the PEMFC is switched off and it does not operate in OCV. Moreover, to avoid unnecessary on/off cycles in the PEMFC system, the cost function of the QP has been defined based on maximizing the efficiency. PEMFC system efficiency is zero when the current/power of the PEMFC is zero. Therefore, QP avoids using PEMFC in low efficiency region as its objective is to maximize it. QP only decides to turn off the PEMFC to avoid over charging when the battery SOC approaches its upper limit.

The only point that should be reminded here is that since the optimization variable in (20) is P_{FC-Sys}, the battery SOC calculation should be related to this optimization variable so that the defined constraint in (22) can be explained. The presented SOC calculation in (1) and (2) can be presented as:

$$\dot{SOC}(k) = f(SOC(k), P_{bat}(k)) \tag{26}$$

Here, the battery power can be substituted by the difference between requested power and the PEMFC system power as:

$$\dot{SOC}(k) = f(SOC(k), P_{req}(k) - \eta_{DC-DC}P_{FC-Sys}(k)) \tag{27}$$

Since $P_{req}(k)$ is obtained by imposing acceleration to the system, (27) can be rewritten in terms of the optimization variable (P_{FC-Sys}), by using a new function (F).

$$\dot{SOC}(k) = F(SOC(k), P_{FC-Sys}(k)) \tag{28}$$

2) Bounded load following strategy (BLFS):

The second EMS of this study is a commonly used rule-based real-time approach in the literature [7, 31]. BLFS is a hysteresis-based EMS to distribute the power between the sources of a FCHEV. It normally limits the operation of the PEMFC stack within ME and MP points and mostly provides three modes of operation including ON/OFF, $P_{FC,min}$, and $P_{FC,max}$ with respect to the battery SOC level and requested power. To ensure a low hydrogen consumption, the PEMFC ME point is used as the P_{FC_min} mode. In fact, the hydrogen consumption and the degradation of the stack are higher between the open circuit voltage and the best efficiency point region of the PEMFC. Therefore, when the PEMFC is turned on, the ME mode is activated. P_{FC_max} mode, which sets the stack on its MP, is triggered when the battery SOC reaches the minimum SOC level. The only time that PEMFC works between OFF and $P_{FC,min}$ is the transitions from OFF to $P_{FC,min}$ due to the slew rate limitations. The details of BLFS are available in [7]. The constraints regarding the battery SOC and PEMFC slew rates are the same as QP strategy in the previous section.

IV. EXPERIMENT AND RESULTS ANALYSIS

To show the effect of online systemic management incorporation into the EMS design, five scenarios, namely the proposed EMSs based on systemic management and the updated map (QP$_{Sys-Up}$ and BLFS$_{Sys-Up}$), the proposed EMSs using commercial controller and the updated map (QP$_{Com-Up}$ and BLFS$_{Com-Up}$), and QP using commercial controller and an outdated map (QP$_{Com-Out}$) are taken into consideration under two driving cycles, worldwide harmonized light-duty vehicles test cycles (WLTC_class 3) and West Virginia Interstate Driving Schedule (CYC_WVUINTER).

In QP$_{Sys-Up}$ and BLFS$_{Sys-Up}$ case studies, the proposed systemic management uses the estimated PEMFC characteristics shown in Figs. 12 and 13 to determine the right current and temperature combinations for supplying the reference power imposed by the EMS to the PEMFC system. In fact, the reference temperature is determined by the optimal power-versus-temperature line and after that FLC controls the cooling fan to reach the reference temperature. In QP$_{Com-Up}$ and BLFS$_{Com-Up}$ case studies, the imposed power by the EMS is supplied by the PEMFC using the commercial fan controller of the PEMFC stack and the updated characteristics. The comparison of QP$_{Sys-Up}$ and BLFS$_{Sys-Up}$ with QP$_{Com-Up}$ and BLFS$_{Com-Up}$ case studies illustrates the effect of including systemic management in the EMS design which is one of the main objectives of this manuscript. QP$_{Com\_Out}$ case study supplies the power by using the commercial fan controller and outdated characteristics of the PEMFC stack. The outdated map belongs to the presented PEMFC in its BOL in Fig. 1a. By using this map, the EMS is fed by false inputs because the characteristics map is different with the utilized PEMFC on the HIL set-up. The comparison of QP$_{Com-Up}$ and QP$_{Com-Out}$

illuminates the importance of online updating in the performance of the vehicle.

Fig. 15 and Fig. 16 compare the performance of the five above-discussed scenarios for WLTC_class 3 and CYC_WVUINTER driving cycles, respectively. As is seen in Figs. 16a and 16a, WLTC_class 3 contains low-, medium-, and high-speed regimes while CYC_WVUINTER solely includes high-speed condition. Figs. 15b and 16b present the supplied power by the PEMFC stack for the five cases. According to these figures, the reference power imposed to PEMFC stack by the EMS is the same in QP_{Sys-Up} and QP_{Com-Up} and also in $BLFS_{Sys-Up}$ and $BLFS_{Com-Up}$ for both driving cycles. However, the reference power of $QP_{Com-Out}$ is different as QP receives data from an outdated map in this case study. Figs. 15c and 16c show the temperature evolution which are different in each case due to the cooling fan operation. Figs. 15d and 16d represent the battery SOC variation at each considered case. As is seen, the battery SOC variation in both QP_{Sys-Up} and QP_{Com-Up} is similar, as opposed to $QP_{Com-Out}$ case. SOC evolution is also the same in the BLFS strategies. The designed EMSs try to meet the requested power from the system by respecting the defined limits for battery SOC and PEMFC stack. Moreover, they tend to keep a high level of battery SOC while the vehicle is under operation. The analyses carried out in Fig. 15 and Fig. 16 show the general performance of the developed EMSs in the discussed driving conditions and scenarios. However, the influence of PEMFC systemic management integration over the performance of the utilized QP and BLFS EMSs should be
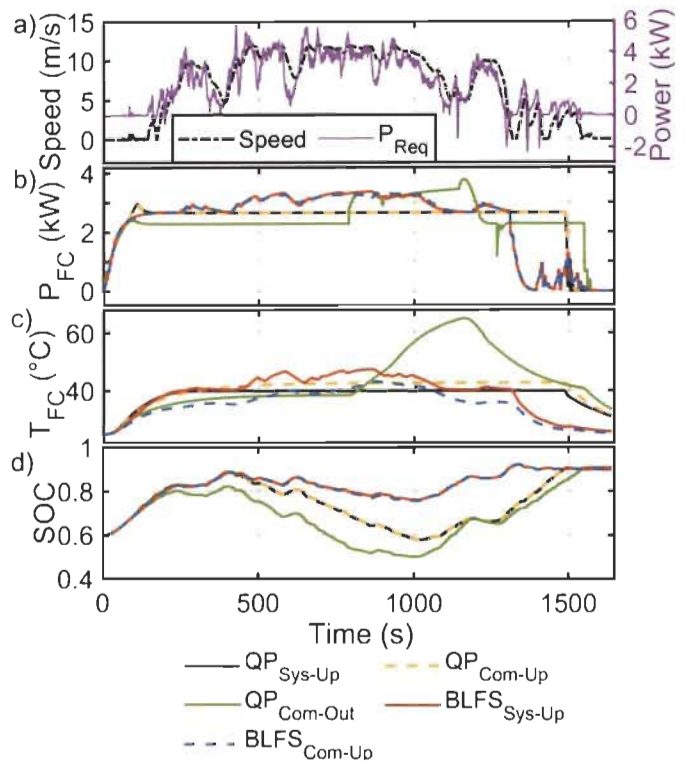
Fig. 16. The EMS performance under CYC_WVUINTER driving cycle, a) driving speed and the corresponding traction power, b) power split by different strategies, c) PEMFC temperature evolution, and d) battery SOC variation.

further considered. In this regard, the distribution of the drawn current from the PEMFC stack to meet the requested power in each of the considered driving scenarios is illustrated in Fig. 17. Form this figure, it is seen that the drawn current from the PEMFC stack by the proposed systemic EMSs (QP_{Sys-Up} and $BLFS_{Sys-Up}$) is clearly lower than the commercial controller case studies (QP_{Com-Up} and $BLFS_{Com-Up}$) under the two considered driving cycles. Fig. 17a and Fig. 17b compare the performance of the QP based EMS with and without systemic management along with the outdated map case study. Fig. 17a shows that the PEMFC stack has worked in almost all the operating current range since the driving cycle contains a lot of changes. However, the QP_{Sys-Up} has managed to supply the power with lower current levels which are in the efficient operation zone of the stack. From Fig. 17b, it is seen that the PEMFC stack has worked mostly in the efficient zone while the QP_{Com-Up} has used higher current levels to fulfil the expectations. QP_{Com_Out} has a very different current distribution compared to other cases as its set signals are based on the outdated characteristics. It goes to very high current region according to Fig. 17b to be able to supply the requested power. According to Fig. 17c and Fig.17d, the systemic BLFS ($BLFS_{Sys-Up}$) uses lower current levels in the efficient zone compared to the commercial controller ($BLFS_{Com-Up}$). Moreover, in Fig. 17c, PEMFC has some transitions between off and almost 18 A owing to the changes in the WLTC_class 3 driving cycle while in Fig. 17d, it mostly operates within ME and MP points.
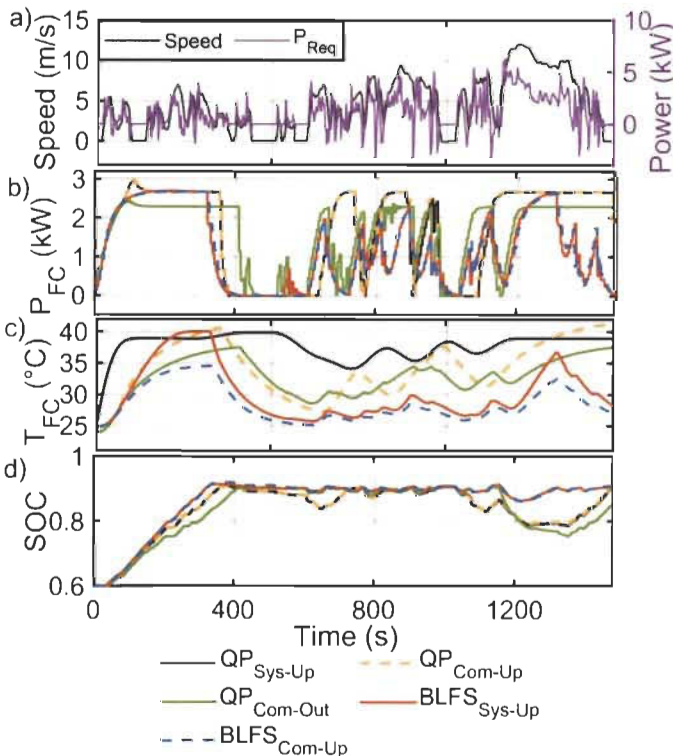
Fig. 18 indicates the hydrogen consumption of the PEMFC

Fig. 15. The EMS performance under WLTC_class 3, a) driving speed and the corresponding traction power, b) power split by different strategies, c) PEMFC temperature evolution, and d) battery SOC variation.

stack as well as the influence of initial and final battery SOC over the performance of the studied cases. In this regard, each test is repeated five times starting with different initial SOCs (60%, 65%, 70%, 75%, and 80%). Subsequently, the difference between initial and final SOC (ΔSOC) versus the hydrogen consumption is plotted. Form this figure, it is clear that under both driving cycles, regardless of the initial and final battery SOC, the QP_{Sys-Up} achievs the lowest and the QP_{Com_Out} reaches the highest hydrogen consumption. Comparing QP_{Sys-Up} and QP_{Com-Up} shows that hydrogen consumption has decreased up to 3.7% and 2.6% in Fig. 18a and Fig. 18b respectively due to the integration of the proposed systemic management. Moreover, comparison of QP_{Com-Up} and QP_{Com_Out} shows that ignorance of adaptation to the PEMFC health state has increased hydrogen consumption up to 3.2% and 6.6% in Fig. 18a and Fig. 18b respectively. Regarding the BLFS, inclusion of the systemic management has declined the hydrogen consumption up to 3.4% in Fig. 18c and 3% in Fig. 18d.
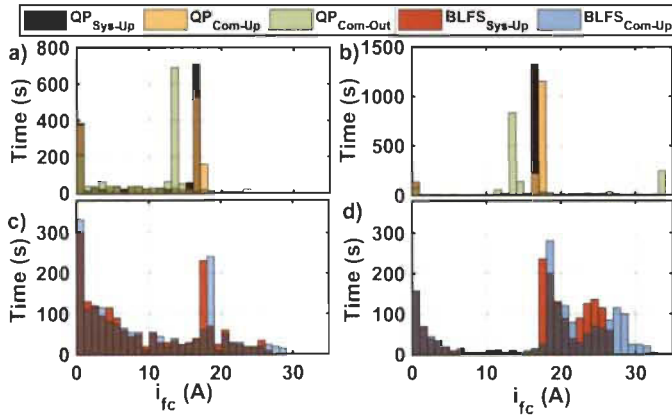

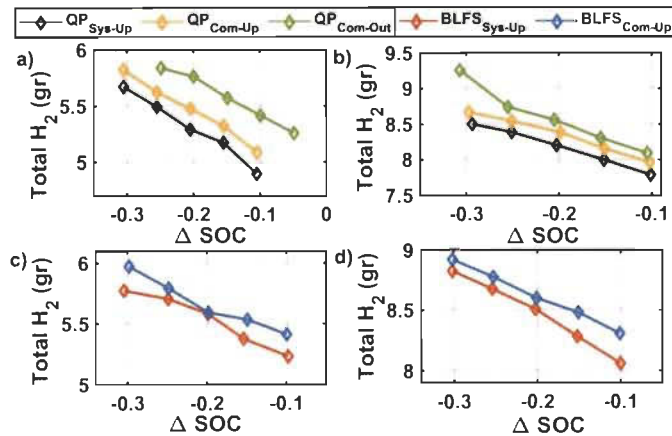Fig. 17. The distribution of the drawn current from the PEMFC stack, a) and c) WLTC_class 3, b) and d) CYC_WVUINTER.

Fig. 18. Hydrogen consumption for various initial Battery SOCs, a) and c) WLTC_class 3, b) and d) CYC_WVUINTER.

V. CONCLUSION

This paper proposes a new methodology to increase the efficiency of an EMS in a low-speed FCHEV. The EMS works based on an online systemic current and temperature

management of the PEMFC stack and determines the reference requested power as well as the reference temperature to efficiently distribute the power between the sources. Since the constraints of the EMS are updated by an online model of the PEMFC, the variation of operating conditions and degradation cannot cause mismanagement in the operation of the vehicle. Two EMSs, namely QP and BFLS, have been developed to verify the effect of the proposed systemic management on the hydrogen consumption. The two strategies, which are premised on the online systemic management (QP_{Sys-Up} and $BLFS_{Sys-Up}$), are tested under two driving cycles (WLTC_class 3 and CYC_WVUINTER) and compared with three other case studies: QP and BFLS using an updated map (QP_{Com-Up} and $BLFS_{Com-Up}$), and QP using an outdated map (QP_{Com_Out}), where the reference temperature to reach the assigned power by the EMSs is determined by the fan commercial controller in all the three cases. The comparative study illustrates that having an outdated PEMFC map can deteriorate the fuel economy of the studied vehicle up to 6.6% (comparison of QP_{Com-Up} and QP_{Com_Out} strategies). Moreover, incorporating the systemic management into the EMSs can enhance the hydrogen economy up to 3.7% in QP and 3.4% in BFLS.

Looking forward, some prospects for extending the scope of this paper remain as follows:

- Testing the effect of the proposed systemic management in this study on the performance of other common EMSs in this domain.

- Extending the idea of systemic management to water management of the PEMFC stack to devise an adaptive purging procedure for vehicular applications. It will create a link between the EMS policy and the purging cycle for a better water distribution.

- Developing an online adaptation scheme and systemic management for the battery pack as the second power source of a FCHEV.

References

[1] Z. Li, A. Khajepour, and J. Song, "A comprehensive review of the key technologies for pure electric vehicles," *Energy*, vol. 182, pp. 824-839, 2019/09/01/ 2019.

[2] N. Sulaiman, M. A. Hannan, A. Mohamed, P. J. Ker, E. H. Majlan, and W. R. Wan Daud, "Optimization of energy management system for fuel-cell hybrid electric vehicles: Issues and recommendations," *Applied Energy*, vol. 228, pp. 2061-2079, 2018/10/15/ 2018.

[3] C. M. Martinez, X. Hu, D. Cao, E. Velenis, B. Gao, and M. Wellers, "Energy Management in Plug-in Hybrid Electric Vehicles: Recent Progress and a Connected Vehicles Perspective," *IEEE Transactions on Vehicular Technology*, vol. 66, no. 6, pp. 4534-4549, 2017.

[4] R. Zhang, J. Tao, and H. Zhou, "Fuzzy Optimal Energy Management for Fuel Cell and Supercapacitor Systems Using Neural Network Based Driving Pattern Recognition," *IEEE Transactions on Fuzzy Systems*, vol. 27, no. 1, pp. 45-57, 2019.

[5] Y. Yan, Q. Li, W. Chen, B. Su, J. Liu, and L. Ma, "Optimal Energy Management and Control in Multimode Equivalent Energy Consumption of Fuel Cell/Supercapacitor of Hybrid Electric Tram," *IEEE Transactions on Industrial Electronics*, vol. 66, no. 8, pp. 6065-6076, 2019.

[6] X. Wu, X. Hu, X. Yin, L. Li, Z. Zeng, and V. Pickert, "Convex programming energy management and components sizing of a

plug-in fuel cell urban logistics vehicle," *Journal of Power Sources.* vol. 423, pp. 358-366, 2019/05/31/ 2019.

[7] M. Carignano, V. Roda, R. Costa-Castelló, L. Valiño, A. Lozano, and F. Barreras, "Assessment of Energy Management in a Fuel Cell/Battery Hybrid Vehicle," *IEEE Access,* vol. 7, pp. 16110-16122, 2019.

[8] H. Lim and W. Su, "Hierarchical Energy Management for Power-Split Plug-In HEVs Using Distance-Based Optimized Speed and SOC Profiles," *IEEE Transactions on Vehicular Technology,* vol. 67, no. 10, pp. 9312-9323, 2018.

[9] J. Chen, C. Xu, C. Wu, and W. Xu, "Adaptive Fuzzy Logic Control of Fuel-Cell-Battery Hybrid Systems for Electric Vehicles," *IEEE Transactions on Industrial Informatics,* vol. 14, no. 1, pp. 292-300, 2018.

[10] Y. Wang, S. J. Moura, S. G. Advani, and A. K. Prasad, "Power management system for a fuel cell/battery hybrid vehicle incorporating fuel cell and battery degradation," *International Journal of Hydrogen Energy.* vol. 44, no. 16, pp. 8479-8492, 2019/03/29/ 2019.

[11] H. Li, A. Ravey, A. N'Diaye, and A. Djerdir, "Online adaptive equivalent consumption minimization strategy for fuel cell hybrid electric vehicle considering power sources degradation," *Energy Conversion and Management.* vol. 192, pp. 133-149, 2019/07/15/ 2019.

[12] X. Hu, C. Zou, X. Tang, T. Liu, and L. Hu, "Cost-optimal energy management of hybrid electric vehicles using fuel cell/battery health-aware predictive control," *IEEE Transactions on Power Electronics,* pp. 1-1, 2019.

[13] N. Bizon and P. Thounthong, "Real-time strategies to optimize the fueling of the fuel cell hybrid power source: A review of issues, challenges and a new approach," *Renewable and Sustainable Energy Reviews,* vol. 91, pp. 1089-1102, 2018/08/01/ 2018.

[14] D. Zhou, A. Al-Durra, I. Matraji, A. Ravey, and F. Gao, "Online Energy Management Strategy of Fuel Cell Hybrid Electric Vehicles: A Fractional-Order Extremum Seeking Method," *IEEE Transactions on Industrial Electronics,* vol. 65, no. 8, pp. 6787-6799, 2018.

[15] K. Ettihir, L. Boulon, and K. Agbossou, "Optimization-based energy management strategy for a fuel cell/battery hybrid power system," *Applied Energy,* vol. 163, pp. 142-153, 2016/02/01/ 2016.

[16] M. Kandidayeni, A. Macias, L. Boulon, and S. Kelouwani, "Efficiency Enhancement of an Open Cathode Fuel Cell through a Systemic Management," *IEEE Transactions on Vehicular Technology,* pp. 1-1, 2019.

[17] L. Yin, Q. Li, T. Wang, L. Liu, and W. Chen, "Real-time thermal Management of Open-Cathode PEMFC system based on maximum efficiency control strategy," *Asian Journal of Control,* vol. 21, no. 4, pp. 1796-1810, 2019.

[18] K. Ou, W.-W. Yuan, M. Choi, S. Yang, and Y.-B. Kim, "Performance increase for an open-cathode PEM fuel cell with humidity and temperature control," *International Journal of Hydrogen Energy.* vol. 42, no. 50, pp. 29852-29862, 2017/12/14/ 2017.

[19] Q. Meyer *et al.,* "Optimisation of air cooled, open-cathode fuel cells: Current of lowest resistance and electro-thermal performance mapping," *Journal of Power Sources,* vol. 291, pp. 261-269, 2015/09/30/ 2015.

[20] Y. Wang, F. Qin, K. Ou, and Y. Kim, "Temperature Control for a Polymer Electrolyte Membrane Fuel Cell by Using Fuzzy Rule," *IEEE Transactions on Energy Conversion,* vol. 31, no. 2, pp. 667-675, 2016.

[21] J. Höflinger, P. Hofmann, and B. Geringer, "Experimental PEM-Fuel Cell Range Extender System Operation and Parameter Influence Analysis," 2019. Available: https://doi.org/10.4271/2019-01-0378

[22] M. Kandidayeni, A. O. M. Fernandez, A. Khalatbarisoltani, L. Boulon, S. Kelouwani, and H. Chaoui, "An Online Energy Management Strategy for a Fuel Cell/Battery Vehicle Considering the Driving Pattern and Performance Drift Impacts," *IEEE Transactions on Vehicular Technology,* pp. 1-1, 2019.

[23] V. H. Johnson, "Battery performance models in ADVISOR," *Journal of Power Sources,* vol. 110, no. 2, pp. 321-329, 2002/08/22/ 2002.

[24] Y. Zhou, A. Ravey, and M.-C. Péra, "Multi-mode predictive energy management for fuel cell hybrid electric vehicles using Markov driving pattern recognizer," *Applied Energy,* vol. 258, p. 114057, 2020/01/15/ 2020.

[25] J. P. F. Trovão, M. Roux, M. É, and M. R. Dubois, "Energy- and Power-Split Management of Dual Energy Storage System for a Three-Wheel Electric Vehicle," *IEEE Transactions on Vehicular Technology,* vol. 66, no. 7, pp. 5540-5550, 2017.

[26] S. Strahl, A. Husar, and M. Serra, "Development and experimental validation of a dynamic thermal and water distribution model of an open cathode proton exchange membrane fuel cell," *Journal of Power Sources,* vol. 196, no. 9, pp. 4251-4263, 2011/05/01/ 2011.

[27] P. W. Majsztrik, M. B. Satterfield, A. B. Bocarsly, and J. B. Benziger, "Water sorption, desorption and transport in Nafion membranes," *Journal of Membrane Science,* vol. 301, no. 1, pp. 93-106, 2007/09/01/ 2007.

[28] S. Strahl, A. Husar, P. Puleston, and J. Riera, "Performance Improvement by Temperature Control of an Open-Cathode PEM Fuel Cell System," *Fuel Cells,* vol. 14, no. 3, pp. 466-478, 2014.

[29] S. Kelouwani, K. Adegnon, K. Agbossou, and Y. Dube, "Online System Identification and Adaptive Control for PEM Fuel Cell Maximum Efficiency Tracking," *IEEE Transactions on Energy Conversion,* vol. 27, no. 3, pp. 580-592, 2012.

[30] J. Lever, M. Krzywinski, and N. Altman, "Model selection and overfitting," *Nature Methods,* vol. 13, p. 703, 08/30/online 2016.

[31] K. Ettihir, L. Boulon, and K. Agbossou, "Energy management strategy for a fuel cell hybrid vehicle based on maximum efficiency and maximum power identification," *IET Electrical Systems in Transportation,* vol. 6, no. 4, pp. 261-268, 2016.

Mohsen Kandidayeni (S'18) was born in Tehran (Iran) in 1989. His educational journey has spanned through different paths. He received the B.S. degree in Mechanical Engineering in 2011, and then did a master's degree in Mechatronics at Arak University (Iran) in 2014. He joined the Hydrogen Research Institute of University of Quebec, Trois-Rivières, QC, Canada, in 2016 and received the Ph.D. degree in Electrical Engineering from this university in 2020. He was a straight-A student during his Master and Ph.D. programs and the recipient of a doctoral scholarship from the Fonds de recherche du Québec–Nature et technologies (FRQNT). His research interests include energy-related topics such as hybrid electric vehicles, fuel cell systems, energy management, Multiphysics systems, modeling and control.

Alvaro Macias F. (M'17) was born in Mexico City, in 1992. He received the B.S. degree in Mechatronics engineering from Tec de Monterrey, Guadalajara, Mexico, in 2015 and the M.S. degree in electrical engineering from Université du Québec à Trois-Rivières, Canada, in 2018. He is currently pursuing the Ph.D. degree in electrical engineering at Université du Québec à Trois-Rivières, Canada. From 2015 to 2016, he worked as Research and Development in the Centro de Investigación y de Estudios Avanzados del Instituto Politécnico Nacional, Mexico. His current research interest includes the development of energy management strategies for fuel cell systems, passive and active system configuration, and fuel cell modeling.

Loïc Boulon (M'10,SM'15) received the master degree in electrical and automatic control engineering from the University of Lille (France), in 2006. Then, he obtained a PhD in electrical engineering from University of Franche-Comté (France). Since 2010, he is a professor at UQTR and he works into the Hydrogen Research Institute (Full Professor since 2016).

His work deals with modeling, control and energy management of multiphysics systems. His research interests include hybrid electric vehicles, energy and power sources (fuel cell systems, batteries and ultracapacitors). He has published more than 120 scientific papers in peer-reviewed international journals and international conferences and given over 35 invited conferences

all over the word. Since 2019, he is the world most cited authors of the topic "Proton exchange membrane fuel cells (PEMFC); Fuel cells; Cell stack" in Elsevier SciVal. In 2015, Loïc Boulon was general chair of the IEEE-Vehicular Power and Propulsion Conference in Montréal (QC, Canada). Prof. Loïc Boulon is now VP-Motor Vehicles of the IEEE Vehicular Technology Society and he found the "International Summer School on Energetic Efficiency of Connected Vehicles" and the "IEEE VTS Motor Vehicle Challenge". He is the holder of the Canada Research Chair in Energy Sources for the Vehicles of the future.

Sousso Kelouwani (M'00–SM'17) received the B.S. and the M.Sc.A. degrees from Université du Québec à Trois-Rivières, Trois-Rivières, QC, Canada, in 2000 and 2002, respectively, and the Ph.D. degree (automation and systems) from École Polytechnique de Montréal, Montréal, QC, Canada, in 2010, all in electrical engineering. Holder of the Canada Research Chair in Energy Optimization of intelligent transportation systems, Sousso Kelouwani is also the holder of the Industrial Research Chair DIVEL in Intelligent Navigation of Autonomous Industrial Vehicles. Full professor of Mechatronics at the Department of Mechanical Engineering at UQTR, he holds four patents in the United States, his research interest focuses on the optimization of energy systems for vehicular applications, advanced driving assistance techniques, eco-energy navigation of autonomous vehicles, hybridization of energy sources for vehicles (batteries, fuel cells, hydrogen generators, etc.) in harsh weather conditions. In 2017, he received the Environment Award of the Grand Prix for Excellence in Transport from the Quebec Transportation Association (AQTr) for the development of a hydrogen range extender based on a hydrogen generator for electric vehicles. He was also a recipient of the Canada Governor General's Gold Medal in 2000. Moreover, he has worked with several Canadian transportation companies to develop intelligent, energy-efficient and driverless vehicles.

5.3 Conclusion

This chapter puts the finishing touches to the development of an upgraded EMS which considers the systemic management and online modeling of a PEMFC stack. In this respect, a methodology for simultaneous management of PEMFC current and temperature is proposed first. Subsequently, this systemic management is incorporated into two online EMSs (QP and BLFS) in a FCHEV.

The developed systemic management strategy is based on a 3D power map, which provides an efficient path based on the stack temperature and the current level of the PEMFC system. It meets the requested power from the stack with high level of efficiency. The obtained results from the conducted experiments highlight the satisfying performance of the proposed methodology by improving the system efficiency up to 13 % and 16 % for constant and variable power profiles respectively.

This EMSs work based on the systemic current and temperature management and determine the reference requested power as well as the reference temperature from the stack to efficiently distribute the power between the sources. Since the constraints of the EMSs are updated by an online model of the PEMFC, the variation of operating conditions and degradation cannot cause mismanagement in the operation of the vehicle. The comparative study illustrates that having an outdated PEMFC map can deteriorate the fuel economy of the studied vehicle up to 6.6% (comparison of QP_{Com-Up} and QP_{Com_Out} strategies). Moreover, incorporating the systemic management into the EMSs can enhance the hydrogen economy up to 3.7% in QP and 3.4% in BFLS.

Next chapter provides a general conclusion along with future direction of this work.

Chapter 6 - Conclusion

FCHEVs represent a gradually increasing segment of the automotive market due to many favorable features. The overall performance of these vehicles, which includes drive quality, fuel economy, and the total cost of ownership, is highly dependent on the design of appropriate EMSs. This dissertation focuses on offering a clear understanding of the relationship between fuel consumption and PEMFC stack systemic management and degradation. This objective is pursued by developing EMSs that adopt a systemic viewpoint towards the management of the PEMFC stack and can embrace the stack performance drifts caused by degradation and operating conditions variation. Driven by this motivation, this thesis mainly discusses the use of online identification techniques for adapting the behavior of a PEMFC model to the performance drifts of the real device and integrating this online model into the EMS formulation of a FCHEV. The development of online PEMFC models by using these techniques prevents one from developing complicated mechanistic models to embrace the influence of all the operating and ambient conditions as well as ageing, which is a highly complicated phenomena to be modeled.

In order to provide a proof of concept for the set goals in this thesis, before going through the development of online estimation algorithms, chapter 2 illustrates the level of inaccuracy that can be caused by having a degraded PEMFC system as well as the amount of improvement that can be reached by having a systemic management. In this regard, an optimal EMS based on DP is designed in this chapter once with one control variable (PEMFC current) and another time with two control variables (PEMFC current and stack temperature) for two PEMFCs with different levels of degradation. The comparison of unidimensional

strategy, which is similar to the ones already available in the literature, and the bidimensional strategy, which is based on the systemic management of the stack, shows that the fuel economy can be increased by 4.1% just by adding the temperature dimension for the tested driving cycles. Moreover, it is observed that if the energy management policy is not adapted to the real state of health of the PEMFC stack, it leads to poor performance of the strategy and increases the fuel consumption up to almost 24.8% in the studied cases in this chapter. The results of this chapter provide a concrete proof for the fruitfulness of the set objectives in this thesis regarding the ameliorating the fuel economy of a FCHEV.

After realizing the importance of adaptation to the real state of a PEMFC system, chapter 3 touches on the important subject of PEMFC online modeling. The online model is expected to provide the real characteristics of the PEMFC system, such as maximum power and efficiency points, to be used in the design of EMS. In this respect, a multi-input semi-empirical model is selected for estimating the behavior of a PEMFC stack and the parameters of this model are identified online using different recursive filters. According to the benchmark study of this chapter, Kalman filter shows a very good performance for online parameters identification of the selected model, which has been proposed by Amphlett et. al. Moreover, a comparative study of linear and nonlinear parameters estimation of the PEMFC model shows that by estimating the maximum current density of the PEMFC, which is a nonlinear parameter in the selected model, the estimation quality of PEMFC characteristics increases noticeably.

While the development of an online PEMFC model based on recursive filters is dealt with in chapter 3, no solution is provided for the initialization of this approach. In fact, initialization plays an important role in achieving accurate results. In this regard, chapter 4

discusses the importance of initialization in improving the online estimation accuracy of the PEMFC characteristics. In this chapter, a benchmark study of three well-known metaheuristic optimization algorithms, which are one of the most reliable approaches for extracting the PEMFC model parameters offline, is performed to find the most dependable one. Subsequently, the selected algorithm, which is SFLA, is used to tune the initial parameters of the PEMFC model and the two (R and Q matrices) variables of Kalman filter. The results of this section show that good estimation of characteristics can be reached quicker and more conveniently by having an appropriate initialization.

After developing a suitable online model for estimating the PEMFC characteristics, this thesis aims at proposing a systemic management for the PEMFC stack and integrating it into the EMS design. To do so, chapter 5 puts forward a concurrent PEMFC current and temperature systemic management to supply the requested power from the stack with high level of efficiency. Moreover, this systemic management is incorporated into the EMS design of a FCHEV in this chapter.

To develop the systemic management approach, the characteristics map of PEMFC is generated to relate the power of the PEMFC stack to its current and temperature. Afterwards, according to the requested power from the PEMFC, a reference temperature is extracted from the map and sent to an optimized fuzzy controller to be reached. In the meantime, the current is being regulated by a PI controller which gives relaxation time to the PEMFC system for reaching the reference temperature. A comparative study between the performance of a commercial controller and the proposed systemic management is conducted in this chapter to illustrate the effectiveness of the suggested strategy. According to this study, the proposed

strategy is able to decrease the hydrogen consumption of the PEMFC system by 13% and 16% for the case of constant and variable power profiles respectively.

Subsequently, in chapter 5, it is shown how the provided bases in terms of online PEMFC modeling and systemic management can be incorporated into the design of EMSs for FCHEVs. These EMSs indicate indeed the eventual purpose of this thesis which is a strategy that leads to the determination of PEMFC current and stack temperature as opposed to the existing strategies which only determine the required PEMFC current. Moreover, the proposed strategies are capable of embracing the drifts in the PEMFC performance due to degradation and operating conditions variation as the model is being updated online. The performed study in this section indicates that including the systemic management into the EMS can enhance the fuel economy up to 3.7%. Moreover, if the PEMFC map becomes outdated, it can degrade the FCHEV performance in terms of fuel economy up to 6.6%.

The overall aim of this thesis was to develop the required techniques for integrating the online modeling and systemic management of a PEMFC stack into the design of an EMS for a FCHEV. Considering the discussed aspects regarding different sections of this thesis, it can be stated that the targeted goals of the thesis have been successfully reached. It has been shown in this thesis that the fuel economy of a real-time EMS for a FCHEV can be improved by 3.7%. Moreover, online updating of the PEMFC characteristics can save the hydrogen consumption up to 6.6%. The effectiveness of the proposed PEMFC online model, systemic management, and the upgraded EMS has been justified by implementing on a small-scale test bench in hydrogen research institute of University of Quebec n Trois-Rivieres. The methodology proposed in this work can serve not only as a general way to design real-time bidimensional EMSs that consider PEMFC systemic management and health-state

estimation, but also as a basis to include more dimensions while designing an EMS in all types of electrified vehicles.

6.1 Recommendations for future directions

While this thesis provides the basis for the efficiency and robustness enhancement of different existing EMSs in the literature for FCHEVs, looking forward, the following attempts should be made to further verify and improve the proposed techniques in this thesis:

6.1.1 The use of online estimation strategies in the design of energy management strategies for fuel cell hybrid electric vehicles

- **Fuel cell hybrid electric vehicle subsystems**

This thesis mainly discussed the employment of online estimation strategies for tracking the performance of the PEMFC system. However, a FCHEV is an arrangement of different subsystems, such as PEMFC, battery pack, and so forth. Each subsystem assumes significant responsibilities and their performance can be improved by precisely estimating their parameters. Regarding the battery, which is one of the most common energy storage systems in FCHEVs, the online estimation strategies have been used for the following purposes [70]:

> ➢ Battery fault estimation [71-73]: The diagnosis and estimation of faults in a battery pack are considered as the chief functions of a battery management system to keep dependable operation of electrified vehicles.

> ➢ Battery SOC estimation [74-76]: The battery SOC is the percentage of the remaining capacity in the cell compared to the total capacity. The SOC level is estimated by using measured current and voltage because it cannot be measured directly. The accurate SOC estimation is critical in vehicular applications, where

one of its usages is to determine when to stop charging and discharging. Over-charging or over-discharging can result in permanent internal damages in the battery pack.

➢ Battery SOH estimation [77-79]: The SOH of a battery can be defined as the comparison of its performance, in terms of charge/discharge capabilities, at the present time with the initial fresh conditions. The precise approximation of SOH can determine whether the battery should be replaced or not.

➢ Battery life estimation [79, 80]: The performance of the battery relies on several aspects, such as operating temperature, driving conditions, depth of discharge, humidity, and SOC. Such aspects make the employment of online battery models essential to estimate the lifetime precisely under various operation conditions.

In light of the discussed points regarding battery, it is clear that the PEMFC is not the only subsystem in a FCHEV that is in need of online estimation. As the FCHEVs come typically in FC-battery architecture, it stands to reason to link the online estimation strategies of these sub-systems to the development a health-conscious and energy-aware EMS to obtain results which are closer to the real state of the components during their lifetime.

To do so, the online state estimation of the power sources should be integrated into the EMS loop while the vehicle is under operation. Therefore, the strategy can make a decision based on the present health state of the components and assure the performance, safety, availability and reliability of power sources. The provided basis in this thesis, regarding the integration of online state estimation of a PEMFC system into the design of an EMS, paves the way for the simultaneous health state estimation of other sources in the EMS design. While designing such holistic EMS, it should be noted that, as explained throughout this

thesis, the online modeling of the PEMFC is required. Because it is the main power source and its maximum efficiency and power point of operation change by the time. Moreover, the battery output voltage decreases through time (capacity fade and resistance increase), and accordingly the battery SOH should be monitored online. The battery SOC also requires to be estimated online as it is an integral part of any rule-based system and is afflicted by the variation of the SOH.

To summarize, in future, the online state estimation of the all the on-board power sources should be considered to be incorporated into the EMS design procedure with respect to the provided foundations in this thesis.

6.1.2 The notion of adopting a systemic approach for developing multi-dimensional energy management strategies

As discussed throughout this thesis, the performance of a PEMFC stack, in terms of power delivery and efficiency, depends on several aspects, such as current, temperature, pressure, and so forth. Regarding the PEMFC as a system provides this opportunity to develop several local management strategies for controlling each of these aspects to enhance the energetic performance of the system to the utmost. This thesis put forward the simultaneous management of temperature and current and its incorporation into the design of an EMS. Learning from the results of this attempt, it is possible to extend this approach to the water management and purge procedure of a PEMFC stack with a view to include them in the EMS development of a FCHEV.

Normally, PEMFCs have three modes of operation: recirculation mode, flow-through mode, and dead-ended anode (DEA) mode [81]. Due to the advantages of simplicity, and

parasitic power and cost decline, DEA mode of operation, where the hydrogen outlet is closed, is the most common approach [82]. However, this method has also some disadvantages, one of which is the water flooding due to anode closure. To avoid this and other problems, one of the most common methods is to utilize a normally closed purge valve at the anode outlet to eliminate excess water and impurities from the cells [83]. Generally, cyclic purging is practiced where the duration and frequency of the purge need to let enough venting and cleaning of the PEMFC under full load conditions. However, this approach can lead to nonuniform water distribution in PEMFCs in dynamic load conditions, such as vehicular applications. Nonuniformity results in poor performance and noticeable cell-to-cell performance variation [84]. One solution for future work could be to devise an adaptive purging procedure for vehicular applications. The thing is that water accumulation changes according to the current flow and the air stoichiometry. In this respect, the purge cycle, which has an important role in the additional water and impurity removal, can be adjusted with respect to the stack voltage to reach a better water distribution. In a FCHEV, the stack voltage changes with respect to the requested power where the allocated power to the PEMFC system is determined by the EMS. In this regard, an adaptive purging should be devised to create a link between the policy of the EMS regarding the PEMFC usage and the purge cycle.

Another idea to extend the prospects of this thesis in this direction is the consideration of the battery pack thermal management or even both battery and PEMFC thermal managements while developing an EMS. It should be reminded that the battery cell temperature has an influence over the performance, reliability and lifespan [85]. Both high and low temperatures can deteriorate the overall performance of the battery and lead to a reduced lifespan due to increased degradation of the battery cell. Moreover, in case of

vehicular applications, since the capacity and charge/discharge rate rise, the concerns related to the battery security become more important [86]. Therefore, the use of a battery thermal management system seems to be necessary in a FCHEV to satisfy the request in higher power and improve the driving performance. Thermal management systems can be divided into active systems and passive systems [87]. Passive systems usually have zero power consumption and utilize tools such as heat pipes, phase change materials, and hydrogels. However, the cooling process is difficult to manage. Active methods mostly employ forced circulation of particular cooling substances such as water and air. The key matter is that under certain conditions, the cooling effect can be very restricted. In this respect, future works should consider the thermal management of battery pack and fuel cell stack both while designing an EMS. The main point here is that the charge/discharge capacity of the battery is highly affected by temperature. This will further influence the performance of the vehicle as the discharge rate ascertain the acceleration performance of a FCHEV. Therefore, the future EMSs should attempt to manage the use of PEMFC and battery in a way to reach a compromise in the thermal performance of these components. Moreover, the addition of supercapacitors to absorb the high dynamic peaks could be fruitful in this direction.

6.1.3 *Machine learning-based algorithms for online state estimation of the PEMFC system*

This thesis focused on the development of recursive filter-based algorithms for estimating the characteristics of a PEMFC semi-empirical model online. However, another potent tool to estimate the characteristics online is machine learning methods like artificial neural networks (ANN). One problem associated to the use of ANNs is that they are very accurate interpolator but very weak extrapolator. In other words, they perform well within the ranges

that they have been trained [88]. As the operating ranges change, they can become unreliable and may need retraining. In this respect, future works can focus on the development of adaptive ANN-based model to estimate the required characteristics of the PEMFC system for the design of an EMS. The performance of the adaptive ANN-based model should be compared with the proposed recursive filter-based online model in this thesis.

One solution for extending the operation range of the ANN-based PEMFC model is to combine it with a sub-model. The main point here is that PEMFC is a Multiphysics system and its performance depends on several factors. Therefore, the key purpose of this sub-model is to provide the ANN-based PEMFC model with the right inputs to have a performant output. For instance, let's assume the purpose is to estimate the hydrogen consumption and the inputs are the electrical power and the outlet coolant temperature in a high-power PEMFC system. It is also known that the outlet temperature of the PEMFC, itself, is related to inlet coolant temperature, the electrical power demand, and flow rate. Therefore, a sub-model, which can be a lookup table that updates the input data into the ANN as a function of the mentioned parameters, can be added to the main ANN-based model to provide the right input for accurate estimation of the characteristics. The interesting aspect of making such hybrid model is that its online adaption will be easier. The look-up table will be updated by new data while the system is under operation and the weights of the ANN-model will be updated conveniently as it does not have many inputs and outputs.

Another aspect of the thesis that can be further developed using the machine learning approaches is the initialization of the recursive filters. In fact, the future works can concentrate on determining the initial values of the unknown parameters for different operating conditions employing ANNs or fuzzy systems. In this way, adaptive recursive

filters can be developed which are completely immune to the sudden and big variations of the ambient and operating conditions.

6.1.4 Improving the performance of passive coupling-based powertrains in FCHEVs

Passive coupling refers to the connection of the power source directly to the DC bus in the FCHEV. This configuration does not require an EMS and benefits from a self-management due to different impedance of the components, for instance PEMFC and SC. As the passive configuration does not have any DC-DC converters, it leads to less weight, cost, and energy losses [89]. However, the downside of a passive hybrid FC vehicle is that the PEMFC is mainly in charge of supplying the requested power. The power split between the PEMFC system and the SC is based on the natural characteristics of each source (internal resistor and open circuit voltage for instance). Therefore, this can result in the occurrence of higher power ripples at the PEMFC side and accordingly rise the degradation rate of the stack.

From the lessons learned throughout this thesis, in future, the performance of the passive coupling-based FCHEVs can be enhanced, from the perspective of energetic efficiency, by developing several local controls for the PEMFC system. Since these configurations are self-coordinated and do not need an EMS, there will not be any concerns for integration into an EMS. As explained in section 7.1.2, water management has an important role in the energetic efficiency of a PEMFC stack. Therefore, the suggested approach in this section can be also applied to hybrid PEMFC system with a passive configuration. Another significant factor in improving the performance of the PEMFC stack is the humidity regulation [67]. In fact, low membrane humidity level leads to the growth of the membrane resistance, which, in turn,

degrades the PEMFC efficiency owing to large ohmic voltage drop. Hence, the water content of the membrane cab be managed with different means, such as anode/cathode purge, or relative humidity regulation to boost the efficiency. Future works can try the use of bubble humidifiers, which are very simple and inexpensive for PEMFC humidification to assess the efficiency improvement.

References

[1]   Z. Zoundi, "CO2 emissions, renewable energy and the Environmental Kuznets Curve, a panel cointegration approach," *Renewable and Sustainable Energy Reviews,* vol. 72, pp. 1067-1075, 5// 2017.

[2]   D. Karamanev, V. Pupkevich, K. Penev, V. Glibin, J. Gohil, and V. Vajihinejad, "Biological conversion of hydrogen to electricity for energy storage," *Energy,* vol. 129, pp. 237-245, 2017/06/15/ 2017.

[3]   J. Larminie, A. Dicks, J. Larminie, and A. Dicks, "Introduction," in *Fuel Cell Systems Explained*, ed: John Wiley & Sons, Ltd,. 2013, pp. 1-24.

[4]   A. F. Ambrose, A. Q. Al-Amin, R. Rasiah, R. Saidur, and N. Amin, "Prospects for introducing hydrogen fuel cell vehicles in Malaysia," *International Journal of Hydrogen Energy,* vol. 42, pp. 9125-9134, 2017/04/06/ 2017.

[5]   H. S. Das, C. W. Tan, and A. H. M. Yatim, "Fuel cell hybrid electric vehicles: A review on power conditioning units and topologies," *Renewable and Sustainable Energy Reviews,* vol. 76, pp. 268-291, 2017/09/01/ 2017.

[6]   N. Sulaiman, M. A. Hannan, A. Mohamed, E. H. Majlan, and W. R. Wan Daud, "A review on energy management system for fuel cell hybrid electric vehicle: Issues and challenges," *Renewable and Sustainable Energy Reviews,* vol. 52, pp. 802-814, 2015/12/01/ 2015.

[7]   X. Hu, N. Murgovski, L. M. Johannesson, and B. Egardt, "Optimal Dimensioning and Power Management of a Fuel Cell/Battery Hybrid Bus via Convex Programming," *IEEE/ASME Transactions on Mechatronics,* vol. 20, pp. 457-468, 2015.

[8]   K. Simmons, Y. Guezennec, and S. Onori, "Modeling and energy management control design for a fuel cell hybrid passenger bus," *Journal of Power Sources,* vol. 246, pp. 736-746, 2014/01/15/ 2014.

[9]   C. Min and G. A. Rincon-Mora, "Accurate electrical battery model capable of predicting runtime and I-V performance," *IEEE Transactions on Energy Conversion,* vol. 21, pp. 504-511, 2006.

[10]   N. Sulaiman, M. A. Hannan, A. Mohamed, E. H. Majlan, and W. R. Wan Daud, "A review on energy management system for fuel cell hybrid electric vehicle: Issues and challenges," *Renewable and Sustainable Energy Reviews,* vol. 52, pp. 802-814, 2015/12/01/ 2015.

[11]   A. Panday and H. O. Bansal, "A Review of Optimal Energy Management Strategies for Hybrid Electric Vehicle," *International Journal of Vehicular Technology,* vol. 2014, pp. 1-19, 2014.

[12]   S. F. Tie and C. W. Tan, "A review of energy sources and energy management system in electric vehicles," *Renewable and Sustainable Energy Reviews,* vol. 20, pp. 82-102, 2013.

[13] O. Erdinc and M. Uzunoglu, "Recent trends in PEM fuel cell-powered hybrid systems: Investigation of application areas, design architectures and energy management approaches," *Renewable and Sustainable Energy Reviews,* vol. 14, pp. 2874-2884, 2010.

[14] N. Sulaiman, M. A. Hannan, A. Mohamed, P. J. Ker, E. H. Majlan, and W. R. Wan Daud, "Optimization of energy management system for fuel-cell hybrid electric vehicles: Issues and recommendations," *Applied Energy,* vol. 228, pp. 2061-2079, 2018/10/15/ 2018.

[15] A. M. Ali and D. Söffker, "Towards Optimal Power Management of Hybrid Electric Vehicles in Real-Time: A Review on Methods, Challenges, and State-Of-The-Art Solutions," *Energies,* vol. 11, p. 476, 2018.

[16] C. M. Martinez, X. Hu, D. Cao, E. Velenis, B. Gao, and M. Wellers, "Energy Management in Plug-in Hybrid Electric Vehicles: Recent Progress and a Connected Vehicles Perspective," *IEEE Transactions on Vehicular Technology,* vol. 66, pp. 4534-4549, 2017.

[17] H. Li, A. Ravey, A. N. Diaye, and A. Djerdir, "A Review of Energy Management Strategy for Fuel Cell Hybrid Electric Vehicle," in *2017 IEEE Vehicle Power and Propulsion Conference (VPPC)*, 2017, pp. 1-6.

[18] Y. Huang, H. Wang, A. Khajepour, B. Li, J. Ji, K. Zhao*, et al.*, "A review of power management strategies and component sizing methods for hybrid vehicles," *Renewable and Sustainable Energy Reviews,* vol. 96, pp. 132-144, 2018/11/01/ 2018.

[19] W. Zhou, L. Yang, Y. Cai, and T. Ying, "Dynamic programming for new energy vehicles based on their work modes Part II: Fuel cell electric vehicles," *Journal of Power Sources,* vol. 407, pp. 92-104, 2018/12/15/ 2018.

[20] W. Zhou, L. Yang, Y. Cai, and T. Ying, "Dynamic programming for New Energy Vehicles based on their work modes part I: Electric Vehicles and Hybrid Electric Vehicles," *Journal of Power Sources,* vol. 406, pp. 151-166, 2018/12/01/ 2018.

[21] R. Zhang and J. Tao, "GA-Based Fuzzy Energy Management System for FC/SC-Powered HEV Considering H2Consumption and Load Variation," *IEEE Transactions on Fuzzy Systems,* vol. 26, pp. 1833-1843, 2018.

[22] Z. Chen, Y. Wu, N. Guo, J. Shen, and R. Xiao, "Energy management for plug-in hybrid electric vehicles based on quadratic programming with optimized engine on-off sequence," in *IECON 2017 - 43rd Annual Conference of the IEEE Industrial Electronics Society*, 2017, pp. 7134-7139.

[23] Z. Chen, C. C. Mi, R. Xiong, J. Xu, and C. You, "Energy management of a power-split plug-in hybrid electric vehicle based on genetic algorithm and quadratic programming," *Journal of Power Sources,* vol. 248, pp. 416-426, 2014/02/15/ 2014.

[24] M. Koot, J. T. B. A. Kessels, B. d. Jager, W. P. M. H. Heemels, P. P. J. v. d. Bosch, and M. Steinbuch, "Energy management strategies for vehicular electric power systems," *IEEE Transactions on Vehicular Technology,* vol. 54, pp. 771-782, 2005.

[25]   Y. Liu, J. Li, Z. Chen, D. Qin, and Y. Zhang, "Research on a multi-objective hierarchical prediction energy management strategy for range extended fuel cell vehicles," *Journal of Power Sources,* vol. 429, pp. 55-66, 2019/07/31/ 2019.

[26]   Q. Li, W. Huang, W. Chen, Y. Yan, W. Shang, and M. Li, "Regenerative braking energy recovery strategy based on Pontryagin's minimum principle for fell cell/supercapacitor hybrid locomotive," *International Journal of Hydrogen Energy,* vol. 44, pp. 5454-5461, 2019/02/26/ 2019.

[27]   S. Xie, X. Hu, Z. Xin, and J. Brighton, "Pontryagin's Minimum Principle based model predictive control of energy management for a plug-in hybrid electric bus," *Applied Energy,* vol. 236, pp. 893-905, 2019/02/15/ 2019.

[28]   H. Li, A. Ravey, A. N'Diaye, and A. Djerdir, "A novel equivalent consumption minimization strategy for hybrid electric vehicle powered by fuel cell, battery and supercapacitor," *Journal of Power Sources,* vol. 395, pp. 262-270, 2018/08/15/ 2018.

[29]   W. Zhang, J. Li, L. Xu, and M. Ouyang, "Optimization for a fuel cell/battery/capacity tram with equivalent consumption minimization strategy," *Energy Conversion and Management,* vol. 134, pp. 59-69, 2017/02/15/ 2017.

[30]   E. Kamal and L. Adouane, "Intelligent Energy Management Strategy Based on Artificial Neural Fuzzy for Hybrid Vehicle," *IEEE Transactions on Intelligent Vehicles,* vol. 3, pp. 112-125, 2018.

[31]   H. Kazemi, Y. P. Fallah, A. Nix, and S. Wayne, "Predictive AECMS by Utilization of Intelligent Transportation Systems for Hybrid Electric Vehicle Powertrain Control," *IEEE Transactions on Intelligent Vehicles,* vol. 2, pp. 75-84, 2017.

[32]   R. Zhang, J. Tao, and H. Zhou, "Fuzzy Optimal Energy Management for Fuel Cell and Supercapacitor Systems Using Neural Network Based Driving Pattern Recognition," *IEEE Transactions on Fuzzy Systems,* vol. 27, pp. 45-57, 2019.

[33]   Y. Yan, Q. Li, W. Chen, B. Su, J. Liu, and L. Ma, "Optimal Energy Management and Control in Multimode Equivalent Energy Consumption of Fuel Cell/Supercapacitor of Hybrid Electric Tram," *IEEE Transactions on Industrial Electronics,* vol. 66, pp. 6065-6076, 2019.

[34]   X. Wu, X. Hu, X. Yin, L. Li, Z. Zeng, and V. Pickert, "Convex programming energy management and components sizing of a plug-in fuel cell urban logistics vehicle," *Journal of Power Sources,* vol. 423, pp. 358-366, 2019/05/31/ 2019.

[35]   Q. Li, B. Su, Y. Pu, Y. Han, T. Wang, L. Yin, *et al.,* "A State Machine Control Based on Equivalent Consumption Minimization for Fuel Cell/ Supercapacitor Hybrid Tramway," *IEEE Transactions on Transportation Electrification,* vol. 5, pp. 552-564, 2019.

[36]   A. Fathy, H. Rezk, and A. M. Nassef, "Robust hydrogen-consumption-minimization strategy based salp swarm algorithm for energy management of fuel cell/supercapacitor/batteries in highly fluctuated load condition," *Renewable Energy,* vol. 139, pp. 147-160, 2019/08/01/ 2019.

[37] M. Carignano, V. Roda, R. Costa-Castelló, L. Valiño, A. Lozano, and F. Barreras, "Assessment of Energy Management in a Fuel Cell/Battery Hybrid Vehicle," *IEEE Access,* vol. 7, pp. 16110-16122, 2019.

[38] D. Zhou, A. Al-Durra, F. Gao, A. Ravey, I. Matraji, and M. Godoy Simões, "Online energy management strategy of fuel cell hybrid electric vehicles based on data fusion approach," *Journal of Power Sources,* vol. 366, pp. 278-291, 2017/10/31/ 2017.

[39] J. Chen, C. Xu, C. Wu, and W. Xu, "Adaptive Fuzzy Logic Control of Fuel-Cell-Battery Hybrid Systems for Electric Vehicles," *IEEE Transactions on Industrial Informatics,* vol. 14, pp. 292-300, 2018.

[40] D. Zhou, A. Ravey, A. Al-Durra, and F. Gao, "A comparative study of extremum seeking methods applied to online energy management strategy of fuel cell hybrid electric vehicles," *Energy Conversion and Management,* vol. 151, pp. 778-790, 2017/11/01/ 2017.

[41] R. Koubaa and L. krichen, "Double layer metaheuristic based energy management strategy for a Fuel Cell/Ultra-Capacitor hybrid electric vehicle," *Energy,* vol. 133, pp. 1079-1093, 2017/08/15/ 2017.

[42] P. M. Muñoz, G. Correa, M. E. Gaudiano, and D. Fernández, "Energy management control design for fuel cell hybrid electric vehicles using neural networks," *International Journal of Hydrogen Energy,* vol. 42, pp. 28932-28944, 2017/11/30/ 2017.

[43] C. Sandoval, V. M. Alvarado, J.-C. Carmona, G. Lopez Lopez, and J. F. Gomez-Aguilar, "Energy management control strategy to improve the FC/SC dynamic behavior on hybrid electric vehicles: A frequency based distribution," *Renewable Energy,* vol. 105, pp. 407-418, 2017/05/01/ 2017.

[44] M. G. Carignano, R. Costa-Castelló, V. Roda, N. M. Nigro, S. Junco, and D. Feroldi, "Energy management strategy for fuel cell-supercapacitor hybrid vehicles based on prediction of energy demand," *Journal of Power Sources,* vol. 360, pp. 419-433, 2017/08/31/ 2017.

[45] T. Fletcher, R. Thring, and M. Watkinson, "An Energy Management Strategy to concurrently optimise fuel consumption & PEM fuel cell lifetime in a hybrid vehicle," *International Journal of Hydrogen Energy,* vol. 41, pp. 21503-21515, 2016/12/14/ 2016.

[46] Z. Hu, J. Li, L. Xu, Z. Song, C. Fang, M. Ouyang, *et al.,* "Multi-objective energy management optimization and parameter sizing for proton exchange membrane hybrid fuel cell vehicles," *Energy Conversion and Management,* vol. 129, pp. 108-121, 2016/12/01/ 2016.

[47] L. Xu, J. Li, and M. Ouyang, "Energy flow modeling and real-time control design basing on mean values for maximizing driving mileage of a fuel cell bus," *International Journal of Hydrogen Energy,* vol. 40, pp. 15052-15066, 2015/11/16/ 2015.

[48]   J. Bernard, S. Delprat, T. M. Guerra, and F. N. Büchi, "Fuel efficient power management strategy for fuel cell hybrid powertrains," *Control Engineering Practice,* vol. 18, pp. 408-417, 2010/04/01/ 2010.

[49]   D. Feroldi, M. Serra, and J. Riera, "Energy Management Strategies based on efficiency map for Fuel Cell Hybrid Vehicles," *Journal of Power Sources,* vol. 190, pp. 387-401, 2009/05/15/ 2009.

[50]   A. A. Shah, K. H. Luo, T. R. Ralph, and F. C. Walsh, "Recent trends and developments in polymer electrolyte membrane fuel cell modelling," *Electrochimica Acta,* vol. 56, pp. 3731-3757, 2011.

[51]   Y. Wang, S. J. Moura, S. G. Advani, and A. K. Prasad, "Power management system for a fuel cell/battery hybrid vehicle incorporating fuel cell and battery degradation," *International Journal of Hydrogen Energy,* vol. 44, pp. 8479-8492, 2019/03/29/ 2019.

[52]   Y. Wang, S. J. Moura, S. G. Advani, and A. K. Prasad, "Optimization of powerplant component size on board a fuel cell/battery hybrid bus for fuel economy and system durability," *International Journal of Hydrogen Energy,* vol. 44, pp. 18283-18292, 2019/07/05/ 2019.

[53]   H. Li, A. Ravey, A. N'Diaye, and A. Djerdir, "Online adaptive equivalent consumption minimization strategy for fuel cell hybrid electric vehicle considering power sources degradation," *Energy Conversion and Management,* vol. 192, pp. 133-149, 2019/07/15/ 2019.

[54]   X. Hu, C. Zou, X. Tang, T. Liu, and L. Hu, "Cost-optimal energy management of hybrid electric vehicles using fuel cell/battery health-aware predictive control," *IEEE Transactions on Power Electronics,* pp. 1-1, 2019.

[55]   N. Bizon and P. Thounthong, "Real-time strategies to optimize the fueling of the fuel cell hybrid power source: A review of issues, challenges and a new approach," *Renewable and Sustainable Energy Reviews,* vol. 91, pp. 1089-1102, 2018/08/01/ 2018.

[56]   D. Zhou, A. Al-Durra, I. Matraji, A. Ravey, and F. Gao, "Online Energy Management Strategy of Fuel Cell Hybrid Electric Vehicles: A Fractional-Order Extremum Seeking Method," *IEEE Transactions on Industrial Electronics,* vol. 65, pp. 6787-6799, 2018.

[57]   K. Ettihir, L. Boulon, and K. Agbossou, "On-line proton exchange membrane fuel cell identification based on a rls algorithm," in *5th International Conference on Fundamentals & Development of Fuel Cells (FDFC 2013),* 2013.

[58]   K. Ettihir, L. Boulon, and K. Agbossou, "Energy management strategy for a fuel cell hybrid vehicle based on maximum efficiency and maximum power identification," *IET Electrical Systems in Transportation,* vol. 6, pp. 261-268, 2016.

[59]   K. Ettihir, L. Boulon, and K. Agbossou, "Optimization-based energy management strategy for a fuel cell/battery hybrid power system," *Applied Energy,* vol. 163, pp. 142-153, 2016/02/01/ 2016.

[60] K. Ettihir, L. Boulon, M. Becherif, K. Agbossou, and H. S. Ramadan, "Online identification of semi-empirical model parameters for PEMFCs," *International Journal of Hydrogen Energy,* vol. 39, pp. 21165-21176, 2014.

[61] S. Kelouwani, N. Henao, K. Agbossou, Y. Dube, and L. Boulon, "Two-Layer Energy-Management Architecture for a Fuel Cell HEV Using Road Trip Information," *IEEE Transactions on Vehicular Technology,* vol. 61, pp. 3851-3864, 2012.

[62] R. N. Methekar, S. C. Patwardhan, R. D. Gudi, and V. Prasad, "Adaptive peak seeking control of a proton exchange membrane fuel cell," *Journal of Process Control,* vol. 20, pp. 73-82, 2010/01/01/ 2010.

[63] D. Li, Y. Yu, Q. Jin, and Z. Gao, "Maximum power efficiency operation and generalized predictive control of PEM (proton exchange membrane) fuel cell," *Energy,* vol. 68, pp. 210-217, 2014/04/15/ 2014.

[64] L. Xu, J. Li, J. Hua, X. Li, and M. Ouyang, "Adaptive supervisory control strategy of a fuel cell/battery-powered city bus," *Journal of Power Sources,* vol. 194, pp. 360-368, 2009.

[65] L. Yin, Q. Li, T. Wang, L. Liu, and W. Chen, "Real-time thermal Management of Open-Cathode PEMFC system based on maximum efficiency control strategy," *Asian Journal of Control,* vol. 0, 2019.

[66] M. Kandidayeni, A. Macias, L. Boulon, and S. Kelouwani, "Optimized Fuzzy Thermal Management of an Open Cathode Fuel Cell System," in *2018 IEEE Vehicle Power and Propulsion Conference (VPPC)*, 2018, pp. 1-6.

[67] K. Ou, W.-W. Yuan, M. Choi, S. Yang, and Y.-B. Kim, "Performance increase for an open-cathode PEM fuel cell with humidity and temperature control," *International Journal of Hydrogen Energy,* vol. 42, pp. 29852-29862, 2017/12/14/ 2017.

[68] Q. Meyer, K. Ronaszegi, G. Pei-June, O. Curnick, S. Ashton, T. Reisch, *et al.,* "Optimisation of air cooled, open-cathode fuel cells: Current of lowest resistance and electro-thermal performance mapping," *Journal of Power Sources,* vol. 291, pp. 261-269, 2015/09/30/ 2015.

[69] Y. Wang, F. Qin, K. Ou, and Y. Kim, "Temperature Control for a Polymer Electrolyte Membrane Fuel Cell by Using Fuzzy Rule," *IEEE Transactions on Energy Conversion,* vol. 31, pp. 667-675, 2016.

[70] X. Hu, F. Feng, K. Liu, L. Zhang, J. Xie, and B. Liu, "State estimation for advanced battery management: Key challenges and future trends," *Renewable and Sustainable Energy Reviews,* vol. 114, p. 109334, 2019/10/01/ 2019.

[71] Q. Yu, R. Xiong, and C. Lin, "Model-Based Sensor Fault Detection for Lithium-Ion Batteries in Electric Vehicles," in *2019 IEEE 89th Vehicular Technology Conference (VTC2019-Spring)*, 2019, pp. 1-4.

[72] J. Wei, G. Dong, and Z. Chen, "Model-based fault diagnosis of Lithium-ion battery using strong tracking Extended Kalman Filter," *Energy Procedia,* vol. 158, pp. 2500-2505, 2019/02/01/ 2019.

[73]   J. Wei, G. Dong, and Z. Chen, "Lyapunov-based thermal fault diagnosis of cylindrical lithium-ion batteries," *IEEE Transactions on Industrial Electronics,* pp. 1-1, 2019.

[74]   Z. Xi, M. Dahmardeh, B. Xia, Y. Fu, and C. Mi, "Learning of Battery Model Bias for Effective State of Charge Estimation of Lithium-Ion Batteries," *IEEE Transactions on Vehicular Technology,* vol. 68, pp. 8613-8628, 2019.

[75]   P. Shrivastava, T. K. Soon, M. Y. I. B. Idris, and S. Mekhilef, "Overview of model-based online state-of-charge estimation using Kalman filter family for lithium-ion batteries," *Renewable and Sustainable Energy Reviews,* vol. 113, p. 109233, 2019/10/01/ 2019.

[76]   M. U. Ali, A. Zafar, S. H. Nengroo, S. Hussain, M. Junaid Alvi, and H.-J. Kim, "Towards a Smarter Battery Management System for Electric Vehicle Applications: A Critical Review of Lithium-Ion Battery State of Charge Estimation," *Energies,* vol. 12, p. 446, 2019.

[77]   X. Li, Z. Wang, L. Zhang, C. Zou, and D. D. Dorrell, "State-of-health estimation for Li-ion batteries by combing the incremental capacity analysis method with grey relational analysis," *Journal of Power Sources,* vol. 410-411, pp. 106-114, 2019/01/15/ 2019.

[78]   L. Cai, J. Meng, D.-I. Stroe, G. Luo, and R. Teodorescu, "An evolutionary framework for lithium-ion battery state of health estimation," *Journal of Power Sources,* vol. 412, pp. 615-622, 2019/02/01/ 2019.

[79]   M. S. H. Lipu, M. A. Hannan, A. Hussain, M. M. Hoque, P. J. Ker, M. H. M. Saad, *et al.,* "A review of state of health and remaining useful life estimation methods for lithium-ion battery in electric vehicles: Challenges and recommendations," *Journal of Cleaner Production,* vol. 205, pp. 115-133, 2018/12/20/ 2018.

[80]   J. Zhu, T. Tan, L. Wu, and H. Yuan, "RUL Prediction of Lithium-Ion Battery Based on Improved DGWO-ELM Method in a Random Discharge Rates Environment," *IEEE Access,* vol. 7, pp. 125176-125187, 2019.

[81]   J. Zhao, Q. Jian, Z. Huang, L. Luo, and B. Huang, "Experimental study on water management improvement of proton exchange membrane fuel cells with dead-ended anode by periodically supplying fuel from anode outlet," *Journal of Power Sources,* vol. 435, p. 226775, 2019/09/30/ 2019.

[82]   Y. Yang, X. Zhang, L. Guo, and H. Liu, "Different flow fields, operation modes and designs for proton exchange membrane fuel cells with dead-ended anode," *International Journal of Hydrogen Energy,* vol. 43, pp. 1769-1780, 2018/01/18/ 2018.

[83]   B. Chen, Z. Tu, and S. H. Chan, "Performance degradation and recovery characteristics during gas purging in a proton exchange membrane fuel cell with a dead-ended anode," *Applied Thermal Engineering,* vol. 129, pp. 968-978, 2018/01/25/ 2018.

[84]   H. Li, Y. Tang, Z. Wang, Z. Shi, S. Wu, D. Song, *et al.,* "A review of water flooding issues in the proton exchange membrane fuel cell," *Journal of Power Sources,* vol. 178, pp. 103-117, 2008/03/15/ 2008.

[85]   X. Hu, Y. Zheng, D. A. Howey, H. Perez, A. Foley, and M. Pecht, "Battery warm-up methodologies at subzero temperatures for automotive applications: Recent advances and perspectives," *Progress in Energy and Combustion Science,* vol. 77, p. 100806, 2020/03/01/ 2020.

[86]   Y. Lyu, A. R. M. Siddique, S. H. Majid, M. Biglarbegian, S. A. Gadsden, and S. Mahmud, "Electric vehicle battery thermal management system with thermoelectric cooling," *Energy Reports,* vol. 5, pp. 822-827, 2019/11/01/ 2019.

[87]   Z. Rao and S. Wang, "A review of power battery thermal energy management," *Renewable and Sustainable Energy Reviews,* vol. 15, pp. 4554-4571, 2011/12/01/ 2011.

[88]   F. J. Asensio, J. I. San Martín, I. Zamora, and O. Oñederra, "Model for optimal management of the cooling system of a fuel cell-based combined heat and power system for developing optimization control strategies," *Applied Energy,* vol. 211, pp. 413-430, 2018/02/01/ 2018.

[89]   A. Macías, M. Kandidayeni, L. Boulon, and J. Trovão, "Passive and Active Coupling Comparison of Fuel Cell and Supercapacitor for a Three-Wheel Electric Vehicle," *Fuel Cells,* vol. n/a.

[90]   M. Ali, M. A. Elhameed, and M. A. Farahat, "Effective Parameters' Identification for Polymer Electrolyte Membrane Fuel Cell Models Using Grey Wolf Optimizer," *Renewable Energy,* 2017.

[91]   O. E. Turgut and M. T. Coban, "Optimal proton exchange membrane fuel cell modelling based on hybrid Teaching Learning Based Optimization – Differential Evolution algorithm," *Ain Shams Engineering Journal,* vol. 7, pp. 347-360, 2016.

[92]   Z. Sun, N. Wang, Y. Bi, and D. Srinivasan, "Parameter identification of PEMFC model based on hybrid adaptive differential evolution algorithm," *Energy,* vol. 90, pp. 1334-1341, 2015.

[93]   C. Restrepo, T. Konjedic, A. Garces, J. Calvente, and R. Giral, "Identification of a Proton-Exchange Membrane Fuel Cell's Model Parameters by Means of an Evolution Strategy," *IEEE Transactions on Industrial Informatics,* vol. 11, pp. 548-559, 2015.

[94]   K. Priya, T. Sudhakar Babu, K. Balasubramanian, K. Sathish Kumar, and N. Rajasekar, "A novel approach for fuel cell parameter estimation using simple Genetic Algorithm," *Sustainable Energy Technologies and Assessments,* vol. 12, pp. 46-52, 2015.

[95]   R. Zhang and J. Tao, "GA-Based Fuzzy Energy Management System for FC/SC-Powered HEV Considering H2 Consumption and Load Variation," *IEEE Transactions on Fuzzy Systems,* vol. 26, pp. 1833-1843, 2018.

[96]   M. Kandi-D, M. Soleymani, and A. A. Ghadimi, "Designing an Optimal Fuzzy Controller for a Fuel Cell Vehicle Considering Driving Patterns," *Scientia Iranica,* vol. 23, pp. 218-227, 2016.

[97]   H. S. Ramadan, M. Becherif, and F. Claude, "Energy Management Improvement of Hybrid Electric Vehicles via Combined GPS/Rule-Based Methodology," *IEEE Transactions on Automation Science and Engineering,* vol. 14, pp. 586-597, 2017.

Publications

Scientific Journals:

2020:

[1]   **M. Kandidayeni**, A. Macias, L. Boulon, and S. Kelouwani, "Efficiency Upgrade of Fuel Cell Hybrid Vehicles' Energy Management Strategies by Online Systemic Management of Fuel Cell," **IEEE Transactions on Industrial Electronics**, 2020 (Accepted).

[2]   **M. Kandidayeni**, A. Macias, L. Boulon, and S. Kelouwani, "Investigating the Impact of Aging and Thermal Management of a Fuel Cell System in Energy Management Strategies," **Applied Energy**, 2020 (Under review).

2019:

[3]   **M. Kandidayeni**, A. Macias, L. Boulon, and S. Kelouwani, "Efficiency Enhancement of an Open Cathode Fuel Cell through a Systemic Management," **IEEE Transactions on Vehicular Technology**, 2019 (doi: 10.1109/TVT.2019.2944996).

[4]   **M. Kandidayeni**, A. O. M. Fernandez, A. Khalatbarisoltani, L. Boulon, S. Kelouwani, and H. Chaoui, "An Online Energy Management Strategy for a Fuel Cell/Battery Vehicle Considering the Driving Pattern and Performance Drift Impacts," **IEEE Transactions on Vehicular Technology**, 2019 (doi: 10.1109/TVT.2019.2936713).

[5]   **M. Kandidayeni**, A. Macias, A. Khalatbarisoltani, L. Boulon, and S. Kelouwani, "Benchmark of proton exchange membrane fuel cell parameters extraction with metaheuristic optimization algorithms," **Energy**, vol. 183, pp. 912-925, 2019/09/15.

[6]   A. O. M. Fernandez, **M. Kandidayeni**, L. Boulon, and H. Chaoui, "An Adaptive State Machine Based Energy Management Strategy for a Multi-Stack Fuel Cell Hybrid Electric Vehicle," **IEEE Transactions on Vehicular Technology**, 2019 (doi: 10.1109/TVT.2019.2950558).

[7]   A. Macías, **M. Kandidayeni**, L. Boulon, and J. Trovão, "Passive and Active Coupling Comparison of Fuel Cell and Supercapacitor for a Three-Wheel Electric Vehicle," **Fuel Cells**, 2019 (doi: 10.1002/fuce.201900089).

[8]   A. K. Soltani, **M. Kandidayeni**, L. Boulon, and D. L. St-Pierre, "Modular Energy Systems in Vehicular Applications," **Energy Procedia**, vol. 162, pp. 14-23, 2019/04/01.

2018:

[9]   **M. Kandidayeni**, A. Macias, A. A. Amamou, L. Boulon, S. Kelouwani, and H. Chaoui, "Overview and benchmark analysis of fuel cell parameters estimation for energy management purposes," **Journal of Power Sources**, vol. 380, pp. 92-104, 2018/03/15.

[10]   **M. Kandidayeni**, A. Macias, A. A. Amamou, L. Boulon, and S. Kelouwani, "Comparative Analysis of Two Online Identification Algorithms in a Fuel Cell System," **Fuel Cells**, vol. 18, pp. 347-358, 2018/06/01.

[11]   A. Amamou, **M. Kandidayeni**, L. Boulon, and S. Kelouwani, "Real time adaptive efficient cold start strategy for proton exchange membrane fuel cells," **Applied Energy**, vol. 216, pp. 21-30, 2018/04/15.

Scientific Conferences:

2020:

[1]   **M. Kandidayeni**, L. Boulon, and S. Kelouwani, "Online Identification of a PEMFC System for Energy Management Purposes," **Young Energy Researchers Conference**, World Sustainable Energy Days", Wels, Austria, 4-6 March, 2020 (Selected work by the committee for oral presentation and exempted from conference fees).

2019:

[2]   **M. Kandidayeni**, L. Boulon, and S. Kelouwani, "Energy Management Strategy Design Considering the Degradation and Thermal Management of a Fuel Cell System," **4e Québec Mines+Énergie (Energy Research Challenge)**", Quebec City, Canada, 18-21 November, 2019 (Winner of the third prize in Energy Research Challenge). (https://mern.gouv.qc.ca/en/challenge-winners-2/)

[3]   **M. Kandidayeni**, L. Boulon, and S. Kelouwani, "Enhancing the Performance of Kalman Filter for Online Identification of a Fuel Cell Semi-Empirical Model," **The 8th International Conference on "Fundamentals & Development of Fuel Cells (FDFC)"**, Nantes, France, February 2019.

[4]   R. Ghaderi, **M. Kandidayeni**, M. Soleimani, and L. Boulon, "Investigation of the Battery Degradation Impact on the Energy Management of a Fuel Cell Hybrid Electric Vehicle," **in 2019 IEEE Vehicle Power and Propulsion Conference (VPPC)**, 2019, pp. 1-6.

2018:

[5]   **M. Kandidayeni**, A. Macias, L. Boulon, and S. Kelouwani, "Optimized Fuzzy Thermal Management of an Open Cathode Fuel Cell System," **in 2018 IEEE Vehicle Power and Propulsion Conference (VPPC)**, 2018, pp. 1-6.

[6]   A. Macias, **M. Kandidayeni**, L. Boulon, and H. Chaoui, "A novel online energy management strategy for multi fuel cell systems," **in 2018 IEEE International Conference on Industrial Technology (ICIT)**, 2018, pp. 2043-2048.

2017:

[7]   **M. Kandidayeni**, A. Macias, C. Depature, L. Boulon, S. Kelouwani, and H. Chaoui, "Real-Time Fuzzy Logic Strategy Scheme for Energetic Macroscopic Representation of a Fuel Cell/Battery Vehicle," **in 2017 IEEE Vehicle Power and Propulsion Conference (VPPC)**, 2017, pp. 1-6.

[8]   **M. Kandidayeni**, L. Boulon, and S. Kelouwani, "Comparative Analysis of Real-Time Identification Methods in a Fuel Cell System," **The 7th International Conference on "Fundamentals & Development of Fuel Cells (FDFC)"**, Stuttgart, Germany, February 2017. (Selected work by the committee for publication in Fuel Cells Journal)

Appendix A – Résumé

L'émission des gaz à effet de serre a été citée comme l'une des principales causes du réchauffement climatique. À cet égard, le secteur des transports est largement blâmé pour la combustion de produits dérivés du pétrole, qui produisent une bonne quantité de ce gaz à effet de serre. Les voitures particulières sont perçues comme les principales sources de rejets de gaz à effet de serre dans ce secteur. Afin de réduire ces émissions, il est crucial de remplacer les véhicules conventionnels par des véhicules propres (zéro émission). [1, 2].

Les véhicules électriques et hybrides pourraient être des alternatives appropriées aux véhicules conventionnels. Cependant, les véhicules hybrides reposent toujours sur les combustibles fossiles et les véhicules électriques présentent quelques inconvénients tels qu'une autonomie limitée ainsi qu'un long temps de recharge. Ces écueils ont ouverts la voie à l'émergence de véhicules hybrides à pile à combustible (VHPAC), fonctionnant à l'hydrogène. Les VHPAC utilisent les piles à combustible (PAC) à membrane échangeuse de protons pour fournir de l'électricité au moteur électrique. Ce type de PAC possède un grand potentiel tel que le fonctionnement à basse température, la haute densité de puissance et l'électrolyte solide [3].

L'autonomie et la durée de vie d'un VHPAC dépendent de la conception des stratégies de gestion énergétique (SGE) appropriées. La majorité des SGE existantes dans la littérature, telles que celles basées sur des règles, basées sur l'optimisation et basées sur l'intelligence, dépendent des modèles de PAC à membrane d'échange de protons [47-49]. À cet égard, la

modélisation des PAC est très importante et une sélection appropriée du modèle doit être faite en fonction des objectifs particuliers du projet. Cependant, l'impact des phénomènes de dégradation et des conditions de fonctionnement de la PAC (température, pression, courant, etc.) sur ses performances énergétiques ont rendu la conception d'un modèle de pile à combustible extrêmement compliquée. Il convient de noter que la littérature présente différents modèles de PAC qui sont capables de faire face aux variations des conditions de fonctionnement [50]. Ces modèles sont déjà convaincants mais pas encore idéaux puisqu'ils ne considèrent pas les phénomènes de dégradation et que leur paramétrage requiert des expériences chronophages.

À cet égard, des efforts considérables ont été déployés pour immuniser la conception de la SGE contre les dérives des performances des PAC en ajoutant un modèle de dégradation au système [51-54]. Cependant, les mécanismes de dégradation et de vieillissement sont très complexes à modéliser. De plus, les paramètres de fonctionnement qui ne sont pas inclus dans le modèle de PAC, tels que l'humidité ou la température ambiante, peuvent également modifier les plages d'efficacité maximale (EM) et de puissance maximale (PM) de la pile. Pour résoudre ces problèmes, deux approches de recherche d'extremum et d'identification en ligne des paramètres du modèle PAC ont été examinées. La première consiste à utiliser des méthodes de recherche d'extrémum qui identifient un point de fonctionnement optimal en utilisant un signal de perturbation périodique en temps réel [40, 55, 56]. De telles stratégies sont intéressantes en raison de leur mise en œuvre simple. Toutefois, elles ne sont pas très efficaces lorsqu'une identification simultanée de plusieurs points de fonctionnement est requise dans les applications en ligne. Pour éviter ce problème, certaines recherches ont été menées en utilisant des filtres récursifs pour l'identification en ligne des paramètres de PAC

et en extrayant les caractéristiques nécessaires du modèle mis à jour. [57-61] ont été réalisés à l'institut de recherche sur l'hydrogène (IRH). Dans [57], Ettihir et al. ont proposé l'utilisation d'un modèle semi-empirique, fonction du courant, avec une méthode récursive pour obtenir les caractéristiques de la PAC en ligne. Ils ont également intégré ce travail dans la conception de SGE d'un VHPAC et ont obtenu des résultats intéressants [58-60]. Kelouwani et al. ont suggéré une étude expérimentale basée sur le traçage de EM de la PAC. Dans cette étude, un modèle polynomial de l'efficacité de la PAC est introduit et la meilleure efficacité est recherchée en ajustant les variables de contrôle (courant, stœchiométrie et température) [61]. Methekar et al. a introduit un contrôle adaptatif d'un système de PAC avec un modèle de Wiener et a suggéré une validation numérique [62]. Dazi et al. ont développé un contrôle prédictif pour déterminer le fonctionnement à PM d'un système de PAC [63]. Dans [64], une stratégie adaptative basée sur le contrôle par supervision est proposée en utilisant une méthode de minimisation de la consommation équivalente. Dans cet article, un algorithme des moindres carrés récursifs est utilisé pour l'identification des performances du PEMFC. Le modèle de PAC utilisé est un modèle semi-empirique très simple, et il n'y a pas de validation expérimentale de ses performances.

A.1 Énoncé du problème et cadre conceptuel de la thèse

En ce qui concerne les travaux étudiés, il peut être déduit que l'emploi de techniques en temps réel doit faire l'objet d'une plus grande attention en vue d'adapter la conception des SGE au comportement réel des PAC. Comme indiqué précédemment, certaines caractéristiques opérationnelles de la PAC, telles que l'EM et la PM, sont généralement considérées comme les variables de conception lors de l'élaboration d'une SGE. Néanmoins, ces caractéristiques varient avec le temps pour plusieurs raisons, telles que la variation des

conditions de fonctionnement (température, pression, humidité, etc.) et les phénomènes de vieillissement et de dégradation. La figure A.1 montre les dérives de performance d'une pile à combustible Horizon de 500 W en termes de puissance disponible. La puissance nominale de la pile en varie en fonction du courant et de la température. La figure A.1a indique une dérive de 20% de la puissance maximale de la pile entre son début de vie (BOL) et sa fin de vie (EOL). La figure A.1b représente les dérives résultant du changement de saison (Température ambiante : 27 °C en été et 20 °C en hiver). Les étoiles représentent la puissance maximale qui varie en fonction des conditions de fonctionnement de la pile et de sa dégradation. Quelle que soit la raison des variations des caractéristiques de la PAC, il est important de les considérer dans le SGE afin d'optimiser le control en temps réel. Il existe plusieurs SGE proposées en ligne et en temps réel pour l'application des VHPAC. Cependant, la majorité des travaux de recherche ne prend pas en considération les caractéristiques réelles du PAC lors de la conception du SGE. La littérature présente quelques travaux de recherche qui propose des SGE considérant les caractéristiques variables de la PAC mais ils sont principalement basés sur la simulation et manquent de validations expérimentales.
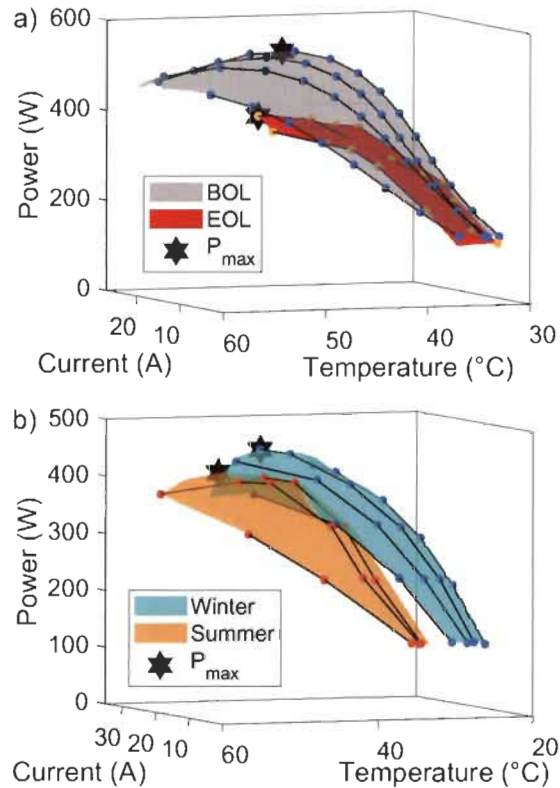
Figure A.1 Variation des caractéristiques d'une PAC dans le temps, a) variation sur la durée de vie, b) variation saisonnière.

Un autre aspect qui a échappé à l'attention de nombreux chercheurs dans le domaine de la conception de SGE pour les VHPAC est l'adoption d'une approche systémique de la gestion énergétique et thermique de la PAC. Les SGE existantes ne contrôlent généralement que le courant requis de la PAC (la gestion de température étant traitée comme un problème de contrôle local à la PAC). Néanmoins, considérer la PAC comme un système offre plusieurs degrés de liberté en termes de contrôle. Les paramètres qui influent les performances de la PAC tels que le courant et la température peuvent être contrôlés simultanément en temps réel. Une puissance demandée de la PAC peut être fournie par différentes combinaisons de ces paramètres de courants et températures pour améliorer l'efficacité [65]. Il est important de noter qu'il existe de nombreux travaux concernant la gestion thermique ou la gestion du

courant de la PAC [66-69]. Cependant, à la connaissance des auteurs, l'intégration d'une gestion simultanée du courant et de la température, qui ont des dynamiques physiques différentes, n'a pas été envisagée jusqu'à présent dans la conception d'un SGE. La figure A.2 indique le concept général proposé par cette thèse pour améliorer l'efficacité et la robustesse des SGE existants. L'ensemble du processus se déroule en ligne pendant le fonctionnement de la PAC. La SGE globale comprend trois étapes, à savoir l'identification des paramètres ainsi que la stratégie de gestion locale, l'extraction d'informations et le partage de puissance. L'objectif est de faire une identification des paramètres en ligne pour adapter le modèle aux dérives de performance de la PAC, puis de définir les meilleurs points de fonctionnement dans l'étape d'extraction des informations tout en ayant une gestion locale. Ensuite, les données obtenues peuvent être utilisées dans l'étape de stratégie de répartition de puissance pour contrôler le flux de puissance entre les différentes sources. Ce processus de trois étapes est appelé EMS global.
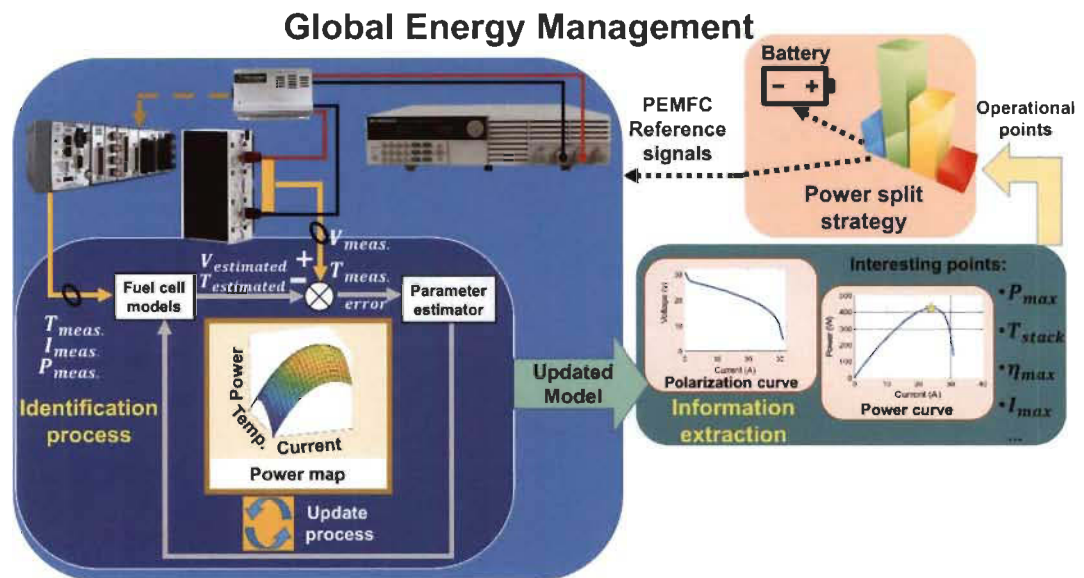

Figure A.2 Le concept général pour la conception d'un SGE global pour un VHPAC.

A.2 Contribution du projet

L'étude de la littérature indique qu'il existe une variété d'approches, en ligne et hors ligne, pour répartir la puissance entre les sources dans un VHPAC. De plus, il existe plusieurs méthodes pour déterminer les meilleures performances de la PAC ou améliorer son efficacité grâce à une gestion locale. Cependant, il convient de noter qu'il n'y a que quelques stratégies qui essaient de lier la répartition de puissance dans un VHPAC avec l'identification des performances en temps réel de la PAC. À cet égard, ce travail vise à utiliser des algorithmes d'estimation des paramètres en ligne afin de s'adapter aux dérives de performance de la PAC. Même si quelques travaux ont été publiés [57-60], une attention méticuleuse devrait être portée au choix du modèle et de la méthode d'estimation.

Mis à part le point mentionné, un aspect central que les chercheurs n'ont pas remarqué jusqu'à présent dans ce domaine est d'envisager une méthode systémique pour la gestion d'une PAC tout en développant une SGE. Dans la littérature, le courant et la température de fonctionnement sont normalement perçus comme des variables de contrôle indépendantes. Néanmoins, la PAC est un système multi-physique avec de fortes interactions dynamiques entre le courant et la température. Une gestion systémique de la PAC permet la conception de stratégies multi-sorties. Cela signifie que la puissance demandée de la PAC peut être fournie par une efficacité plus élevée car elle peut utiliser différentes combinaisons de courant et de température de fonctionnement.

À cet égard, deux directions principales ont été suivies dans cette thèse :

- Prévoir une rigueur scientifique pour la base proposée par les études précédentes afin de choisir un modèle de PAC et une méthode d'identification appropriés en effectuant une étude comparative.

- Faire avancer le concept en intégrant un modèle à entrées multiples et ses gestions de courant et thermique dans la conception de la stratégie.

A.2.1 Objectifs

L'objectif principal est d'intégrer l'estimation des paramètres en ligne et la gestion systémique d'une PAC dans la conception d'une stratégie de gestion énergétique et thermique en ligne dans un VHPAC. À cette fin, les objectifs suivants sont fixés :

➢ Réaliser une étude comparative pour donner une structure solide au concept :

Les études précédentes sont basées sur un modèle à entrée unique, qui ne dépend que du courant. Les autres conditions de fonctionnement, telles que la température, la pression, etc., sont considérées comme des perturbations. Dans ce travail, une étude comparative est menée dans le but de sélectionner un modèle à entrées multiples, qui englobe les principales conditions de fonctionnement, telles que le courant, la température et la pression. De plus, une méthode d'identification des paramètres en ligne appropriée est sélectionnée pour compenser les incertitudes du modèle dues à la dégradation et les conditions de fonctionnement qui ne sont pas prises en compte dans le modèle. Comme ce travail vise à concevoir une stratégie multidimensionnelle, il est nécessaire d'avoir un modèle fiable à entrées multiples.

➢ Gestion énergétique et thermique de la PAC :

L'étude comparative conduit à la sélection d'une méthode d'estimation des paramètres de la PAC ainsi que d'un modèle multi-entrées pour prédire le comportement de la PAC. La température est l'une des entrées du modèle

électrochimique à entrées multiples choisi, et sa valeur est mesuré en ligne sur une vraie pile à combustible. Cependant, la régulation de la température de la PAC, qui a un effet considérable sur ses performances, n'est pas possible avec un modèle électrochimique. A cet égard, un modèle thermique de la pile à combustible, qui permet de contrôler la température en agissant sur le ventilateur, est nécessaire. L'objectif est d'utiliser un modèle thermique en plus du modèle électrochimique pour assurer une gestion énergétique et thermique locale de la pile. Cette gestion systémique permet d'atteindre efficacement le niveau de puissance souhaité en choisissant le bon niveau de température et de courant.

➢ Intégration de la gestion systémique de la PAC dans une SGE pour un VHPAC :

Le modèle proposé ainsi que la gestion locale de la PAC sont utilisés pour concevoir une SGE globale. L'idée principale est d'effectuer une identification de modèle en temps réel pour trouver les meilleurs points de fonctionnement à travers une étape d'extraction d'informations. Par la suite, la stratégie de partage de puissance peut utiliser les données fournies par le modèle de PAC mis à jour pour distribuer de manière optimale le flux de puissance. L'autre contribution de cette SGE est qu'elle permet de contrôler simultanément la température et le courant de la pile en temps réel.

A.3 Méthodologie

Après avoir discuté de la motivation et mené une étude approfondie de la littérature dans la première étape (chapitre 1), la deuxième étape vise à fournir une base concrète pour soutenir l'hypothèse selon laquelle la modélisation en ligne d'une PAC et sa gestion

systémique peut conduire à l'amélioration des performances d'une SGE dans un VHPAC. À cet égard, une SGE optimale basée sur une programmation dynamique (DP) est formulée pour comparer la consommation d'hydrogène d'un VHPAC, simulé pour différents scénarios. Dans le premier scénario, la consommation d'hydrogène du véhicule est étudiée en développant une programmation dynamique unidimensionnelle pour déterminer la trajectoire optimale du courant de PAC tout en utilisant deux PAC avec différents niveaux de dégradation. Cette analyse montrera l'effet de la dégradation de la PAC sur l'économie de carburant du véhicule. Dans le deuxième scénario, une programmation dynamique bidimensionnelle est développée pour la nouvelle étude de cas de PAC afin de déterminer la trajectoire optimale du courant et du rapport cyclique du ventilateur de refroidissement. Ensuite, les résultats sont comparés à la SGE unidimensionnelle pour montrer qu'il est important de considérer la PAC en tant que système lors de la conception d'une SGE.

La troisième étape de ce travail se concentre sur l'identification en ligne des paramètres d'une PAC. Comme il existe quelques preuves de concept dans ce domaine, cette étape apporte une rigueur scientifique par : 1) Une revue de la littérature pour déterminer l'état actuel des informations sur le sujet proposé. Par la suite, les méthodes envisagées sont classées en termes de précision, d'applicabilité dans des situations en ligne et de gestion de l'énergie; 2) une étude comparative par simulation sur la base des candidats de la première étape pour sélectionner un modèle de PAC à entrées multiples approprié et une méthode d'identification pour les étapes ultérieures ; 3) une validation expérimentale du modèle et de la technique d'identification sélectionnés.

La quatrième étape de cette thèse porte sur l'initialisation des filtres récursifs pour le problème d'estimation des paramètres de PAC en ligne. À cet égard, une étude comparative

de trois algorithmes d'optimisation métaheuristique bien connus est effectuée pour introduire une technique fiable pour le réglage initial du filtre récursif. Il convient de noter que les algorithmes métaheuristiques sont l'approche la plus courante dans la littérature pour extraire les paramètres d'un modèle de PAC. La qualité de l'estimation en ligne des caractéristiques des PAC est examinée pour différentes valeurs initiales.

La dernière étape de ce travail porte sur le développement d'une gestion simultanée du courant et de la température à travers la cartographie des caractéristiques des PAC et l'intégration de cette approche à la conception SGE d'un VHPAC. Le principal défi ici est la différence entre la dynamique rapide du courant et la dynamique lente de la température. La gestion systémique offre la possibilité d'avoir un contrôle local sur la PAC pour améliorer ses performances en temps réel. Une telle gestion systémique convient à des fins de gestion de l'énergie. À cet égard, la gestion de la température et du courant obtenue à partir de cette étape ouvre la voie à la conception de SGE qui peuvent conduire à des résultats très pertinents. La stratégie proposée à ce stade vise principalement à améliorer les performances d'un VHPAC en termes d'économie de carburant en utilisant une gestion systémique en ligne de la PAC. Cette stratégie est en fait le but ultime de cette thèse car elle prend en compte à la fois les dérives de performance d'une PAC et sa gestion thermique. Une caractéristique distinctive de cette stratégie est de générer deux signaux de référence (courant et température de PAC) pour atteindre l'optimalité dans le partage de puissance, contrairement aux stratégies existantes qui n'ont qu'une seule variable de contrôle (courant de PAC). Il convient de mentionner que la SGE est validée expérimentalement sur un banc d'essai développé pour le véhicule Némo de l'IRH. Nemo est un véhicule à hydrogène à l'échelle du laboratoire pour la validation.

A.4 Résultats et analyse

Le chapitre 2 présente l'importance de la gestion systémique et de l'identification en ligne des PAC dans le développement d'une SGE pour les VHPAC. À cet égard, une stratégie optimale basée sur la programmation dynamique est développée dans ce chapitre. La stratégie proposée est conçue avec une variable de contrôle (courant de PAC) et avec deux variables de contrôle (courant et température de la PAC) pour deux PAC avec différents niveaux de dégradation. La comparaison de la stratégie unidimensionnelle, similaire à celles déjà disponibles dans la littérature, et de la stratégie bidimensionnelle, basée sur la gestion systémique de la PAC, montre que l'économie de carburant peut être augmentée de 4,1% en ajoutant simplement la température comme variable de contrôle. De plus, on constate que si la politique de gestion de l'énergie n'est pas adaptée à l'état réel de santé de la PAC, elle conduit à une mauvaise performance de la stratégie et augmente la consommation de carburant jusqu'à près de 24,8% dans les cas étudiés dans ce chapitre. Les résultats de ce chapitre apportent une preuve concrète de la pertinence des objectifs fixés dans cette thèse concernant l'amélioration de l'économie de carburant d'un VHPAC.

Dans le chapitre 3, un modèle semi-empirique à entrées multiples est sélectionné pour estimer le comportement d'une PAC et les paramètres de ce modèle sont identifiés en ligne à l'aide de différents filtres récursifs. Selon l'étude comparative des filtres récursifs, le filtre de Kalman montre une très bonne performance pour l'identification en ligne des paramètres du modèle sélectionné, qui a été proposée par Amphlett et. al. De plus, une étude comparative de l'estimation des paramètres linéaires et non linéaires du modèle de PAC montre que l'estimation de la densité de courant maximale de la PAC, qui présente un paramètre non linéaire dans le modèle sélectionné, augmente la qualité d'estimation.

Le chapitre 4 discute l'importance de l'initialisation pour améliorer la précision d'estimation en ligne des caractéristiques des PAC. Dans ce chapitre, une étude comparative de trois algorithmes d'optimisation métaheuristique bien connus est effectuée pour trouver celui qui est le plus fiable. Par la suite, l'algorithme sélectionné, appelé ''shuffled frog leaping algorithm'' (SFLA), est utilisé pour régler les paramètres initiaux du modèle de PAC et les deux variables du filtre de Kalman (matrices R and Q). Les résultats de cette section montrent qu'une bonne estimation des caractéristiques peut être atteinte plus rapidement et plus facilement en ayant une initialisation appropriée.

Le chapitre 5 propose une gestion systémique simultanée du courant et de la température des PAC pour fournir la puissance demandée avec un haut niveau d'efficacité. De plus, cette gestion systémique est intégrée dans la conception stratégique d'un VHPAC dans ce chapitre.

À cet égard, dans le but de développer l'approche de gestion systémique, la carte des caractéristiques de la PAC est générée pour relier sa puissance au courant et à la température. Par la suite, selon la puissance demandée de la PAC, une température de référence est extraite de la carte et envoyée à un contrôleur de logique floue optimisée pour être atteinte. En attendant, le courant est régulé par un régulateur PI qui donne un temps de relaxation à la PAC pour atteindre la température de référence. Une étude comparative entre la performance d'un contrôleur commercial et la gestion systémique proposée est réalisée dans ce chapitre pour illustrer l'efficacité de la stratégie offerte. Selon cette étude, la stratégie proposée est capable de diminuer la consommation d'hydrogène du système de PAC de 13% et 16% pour le cas de profils de puissance constants et variables, respectivement.

Par la suite, la modélisation en ligne des piles à combustible et la gestion systémique sont intégrées dans la conception de la SGE pour les VHPAC. La SGE optimale est basée sur une

fonction de coût quadratique et elle permet de contrôler simultanément le courant et la température de PAC au contraire des stratégies existantes qui ne contrôlent que le courant de la pile. De plus, cette stratégie est capable de compenser les dérives de performances de la PAC car le modèle est mis à jour en ligne. L'étude réalisée dans cette section indique que l'inclusion de la gestion systémique dans la stratégie peut améliorer l'économie de carburant jusqu'à 3,7%. De plus, si la carte de la PAC est considérée statique, cela peut dégrader les performances du véhicule en termes d'économie de carburant jusqu'à 6,6%.

A.5 Discussion des articles

A.5.1 Article 1: Investigating the Impact of Aging and Thermal Management of a Fuel Cell System in Energy Management Strategies

Cet article se concentre sur l'évaluation de l'influence de la dégradation et de la gestion thermique d'une PAC sur l'économie de carburant d'un VHPAC. À cet égard, une programmation dynamique déterministe est formulée de manière unidimensionnelle et bidimensionnelle pour une PAC neuve et pour une PAC vieillie. Semblable aux SGE existantes dans la littérature, la programmation dynamique unidimensionnelle ne détermine que le courant requis de la PAC, tout en respectant la limitation des sources d'énergie. Cependant, la programmation dynamique bidimensionnelle détermine le courant et la température requis de la PAC pour fournir la puissance. La prise en compte de la température en plus du courant est une nouvelle étape dans la conception de la SGE qui a échappé aux attentions des études précédentes. Les performances des stratégies formulées sont évaluées sous deux cycles de WLTC_class 2 et CYC_WVUINTER. L'analyse de divers scénarios indique que l'intégration de la température peut améliorer l'économie de carburant jusqu'à

4,1%. De plus, le vieillissement de la PAC peut dégrader l'économie de carburant jusqu'à 14,7% en stratégie unidimensionnelle. Les résultats finaux indiquent également que si la politique de gestion de l'énergie pour la distribution d'énergie entre la PAC et la batterie n'est pas mise à jour, elle peut augmenter la consommation d'hydrogène jusqu'à 24,8%.

A.5.2 Article 2: Overview and benchmark analysis of fuel cell parameters estimation for energy management purposes

Un examen approfondi des étapes nécessaires de la modélisation à l'utilisation des techniques d'identification pour la conception des stratégies de gestion énergétique en ligne des VHPAC est effectué dans cet article. À cet égard, tout d'abord, des approches de modélisation des PAC sont étudiées dans lesquelles les modèles semi-empiriques sont distingués comme l'un des modèles les plus adaptés à des applications en ligne. Deuxièmement, les méthodes d'identification des paramètres des PAC sont discutées et l'une des catégories qui est très appropriée pour la conception des stratégies de gestion énergétique en temps réel est sélectionnée pour une analyse plus approfondie. Enfin, une étude comparative de trois techniques potentielles d'identification des paramètres, algorithme des moindres carrés récursifs, filtre de Kalman, et filtre de Kalman étendu, est réalisée en utilisant deux modèles de PAC semi-empiriques. Les résultats de l'étude comparative indiquent qu'en cas d'analyse linéaire, l'intégration du filtre de Kalman avec le modèle proposé par Amphlett et. al a une performance supérieure par rapport aux autres combinaisons. En plus, il a été conclu que la méthode d'identification non linéaire, au moyen de filtre de Kalman étendu et le modèle d'Amphlett et. al, donne l'estimation de courbe de polarisation la plus précise.

A.5.3 Article 3: Benchmark of proton exchange membrane fuel cell parameters

extraction with metaheuristic optimization algorithms

Cet article étudie les performances de trois algorithmes d'optimisation métaheuristique, à savoir SFLA, Imperialist Competitive Algorithm (ICA) et fire fly algorithm (FOA), dans un problème d'extraction de paramètres de la PAC. À cet égard, la comparaison des performances des algorithmes est effectuée en utilisant la somme de l'erreur quadratique entre la tension mesurée et estimée de la PAC pour deux études de cas disponibles dans la littérature sur 100 essais indépendants. Par la suite, la précision des algorithmes est jugée sur la base de leur meilleure valeur de fitness, pire valeur de fitness, variance et écart type. Enfin, l'algorithme sélectionné à partir de l'étape de comparaison est utilisé pour identifier les paramètres du modèle d'une PAC Horizon de 500 W à cathode ouverte. Cette nouvelle étude propose une température de PAC variable contrairement aux autres études de cas existantes dans la littérature. Les résultats finaux de cette étude indiquent qu'en ce qui concerne la meilleure somme d'erreur quadratique, SFLA surpasse légèrement ICA et FOA dans les deux études de cas. Cependant, les résultats montrent que SFLA fonctionne 20% mieux que ICA et deux fois mieux que FOA dans la première et deuxième étude de cas. De plus, la variance et l'écart type de SFLA sont sensiblement inférieurs à ceux des autres algorithmes, ce qui justifient la précision et la répétabilité de cette méthode.

A.5.4 Article 4: Efficiency Enhancement of an Open Cathode Fuel Cell through

a Systemic Management

Dans ce manuscrit, une stratégie de gestion systémique est proposée pour améliorer l'efficacité d'un système de PAC à cathode ouverte pour différents niveaux de puissance demandés. Cette stratégie se concentre sur l'utilisation de la cartographie 3D pour déterminer

la température de référence du schéma de contrôle. À cet égard, un certain nombre d'expériences sont menées pour obtenir une carte de puissance 3D pour différentes températures et courants. Cette carte de puissance fournit un trajet efficace basé sur la température et le niveau de courant du système de la PAC et détermine la température de référence pour chaque niveau de puissance demandé du système. Enfin, un contrôleur logique floue optimisé est utilisé pour atteindre la température de référence définie lorsque le courant de la PAC est contrôlé par un contrôleur PI. Les résultats obtenus à partir des expériences mettent en évidence les performances satisfaisantes de la méthodologie proposée en améliorant l'efficacité du système jusqu'à 13% et 16% pour des profils de puissance constants et variables respectivement.

A.5.5 Article 5: Efficiency Upgrade of Fuel Cell Hybrid Vehicles Energy Management Strategies by Online Systemic Management of Fuel Cell

Cet article propose une nouvelle méthodologie pour augmenter l'efficacité d'une SGE pour un VHPAC à basse vitesse. La SGE fonctionne sur la base d'une gestion systémique en ligne du courant et de la température de la PAC. Il détermine la puissance de référence demandée ainsi que la température de référence de la PAC pour répartir efficacement la puissance entre les sources. Du fait que les contraintes de la SGE sont mises à jour par un modèle en ligne de la PAC, la variation des conditions de fonctionnement et la dégradation ne peuvent plus perturber la gestion énergétique du véhicule. La stratégie utilisée est basée sur une programmation quadratique. Cette stratégie, qui repose sur la gestion systémique en ligne, a été testée pour deux cycles différents (WLTC_class 3 and CYC_WVUINTER) et comparée à deux autres cas :

- Programmation quadratique à l'aide d'une carte mise à jour et programmation quadratique à l'aide d'une carte obsolète.

- La température de référence pour atteindre la puissance assignée par la programmation quadratique est déterminée par le contrôleur commercial dans les deux cas.

L'étude comparative illustre que le fait d'avoir une carte obsolète de la PAC peut détériorer l'économie de carburant du véhicule étudié jusqu'à 6,6%. De plus, l'intégration de la gestion systémique dans la programmation quadratique peut améliorer l'économie de l'hydrogène jusqu'à 3,7%.

A.5.6 Article 6: *Comparative Analysis of Two Online Identification Algorithms in a Fuel Cell System*

Dans cet article, deux algorithmes récursifs bien connus (Algorithme des moindres carrés récursifs et algorithme récursif du maximum de vraisemblance) sont comparés pour l'estimation en ligne des paramètres d'un modèle de PAC semi-empirique à entrées multiples. À cet égard, tout d'abord, un modèle de PAC semi-empirique est sélectionné pour atteindre un compromis satisfaisant entre le temps de calcul et la signification physique. Par la suite, les algorithmes sont utilisés pour identifier les paramètres du modèle. Enfin, les résultats expérimentaux obtenus par les algorithmes sont discutés et leur robustesse est étudiée. Les résultats indiquent que les deux algorithmes sont capables d'estimer la tension de sortie à un niveau satisfaisant. Cependant, l'algorithme récursif du maximum de vraisemblance a montré plus de robustesse dans le traitement des données de mesure bruitées Il convient de rappeler que cette robustesse pourrait conduire à des capteurs et des instruments de mesure moins coûteux. De plus, il convient de noter que la plage d'altération des paramètres semi-

empiriques était acceptable. Ces travaux pourront être intégrés dans la conception d'une gestion globale de l'énergie pour les VHPAC.

A.5.7 Article 7: An Online Energy Management Strategy for a Fuel Cell/Battery Vehicle Considering the Driving Pattern and Performance Drift Impacts

Cet article présente une nouvelle SGE multimode en ligne pour un VHPAC. Cette stratégie est principalement composée d'un classificateur de conditions de conduite (basé sur la carte auto adaptative) et d'un contrôleur à logique floue multimode. La fonction d'appartenance de sortie est constamment ajustée en fonction de l'estimation en ligne des limites PM et EM de la PAC par un filtre de Kalman et un modèle semi-empirique. La carte auto adaptative développée reconnaît les conditions de conduite et active le mode le plus approprié du contrôleur à logique floue à chaque mise à jour pour fournir efficacement la puissance demandée du véhicule. Les performances de la stratégie en ligne proposée sont comparées à un contrôleur de logique floue optimisé hors ligne sous un cycle combiné de CYC_NewYorkBus, CYC_UDDS et WLTC_class 3. Un résultat satisfaisant est obtenu avec seulement une différence de 2% en termes de coût total de la consommation d'hydrogène et de cycles marche/arrêt du système PAC. De plus, les performances de la stratégie proposée sont testées lorsque le système PAC subit une dérive de seize pour cent concernant la PM. Dans ce cas, la stratégie en ligne proposée s'adapte à l'état réel du système de PAC et améliore les performances énergétiques du véhicule de 8% par rapport au contrôleur multimode hors ligne.

Appendix B – Article 6

B.1 Objectives

This paper aims at providing a basis for easy integration of a PEMFC real behavior into the design of real-time EMSs. In this regard, two recursive algorithms are introduced, and tested to identify the parameters of a PEMFC model online. The utilized PEMFC model is a semi-empirical which has eight parameters for identification. This model requires the current, stack temperature, and pressure as inputs and estimates the PEMFC voltage as the output. This integration provides one with online characteristics of a PEMFC, such as polarization curve, maximum power, and efficiency, which can be used in an EMS loop to update the constraints and related control laws. The parameters of such model have been only estimated offline with various optimization algorithms in previous studies [90-94]. However, in this work, parameter identification is performed online to counteract uncertainties that occur slowly over time, such as ageing, and quickly due to change of the operating conditions which are not considered in the model.

Compared to other similar works in the literature, the main contribution of this work is the online parameters estimation of a multi-input (current, temperature, and pressure) semi-

empirical model with eight parameters, as opposed to a single-input (current) model with four parameters used in [57-60, 64]. Since the intrinsic dynamic of current, temperature, and pressure are completely different, a multi-input model identification is more challenging than a single-input one. Moreover, a careful experimental study for comparing the effectiveness of the utilized identification methods is given along with a step-by-step explanation for adapting the algorithms to this particular problem. It should be noted that as a first step for online identification of PEMFC parameters, this paper mainly provides the proof of concept by utilizing two common algorithms and does not go through the details for selecting a suitable model and identification technique. These concerns are dealt with in Article 3.

B.2 Methodology

This paper proposes online identification of a multi-input PEMFC model to track the performance drifts due to the influence of degradation phenomenon and the operating conditions, which are not considered in the model, over the output voltage of a FC system. In this regard, firstly, a semi-empirical model is selected to reach a satisfactory compromise between computational time and physical meaning. This model has four tuning parameters for activation loss, three parameters for Ohmic loss, and one parameter for concentration loss. Although the model is nonlinear, the targeted parameters for identification have a linear structure. Therefore, two recursive identification algorithms, namely recursive least square (RLS) and recursive maximum likelihood (RML), are utilized to update the parameters of the chosen model online. RLS algorithm is based on the concept of minimizing the error related to input signal and gives excellent performance when operating in time varying conditions. Assuming that noise is serially uncorrelated and independent of the elements of the regression vector, it can be applied to a linear-in-parameter system to estimate the

parameters, and the model can be called a linear regression. RML algorithm holds a striking resemblance to RLS. The main difference here is that the disturbance acting on the output of the system is modeled as a moving average of a serially uncorrelated white noise sequence. In this case, the unobserved components are approximated by the residuals, which are the values of the estimation error. Various scenarios, four noise levels and two PEMFCs with different levels of degradation, have been considered to test the performance of the algorithms.

B.3 Synopsis of the results analyses

Different analyses have been performed in this paper to clarify the effectiveness of the discussed algorithms and the PEMFC model. Each algorithm is used to tune the parameters of the semi-empirical model for two real PEMFCs with different degradation levels. In order to check the robustness of the algorithms, a random noise is added to the measured voltage, and the noisy signal is sent to the process of identification. Regarding the comparison of the algorithms to one another, the mean square error (MSE) and the peak signal to noise ratio (PSNR) have been utilized. MSE and PSNR are two error metrics used to compare the estimation quality. PSNR calculates the peak signal-to-noise ratio, in decibels, between the two original signal and estimated signal. The higher the PSNR, the better the quality of the estimation. The MSE represents the cumulative squared error between the estimated voltage and the measured voltage. The lower the value of MSE, the lower the error. The voltage estimation quality of the algorithms in terms of PSNR and MSE is compared for four cases, namely zero noise, a random noise with variance of 0.25, a random noise with variance of 0.5, and a random noise with variance of 0.75. Zero noise refers to the normal measurement, and the other cases show the addition of random noise with different variances to test the

robustness of the algorithms. The obtained results confirm that, in case of normal measured data (zero noise), RLS performs better than RML to some extent. However, as the level of noise increases, RML algorithm indicates superior performance compared to RLS. This result implies that RML algorithm is more robust than RLS while confronting some noises in the system.

Figure B.1 compares the polarization curves obtained by the estimated parameters with RML and RLS algorithms for the noise level of 0.25. As is clear in this figure, the estimated polarization curve by RML algorithm is closer to the reference, which comes from the experimental data, than RLS. This figure also shows the influence of noise in the polarization curve estimation. Looking more closely, it can be concluded that a small change in the voltage estimation can cause a noticeable change in the polarization curve estimation. The difference between the PSNR values of RML and RLS algorithms for the noise level of 0.25 is not a lot. However, this slight difference causes an obvious change in the polarization curve prediction.
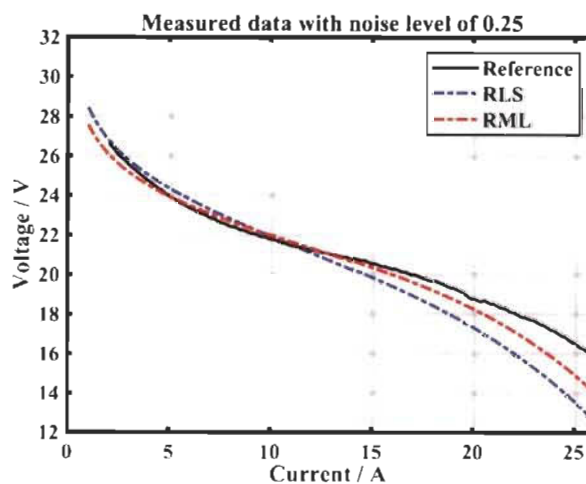

Figure B.1 The comparison of polarization curves obtained by the utilized algorithms.

B.4 Conclusion

In this paper, two well-known recursive algorithms are compared for online estimation of a multi-input semi-empirical PEMFC model parameters. In this respect, firstly, a semi-empirical FC model is selected to reach a satisfactory compromise between computational time and physical meaning. Subsequently, the algorithms are explained and implemented to identify the parameters of the model. Finally, experimental results achieved by the algorithms are discussed and their robustness is investigated. The main results achieved from the experimental implementation and test of the algorithms indicate that both of the algorithms are capable of estimating the output voltage to a satisfactory level. However, RML has shown more robustness in dealing with noisy measurement data. It is worth reminding that this robustness might lead to less expensive sensors and measurement instruments. Moreover, it should be noted that the range of alteration in the semi-empirical parameters was acceptable. In future, this work can be integrated into the design of global energy management for FCHEVs.

Fuel Cells

Comparative Analysis of Two Online Identification Algorithms in a Fuel Cell System▲

M. Kandidayeni[1]*, A. Macias[1], A. A. Amamou[1], L. Boulon[1,2], S. Kelouwani[1]

[1] Université du Québec à Trois-Rivières, Hydrogen Research Institute, Trois-Rivières, QC, Canada
[2] Canada Research Chair in Energy Sources for the Vehicles of the Future

Abstract

Output power of a fuel cell (FC) stack can be controlled through operating parameters (current, temperature, etc.) and is impacted by ageing and degradation. However, designing a complete FC model which includes the whole physical phenomena is very difficult owing to its multivariate nature. Hence, online identification of a FC model, which serves as a basis for global energy management of a fuel cell vehicle (FCV), is considerably important. In this paper, two well-known recursive algorithms are compared for online estimation of a multi-input semi-empirical FC model parameters. In this respect, firstly, a semi-empirical FC model is selected to reach a satisfactory compromise between compu-

tational time and physical meaning. Subsequently, the algorithms are explained and implemented to identify the parameters of the model. Finally, experimental results achieved by the algorithms are discussed and their robustness is investigated. The ultimate results of this experimental study indicate that the employed algorithms are highly applicable in coping with the problem of FC output power alteration, due to the uncertainties caused by degradation and operation condition variations, and these results can be utilized for designing a global energy management strategy in a FCV.

Keywords: Fuel Cells, Global Energy Management, Online Identification, Recursive Algorithms, Semi-empirical Calculations

1 Introduction

Proton exchange membrane fuel cell (PEMFC) is a promising alternative energy conversion device in automotive applications, due to high efficiency and low adverse environmental impacts [1]. Fuel cell vehicles (FCVs) have shown a steady increase in the automotive market. However, their successful market penetration requires more improvement in terms of performance, reliability, and cost [2]. Hybridization of PEMFC with other sources, such as batteries and supercapacitors (SCs), has been suggested as an effective measure to improve the mentioned factors in a FCV. Common structures for hybridization of FCVs are FC-battery, FC-SC, and FC-battery-SC. All of these structures have their own advantages and disadvantages [3]. With all the favorable aspects of hybridization,

the overall performance of FCVs, regarding fuel and energy consumption, still relies on the powertrain components efficiency and accurate coordination of sources. In this regard, several energy management strategies (EMSs), namely rule-based, optimization-based and intelligent-based, have been proposed for the mentioned hybrid structures in literature [4–6]. Some examples of very recent proposed online EMSs can be found in [7–11]. In [7], an online EMS based on data fusion approach is suggested. Three FLCs are then optimized and adapted, by Dempster-Shafer evidence theory, to three driving conditions predicted by support vector machine. However, the design constraints of the controllers come from a static efficiency-power map of a PEMFC. In [8], an adaptive control method, based on tuning the FLC parameters for different conditions, is proposed. This work remarks on the decline of PEMFC output voltage due to degradation and suggests the rule base values modification under this condition.

['] *Corresponding author: mohsen.kandi.dayeni@uqtr.ca*

ORIGINAL RESEARCH PAPER

In [9], an online EMS based on extremum seeking method is suggested to maintain the PEMFC operating points in high efficiency region by means of a band-pass filter. A two-layer EMS composed of rule-based approach and particle swarm optimization has been proposed for real-time control of FCVs in [10]. The rule-based of this work is based on a static PEMFC map. In [11], an EMS based on short-term energy estimation is developed to maintain the SC state of energy within a defined limit. The PEMFC limits are based on a quasistatic model, and determining the power rate limits to avoid premature ageing is pointed out as a remaining issue.

Literature consideration shows that many of the existent EMSs in literature are based on parametric PEMFC models, especially static models [12–14]. However, the performance of PEMFCs is influenced by the operating conditions variation (temperature, pressure, current, etc.), degradation, and ageing phenomena. Such performance drifts have made the design of a complete PEMFC model immensely complicated. There exists various PEMFC models capable of dealing with the variations of the operating conditions [15–19]. These models are by some means convincing, though not perfect, with regard to coping with the operating conditions variations. However, ageing phenomena modeling, which is a very complicated process, has not been resolved yet. In this respect, some researches have been conducted to track the real performance of a fuel cell system online. These works can be divided into two categories. The first category is based on extremum seeking strategies, such as maximum power point tracking [20–23]. The second category is based on a parametric identification coupled with an optimization algorithm. This approach is based on models and offers two solutions: (i) a straight solution is to use a model which considers the multi-physics behavior of the PEMFC. As previously mentioned, such a model is itself a study limitation; (ii) the second solution is to utilize an online parameter estimation for a gray-box or black box model. Several studies have made a contribution concerning the online identification coupled with an optimization of PEMFC to obtain the best performance. Ettihir et al. have proposed the utilization of a semi-empirical model, which is only a function of current, with a recursive least square method to get the characteristics of the PEMFC online [24]. They have integrated their work into the EMS design of a FCV as well, and achieved interesting results [25–27]. Kelouwani et al. have suggested an experimental study based on tracing the maximum efficiency of the PEMFC. In this study, a polynomial model of the PEMFC efficiency is introduced and the best efficiency is looked after by adjusting the control variables [28]. Methekar et al. have introduced an adaptive control of a fuel cell system with a Wiener model [29]. Dazi et al. have developed a predictive control to ascertain the maximum power operation of a fuel cell system [30]. In [31], an adaptive supervisory control strategy for a FC-battery bus based on equivalent consumption minimisation is proposed. In this paper, an algorithm has been used for charge-sustaining and a recursive least square has been employed for performance identification of the PEMFC. The utilized PEMFC model of this work is a single input semi-empirical model, which is only a function of current. The studied papers indicate that many online and real-time EMSs have been proposed for FCVs. However, only a few of them, like [24–27, 31], have tried to take into account the real characteristics of the PEMFCs.

This paper aims at providing a basis for easy integration of a PEMFC real behavior into the design of real-time EMSs. In this regard, two recursive algorithms are introduced, and tested to identify the parameters of a semi-empirical model online. This integration provides one with online characteristics of a PEMFC, such as polarization curve, maximum power, and efficiency, which can be used in an EMS loop to update the constraints and related control laws. Compared to other works, the main contribution of this work is online parameters estimation of a multi-input (current, temperature, and pressure) semi-empirical model, which has eight parameters, simultaneously, as opposed to a single-input (current) model with four parameters used in [24–27, 31]. Since the intrinsic dynamic of current, temperature, and pressure are completely different, a multi-input model identification is more challenging than a single-input one. Moreover, a careful experimental study for comparing the effectiveness of the utilized identification methods is given along with a step-by-step explanation for adapting the algorithms to this particular problem. It should be noted that the employed PEMFC model in this work is a combination of the models introduced in [32–34]. The parameters of such model have been only estimated offline with various optimization algorithms in previous studies [35–39]. However, in this work, parameter identification is performed online to counteract uncertainties that occur slowly over time, such as ageing, and quickly due to change of the operating conditions which are not considered in the model. The remainder of this paper is organized as follows. The explanation on how the proposed method of this work can be integrated into EMS design is given in Section 2. The PEMFC model is presented in Section 3. Section 4 deals with the explanation of identification algorithms. The obtained results of the work are discussed in Section 5. Finally, the conclusion is given in Section 6.

2 Integration into Energy Management Design

The EMS of a multi-source system, like a FCV, can be designed in a way to increase system efficiency, lifetime, and autonomy by defining the operating points of the components. However, defining the operating points in a PEMFC is challenging since they steadily move across the operating space. With regard to FCVs, it is interesting to run the PEMFC at its efficient power range. As discussed earlier, many of the designed EMSs in literature have used some constraints such as the maximum and minimum power range of the PEMFC. However, the power-current profile of a PEMFC changes due to the effect of operating conditions, such as temperature, and other disturbances like ageing phenomena. The variation of PEMFC characteristics acts like uncertainties in EMSs. When these var-

iations are not tracked, they cause mismanagement in the EMS since they change the assumed limits in the controller. In this regard, this section describes how the results of this work can be included in the design of a global energy management in a FCV. The whole process is conducted online while the PEMFC is under operation. The global EMS comprises three stages, namely parameter identification, information extraction, and power split strategy. The objective is to do an online parameter identification to adapt the model to the performance drifts of the PEMFC, and then define the best operating points in the information extraction stage. Afterwards, the obtained data can be used in the power split strategy stage to control the power flow between the sources. This three-stage process is called global EMS, and is shown in Figure 1. It should be noted that this paper mainly deals with the design of the first two stages, which are the core of the explained global EMS. In fact, this paper focuses on the implementation of the recursive algorithms for estimating the parameters of a semi-empirical PEMFC model online, which is the first stage. Subsequently, the output of the identification process is employed for finding the maximum power of the PEMFC at each moment, which is the second stage. Finding the maximum power in the information extraction step is one given example out of several possibilities, such as maximum efficiency point (η_{max}), minimum voltage (V_{min}), maximum current (I_{max}), and so forth. The future works can use the provided basis in this article to design an online power split strategy.

In order to show the importance of taking the real behavior of the PEMFC into consideration, two PEMFCs with different levels of degradation are used in this paper. The exact age of each PEMFC has not been properly tracked. However, the polarization curves and the maximum deliverable powers of each PEMFC are shown in Figure 2, as a method of distin-

guishing the current state of each one. As it is observed, the rated power of one of the PEMFCs is almost 400 W while the other one is 300 W. Throughout this manuscript, the less aged PEMFC, which has a higher rated power, is called Normal PEMFC, and the more aged one with less rated power is called Degraded PEMFC. The characteristics of a brand-new PEMFC, which has been obtained from the data sheet, are represented in Figure 2 as well to clarify the difference between the employed PEMFCs in this work and a new one.

It should be noted that the experimental polarization curves have been obtained by drawing a fixed current from the fuel cells and measuring their output voltage. By slowly stepping up the load, the fuel cell voltage response can be seen and recorded. After each increase in the level of current, 15 to 25 minutes have been allowed to the fuel cells to reach equilibrium. All tests have been conducted in a stable environment in
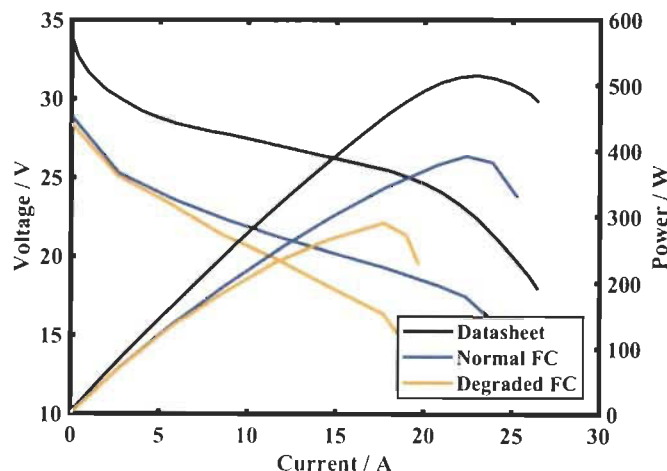

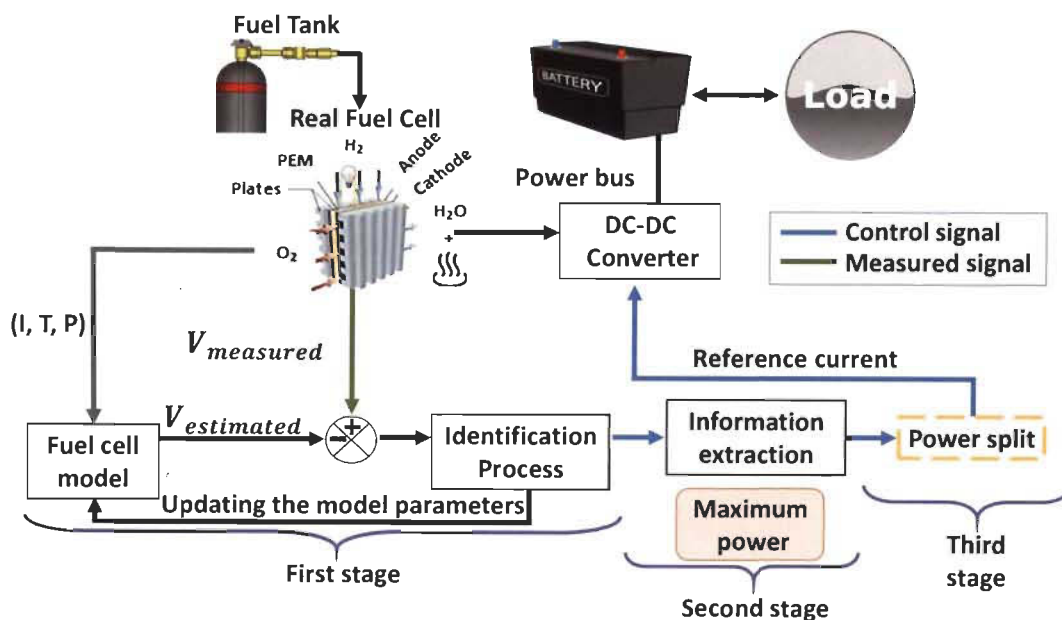Fig. 2 Polarization and power curves of new (from data sheet), Normal, and Degraded PEMFCs.

Fig. 1 Global energy management (I, T, and P refer to operating current, temperature, and pressure, respectively).

the test center of Hydrogen Research Institute (IRH) of Université du Québec à Trois-Rivières to maintain the conditions. Another point which needs to be mentioned is that the employed PEMFCs in this work are Horizon H-500 PEMFCs. The characteristics of a Horizon H-500 PEMFC is listed in Table 1. The difference between the rated power, shown in Table 1, and the utilized PEMFCs is due to the degradation. According to manufacturer, the H_2 pressure should be regulated between 0.5 to 0.6 bar. Hence, it can be stated that in the utilized air-breathing PEMFCs, the pressure is constant.

3 Fuel Cell Modeling

An electrochemical based PEMFC model has been utilized in this paper. In this type of model, the output voltage of FC (V_{FC}) is considered as the sum of cell reversible voltage (E_{Nernst}) and voltage drops, namely activation (V_{act}), ohmic (V_{ohmic}), and concentration or mass transport (V_{con}). This type of model considers the same behavior for all cells. The general formulation of an electrochemical FC model is as follows:

$$V_{FC} = n \times (E_{Nernst} + V_{act} + V_{ohmic} + V_{con}) \qquad (1)$$

where the unit of V_{FC} and the voltage drops is volt and n is the number of cells. In this work, E_{Nernst}, which is the potential of FC without load in an open circuit, is calculated based on the following theoretical formula, proposed in [33].

$$E_{Nernst} = 1.229 - 0.85 \times 10^{-3}(T - 298.15)$$
$$+ 4.3085 \times 10^{-5}T[\ln(P_{H_2}) + 0.5\ln(P_{O_2})] \qquad (2)$$

where T is the stack temperature (K), P_{H_2}, and P_{O_2} are the partial pressure (Pa) of hydrogen in anode side and oxygen in cathode side. V_{act} is obtained by means of Eq. (3), introduced in [33].

$$V_{act} = \Upsilon_1 + \Upsilon_2T + \Upsilon_3T\ln(CO_2) + \Upsilon_4T\ln(i) \qquad (3)$$

$$CO_2 = P_{O_2}/5.08 \times 10^6 e^{-(498/T)} \qquad (4)$$

where i is the FC operating current (A), CO_2 is the oxygen concentration (mol cm^{-3}), and the Υ_n (n = 1 ⋯ 4) is the empirical coefficients, based on fluid mechanics, thermodynamics, and electrochemistry and may differ depending on the cell material and manufacture.

The formulation of V_{ohmic}, shown in Eq. (5), is based on the proposed structure in [34]. This structure introduces an appreciable method to avoid struggling with the computation of water content and distribution. Eq. (5) is a function of temperature, due to the fact that diffusivities and water partial pressures change with temperature, and current, since proton and water fluxes alter with the current.

$$V_{ohmic} = -iR_{internal} = -i(\xi_1 + \xi_2T + \xi_3i) \qquad (5)$$

where ξ_n (n = 1 ⋯ 3) are the parametric coefficients. The range of the parameters of ohmic region is validated by the value of $R_{internal}$, which is the internal resistor (Ω). The range of internal resistor has been obtained by current interrupt test, which is explained later in this section. V_{con} is computed with the help of Eq. (6), proposed in [32, 40].

$$V_{con} = \alpha I^G \ln(1 - \beta I_d) \qquad (6)$$

where α is a semi-empirical parameter related to the diffusion mechanism and it is between 0.3 to 1.8 [23], I_d is the current density (A cm^{-2}), G (between 1 and 4) is a dimensionless number which is related to the water flooding phenomena, and β is the inverse of the limiting current density (A^{-1} cm^2). The value of β is 1.2381.

The introduced PEMFC model comprises 8 time-varying parameters, which need to be identified. In order to embrace the influence of degradation phenomenon, which happens slowly over time, and the operating conditions, which are not included in the model like humidity, the parameters should be identified online to adapt the model to real state of the PEMFC. Table 2 shows the targeted parameters for identification and their expected range of variation. The reported ranges

Table 1   Horizon H-500 PEMFC characteristics.

PEMFC Technical specification	
Type of FC	PEM
Number of cells	36
Active area	52 cm^2
Rated power	500 W
Rated performance	22 V @ 23.5 A
Max-current (shutdown)	42 A
Hydrogen pressure	50–60 kPa (0.5–0.6 bar)
Rated H_2 consumption	7 L min^{-1}
Ambient temperature	5 to 30 °C
Max-stack temperature	65 °C
Cooling	Air (integrated cooling fan)

Table 2   Targeted Parameters for estimation.

Parameters	Range	
	Minimum	Maximum
Υ_1	–1.997	–0.8532
Υ_2	0.001	0.005
Υ_3	3.6×10^{-5}	9.8×10^{-5}
Υ_4	-2.6×10^{-4}	-0.954×10^{-4}
α	0.0135	0.5
ξ_1		
ξ_2	Current interrupt test	
ξ_3		

have been adopted from previous studies [35–39], and the obtained values for the parameters of the employed PEMFC in this work may be slightly different. This deviation in the range is mainly due to the various used material in the fuel cells, fabrication methods, state of health of the reported fuel cells, and so forth.

3.1 Resistor Measurement

In order to relate the targeted parameters for estimating the internal resistor of the PEMFC to the realistic physical meaning, some measurements from the real value of resistor are needed. Therefore, in this paper, the current interrupt method is used as an electrochemical technique to obtain a range for the resistor variation with regard to current and temperature [41–44]. The efficacy of this method for measuring the ohmic resistance has been already investigated in [44]. Current interrupt test revolves around the idea of rapid acquisition of the measured voltage to separate ohmic from activation loss. Because, ohmic loss fades faster than electrochemical losses after the interruption of the current. Hence, the ohmic loss can be measured from the difference between the voltage immediately before and after the interruption. In comparison to other electrochemical methods such as electrochemical impedance spectroscopy, which is an effective frequency based method, current interrupt benefits from convenient data analysis. However, one of the challenges in current interrupt method is to obtain the point in which the voltage jumps and a fast oscilloscope is needed to deal with this problem. In this paper, the procedure for performing the current interrupt test is strictly according to [44].

Table 3 shows different current levels in which the current has been interrupted as well as the corresponded temperature of each point. The PEMFC has been given enough time to reach a stable temperature for each current level before conducting the test. Moreover, the test has been done in a forced convection condition in which the fans of the PEMFCs have worked with a constant duty cycle of 34%.

Table 3 Current levels and PEMFC stack temperature during resistor measurement.

Current / A	Temperature / °C (Normal PEMFC)	Temperature / °C (Degraded PEMFC)
3	23.2	22.49
6	25	24.87
9	26.25	26.15
12	28.2	28.1
15	30.9	30.8
18	33.7	34.7
21	38.15	–
24	44.7	–
25	49.4	–

Figure 3 presents the variation of the resistor with respect to current and temperature for both of the Normal and Degraded PEMFCs. As it is seen, the value of resistor in the Degraded PEMFC is more than the Normal PEMFC. These measurements are used as a tool to check the range of estimated resistor by the identification algorithms.

4 Parameter Identification Algorithms

With respect to the aims and objectives of the problem, the process of identification can be conducted offline or online. In offline identification, the process data is first gathered in a data storage, and then it is transferred to a computer and evaluated. However, in online identification, which is the focus of this work, information is processed online after each sample [45]. In online identification, there is no need to save the information because the recursive algorithms are used, and the model is updated as the data comes in. The aim of this work is to apply and compare two commonly algorithms in self-tuning control for the problem of PEMFC parameters estimation. RLS is used to deal with linear regression model estimation, and RML can be used to estimate the parameters and the noise dynamics, as described below.

4.1 RLS Algorithm

RLS algorithm is based on the concept of minimizing the error related to input signal. RLS gives excellent performance when operating in time varying conditions. Assuming that noise is serially uncorrelated and independent of the elements of the regression vector, RLS algorithm can be applied to a linear-in-parameter system to estimate the parameters, and the model can be called a linear regression. The utilized RLS in this work is formulated as below.
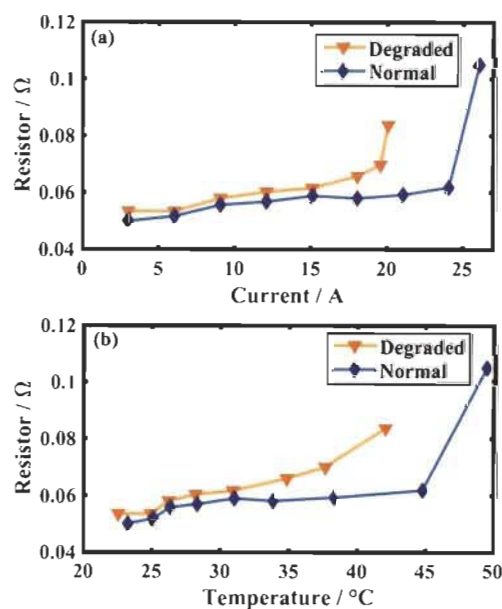

Fig. 3 Resistor change with respect to current (a), and temperature (b).

$$y(t) = \theta(t)^T \varphi(t) + v(t) \tag{7}$$

$$\theta(t) = \theta(t-1) + k(t)E(t) \tag{8}$$

$$k(t) = \lambda^{-1}P(t-1)\varphi(t)/\left(1 + \lambda^{-1}\varphi^T(t)P(t-1)\varphi(t)\right) \tag{9}$$

$$P(t) = \lambda^{-1}P(t-1) - \lambda^{-1}k(t)\varphi^T(t)P(t-1) + BI \tag{10}$$

$$\lambda(t) = \omega - \left(1 - \omega/\varphi^T(t)P(t-1)\varphi(t)\right); \varphi^T(t)P(t-1)\varphi(t) > 0 \tag{11}$$

$$\lambda(t) = 1; \varphi^T(t)P(t-1)\varphi(t) = 0 \tag{12}$$

$$E(t) = u(t) - \varphi^T(t)\theta(t-1) \tag{13}$$

where $y(t)$ is the estimated output, $\theta(t)$ is the parameter vector, $\phi(t)$ is the regression vector, $v(t)$ is the uncertainty on the output, $k(t)$ is the Kalman gain, $E(t)$ is the error, λ is a directional forgetting factor, $P(t)$ is the covariance matrix, B is a constant that increases the covariance matrix instantly, I is the identity matrix, ω is the forgetting factor ($0 < \omega < 1$), and $u(t)$ is the measured output. It should be noted that the estimates are assumed to be unbiased in RLS. This assumption implies that regression vector and the noise are independent and $v(t)$ is a white noise. Forgetting factor and covariance matrix play an important role in the estimation quality of a time-varying system. The estimation algorithms are susceptible to estimator windup, which stems from the forgetting factor, and faults in the approximation, which might be due to large parameters change. Therefore, in this paper, a directional forgetting factor has been utilized to prevent the identification process from becoming undependable when the system is not constantly excited [46]. Table 4 clarifies how the introduced PEMFC model can be fitted in the RLS structure for parameter estimation process.

One point that needs to be mentioned is that the initialization of the parameters vector is very important to achieve realistic outcomes from the identification process in both RLS and RML algorithms. In this regard, a preprocessing of data is performed in this paper to avoid increasing the computational time or divergence and also get close to realistic results. The preprocessing of data is conducted by the Curve Fitting Toolbox™ of MATLAB software. This toolbox utilizes the least square methods to fit the data. Fitting requires a parametric model which can relate the real data to the predictor data. In

this work, the employed fuel cell model is linear in coefficients. Therefore, linear least square, which minimizes the summed square of the difference between the observed response value and the fitted response value, is used to fit the model to experimental data. The utilized experimental data in the preprocessing stage comes from the conducted test for obtaining the polarization curves of the fuel cells, presented in Figure 2, which is a proper representative of its behavior.

4.2 RML Algorithm

On the condition that the noise is related to the regression vector, the model cannot be considered as a linear regression due to unobserved data. In this condition, RLS algorithm cannot be employed since the model is not a linear regression, and RML algorithm can be introduced. RML algorithm holds a striking resemblance to RLS. The main difference here is that the disturbance acting on the output of the system ($v(t)$) is modeled as a moving average of a serially uncorrelated white noise sequence. In this case, the unobserved components ($e(t)$, $e(t-1), \cdots e(t-r)$) are approximated by the residuals, which are the values of the estimation error ($E(t)$). RML algorithm is formulated as below.

$$y(t) = \theta(t)^T \varphi(t) + v(t) \tag{14}$$

$$v(t) = e(t) + c_1(t)e(t-1) + \ldots + c_r(t)e(t-r) \tag{15}$$

$$\theta(t) = \theta(t-1) + k(t)E(t) \tag{16}$$

$$k(t) = \lambda^{-1}P(t-1)\Psi(t)/\left(1 + \lambda^{-1}\Psi^T(t)P(t-1)\Psi(t)\right) \tag{17}$$

$$\Psi(t) = \varphi(t)/C(q^{-1}) \tag{18}$$

$$P(t) = \lambda^{-1}P(t-1) - \lambda^{-1}k(t)\Psi^T(t)P(t-1) + BI \tag{19}$$

$$\lambda(t) = \omega - \left(1 - \omega/\varphi^T(t)P(t-1)\varphi(t)\right); \varphi^T(t)P(t-1)\varphi(t) > 0 \tag{20}$$

$$\lambda(t) = 1; \varphi^T(t)P(t-1)\varphi(t) = 0 \tag{21}$$

$$E(t) = u(t) - \varphi^T(t)\theta(t-1) \tag{22}$$

where e is the residuals calculated by the values of error, c is the added parameter for error prediction, $\Psi(t)$ is a filter, q^{-1} is the delayed operator, and C is the estimated polynomial of the parameter c ($1 + c_1q^{-1} + \cdots + c_rq^{-r}$). The number of parameter c, which is shown by r in the formulas, has been chosen three in this particular case with respect to the conducted trials, and it can be increased or decreased in other problems.

It should be noted that with respect to the introduced structure for the RML algorithm, which contains a model for predicting error, the introduced semi-empirical model should be extended as below to consider the error model as well.

Table 4 Description of the parameters of RLS.

RLS parameters	Implementation description
$\theta(t)$	$[\Upsilon_1, \Upsilon_2, \Upsilon_3, \Upsilon_4, \xi_1, \xi_2, \xi_3, \alpha]$
$\phi(t)$	$[1, T, T\ln(CO_2), T\ln(i), -i, -iT, -i^2, I^G\ln(1 - \beta I_d)]$
$y(t)$	Estimated V_{FC} by RLS
$u(t)$	Measured V_{FC} from the real PEMFC

$$V_{FC} = n \times \frac{(E_{Nernst} + V_{act} + V_{ohmic} + V_{con} + c_1(t)e(t-1) +}{c_2(t)e(t-2) + c_3(t)e(t-3))}$$

(23)

Table 5 shows how the introduced RML algorithm in this section can be coupled to the PEMFC model.

5 Experimental Results and Discussion

The performance of the described algorithms has been tested on a developed test bench in the Hydrogen Research Institute. In this test bench, as shown in Figure 4, a Horizon H-500 air breathing PEMFC is connected to a National Instrument CompactRIO through its controller. A programmable DC electronic load is used to request load profiles from the PEMFC. According to the manufacturer, the difference between the atmospheric pressure in the cathode side and the pressure of the PEMFC in the anode side should be about 50.6 kPa. The pressure in the anode side is set to 55.7 kPa. The explained semi-empirical model and parameter identification algorithms have been developed in MATLAB and implemented in Lab VIEW software *via* Math Script Module. A current profile is applied to the PEMFCs *via* the load, which is connected to the LabVIEW software and PC *via* USB connection. The measured data (temperature and voltage) from the real PEMFC is transferred to the PC, by means of the CompactRIO,

to be used in the implemented model for identification process. The communication between the CompactRIO and the PC is *via* Ethernet connection every 100 milliseconds. In this regard, the identification algorithms receive the measured data every 100 milliseconds and identify the parameters of the model at each step. Then the updated model is used to plot polarization curve as well as the power-versus-current curve. The current correspondent to the maximum power is obtained from the power-versus-current profile, and it is requested from the PEMFCs *via* the load.

This work aims to increase the accuracy of the extracted information, which is maximum power herein, from the updated model. Later on, this information extraction basis can be integrated into the EMS designs to achieve more realistic results. Two main analyses have been performed in this section to clarify the effectiveness of the discussed algorithms and the PEMFC model. The first analysis is to compare the performance of the identification algorithms, and the second analysis is to show the relevance of the achieved results to real physical values.

Figure 5 indicates the utilized current profile to test the performance of the identification algorithms. This current profile has been created by means of UDDS driving profile which represents the city driving condition. To do so, the UDDS driving profile has been used as the input of IEEE VTS Motor Vehicles Challenge [47], and the resulting requested current from the PEMFC has been scaled within the operating range of the presented PEMFCs in the test bench. Since this current profile comes from a driving cycle, it can imitate a real situation that may happen to a used fuel cell system in a vehicle. However, the application of this work is not just limited to vehicles. The represented current profile, shown in Figure 3, has been applied to two described PEMFCs with different levels of degradation.

Figures 6 and 7 represent the estimated voltage and temperature variation for the Degraded and Normal PEMFCs, respectively. As is clear in these figures, both of RLS and RML algorithms are potentially capable of estimating voltage precisely. It is difficult to form an opinion about the performance comparison of the algorithms solely by means of these figures.

Regarding the comparison of the algorithms to one another, the mean square error (MSE) and the peak signal to noise ratio (PSNR) have been employed. MSE and PSNR are two error metrics used to compare the estimation quality. PSNR calculates the peak signal-to-noise ratio, in decibels, between the two original signal and estimated signal. In this paper, the original signal is the measured output voltage of the PEMFC and the estimated signal is the PEMFC estimated output voltage by the algorithms. The higher the PSNR, the better the quality of the estimation. The MSE represents the cumulative squared error between the estimated volt-

Table 5 Description of the parameters of RML.

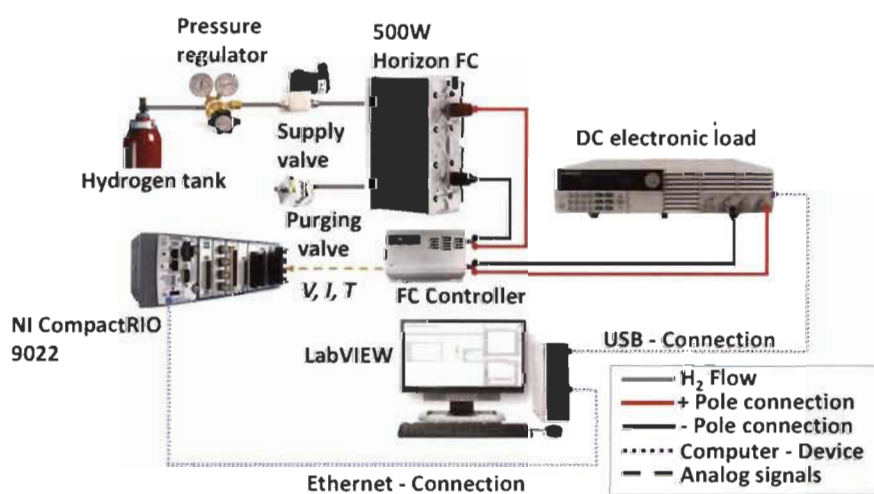| RML parameters	Implementation description
$\theta(t)$	$[\Upsilon_1, \Upsilon_2, \Upsilon_3, \Upsilon_4, \xi_1, \xi_2, \xi_3, \alpha, c_1, c_2, c_3]$
$\phi(t)$	$[1, T, Tln(CO_2), Tln(i), -i, -iT, -i^2, I^G ln(1 - \beta I_d), e(t-1), e(t-2), e(t-3)]$
$y(t)$	Estimated V_{FC} by RML
$u(t)$	Measured V_{FC} from the real PEMFC
$C(q^{-1})$	$(1 + c_1 q^{-1} + c_2 q^{-2} + c_3 q^{-3})$

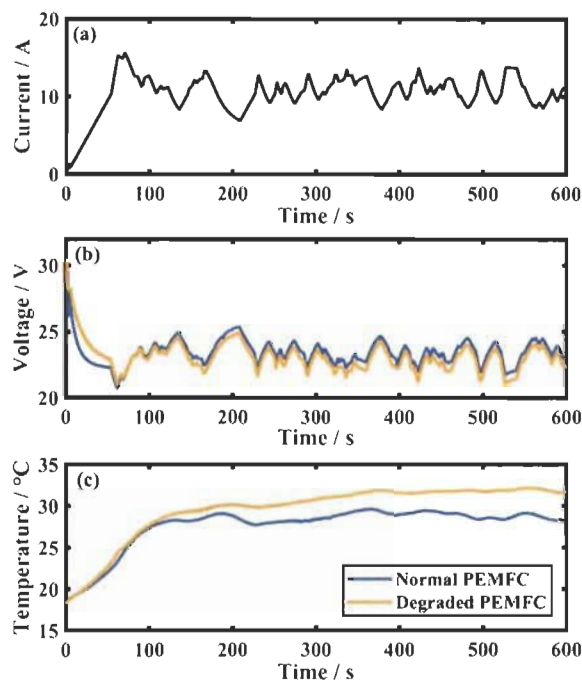Fig. 4 Developed test bench at Hydrogen Research Institute.

Fig. 5 Applied current profile (a), and corresponded voltage (b), and temperature (c) in the test bench.

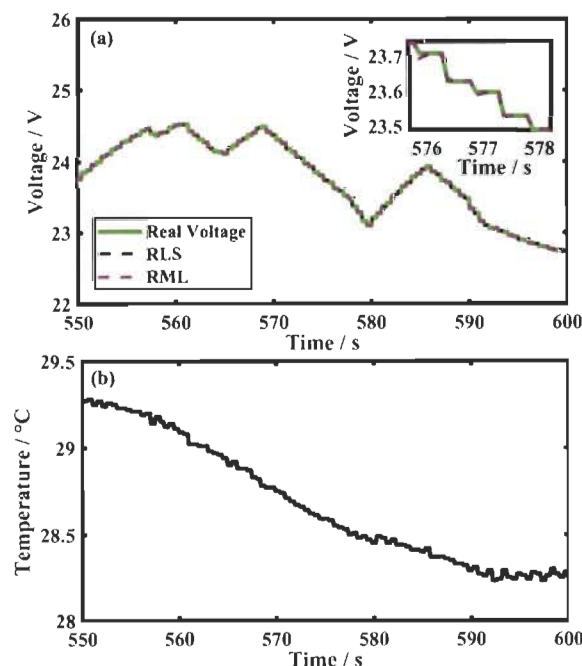Fig. 6 Estimated output voltage (a), and temperature change (b), of the Degraded PEMFC.

Fig. 7 Estimated output voltage (a), and temperature change (b), of the Normal PEMFC.

age and the measured voltage. The lower the value of MSE, the lower the error.

As mentioned earlier, the utilized algorithms in this work have been implemented in LabVIEW software for experimental validation. The PEMFC is connected to a National Instrument CompactRIO, which provides access to the PEMFC voltage and temperature sensors' measurements. In order to check the robustness of the algorithms, a random noise is added to

the voltage measurement in the LabVIEW, and the noisy signal is sent to the process of identification, which is done by the algorithms. It should be reminded that the purpose of identification is to estimate output voltage of the PEMFC and that is why the noise is added to the voltage measurement. Figure 8 presents the obtained PSNR values for different cases. Four cases, namely zero noise, a random noise with variance of 0.25, a random noise with variance of 0.5, and a random noise with variance of 0.75, have been considered in this analysis. Zero noise refers to the normal measurement, and the other cases show the addition of random noise with different variances to test the robustness of the algorithms. As it is seen in Figure 8, in case of normal measured data (zero noise), RLS performs better than RML to some extent. However, as the level of noise increases RML algorithm indicates superior performance compared to RLS. This result implies that RML algorithm is more robust than RLS while confronting some noises in the system.

Figure 9 presents the comparison of the algorithms based on MSE metric for the same discussed four cases. The achieved results of MSE analysis is in agreement with the results of PSNR, regarding the robustness of the algorithms. It is clear that the value of MSE for RLS is marginally lower that RML in normal measured data, and in higher noise levels, the MSE value of RML is lower than RLS, which shows its robustness against noise.

Regarding the investigation of the result relevance to the physical meaning, current interrupt method, as explained in Section 3.1, has been used to obtain a reference range for assessing the resistor estimation by algorithms. In fact, current interrupt test, which is an electrochemical technique, is used to measure the evolution of resistor with respect to the temper-
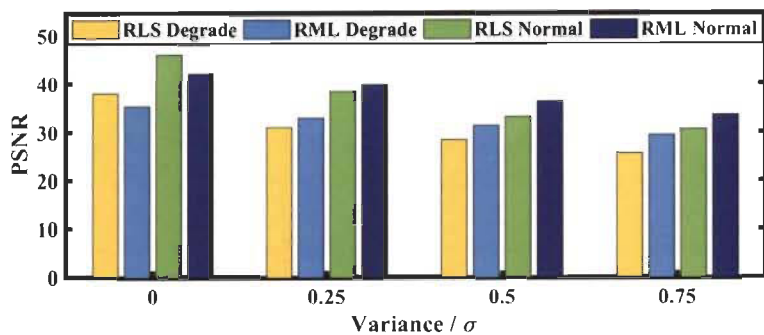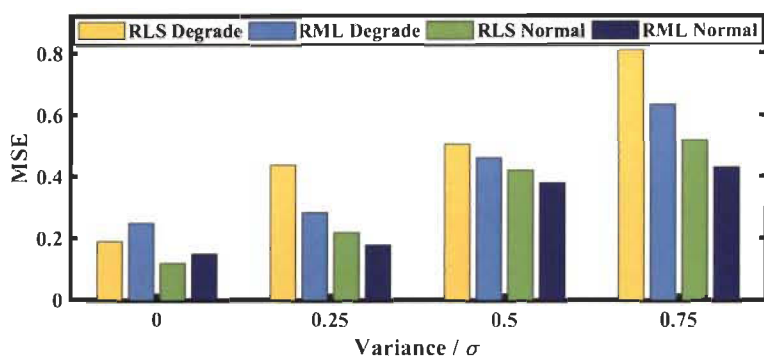
Fig. 8 Comparison of the algorithms based on PSNR.

Fig. 9 Comparison of the algorithms based on MSE.

ature and current. This measurement clarifies the range of the resistor for the whole stack and is a helpful tool to check the achieved results by the both algorithms. Figure 10 shows the estimated values of the $R_{internal}$ in the Normal and Degraded PEMFCs, which are within the obtained ranges of the current interrupt test presented in Figure 3. The observed evolution in the trend of resistor, particularly between 0 to 100 seconds, is due to the sharp rise of current in the used current profile, shown in Figure 5, in this time period. This sudden increase in the current also leads to a temperature rise, which affects the resistor. The resistor is influenced by not only the current but also the temperature. According to Figure 10, the ohmic resistance value in the Degraded PEMFC is more than the Normal PEMFC.

Table 6 provides information on the average value of the semi-empirical parameters, obtained by both of the identification methods. There is not a lot of information about the range of the semi-empirical parameters in literature and even in the
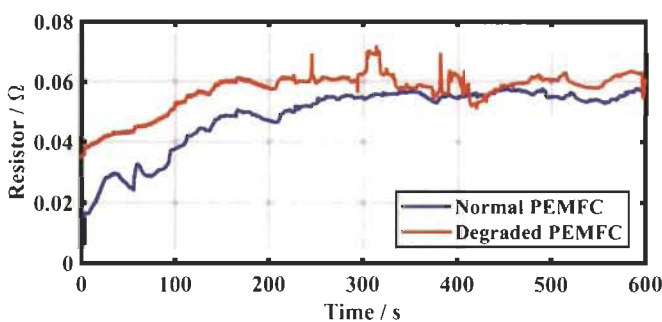
few existing manuscripts, there is not any explanation about the age and degradation level of the PEMFCs. However, the achieved parameters in this manuscript seem to be almost in the same range as in Table 2.

Figure 11 represents the evolution of the activation region parameters of the Normal PEMFC with RLS algorithm. Since the performance of the algorithms has been already discussed over the previous figures and the average values of the estimated parameters for both PEMFCs have been reported in Table 6, the parameters identified by RLS approach are only shown in Figure 11 to give an idea of parameters variation. As is seen in this figure, the parameters are time-varying and the small variation of the parameters overtime shows that the selected PEMFC model has an acceptable accuracy, otherwise the parameters would fluctuate a lot to compensate the lack of accuracy in the model.

The variation of the concentration region parameter, achieved by RLS, is shown in Figure 12. It should be noted that the severity of degradation influence is ambiguous over each specific parameter. However, it can be ensured that in case of disturbance occurrence due to degradation, the parameters change to embrace its effect.

Figure 13 represents the comparison of the polarization and power curves of Normal and Degraded PEMFCs with the estimated ones, obtained by RLS algorithm for zero noise condition. It should be noted that the polarization curve changes continuously mainly due to the temperature change. As it is seen, maximum power is achieved in the high current region, where the concentration part begins. In this regard, by employing the recursive algorithms in the parameter estimation of a PEMFC model, the polarization curve and maximum power can be obtained at each moment, and be used in power splitting or global EMSs.

Fig. 10 Evolution of the estimated ohmic resistance in the PEMFCs.

Table 6 The average obtained values of the semi-empirical parameters.

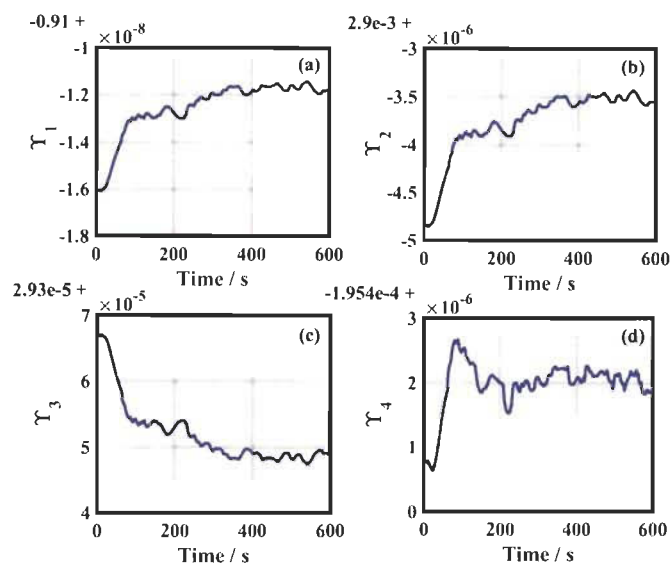| Parameters	Degraded PEMFC		Normal PEMFC	
	RLS	RML	RLS	RML
Υ_1	−1.19	−1.19	−0.91	−0.91
Υ_2	4.01×10^{-3}	4.01×10^{-3}	2.9×10^{-3}	2.9×10^{-3}
Υ_3	9.68×10^{-5}	9.53×10^{-5}	7.71×10^{-5}	7.78×10^{-5}
Υ_4	-9.56×10^{-5}	-1.05×10^{-4}	-1.97×10^{-4}	-1.93×10^{-4}
α	7.95×10^{-1}	7.95×10^{-1}	9.94×10^{-1}	9.94×10^{-1}
ξ_1	9.94×10^{-2}	9.94×10^{-2}	1.07×10^{-2}	1.07×10^{-2}
ξ_2	-2.92×10^{-4}	-2.92×10^{-4}	-9.90×10^{-6}	-1.00×10^{-5}
ξ_3	-1.22×10^{-5}	-1.22×10^{-5}	8.54×10^{-5}	8.54×10^{-5}
c_1	−	2.50×10^{-1}	−	2.50×10^{-1}
c_2	−	3.00×10^{-1}	−	3.00×10^{-1}
c_3	−	5.00×10^{-2}	−	5.00×10^{-2}

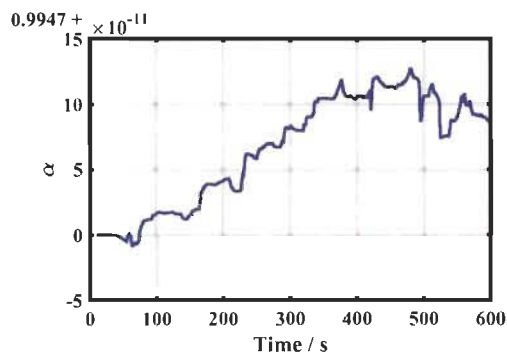Fig. 11 The fluctuation of activation region parameters.

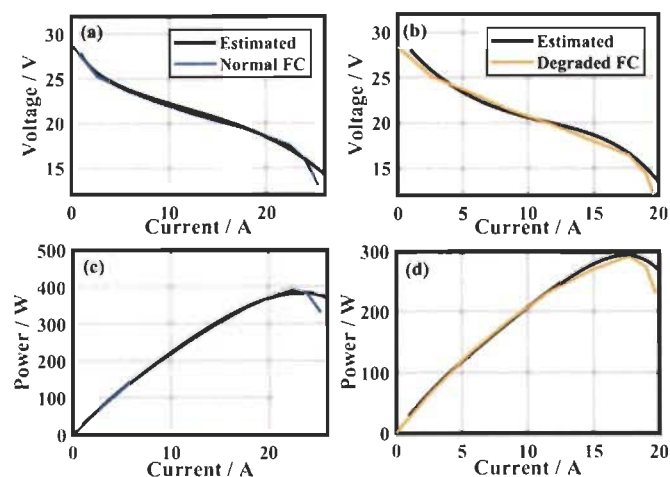

Fig. 12 The fluctuation of concentration region parameter.

Fig. 13 Polarization curve and corresponded power curve of Normal PEMFC (a, c), and Degraded PEMFC (b, d).
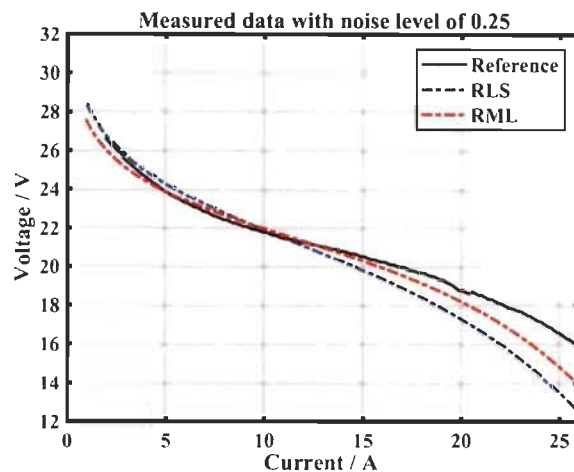

Fig. 14 The comparison of polarization curves obtained by algorithms.

which comes from the experimental data, than RLS. This figure also shows the influence of noise in the polarization curve estimation. Looking more closely at Figure 14, it can be concluded that a small change in the voltage estimation can cause a noticeable change in the polarization curve estimation. The difference between the PSNR values of RML and RLS algorithms, presented in Figure 8, for the noise level of 0.25 is not a lot. However, this slight difference causes an obvious change in the polarization curve prediction.

6 Conclusions

This paper proposes online identification of a multi-input PEMFC model to track the performance drifts due to the influence of degradation phenomenon and the operating conditions, which are not considered in the model, over the output voltage of a fuel cell system. In this regard, a semi-empirical PEMFC model is selected and two identification algorithms, RLS and RML, are utilized to update the chosen model. Various scenarios, four noise level cases, and two PEMFCs with different levels of degradation, have been considered to test the performance of the algorithms. The main results achieved from the experimental implementation and test of the algorithms indicate that both of the algorithms are capable of estimating the output voltage to a satisfactory level. However, RML has shown more robustness in dealing with noisy measurement data. It is worth reminding that this robustness might lead to less expensive sensors and measurement instruments. Moreover, it should be noted that the range of alteration in the semi-empirical parameters was acceptable. In future, this work can be integrated into the design of global energy management for FCVs.

Acknowledgements

Figure 14 compares the polarization curves obtained by the estimated parameters with RML and RLS algorithms for the noise level of 0.25. As is clear in Figure 14, the estimated polarization curve by RML algorithm is closer to the reference,

List of Symbols

Latin Letters

a_n	Output coefficient
b_m	Input coefficient
c_r	Error coefficient
C	Estimated polynomial
CO_2	Oxygen concentration / mol cm^{-3}
E	Estimation error
E	Error
E_{Nernst}	Cell reversible voltage / V
G	Dimensionless number
i	FC operating current / A
I	Identity matrix
I_d	Current density / A cm^{-2}
q^{-1}	Delayed operator
k	Kalman gain
n	Number of cells
P	Covariance matrix
P_{H2}	Hydrogen partial pressure / Pa
P_{O2}	Oxygen partial pressure / Pa
$R_{internal}$	Total internal resistance of the fuel cell / Ω
T	Stack temperature / K
U	Input
V	Noise
V_{act}	Activation voltage drop / V
V_{con}	Concentration voltage drop / V
V_{FC}	Output voltage of fuel cell / V
V_{ohmic}	Ohmic voltage drop / V
X	Regression vector
Y	Output

Greek Letters

A	Semi-empirical parameter related to diffusion mechanism
B	Inverse of the limiting current density / A^{-1} cm^{-2}
B	Constant
E	Residuals
ξ_n	Parametric coefficients related to ohmic resistance
θ	Parameter vector
Υ_n	Experiential coefficients related to activation loss
Φ	Linear regression vector
ϕ_0	Residual regression vector
Λ	Directional forgetting factor
Ψ	Filter
Ω	Forgetting factor

References

[1] U. Winter, H. Weidner, *Fuel Cells* **2003**, *3*, 76.

[2] C. Kompis, K. Malek, *Fuel Cells* **2016**, *16*, 760.

[3] N. Sulaiman, M. A. Hannan, A. Mohamed, E. H. Majlan, W. R. Wan Daud, *Renewable Sustainable Energy Rev.* **2015**, *52*, 802.

[4] A. Panday, H. O. Bansal, *Int. J. Veh. Technol.* **2014**, *2014*, 1.

[5] S. F. Tie, C. W. Tan, *Renewable Sustainable Energy Rev.* **2013**, *20*, 82.

[6] O. Erdinc, M. Uzunoglu, *Renewable Sustainable Energy Rev.* **2010**, *14*, 2874.

[7] D. Zhou, A. Al-Durra, F. Gao, A. Ravey, I. Matraji, M. Godoy Simões, *J. Power Sources* **2017**, *366*, 278.

[8] J. Chen, C. Xu, C. Wu, W. Xu, *IEEE Trans. Ind. Inf.* **2018**, *14*, 292.

[9] D. Zhou, A. Ravey, A. Al-Durra, F. Gao, *Energy Convers. Manage.* **2017**, *151*, 778.

[10] R. Koubaa, L. Krichen, *Energy* **2017**, *133*, 1079.

[11] M. G. Carignano, R. Costa-Castelló, V. Roda, N. M. Nigro, S. Junco, D. Feroldi, *J. Power Sources* **2017**, *360*, 419.

[12] L. Xu, J. Li, M. Ouyang, *Int. J. Hydrogen Energy* **2015**, *40*, 15052.

[13] J. Bernard, S. Delprat, T. M. Guerra, F. N. Büchi, *Control Eng. Pract.* **2010**, *18*, 408.

[14] D. Feroldi, M. Serra, J. Riera, *J. Power Sources* **2009**, *190*, 387.

[15] A. A. Shah, K. H. Luo, T. R. Ralph, F. C. Walsh, *Electrochim. Acta* **2011**, *56*, 3731.

[16] M. Eikerling, *Fuel Cells* **2016**, *16*, 663.

[17] M. Karimi, J. Yahyazadeh, A. Rezazade, *Fuel Cells* **2016**, *16*, 530.

[18] K. Ou, Y. X. Wang, Y. B. Kim, *Fuel Cells* **2017**, *17*, 299.

[19] P. Xu, S. Xu, *Fuel Cells* **2017**, *17*, 794.

[20] N. Bizon, *Appl. Energy* **2013**, *104*, 326.

[21] Z.-d. Zhong, H.-b. Huo, X.-j. Zhu, G.-y. Cao, Y. Ren, *J. Power Sources* **2008**, *176*, 259.

[22] F. X. Chen, Y. Yu, J. X. Chen, *Fuel Cells* **2017**, *17*, 671.

[23] A. Harrag, S. Messalti, *Fuel Cells* **2017**, *17*, 816.

[24] K. Ettihir, L. Boulon, K. Agbossou, paper presented at the 5th International Conference on Fundamentals & Development of Fuel Cells (FDFC 2013), Karlsruhe, Germany, **2013**.

[25] K. Ettihir, L. Boulon, K. Agbossou, *IET Electr. Syst. Transp.* **2016**, *6*, 261.

[26] K. Ettihir, L. Boulon, K. Agbossou, *Appl. Energy* **2016**, *163*, 142.

[27] K. Ettihir, L. Boulon, M. Becherif, K. Agbossou, H. S. Ramadan, *Int. J. Hydrogen Energy* **2014**, *39*, 21165.

[28] S. Kelouwani, N. Henao, K. Agbossou, Y. Dube, L. Boulon, *IEEE Trans. Veh. Technol.* **2012**, *61*, 3851.

[29] R. N. Methekar, S. C. Patwardhan, R. D. Gudi, V. Prasad, *J. Process Control* **2010**, *20*, 73.

[30] D. Li, Y. Yu, Q. Jin, Z. Gao, *Energy* **2014**, *68*, 210.

[31] L. Xu, J. Li, J. Hua, X. Li, M. Ouyang, *J. Power Sources* **2009**, *194*, 360.

[32] L. Pisani, G. Murgia, M. Valentini, B. D'Aguanno, *J. Power Sources* **2002**, *108*, 192.

[33] R. F. Mann, J. C. Amphlett, M. A. I. Hooper, H. M. Jensen, B. A. Peppley, P. R. Roberge, *J. Power Sources* **2000**, *86*, 173.

[34] J. C. Amphlett, R. M. Baumert, R. F. Mann, B. A. Peppley, P. R. Roberge, T. J. Harris, *J. Electrochem. Soc.* **1995**, *142*, 9.

[35] M. Ali, M. A. Elhameed, M. A. Farahat, *Renewable Energy* **2017**, *111*, 455.

[36] O. E. Turgut, M. T. Coban, *Ain Shams Eng. J.* **2016**, *7*, 347.

[37] Z. Sun, N. Wang, Y. Bi, D. Srinivasan, *Energy* **2015**, *90*, 1334.

[38] C. Restrepo, T. Konjedic, A. Garces, J. Calvente, R. Giral, *IEEE Trans. Ind. Inf.* **2015**, *11*, 548.

[39] K. Priya, T. Sudhakar Babu, K. Balasubramanian, K. Sathish Kumar, N. Rajasekar, *Sustainable Energy Technol. Assess.* **2015**, *12*, 46.

[40] G. Squadrito, G. Maggio, E. Passalacqua, F. Lufrano, A. Patti, *J. Appl. Electrochem.* **1999**, *29*, 1449.

[41] A. Husar, S. Strahl, J. Riera, *Int. J. Hydrogen Energy* **2012**, *37*, 7309.

[42] J. Wu, X. Yuan, H. Wang, M. Blanco, J. Martin, J. Zhang, *Int. J. Hydrogen Energy* **2008**, *33*, 1735.

[43] K. R. Cooper, M. Smith, *J. Power Sources* **2006**, *160*, 1088.

[44] T. Mennola, M. Mikkola, M. Noponen, T. Hottinen, P. Lund, *J. Power Sources* **2002**, *112*, 261.

[45] R. Isermann, *Automatica* **1980**, *16*, 575.

[46] L. Cao, H. Schwartz, *Automatica* **2000**, *36*, 1725.

[47] C. Depature, S. Jemei, L. Boulon, A. Bouscayrol, N. Marx, S. Morando, A. Castaings, IEEE Vehicle Power and Propulsion Conference (VPPC), Hangzhou, **2016**, IEEE, pp. 1.

Appendix C – Article 7

Authors: M. Kandidayeni, A. Macias, L. Boulon, and S. Kelouwani

C.1 Objectives

The performance of an FCHEV is impacted by several interrelated factors which put the design of an EMS in critical position [6]. Regardless of the type of the hybrid vehicle, the existing EMSs fall under two categories of rule-based and optimization-based [12, 18]. The rule-based strategies are usually heuristic and lead to limited and sub-optimal solutions. In this regard, the researchers have turned attentions on the optimization methods, which assure optimal or near-optimal solutions in theory and can also provide new guidelines for refining the rule-based methods [95, 96]. However, the performance of the optimization-based strategies depends to a great extent on the driving pattern and they achieve different efficiency with respect to the driving conditions. In this light, the use of traffic condition and driving information in the design of an EMS has come under the attention of many researchers [30, 31, 97]. This line of work is known as intelligent-based EMS category and can be integrated into both of ruled-based and optimization-based strategies [16]. Apart from the importance of considering the driving condition, it is also essential to take into account

the performance drifts of the FC system in EMS formulation of an FCHEV. The performance of a FC system is impacted by several factors such as the variation of operation conditions and degradation phenomenon and it can lead to the mismanagement of the preset controller in the vehicle.

In the light of the discussed issues, the main objective of this article is to propose a novel adaptive soft-computing based EMS for a FCHEV, composed of a FC system and a battery pack. This strategy embraces the influence of driving condition and operating point variation of the stack. This is one of the first attempts, if any, to merge both of driving pattern recognition and adaptation to the performance drifts of the FC system in a single EMS.

C.2 Methodology

This paper puts forward an online multi-mode EMS to efficiently split the power among the components while embracing the effects of the driving conditions and performance degradation of the fuel cell system. The core of the suggested strategy is an online self-organizing map (SOM) driving profile classifier and a multi-mode FLC with online updating of the output defuzzification, as shown in Figure C.1.
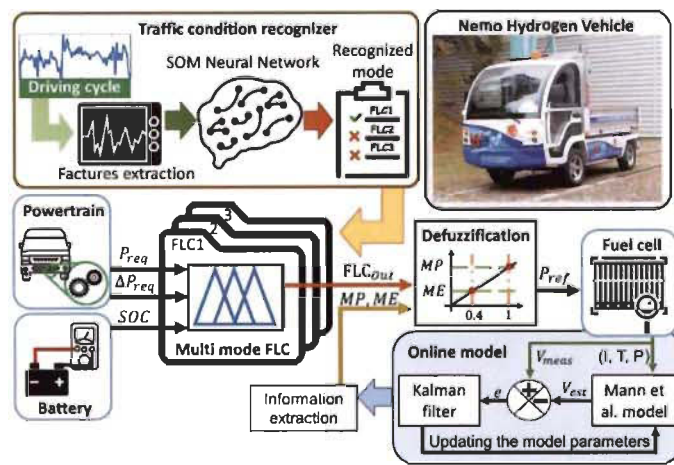

Figure C.1 The general architecture of the proposed online multi-mode EMS.

A SOM is first trained to cluster the driving patterns. The SOM competitive layer in this work is composed of ten driving features as inputs and it classifies the driving patterns into three classes in the output. To the best of the authors' knowledge, SOM has not already been used as a driving condition recognition tool. Subsequently, a three-mode fuzzy logic controller (FLC) is designed and optimized offline by the genetic algorithm for each driving pattern. Each FLC has three inputs including requested power, derivation of requested power, and battery state of charge (SOC), and one output, which determines the portion of required power form the PEMFC system. Unlike the other similar works, the defuzzification of the FLC output is done based on the estimation of maximum power and maximum efficiency of the real FC system through an online model composed of a PEMFC semi-empirical model coupled with KF. Finally, the SOM is utilized to recognize the driving mode at each sequence and accordingly activate the most suitable mode of the FLC to meet the requested power by efficient use of the energy sources. Contrary to most of the existing papers in the literature which are based on simulation, the obtained results of this work have been validated on a developed test bench by using hardware-in-the-loop (HIL) technique. To highlight the influence of tracing the real state of a FC system while designing an EMS, two PEMFCs with different degrees of degradation are used in the experimental section of this paper.

C.3 Synopsis of the results analyses

To study the performance of the proposed online multi-mode EMS, two principal scenarios are taken into consideration. In the first scenario, a combined driving cycle is imposed to the vehicle as the input and the performance of the online proposed EMS is compared with an offline-optimized EMS in terms of hydrogen consumption and efficient use of the energy sources. The new FC system is used throughout the first scenario. It should be noted that this

offline strategy knows the driving cycle in advance as opposed to the online multi-mode EMS. From the obtained results, it is clear that the FC system is being used to supply the main portion of the requested power in a stable manner, compared to the battery, which is mostly responsible for absorbing the fast transitions. The optimal offline strategy keeps the SOC in a higher level compared to the online strategy due to its priory knowledge about the requested power.

In the second scenario, the capability of the proposed EMS to deal with the FC system performance drifts is scrutinized. In this respect, the EMS test with the combined driving cycle is repeated, but by using the old PEMFC. Moreover, to signify the importance of the online PEMFC characteristics tracking, once the test is performed by deactivating the online identification, and the second time it is done by activating it. According to the obtained results, the offline multi-mode strategy experiences a lot of start-ups and shutdowns in the beginning (400 s) in the FC system as it tries to recharge the battery by using the PEMFC in high power. However, it is not aware of the fact that the FC system has been degraded and its MP and ME points have changed. Therefore, it demands for a power level that is out of the ability of the FC to supply and causes these on/off cycles.

On the other hand, in case of the proposed online EMS, in the first 100 s, the identification is performed to realize the real characteristics of the FC system and update the defuzzification tuning of the controller. After that, the FC system works in the high-power area to recharge the battery pack to a certain level in addition to supplying the requested power without having any on/off cycles. As a result, the online multi-mode EMS utilizes the FC system more efficiently which can prolong its lifetime besides improving the fuel economy of the vehicle. Table C-1 compares the obtained cost by each of the EMSs in both scenarios. According to this table, the proposed online multi-mode strategy shows a very close performance to the optimal FLC in

scenario 1. This close performance demonstrates that the proposed online EMS is able to handle unknown driving conditions with an acceptable fuel economy. The presented results of scenario 2 also confirms the satisfactory adaptation of the proposed EMS to the performance drifts of the FC system, which is a distinguishing feature of this suggested EMS. This adaptation to the real state of the FC system has made 8% of performance improvement in the online multi-mode strategy in scenario 2.

Table C-1   The cost comparison of the EMSs in the two performed scenarios

Cost (USD)	Scenario 1		Scenario 2	
	Optimized FLC	Online Multi-mode	Offline multi-mode	Online multi-mode
H_2	28.82	26.96	28.92	25.56
ON/OFF cycles	0	0	0.80	0
Recharge penalty	13	6.00	7.98	8.99
Total	32.16	32.96	37.70	34.55

C.4 Conclusion

This paper presents a new online multi-mode EMS for a FCHEV. This EMS is mainly composed of a SOM based driving condition classifier and a multi-model FLC. The FLC output MF is constantly adjusted based on the online estimation of the FC system MP and ME boundaries by KF and a semi-empirical PEMFC model. The developed SOM recognizes the driving condition and activates the most proper mode of the FLC at each update to efficiently supply the request power from the vehicle. The performance of the proposed online strategy is compared with an offline optimized FLC under a combined driving cycle of CYC_NewYorkBus, CYC_UDDS, and WLTC_class 3 and a satisfactory result is obtained with only a two-percent difference in terms of the total cost of hydrogen consumption and

on/off cycles of the FC system. Moreover, the performance of the proposed EMS is tested when the FC system undergoes a sixteen-percent drift regarding the maximum power. In this case, the proposed online EMS adapts to the real state of the FC system and improves the performance of the vehicle by eight percent compared to the offline multi-mode controller.

An Online Energy Management Strategy for a Fuel Cell/Battery Vehicle Considering the Driving Pattern and Performance Drift Impacts

Mohsen Kandidayeni ⏺, *Student Member, IEEE,* Alvaro Omar Macias Fernandez ⏺, *Student Member, IEEE,*
Arash Khalatbarisoltani ⏺, *Student Member, IEEE,* Loïc Boulon, *Senior Member, IEEE,*
Sousso Kelouwani ⏺, *Senior Member, IEEE,* and Hicham Chaoui ⏺, *Senior Member, IEEE*

Abstract—Energy management strategy (EMS) has a profound influence over the performance of a fuel cell hybrid electric vehicle since it can maintain the energy sources in their high efficacy zones leading to efficiency and lifetime enhancement of the system. This paper puts forward an online multi-mode EMS to efficiently split the power among the components while embracing the effects of the driving conditions and performance degradation of the fuel cell system. In this regard, firstly, a self-organizing map (SOM) is trained to cluster the driving patterns. The SOM competitive layer in this work is composed of ten driving features as inputs and it classifies the driving patterns into three classes in the output. Subsequently, a three-mode fuzzy logic controller (FLC) is designed and optimized offline by the genetic algorithm for each driving pattern. Unlike the other similar works, the output membership function of the FLC is designed based on the online identification of the maximum power and efficiency of the fuel cell system which change over time. Finally, the SOM is utilized to recognize the driving mode at each sequence and accordingly activate the most suitable mode of the FLC to meet the requested power by efficient use of the energy sources. The performance of the proposed EMS has been validated by using the hardware-in-the-loop platform for several scenarios. The experimental results analyses indicate the promising performance of the suggested methodology in terms of ameliorating hydrogen economy and the fuel cell system lifetime.

Index Terms—Driving condition prediction, fuel cell hybrid electric vehicle, fuzzy logic control, PEMFC online parameter estimation, self-organizing map.

M. Kandidayeni, A. O. Macias Fernandez, A. Khalatbarisoltani, and L. Boulon are with the Hydrogen Research Institute and the Department of Electrical and Computer Engineering, Université du Québec à Trois-Rivières, Trois-Rivières, QC G8Z 4M3, Canada (e-mail: mohsen.kandi.dayeni@uqtr.ca; alvaro.omar.macias.fernandez@uqtr.ca; arash.khalatbarisoltani@uqtr.ca; loic.boulon@uqtr.ca).

S. Kelouwani is with the Hydrogen Research Institute and the Department of Mechanical Engineering, Université du Québec à Trois-Rivières, Trois-Rivières, QC G9A 5H7, Canada (e-mail: sousso.kelouwani@uqtr.ca).

H. Chaoui is with the Intelligent Robotic and Energy Systems Research Group, Department of Electronics, Carleton University, Ottawa, ON K1S 5B6, Canada (e-mail: hicham.chaoui@carleton.ca).

Digital Object Identifier 10.1109/TVT.2019.2936713

I. INTRODUCTION

TRANSPORTATION is broadly held responsible for producing carbon dioxide emissions resulting from the burning of fossil fuels, such as gasoline, in internal combustion engines [1]. Pure electric and hybrid electric vehicles have been thought-provoking transitional alternates for conventional vehicles although the latter is still dependent on fossil fuels and the former has limited driving range in addition to long recharging time [2]. These shortfalls have also provided the basis for the advent of new power sources such as proton exchange membrane (PEM) fuel cells (FCs) in vehicular applications, which are presenting a steadily growing division of the automotive market [3]. Fuel cell hybrid electric vehicles (FCHEVs) usually utilize a PEMFC as the primary power source and a battery pack or/and a supercapacitor as the secondary power source. Therefore, the performance of an FCHEV is impacted by several interrelated factors which put the design of an energy management strategy (EMS) in critical position [4]. Regardless of the type of the hybrid vehicle, the existing EMSs fall under two categories of rule-based and optimization-based [5], [6]. The rule-based strategies are usually heuristic and lead to limited and sub-optimal solutions. In this regard, the researchers have turned attentions on the optimization methods, which assure optimal or near-optimal solutions in theory and can also provide new guidelines for refining the rule-based methods [7], [8]. Optimization-based strategies can be divided into two groups of global and real-time strategies depending on the defined cost function. The former utilizes the cost function over a fixed driving cycle and is beneficial for realizing the optimal policy. However, it is not applicable in real-time control of the vehicle owing to its dependency on the driving profile. The latter, nonetheless, uses an instantaneous cost function based on the variables of the system. Equivalent consumption minimization strategy (ECMS) and Pontryagin's minimum principle (PMP) are two widely used real-time optimization strategies in hybrid electric vehicles [9]–[12]. One of the key issues here is the high instantaneous computational time. Furthermore, the estimation of the equivalent factor in ECMS and the initialization of the co-state in PMP, which are sensitive to transient dynamic and the driving pattern, are quite challenging tasks [13], [14].

In light of the discussed matters, the use of traffic condition and driving information in the design of an EMS has come under the attention of many researchers [15]–[17]. This line of work is known as intelligent-based EMS category and can be integrated into both of ruled-based and optimization-based strategies [18]. Intelligent-based EMSs mainly consist in the use of car navigation data (global positioning system, vehicle geographical information system or vehicle telematics) and the history of motion for recognizing and predicting the driving condition [19]. Several approaches based on fuzzy logic control (FLC) [20], neural networks (NNs) [21], and other machine learning-based techniques [22] have been introduced in this respect. In [23], the driving data is clustered by using a hierarchical algorithm and support vector machine (SVM) is used for the recognition of the traffic condition. In [24], multi-layer perceptron (MLP) NN is trained to recognize the driving pattern and activates the controller. In [25], back propagation NN along with metaheuristic algorithms is used to formulate a dynamic programming-based predictive EMS to reduce the fuel consumption. In [26], the suggested strategy comprises two steps: generation of optimal EMS for the long trip by using an estimation of distribution optimization algorithm and refining the optimal EMS with regard to actual traffic conditions in the short-term. In [27], combination of PMP with NN, in [28], learning vector quantization NN with GA, and in [29], probabilistic SVM with a data fusion based method are proposed for developing the EMS. In [30], an adaptive control based on tuning the FLC parameters for different loads is proposed. The authors state that the PEMFC voltage declines due to degradation after a while and under this condition the rule-based values should be reconsidered.

Apart from the importance of considering the driving condition, it is also essential to take into account the performance drifts of the FC system in EMS formulation of an FCHEV. The performance of a FC system is impacted by several factors such as the variation of operation conditions and degradation phenomenon. The previous works of the authors have touched upon the procedure for updating the parameters of a FC system online [31], [32]. However, they have not been integrated into the EMS design yet. There are some works in the literature regarding the online identification of the PEMFC model in an EMS. Some of them are based on the extremum seeking methods in which a periodic perturbation signal is utilized to find an optimal operating point in real-time [33]–[35]. Such strategies are employed in the formulation of an EMS mainly due to their easy implementation. However, they cannot be very effective when simultaneous identification of several operating points are required in online applications. Because they need a separate search line for each intended characteristic such as maximum efficiency (ME) and maximum power (MP). This problem can be avoided by utilizing recursive filters for online identification of the PEMFC parameters and extracting the necessary characteristics from the updated model. There are a few EMSs on this basis in the literature for FCHEVs. In [36], [37], the authors employ the recursive least square (RLS) and the square root unscented Kalman filter (KF) for updating a single-input (current) PEMF model while designing hysteresis and PMP based EMSs for a FCHEV. They indicate that the classical EMSs

TABLE I
NEMO PARAMETER DEFINITION

Specification	Parameter	Value
Vehicle's parameters	Rolling resistance	0.015
	Aerodynamic drag	0.42
	Frontal area (m^2)	4
	Density of air (kg/m^3)	1.2
	Mass factor	1.035
	Mass (kg)	896
	Maximum speed (km/h)	40
3-phase induction machine	Power (W)	5690
	Frequency(Hz)	131.1
FC system	Rated power	4 kW
Battery	voltage (V)	72
	Capacity (Ah)	120

are not very efficient when there are drifts in the FC system. In [38], the authors propose a supervisory controller while the PEMFC model is being updated by a simple current dependent model.

This paper proposes a novel adaptive soft-computing based EMS for a FCHEV, composed of a FC system and a battery pack. This is one of the first attempts, if any, to merge both of driving pattern recognition and adaptation to the performance drifts of the FC system in a single EMS. The core of the suggested strategy is an online self-organizing map (SOM) driving profile classifier and a multi-mode FLC with online updating of the output defuzzification. To the best of the authors' knowledge, SOM has not already been used as a driving condition recognition tool. Moreover, the other contribution of this work lies in the formulation of the FLC to adapt to the real state of the FC system. Each FLC has three inputs including requested power, derivation of requested power, and battery state of charge (SOC), and one output, which determines the portion of required power form the PEMFC system. The defuzzification of the FLC output is done based on the estimation of MP and ME of the real FC system through an online model composed of a PEMFC semi-empirical model coupled with KF. Contrary to most of the existing papers in the literature which are based on simulation, the obtained results of this work have been validated on a developed test bench by using hardware-in-the-loop (HIL) technique. To highlight the influence of tracing the real state of a FC system while designing an EMS, two PEMFCs with different degrees of degradation are used in the experimental section of this paper.

Section II deals with the modeling description of the vehicle. The methodology for designing the proposed EMS is detailed in Section III. Section IV clarifies the obtained results from different considered scenarios. Finally, the conclusion along with some remarks is presented in section V.

II. FUEL CELL HYBRID ELECTRIC VEHICLE SYSTEM

A. Hardware-in-the-Loop Platform and Power Train System Modeling

The system used in this work is based on a low-speed FCHEV called Nemo. The main characteristics of the vehicle are listed in Table I.
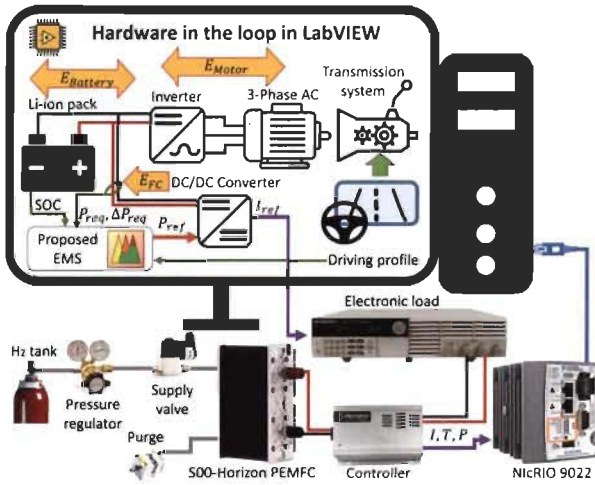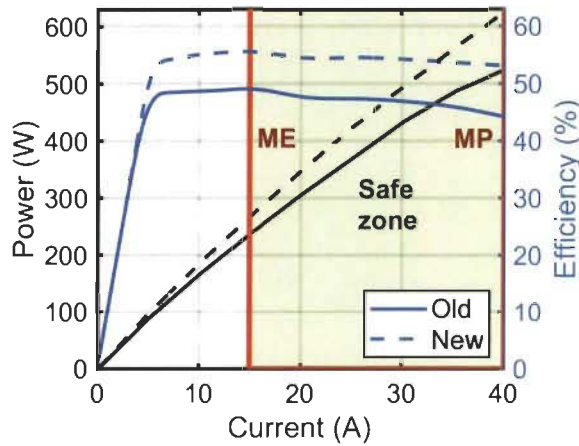
Fig. 1.   The HIL set-up for testing the EMS.

Fig. 2.   The old and new PEMFCs' characteristics.

TABLE II
THE TECHNICAL FEATURES OF THE H-500 HORIZON PEMFC

PEMFC Technical specification	
Type of FC	PEM
Number of cells	36
Active area	56 cm^2
Max Current (shutdown)	42 A
Hydrogen pressure	50-60 kPa (0.5-0.6 Bar)
Rated H$_2$ consumption	7 SLPM
Ambient temperature	5 to 30 °C
Max stack temperature	65 °C
Cooling	Air (integrated cooling fan)

TABLE III
THE UTILIZED BATTERY PACK DATA

Specification	Parameter	Value
	Maximum current continuous	C/1 A
	Capacity	6 Ah
SAFT Rechargeable	Nominal voltage	3.65 V
lithium-ion battery cell	No. of cells in series	20
	No. of cells in parallel	13
	Cell mass	0.34 kg
	Coulombic efficiency	0.99

PEMFC is called old PEMFC and the other one is referred to as new PEMFC. Fig. 2 also shows the safe zone operating range, between the ME and MP boundaries, of these FC systems. The EMSs should try to operate the PEMFC in this safe zone to increase the lifetime and fuel economy of the system. It should be noted that according to [37], a dynamic limitation of 50 Ws^{-1}, which means a maximum of 10% of the maximum power per second for rising, and also 30% of the maximum power per second for falling, as suggested in [39], have been considered for the operation of the PEMFC stack.

According to Fig. 1, the FC system, as the primary power source, is connected to the DC bus via a DC-DC converter, and the battery pack, as the secondary source, is directly linked to the bus to sustain the voltage of the DC-link. The force of the hybrid vehicle, considering the speed (V_{HV}) and mass (m), can be calculated by taking into account the traction (F_{tr}) and resistive (F_{res}) forces as follows:

$$\begin{cases} m\frac{d}{dt}V_{HV} = F_{tr} - F_{res} \\ F_{res} = mgf_r + 0.5\rho_a C_d A_f V^2 + mg\alpha \\ F_{tr} = (V_{HV-ref} - V_{HV})Cs(t) + F_{res} \end{cases} \quad (1)$$

Where a family of PI controller is used to force the vehicle to follow the driving cycle and assure achieving the reference speed of the vehicle. The vehicle requested power from the electric motor side can be then expressed as:

$$P_{req} = (V_{HV} \times F_{tr})/\eta_{EM}\eta_t\eta_{dc-ac} \quad (2)$$

Where η_t is the transmission efficiency (92%), η_{EM} is the motor average efficiency (90%), and η_{dc-ac} is the inverter efficiency (95%). A lithium-ion battery pack is used to help the FC stack to meet the energy demand from the electric motor side. The important parameters of the battery are listed in Table III. An internal resistance based model is used for modeling the behavior of this energy storage system [40]. Fig. 3 shows the
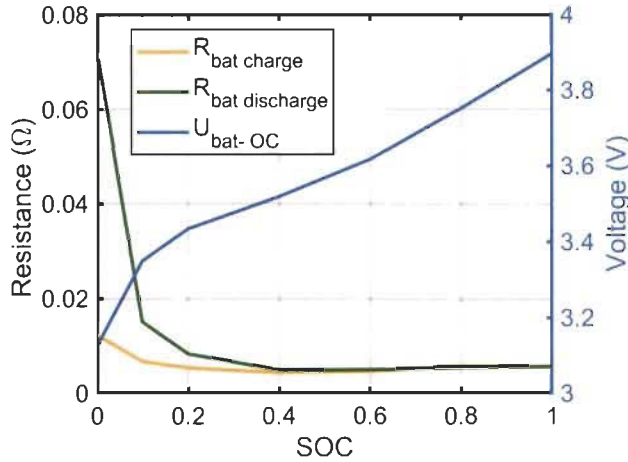
For the purpose of this paper, a HIL set-up, as shown in Fig. 1, is designed for evaluating the performance of the EMS. The FC system is the real component of this HIL simulator and the other ones are the mathematical models. In this set-up, a Horizon 500-W air breathing PEMFC, which is connected to a National Instrument CompactRIO through its controller, is utilized. The FC controller controls the mounted axial fan which is responsible for cooling the stack and supplying the necessary oxygen. The information between the CompactRIO and the PC is transferred by an Ethernet connection every 100 milliseconds. Temperature, current, and voltage of the FC system are recorded and used for the online modeling. An 8514 BK Precision DC Electronic Load is used to request the load profile, imposed by the DC-DC converter, from the FC system. According to Table I, the Nemo FCHEV has a 4-kW FC system. In this regard, the FC output voltage in the HIL set-up is scaled up after the converter to meet the requested power. To emphasize the significance of tracking the real behavior of the FC system while designing an EMS, two H-500 Horizon PEMFCs with different degrees of degradation are used in this work. The MP and ME curves of each of the FC systems are presented in Fig. 2 and their other characteristics are listed in Table II. Hereafter in this manuscript, the degraded

Fig. 3.   The relationship of SOC with U_{bat-OC} and R_{bat} per cell.

relationship of battery SOC with each of open circuit voltage (U_{bat-OC}), internal resistance (R_{bat}) changes in charge, and internal resistance changes in discharge. The battery current (I_{bat}), bus voltage (U_{bus}), and SOC are calculated based on (3)–(5) respectively.

$$I_{bat} = \frac{(U_{bat-OC} - \sqrt{U_{bat-OC}^2 - 4 \times R_{bat} \times P_{bat}}}{2 \times R_{bat}}$$

(3)

$$U_{bus} = U_{bat-OC} - I_{bat} \times R_{bat}$$

(4)

$$SOC(t_f) = SOC(t_0) - \eta_C \frac{\int_{t_0}^{t} I_{bat} dt}{C_{bat}}$$

(5)

where P_{bat} is the battery pack power, C_{bat} is the capacity, and η_C is the coulombic efficiency.

The FC system modeling is premised on a semi-empirical equation proposed by Mann et al. [41]. This model calculates the stack voltage for a number of cells connected in series. In fact, this model is being used for two purposes.

First, for tuning the EMS parameters before its implementation on the real system to make sure that it does not damage the real FC system. Second, it is used in the online characteristics estimation process of the real FC stack while it is under operation.

$$V_{FC} = N(E_{Nernst} + V_{act} + V_{ohmic} + V_{con})$$

(6)

$$E_{Nernst} = 1.229 - 0.85 \times 10^{-3}(T - 298.15)$$

$$+ 4.3085 \times 10^{-5} T [\ln(P_{H2}) + 0.5\ln(P_{O2})]$$

(7)

$$\begin{cases} V_{act} = \xi_1 + \xi_2 T + \xi_3 T \ln(CO_2) + \xi_4 T \ln(i_{FC}) \\ CO_2 = \frac{P_{O2}}{5.08 \times 10^{-6} \exp(-498/T)} \end{cases}$$

(8)

$$V_{ohmic} = -i_{FC} R_{internal} = -i_{FC}(\zeta_1 + \zeta_2 T + \zeta_3 i_{FC})$$

(9)

$$V_{con} = B \ln\left(1 - \frac{J}{J_{max}}\right)$$

(10)

Where V_{FC} is the output voltage (V), N is the number of cells, E_{Nernst} is the reversible cell potential (V), V_{act} is the activation loss (V), V_{ohmic} is the ohmic loss (V), V_{con} is the concentration loss (V), T is the stack temperature (K), P_{H2} is the hydrogen partial pressure in anode side (Nm^{-2}), P_{O2} is the oxygen partial pressure in cathode side (Nm^{-2}), $\xi_n(n = 1 \ldots 4)$ are the semi-empirical coefficients based on fluid mechanics, thermodynamics, and electrochemistry, CO_2 is the oxygen concentration ($mol\ cm^{-3}$), i_{FC} is the PEMFC operating current (A), $R_{internal}$ is the internal resistor (Ω), $\zeta_n(n = 1 \ldots 3)$ are the parametric coefficients, B is a parametric coefficient (V), J is the actual current density ($A\ cm^{-2}$), and J_{max} is the maximum current density ($A\ cm^{-2}$). The hydrogen flow is computed by a first order function approximation based on the experimental data, where a and b are fitting parameters [37].

$$H_{2,flow} = a + b * i_{FC}$$

(11)

The FC system is connected to the DC bus through a DC-DC converter. This converter is modeled by using a smoothing inductor and a boost chopper as formulated in (12) and (13). The detailed explanation of the converter model can be found in [42].

$$L \frac{d}{dt} i_{FC} = V_{FC} - V_{hFC} - r_L i_{FC}$$

(12)

$$\begin{cases} V_{hFC} = m_{hfc} U_{bat} \\ i_{hFC} = m_{hfc} i_{FC} \eta_{hFC}^j \end{cases} \text{with } j = \begin{cases} 1 \text{ if } P_{conv} > 0 \\ -1 \text{ if } P_{conv} < 0 \end{cases}$$

(13)

Where L is the converter inductance (H), V_{hFC} is the input voltage in the chopper (V), r_L is the converter resistance (Ω), m_{hfc} is the modulation ratio, and η_{hFC}^j is the converter efficiency. In fact, the converter uses a voltage controller to determine the required coil current by minimizing the error between the actual and reference voltage of the FC system. Then a current controller is used to determine m_{hfc} which boosts the output voltage to the desired value.

III. ENERGY MANAGEMENT STRATEGY DESIGN

The proposed EMS in this work aims at dealing with two important uncertainties, namely driving pattern changes and performance drifts of the FC system. The general structure of the suggested EMS is shown in Fig. 4. As is seen in this figure, the proposed online EMS comprises three important parts, namely traffic condition recognizer, online PEMFC modeling, and multi-mode FLC. The SOM is employed to determine the driving mode at each sequence and consequently trigger the most appropriate mode of the multi-mode FLC to satisfy the requested power. The updated characteristics of the online PEMFC stack model are also utilized to tune the output of the FLC with respect to the performance drifts of the PEMFC system. The development of each part is carefully described hereinafter.

A. Traffic Condition Recognizer

In this work, SOM, as an unsupervised learning method, is used for recognizing the driving condition. Kohonen presented
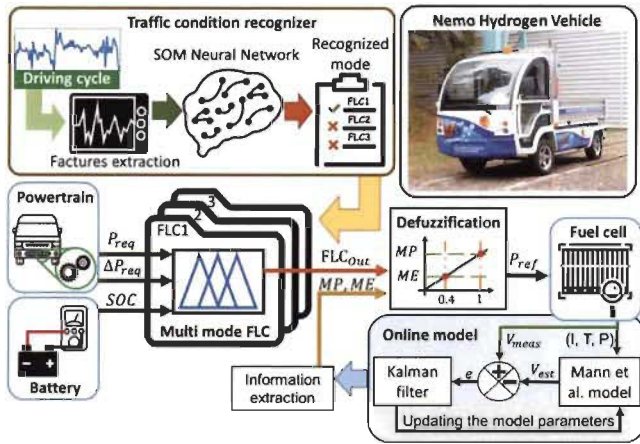
Fig. 4. The general architecture of the proposed online multi-mode EMS.

Individuality	Description
Driving features	■ Average speed (km/h) ■ Idle time (%) ■ Speed standard deviation (km/h) ■ Average acceleration (km/h²) ■ Maximum acceleration (km/h²) ■ Average deceleration (km/h²) ■ Maximum acceleration (km/h²) ■ Percentage of low-speed (%) ■ Percentage of middle-speed (%) ■ Percentage of high-speed (%)
Driving schedule (DS)	• Urban and extra urban DS (CYC_ECE_EUDC) • Federal test procedure DS (CYC_FTP) • Highway Fuel Economy Test (CYC_HWFET) • Indian highway DS (cyc_india_hwy) • Indian Urban DS (cyc_india_urban) • Supplemental Federal Test Procedure (CYC_SC03) • City of Tehran's DS (CYC_TEH_CAR) • Urban Dynamometer DS (CYC_UDDS) • West Virginia Interstate (CYC_WVUINTER) • West Virginia Suburban (CYC_WVUSUB) • California Air Resources DS (CYC_UNIF01) • The Unified DS (CYC_LA92)

this form of unsupervised competitive ANN in 1982 and it has been well studied and implemented in different problems [43]. In SOM, each of the neurons is associated to all the network inputs and to the neighborhood of the nearby neurons. Contrary to the utilized supervised methods, such as MLP and SVM, in driving condition recognition, SOM can update its weights without the need for a priori known labeled output. Compared to other unsupervised methods, like k-means and linear vector quantization, SOM preserves the structure of the original data, is very conducive to the interpretation of the clusters, and teaches the adjacent neurons to distinguish the neighboring sections of the input space. SOM has four phases of training as initialization, competition, cooperation, and adaptation.

In the training process, initially, each neuron is entirely linked to all the source nodes in the input vector and the weights of all the connections are assigned with small random values.

Then, the competition phase is performed by calculating the inner product between neuron j's weight vector (W_j) and the input vector (X). The winning neuron $(i(X))$ is determined by:

$$\begin{cases} i\ (X) = \arg\min_j X - W_j \\ \text{with} \begin{cases} X = [X_1, X_2, \ldots, X_m]^T \\ W_j = [W_{j1}, W_{j2}, \ldots, W_{jm}]^T, \ j = 1, 2, \ldots, l \end{cases} \end{cases} \tag{14}$$

where m is the dimension of the input vector, and l is the total number of neurons in the network. In the cooperation phase, the neurons in the neighborhood of the excited neuron are also tuned based on the principle of lateral interaction among the activated neurons of the human brain. This topological neighborhood is defined by:

$$\begin{cases} h_{j,i(X)} = \exp\left(-d_{j,i}^2/2\sigma^2\right) \\ \text{with} \begin{cases} d_{j,i}^2 = r_j - r_i{}^2 \\ \sigma\ (n) = \sigma_0 \exp\left(-n/\tau_1\right), \ n = 0, 1, 2, \ldots, \end{cases} \end{cases} \tag{15}$$

where $h_{j,i(X)}$ is the topological function, $d_{j,i}$ is the lateral distance, σ is the standard deviation, r_j is the position of the activated neuron, r_i is the position of the wining neuron, σ_0 is the initial value of the σ, and τ is the time constant. Finally, in

the adaptation phase, it is required that the weights of the wining neuron and its neighbors get updated. The weight adaptation is defined as:

$$\begin{cases} W_j\ (n+1) = W_j\ (n) + \eta\ (n)\ h_{j,i(X)}\ (n)\ (X\ (n) - W_j\ (n)) \\ where: \eta\ (n) = \eta_0 \exp\left(-n/\tau_2\right), \ n = 0, 1, 2, \ldots, \end{cases} \tag{16}$$

where $\eta(n)$ is the learning-rate parameter of the algorithm. The initial value of learning rate (η_0) is usually defined as 0.1 and gradually decreases to around 0.01. Once the SOM is trained, it can be used to classify the new input data based on the defined clusters.

In this manuscript, the input layer consists of ten neurons which are among ten important driving features introduced in [23], [28]. Each of these neurons corresponds to one driving feature. Table IV lists the used features and driving schedules for SOM training. All the driving cycles have been scaled down according to the maximum speed of the Nemo vehicle, which is 40 km/h. In this way, the real driving patterns are best represented. The number of driving features in the input layer can vary from 2 to 62 in the literature. However, the chosen features of this work are among the most used ones. In order to train the SOM to classify the input features, twelve driving cycles are employed. Since SOM learns to classify the data based on how they are grouped in the input space, the driving cycles are chosen in a way to reach a homogeneous distribution of data. In other words, the chosen driving cycles cover all the driving conditions. To extract the statistical features, the driving cycles are decomposed into micro-trips and all the features are calculated for each micro-trip [20]. Concerning the number of output layer neurons, based on which the clusters are defined, Silhouette criterion is used. In this regard, SOM is trained for different number of output neurons (2, 3, ..., 6) by using the same input data. In each case, the Silhouette value is calculated for all the data of each cluster and its mean values are shown
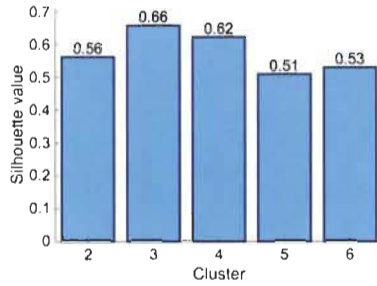
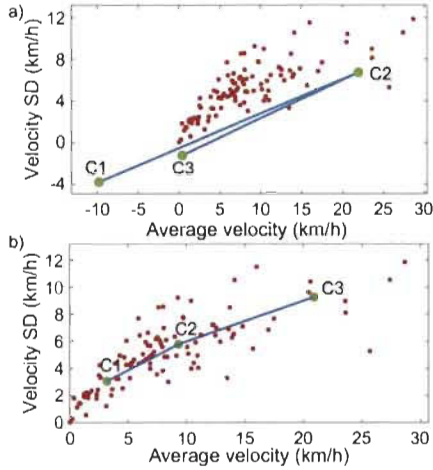Fig. 5. The mean of Silhouette value for each cluster.

Fig. 6. The SOM based driving condition recognizer weight positions. (a) Initial weight positions. (b) The trained SOM weight positions.

Fig. 7. Recognition results for the combined driving cycle.

TABLE V
KF CUSTOMIZATION FOR THE IDENTIFICATION PROBLEM

Operators	SYMBOLS	Implementation description
State vector	$x(t)$	$[\xi_1, \xi_2, \xi_3, \xi_4, \zeta_1, \zeta_2, \zeta_3, B]$
Measurement vector	$H(t)$	$[1, T, Tln(CO_2), Tln(i), -i, -iT, -i^2, ln(1-\frac{J}{J_{max}})]$
Transition matrix	$F(t+1|t)$	Identity matrix
Measured output	$y(t)$	Measured V_{FC} from the real FC

of the SOM driving condition recognizer, as shown in Fig. 7. As it can be seen, the classifier is capable of recognizing new driving data without switching or confusing the conditions. It is worth noting that the CYC_NewYorkBus and WLTC_class 3 driving cycles are completely new for the classifier and have not been used in its training phase.

B. Fuel Cell Online Modeling

As previously mentioned, the parameters of a PEMFC model vary slowly over time since the device is affected by degradation and operating conditions. KF, as an optimal estimator, has been suggested for online parameter estimation of a FC system in the previous work of the authors [31]. KF can conclude the parameters of interest from imprecise and uncertain observations. This filter estimates the current state variables firstly and then updates them when the next measurement is received. The standard form of KF, introduced in [44], has been used in this paper. Table V defines some of the important parameters of KF in this work. The details about initialization and customization of KF for updating the parameters of the introduced PEMFC semi-empirical model, in Section II, are comprehensively discussed in [31]. The ME and MP of the PEMFC are extracted from the updated model and used in the multi-mode FLC. Fig. 8 shows the capability of the online model in estimating the output voltage of the old FC system for the presented current and temperature profiles. Moreover, the hydrogen flow obtained by the model is compared with the measured one. Fig. 9 shows the predicted maximum power and efficiency curves of the old FC system.

C. Multi-Mode Fuzzy Logic Controller

Fuzzy logic systems are designed to provide a number of strategic rules by means of linguistic labels. Several reasons, such as imprecise modeling of a vehicle's components, their nonlinear behavior, and the unknown behavior of exogenous

in Fig. 5. This value demonstrates how analogous an entity is to its own cluster (consistency) compared to other clusters (segregation). Silhouette value changes from −1 to +1, where higher values denote that the entity fits well to its own cluster. According to Fig. 5, by grouping the driving data into three clusters, more cohesion clusters are attained. Therefore, three neurons are selected for the output layer of SOM to classify the driving data into three classes of slow-speed, medium-speed, and high-speed driving profiles.

After training the SOM classifier, it can be used online for determining the driving conditions. In this respect, as suggested in [24], a sampling window size of 150 s and an updating window size of 50 s are employed to extract the statistical driving features while avoiding frequently mode switches. This means that each recognition is based on the driving features of the previous 150-s window and is updated every 50 s. Fig. 6 demonstrates the 2D SOM weight positions based on average velocity and standard deviation (SD) in the initial phase and at the end of self-organization. As is seen in Fig. 6a, primary weights are scattered over the input space after the initialization. The red spots show the training vectors. However, after 1000 epochs, the neurons have moved towards the various training groups by updating the weights of the winner neurons and their neighbors according to Fig. 6b.

A combined driving cycle, made up of CYC_NewYorkBus, CYC_UDDS, and worldwide harmonized light-duty vehicles test cycles (WLTC_class 3), is used to assess the performance
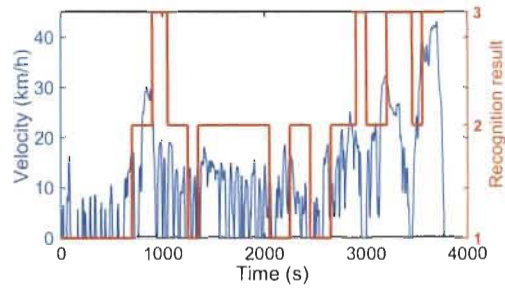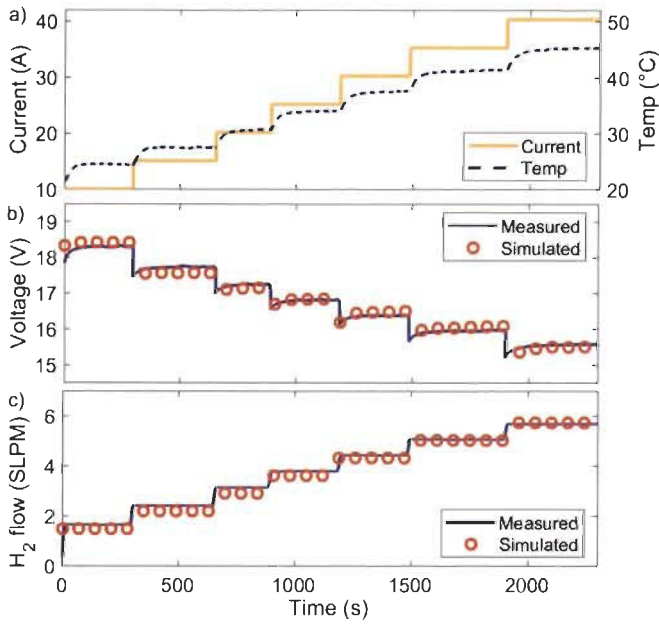
Fig. 8. The output voltage and hydrogen estimation analysis. (a) The demanded current profile from the FC system and the corresponded stack temperature, (b) online voltage estimation, and (c) comparison of H2 rate between the model and the real PEMFC.
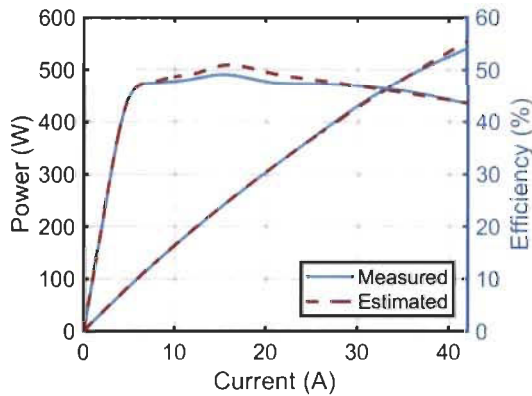

Fig. 9. The analysis of power and efficiency curves estimation by using the extracted parameters at 600 s.
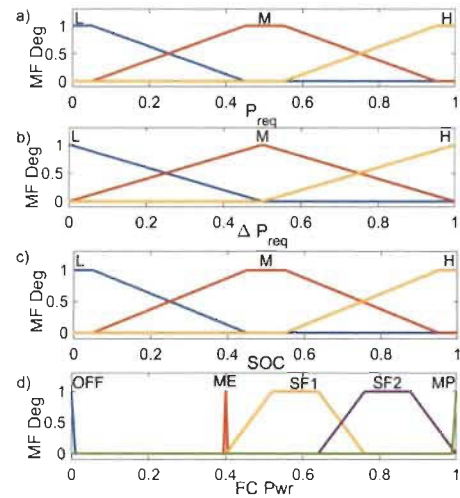

Fig. 10. The primary distribution of the input and output MFs. (a) Input 1: Requested power. (b) Input 2: Requested power derivation. (c) Input 3: Battery SOC. (d) Output: Reference power of the FC system.
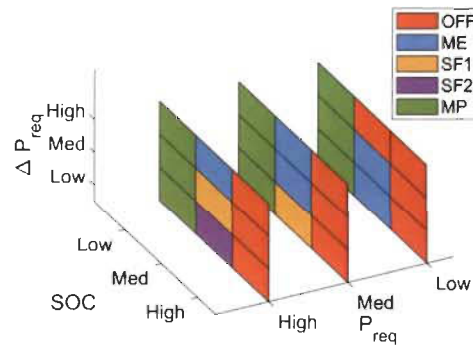

Fig. 11. The designed FLC rule base. (Fuzzy system: Mamdani, Inference mechanism: AND (minimum operator), and diffuzication: centroid). The output MF labels are shown in the legend of this figure.

factors, like traffic, weather, etc., can be counted for suitability of utilizing a FLC in EMS design of FCHEVs.

The proposed FLC has three inputs, which are demanded power, the derivation of the demanded power, and battery SOC. Choosing the requested power derivation as an input, besides the other two inputs, helps at using the PEMFC system in a more stable manner. The only output of the utilized FLC is the required power from the FC system. The initial input and output membership functions (MFs) are shown in Fig. 10. As is clear in this figure, the output MF is defined based on the ME and MP points of the FC system. The output of the FLC, which is between 0 and 1, goes under a defuzzification process to be transformed into a real quantifiable value. The defuzzification is done by utilizing a linear function in which the slope is defined by means of the estimated values of ME and MP points through the previously described online PEMFC modeling. In

this way, as the FC system goes under degradation, the output MF is updated with respect to the real state of the FC system. Moreover, the distribution of the variables of the output MF stays the same though the transformation gains of the defuzzification process change. The fuzzy reasoning rules, shown in Fig. 11, are laid down based on the heuristic expertise. The initial MFs are also tuned heuristically and then improved by GA which is a metaheuristic approach. Since the optimization of fuzzy MFs is a classic method and is available in other similar works [7], its explanation has been considered redundant in this paper. The utilized objective function for performing the MFs adjustment is presented in (17). The constructing parameters of the input and output MFs, which come to 23, are considered as decision variables for optimizing the FLC. To perform the optimization process, GA utilizes some natural procedures, such as crossover and mutation, to leave out the unfavorable populations and keep the most meritorious ones to create new generations. In this context, the process of survival of the fittest refers to the minimization trend of the defined objective function. The number of generations is set to 100, the population size is 200, the elite

count is 10, and the crossover fraction is 0.8.

$$\begin{array}{c} min \\ (params.) \end{array} \quad J = w_1 \sum_{j=1}^{K} m_{H2} + w_2 \sum_{j=1}^{K} N_{on/off} + \$_{RP}$$

$$P_{MFs_{k, min}} \leq P_{MFs_k} \leq P_{MFs_{k, max}} \quad (k = 1 \ldots 23)$$

$$ME \leq P_{FC} \leq MP$$

$$0.5 \leq SOC \leq 1 \tag{17}$$

Where J is the objective function, w_1 is the cost conversion factor for hydrogen, w_2 the durability cost conversion factor, m_{H2} is the hydrogen consumption, $N_{on/off}$ is the number of on/off cycles in the PEMFC, $\$_{RP}$ is the cost of the recharge penalty (USD), P_{MFs} is the parameter for defining the MFs, and P_{FC} is the FC system power. The values of w_1 and w_2 are 2.3 USD/kg H2 and 0.032 USD respectively. These values have been defined based on the 2020 technical targets put forward by the U.S. Department of Energy in the Multi-Year Research, Development, and Demonstration Plan. The optimization process of the fuzzy controllers has been done by considering a recharge penalty step ($\$_{RP}$) at the end of each profile. In this way, the battery is fully recharged by using the maximum power point of the PEMFC stack at the end of each test and the USD cost of the additional required hydrogen is added to the total cost function. It should be noted that the recharge step is performed by setting the stack on its maximum power to punish the strategy if it finishes in low SOC level.

The multi-mode controller should be developed in a way to embrace all the traffic conditions since it is supposed to work online without a prior knowledge of the driving cycle. As the driving data are clustered into three classes by the developed SOM recognizer, one optimized FLC needs to be developed for each class and then the three controllers should be put together to form the multi-mode FLC. Each optimized FLC can be considered as the near optimal controller for each class of the driving data. However, due to the high volume of data that each cluster contains, the optimization process would be very time-consuming for all the driving data. In this regard, a representative driving cycle is developed for each of the driving profile to reduce the required time for optimization process. Fig. 12 shows the extracted representative driving cycles, namely low-speed, medium-speed, and high-speed, and their average velocities. These driving cycles are used as the input driving data for the process of FLC optimization. Each of them is composed of the nearest micro-trips to the center of cluster they belong to. The cluster centers have been already calculated by the developed SOM. The distance between each cluster center and each micro-trip is calculated by the Euclidean distance $(ed(x,y))$ as:

$$ed(x,y) = \sqrt{\sum_{i=1}^{n} (x_i - y_i)^2} \tag{18}$$

where $x = (x_1, x_2, \ldots, x_{10})$ is the cluster center vector, $y = (y_1, y_2, \ldots, y_{10})$ is the micro-trip vector, and n is the number of driving features, which is 10 in this work. There are three cluster center vectors and 130 micro-trip vectors where each vector contains 10 elements. The distance between each cluster
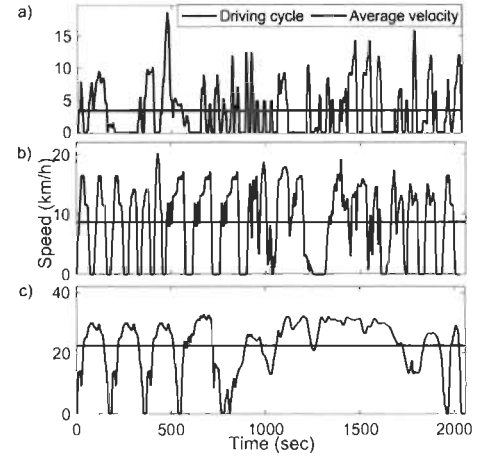

Fig. 12. The extracted representative driving cycles. (a) Low-speed profile. (b) medium-speed profile, and (c) high-speed profile.

center and all the micro-trips is calculated and then the nearest micro-trips to the center are combined to reach an almost 2000-s representative cycle for every cluster. As explained before, the defuzzification function of the output MF is updated when a noticeable drift is observed in the maximum operating points of the FC system, which are available from the online semi-empirical model.

D. Primary Evaluation of the Proposed Strategy

To have a primary assessment of the developed multi-mode controller and the SOM classifier, a comparative analysis, in terms of the costs of H2, ON/OFF cycles, final SOC recharge penalty, and the total cost, is performed for five cases, as explained further in this section. The main purpose of the first three cases is to examine the performance of the SOM classifier of the proposed online multi-mode EMS regarding unnecessary switches. Case 4 is a real challenge between the proposed multi-mode EMS and one optimized fuzzy controller. Finally, Case 5 evaluates the performance of the proposed EMS under a new driving condition and compares it with two other strategies.

Case 1. low-speed (LS) driving profile (Fig. 12a): In this case, the performance of the online multi-mode EMS is compared with only the first mode of the controller (FLC1), which is an offline optimized single-fuzzy EMS specifically designed for LS driving profile. According to Table VI, the performance of the both controllers is completely the same indicating the SOM classifier has used the correct mode.

Case 2. medium-speed (MS) driving profile (Fig. 12b): The second case compares the performance of the online multi-mode EMS with the second mode of the controller (FLC2), which is an offline optimized single-fuzzy EMS specifically designed for MS driving profile. Table VI shows that the total cost of the online multi-mode EMS is 2% more than the FLC2, which can be owing to very few switches in the recognition process.

Case 3. high-speed (HS) driving profile (Fig. 12c): This case compares the performance of the online multi-mode EMS with the third mode of the controller (FLC3), which is an offline optimized single-fuzzy EMS specifically designed for HS driving

TABLE VI
COMPARISON OF THE MULTI-MODE CONTROLLER AND THE OPTIMIZED
CONTROLLER OF EACH REPRESENTATIVE DRIVING CYCLE

Case study	Cost (USD) / EMS	H_2	ON/OFF cycles	Recharge penalty	Total
Case 1	Opt. for LS	12.49	0	8.21	20.70
	Multi-mode	12,49	0	8.21	20.70
Case 2	Opt. for MS	12.72	0	10.55	23.27
	Multi-mode	13.25	0	10.51	23.76
Case 3	Opt. for HS	13.67	0	18.01	31.67
	Multi-mode	14.15	0	17.66	31.81
Case 4	Opt. for rep.	35.64	2.97	2.38	41
	Multi-mode	34.16	2.78	2.52	39.48
Case 5	Opt. for rep.	28.05	0	3.84	31.90
	Multi-mode	25.66	0	3.92	29.58
	BLFS	28.76	0	3.00	31.76

profile. Table VI indicates that the proposed EMS can closely approach the optimized results obtained by FLC3 with less than one percent difference in the total cost. Obviously, the proposed EMS does not have unnecessary switches for determining the mode of operation.

Case 4. representative (Rep.) driving profile: This case compares the performance of the online multi-mode EMS with an offline optimized single-fuzzy EMS (Opt. for rep.) particularly designed for the Rep. driving profile. The Rep. driving profile is a concatenation of LS, MS, and HS profiles. The online multi-mode EMS has three optimized FLCs corresponding to each of LS, MS, and HS conditions inside the Rep. driving profile while the Opt. for rep. EMS is only one optimized FLC for the whole driving profile. According to Table VI, it can be seen that the online multi-mode EMS outperforms the Opt. for rep. EMS by 3.7 percent in terms of the total cost. This superior performance shows the applicability of the proposed multimode EMS.

Case 5. combined driving profile (Fig. 7): So far, all the discussed cases have been done by using the known driving profiles. However, in this case study, to better clarify the effectiveness and flexibility of the online multi-mode controller in real-time unknown driving conditions, its performance is compared with the Opt. for rep. EMS under combined driving profile, which is a new driving condition for both of the strategies. Moreover, the performance of the proposed strategy is compared with one of the commonly used real-time strategies in the literature called bounded load following strategy (BLFS) [39], [45]. BLFS is a hysteresis based energy management to split the power among the components of a fuel cell hybrid electric vehicle. BLFS normally provides three modes of operation for the PEMFC stack including ON/OFF, P_{FC_min}, and P_{FC_max} with respect to the battery SOC level. To assure a low hydrogen consumption, the maximum efficiency of the PEMFC stack is selected as the P_{FC_min} mode. This choice stems from the fact that the hydrogen consumption and the degradation of the stack is higher within the open circuit voltage and the best efficiency point area of the PEMFC. Therefore, when the PEMFC is turned on, the ME mode is activated. P_{FC_max} mode, which sets the stack on its maximum power, is triggered when the battery SOC reaches the
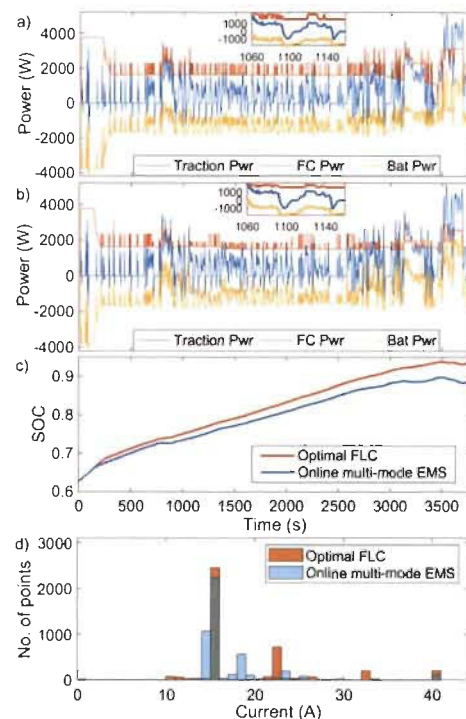

Fig. 13. Scenario 1 for evaluation of the proposed multi-mode EMS. (a) Power split by the optimal FLC, (b) power split by the online multi-mode strategy, (c) battery SOC comparison of the two strategies, and (d) PEMFC operating points distribution.

minimum SOC level. Furthermore, the P_{FC_max} mode assists the battery pack in high traction power operations. The battery SOC can fluctuate between 45% and 95% ($0.45 \leq SOC \leq 95$) [39]. As reported by Table VI, the proposed multi-mode EMS outperforms the Opt. for rep. and the BLFS strategies by almost 7 percent. This performance distinction indicates that the proposed EMS performs well when confronting new driving conditions.

IV. EXPERIMENT AND RESULTS ANALYSIS

The performance of the proposed online multi-mode EMS is comprehensively studied in this section. In this respect, two principal scenarios are taken into consideration. Both of these scenarios have been implemented on the developed test bench to have realistic perception of the FCHEV performance.

In the first scenario, the combined driving cycle, introduced in Section II, is imposed to the vehicle as the input and the performance of the proposed EMS is compared with the offline-optimized EMS in terms of hydrogen consumption and efficient use of the energy sources. The new FC system is used throughout the first scenario. Fig. 13 presents the obtained results from the performed test in scenario 1. Fig. 13a shows the traction power, obtained from imposing the combined driving cycle to the system, the supplied power by FC system, and the battery pack for the case of offline optimized EMS. It should be noted that this offline strategy knows the driving cycle in advanced as opposed to the online multi-mode EMS. Fig. 13b indicates the traction power and its split between the FC and the battery pack for the case of online multi-mode strategy. From these two figures, it
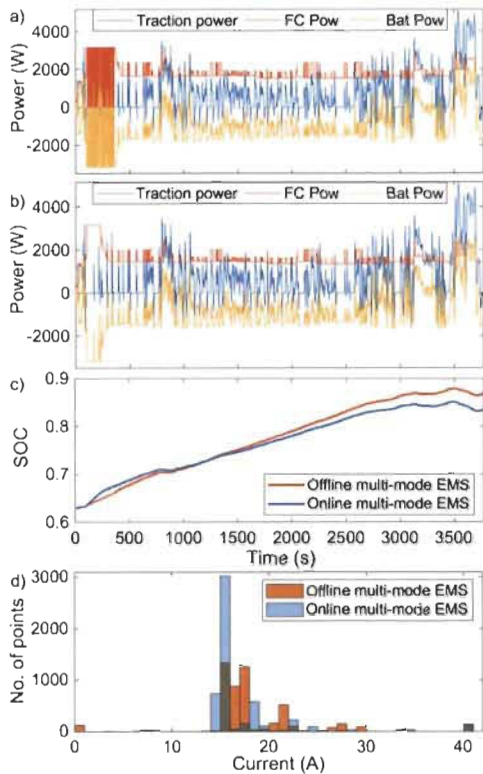
Fig. 14. Scenario 2 for assessing the online performance tracking of the FC system significance in the proposed multi-mode EMS. (a) Power split by the online multi-mode EMS, (b) power split by the offline multi-mode strategy, (c) battery SOC comparison of the strategies, and (d) PEMFC operating points distribution.

is clear that the FC system is being used to supply the main portion of the requested power in a stable manner, compared to the battery, which is mostly responsible for absorbing the fast transitions. Fig. 13c compares the battery SOC of the optimal and multi-mode controllers. It is obvious that the optimal strategy keeps the SOC in a higher level due to its priory knowledge about requested power. Fig. 13d presents the distribution of the FC operating points while meeting the requested power. Form Fig. 13d, it is clear that the proposed strategy is capable of limiting the operation of the FC system within the safe zone, which is between MP and ME, and tends to operate the FC system in the high efficient zone, which is around 15A, most of the time.

In the second scenario, the capability of the proposed EMS to deal with the FC system performance drifts is scrutinized. In this respect, the EMS test with the combined driving cycle is repeated, but by using the old PEMFC. Moreover, to signify the importance of the online PEMFC characteristics tracking, once the test is performed by deactivating the online identification, and the second time it is done by activating it. Fig. 14 shows the obtained outcomes of these tests. Fig. 14a and Fig. 14b represent the power split for offline and online multi-mode EMSs respectively. According to Fig. 14a, the offline multi-mode strategy experiences a lot of start-ups and shutdowns in the first 400 s in the FC system as it tries to recharge the battery by using the PEMFC in high power. However, it is not aware of the fact that

TABLE VII
The Cost Comparison of the EMSs in the Two Performed Scenarios

Cost (USD)	Scenario 1		Scenario 2	
	Optimized FLC	Online Multi-mode	Offline multi-mode	Online multi-mode
H_2	28.82	26.96	28.92	25.56
ON/OFF cycles	0	0	0.80	0
Recharge penalty	13	6.00	7.98	8.99
Total	32.16	32.96	37.70	34.55

the FC system has been degraded and its MP and ME points have changed. Therefore, it demands for a power level that is out of the ability of the FC to supply and causes these on/off cycles.

On the other hand, in case of the proposed online EMS as shown in Fig. 14b, in the first 100 s, the identification is performed to realize the real characteristics of the FC system and update the defuzzification tuning of the controller. After that, the FC system works in the high power area to recharge the battery pack to a certain level in addition to supplying the requested power without having any on/off cycles. Fig. 14c compares the SOC level of the battery for both cases and Fig. 14d demonstrates the FC system operating points distribution. From Fig. 14d, it is clear that the online multi-mode EMS utilizes the FC system more efficiently which can prolong its lifetime besides improving the fuel economy of the vehicle. Table VII compares the obtained cost by each of the EMSs in both scenarios. According to this table, the proposed online multi-mode strategy shows a very close performance to the optimal FLC in scenario 1. This close performance demonstrates that the proposed online EMS is able to handle unknown driving conditions with an acceptable fuel economy. The presented results of scenario 2 also confirms the satisfactory adaptation of the proposed EMS to the performance drifts of the FC system, which is a distinguishing feature of this suggested EMS. This adaptation to the real state of the FC system has made 8% of performance improvement in the online multi-mode strategy in scenario 2.

V. Conclusion

This paper presents a new online multi-mode EMS for a FCHEV. This EMS is mainly composed of a SOM based driving condition classifier and a multi-model FLC. The FLC output MF is constantly adjusted based on the online estimation of the FC system MP and ME boundaries by KF and a semi-empirical PEMFC model. The developed SOM recognizes the driving condition and activates the most proper mode of the FLC at each update to efficiently supply the request power from the vehicle. The performance of the proposed online strategy is compared with an offline optimized FLC under a combined driving cycle of CYC_NewYorkBus, CYC_UDDS, and WLTC_class 3 and a satisfactory result is obtained with only a two-percent difference in terms of the total cost of hydrogen consumption and on/off cycles of the FC system. Moreover, the performance of the proposed EMS is tested when the FC system undergoes a sixteen-percent drift regarding the maximum power. In this case, the proposed online EMS adapts to the real state of the FC

system and improves the performance of the vehicle by eight percent compared to the offline multi-mode controller.

Although this work has well established the potential of the proposed online EMS, some prospects for extending the scope of this paper remain as follows:

- Incorporating an online battery management system into the presented strategy to reach a holistic EMS.
- Performing a lifetime and ageing study of the energy sources under the proposed EMS.

REFERENCES

[1] W. R. Black and N. Sato, "From global warming to sustainable transport 1989–2006," *Int. J. Sustain. Transp.*, vol. 1, pp. 73–89, 2007.

[2] A. Khaligh and Z. Li, "Battery, ultracapacitor, fuel cell, and hybrid energy storage systems for electric, hybrid electric, fuel cell, and plug-in hybrid electric vehicles: State of the art," *IEEE Trans. Veh. Technol.*, vol. 59, no. 6, pp. 2806–2814, Jul. 2010.

[3] S. Samuelsen, "The automotive future belongs to fuel cells range, adaptability, and refueling time will ultimately put hydrogen fuel cells ahead of batteries," *IEEE Spectrum*, vol. 54, no. 2, pp. 38–43, Feb. 2017.

[4] N. Sulaiman, M. A. Hannan, A. Mohamed, E. H. Majlan, and W. R. Wan Daud, "A review on energy management system for fuel cell hybrid electric vehicle: Issues and challenges," *Renewable Sustain. Energy Rev.*, vol. 52, pp. 802–814, 2015.

[5] Y. Huang et al., "A review of power management strategies and component sizing methods for hybrid vehicles," *Renewable Sustain. Energy Rev.*, vol. 96, pp. 132–144, 2018.

[6] S. F. Tie and C. W. Tan, "A review of energy sources and energy management system in electric vehicles," *Renewable Sustain. Energy Rev.*, vol. 20, pp. 82–102, 2013.

[7] R. Zhang and J. Tao, "GA-based fuzzy energy management system for FC/SC-powered HEV considering H_2 consumption and load variation," *IEEE Trans. Fuzzy Syst.*, vol. 26, no. 4, pp. 1833–1843, Aug. 2018.

[8] M. Kandi-D, M. Soleymani, and A. A. Ghadimi, "Designing an optimal fuzzy controller for a fuel cell vehicle considering driving patterns," *Scientia Iranica*, vol. 23, pp. 218–227, 2016.

[9] J. Han, D. Kum, and Y. Park, "Synthesis of predictive equivalent consumption minimization strategy for hybrid electric vehicles based on closed-form solution of optimal equivalence factor," *IEEE Trans. Veh. Technol.*, vol. 66, no. 7, pp. 5604–5616, Jul. 2017.

[10] Y. Ren and Z. Wu, "Research on the energy management strategy of hybrid vehicle based on Pontryagin's minimum principle," in *Proc. 10th Int. Conf. Intell. Human–Mach. Syst. Cybern.*, 2018, pp. 356–361.

[11] A. Rezaei, J. B. Burl, and B. Zhou, "Estimation of the ECMS equivalent factor bounds for hybrid electric vehicles," *IEEE Trans. Control Syst. Technol.*, vol. 26, no. 6, pp. 2198–2205, Nov. 2018.

[12] C. Zheng, W. Li, and Q. Liang, "An energy management strategy of hybrid energy storage systems for electric vehicle applications," *IEEE Trans. Sustain. Energy*, vol. 9, no. 4, pp. 1880–1888, Oct. 2018.

[13] Z. Chen, R. Xiong, and J. Cao, "Particle swarm optimization-based optimal power management of plug-in hybrid electric vehicles considering uncertain driving conditions," *Energy*, vol. 96, pp. 197–208, 2016.

[14] A. Ali and D. Söffker, "Towards optimal power management of hybrid electric vehicles in real-time: A review on methods, challenges, and state-of-the-art solutions," *Energies*, vol. 11, 2018, Art. no. 476.

[15] H. Kazemi, Y. P. Fallah, A. Nix, and S. Wayne, "Predictive AECMS by utilization of intelligent transportation systems for hybrid electric vehicle powertrain control," *IEEE Trans. Intell. Veh.*, vol. 2, no. 2, pp. 75–84, Jun. 2017.

[16] H. S. Ramadan, M. Becherif, and F. Claude, "Energy management improvement of hybrid electric vehicles via combined GPS/rule-based methodology," *IEEE Trans. Autom. Sci. Eng.*, vol. 14, no. 2, pp. 586–597, Apr. 2017.

[17] E. Kamal and L. Adouane, "Intelligent energy management strategy based on artificial neural fuzzy for hybrid vehicle," *IEEE Trans. Intell. Veh.*, vol. 3, no. 1, pp. 112–125, Mar. 2018.

[18] C. M. Martinez, X. Hu, D. Cao, E. Velenis, B. Gao, and M. Wellers, "Energy management in plug-in hybrid electric vehicles: Recent progress and a connected vehicles perspective," *IEEE Trans. Veh. Technol.*, vol. 66, no. 6, pp. 4534–4549, Jun. 2017.

[19] A. Fotouhi, R. Yusof, R. Rahmani, S. Mekhilef, and N. Shateri, "A review on the applications of driving data and traffic information for vehicles' energy conservation," *Renewable Sustain. Energy Rev.*, vol. 37, pp. 822–833, 2014.

[20] M. K. Dayeni and M. Soleymani, "Intelligent energy management of a fuel cell vehicle based on traffic condition recognition," *Clean Technol. Environ. Policy*, vol. 18, pp. 1945–1960, 2016.

[21] Z. Chen, C. C. Mi, J. Xu, X. Gong, and C. You, "Energy management for a power-split plug-in hybrid electric vehicle based on dynamic programming and neural networks," *IEEE Trans. Veh. Technol.*, vol. 63, no. 4, pp. 1567–1580, May 2014.

[22] Y. L. Murphey, J. Park, Z. Chen, M. L. Kuang, M. A. Masrur, and A. M. Phillips, "Intelligent hybrid vehicle power control—Part I: Machine learning of optimal vehicle power," *IEEE Trans.Veh. Technol.*, vol. 61, no. 8, pp. 3519–3530, Oct. 2012.

[23] Z. Chen, L. Li, B. Yan, C. Yang, C. M. Martínez, and D. Cao, "Multimode energy management for plug-in hybrid electric buses based on driving cycles prediction," *IEEE Trans. Intell. Transp. Syst.*, vol. 17, no. 10, pp. 2811–2821, Oct. 2016.

[24] R. Zhang, J. Tao, and H. Zhou, "Fuzzy optimal energy management for fuel cell and supercapacitor systems using neural network based driving pattern recognition," *IEEE Trans. Fuzzy Syst.*, vol. 27, no. 1, pp. 45–57, Jan. 2019.

[25] J. Liu, Y. Chen, J. Zhan, and F. Shang, "An on-line energy management strategy based on trip condition prediction for commuter plug-in hybrid electric vehicles," *IEEE Trans. Veh. Technol.*, vol. 67, no. 5, pp. 3767–3781, May 2018.

[26] H. Lim and W. Su, "Hierarchical energy management for power-split plug-in HEVs using distance-based optimized speed and SOC profiles," *IEEE Trans. Veh. Technol.*, vol. 67, no. 10, pp. 9312–9323, Oct. 2018.

[27] H. Tian, X. Wang, Z. Lu, Y. Huang, and G. Tian, "Adaptive fuzzy logic energy management strategy based on reasonable SOC reference curve for online control of plug-in hybrid electric city bus," *IEEE Trans. Intell. Transp. Syst.*, vol. 19, no. 5, pp. 1607–1617, May 2018.

[28] K. Song et al., "Multi-mode energy management strategy for fuel cell electric vehicles based on driving pattern identification using learning vector quantization neural network algorithm," *J. Power Sources*, vol. 389, pp. 230–239, 2018.

[29] D. Zhou, A. Al-Durra, F. Gao, A. Ravey, I. Matraji, and M. G. Simões, "Online energy management strategy of fuel cell hybrid electric vehicles based on data fusion approach," *J. Power Sources*, vol. 366, pp. 278–291, 2017.

[30] J. Chen, C. Xu, C. Wu, and W. Xu, "Adaptive fuzzy logic control of fuel-cell-battery hybrid systems for electric vehicles," *IEEE Trans. Ind. Inform.*, vol. 14, no. 1, pp. 292–300, Jan. 2018.

[31] M. Kandidayeni, A. Macias, A. A. Amamou, L. Boulon, S. Kelouwani, and H. Chaoui, "Overview and benchmark analysis of fuel cell parameters estimation for energy management purposes," *J. Power Sources*, vol. 380, pp. 92–104, 2018.

[32] M. Kandidayeni, A. Macias, A. A. Amamou, L. Boulon, and S. Kelouwani, "Comparative analysis of two online identification algorithms in a fuel cell system," *Fuel Cells*, vol. 18, pp. 347–358, 2018.

[33] N. Bizon and P. Thounthong, "Real-time strategies to optimize the fueling of the fuel cell hybrid power source: A review of issues, challenges and a new approach," *Renewable Sustain. Energy Rev.*, vol. 91, pp. 1089–1102, 2018.

[34] D. Zhou, A. Al-Durra, I. Matraji, A. Ravey, and F. Gao, "Online energy management strategy of fuel cell hybrid electric vehicles: A fractional-order extremum seeking method," *IEEE Trans. Ind. Electron.*, vol. 65, no. 8, pp. 6787–6799, Aug. 2018.

[35] D. Zhou, A. Ravey, A. Al-Durra, and F. Gao, "A comparative study of extremum seeking methods applied to online energy management strategy of fuel cell hybrid electric vehicles," *Energy Convers. Manage.*, vol. 151, pp. 778–790, 2017.

[36] K. Ettihir, M. Higuita Cano, L. Boulon, and K. Agbossou, "Design of an adaptive EMS for fuel cell vehicles," *Int. J. Hydrogen Energy*, vol. 42, pp. 1481–1489, 2017.

[37] K. Ettihir, L. Boulon, and K. Agbossou, "Optimization-based energy management strategy for a fuel cell/battery hybrid power system," *Appl. Energy*, vol. 163, pp. 142–153, 2016.

[38] L. Xu, J. Li, J. Hua, X. Li, and M. Ouyang, "Adaptive supervisory control strategy of a fuel cell/battery-powered city bus," *J. Power Sources*, vol. 194, pp. 360–368, 2009.

[39] M. Carignano, V. Roda, R. Costa-Castelló, L. Valiño, A. Lozano, and F. Barreras, "Assessment of energy management in a fuel cell/battery hybrid vehicle," *IEEE Access*, vol. 7, pp. 16110–16122, 2019.

[40] V. H. Johnson, "Battery performance models in ADVISOR," *J. Power Sources*, vol. 110, pp. 321–329, 2002.

[41] R. F. Mann, J. C. Amphlett, M. A. I. Hooper, H. M. Jensen, B. A. Peppley, and P. R. Roberge, "Development and application of a generalised steady-state electrochemical model for a PEM fuel cell," *J. Power Sources*, vol. 86, pp. 173–180, 2000.

[42] J. P. F. Trovão, M. Roux, É. Ménard, and M. R. Dubois, "Energy- and power-split management of dual energy storage system for a three-wheel electric vehicle," *IEEE Trans. Veh. Technol.*, vol. 66, no. 7, pp. 5540–5550, Jul. 2017.

[43] T. Kohonen, E. Oja, O. Simula, A. Visa, and J. Kangas, "Engineering applications of the self-organizing map," *Proc. IEEE*, vol. 84, no. 10, pp. 1358–1384, Oct. 1996.

[44] S. S. Haykin, *Kalman Filtering and Neural Networks*. Hoboken, NJ, USA: Wiley, 2001.

[45] K. Ettihir, L. Boulon, and K. Agbossou, "Energy management strategy for a fuel cell hybrid vehicle based on maximum efficiency and maximum power identification," *IET Elect. Syst. Transp.*, vol. 6, pp. 261–268, 2016.

Loïc Boulon (M'10–SM'16) received the master's degree in electrical and automatic control engineering from the University of Lille, Lille, France, in 2006, and the Ph.D. degree in electrical engineering from the University of Franche-Comté, Besançon, France. Since 2010, he has been a Professor with the Université du Québec à Trois-Rivières (Canada) and is with the Hydrogen Research Institute (Full Professor since 2016). He has authored or coauthored more than 100 scientific papers in peer-reviewed international journals and international conferences. His work deals with modeling, control, and energy management of multiphysics systems. His research interests include hybrid electric vehicles, energy and power sources (especially battery in cold weather operation), and fuel cell systems. Prof. Boulon was General Chair for the IEEE-Vehicular Power and Propulsion Conference in Montréal, QC, Canada, in 2015. He is the VP-Motor Vehicles of the IEEE Vehicular Technology Society and holds the Canada Research Chair in Energy Sources for the Vehicles of the Future.

Mohsen Kandidayeni (S'18) received the master's degree in mechatronics from Arak University, Arak, Iran, in 2014. He is currently working toward the Ph.D. degree with the Université du Québec à Trois-Rivières (UQTR), Trois-Rivières, QC, Canada, working on energy-related topics such as hybrid electric vehicles, fuel cell systems, energy management, multiphysics systems, modeling and control. His research interests include renewable energy, fuel cell, transportation, intelligent transport systems, vehicular systems control, and hybrid electric and electric vehicles.

Sousso Kelouwani (M'00–SM'17) received the B.S. and the M.Sc.A. degrees from the Université du Québec à Trois-Rivières (UQTR), Trois-Rivières, QC, Canada, in 2000 and 2002, respectively, and the Ph.D. degree (automation and systems) from the École Polytechnique de Montréal, Montréal, QC, Canada, in 2010, all in electrical engineering. Since 2018, he has been a Full Professor of mechatronics with the Department of Mechanical Engineering, UQTR. Before starting his doctoral studies, he worked in research and development in the field of cell phone application optimization for Cilys 53 Inc. (2002–2005) and Openwave Inc. (2005–2006). He has also worked with several Canadian transportation companies to develop intelligent, energy-efficient, and driverless vehicles, and holds three U.S. patents. His research interests include optimization of energy systems for vehicular applications, advanced driving assistance techniques, ecoenergy navigation of autonomous vehicles, and hybridization of energy sources for vehicles with low ecological impact (battery, fuel cell, hydrogen generator, etc.) in harsh weather conditions. Prof. Kelouwani was the recipient of the Environment Award of the Grand Prix for Excellence in Transport from the Quebec Transportation Association (AQTr) in 2018 for the development of a hydrogen range extender based on a hydrogen generator for electric vehicles, and also the Canada Governor General's Gold Medal in 2000. He holds the Industrial Research Chair DIVEL in Intelligent Navigation of Autonomous Industrial Vehicles.

Alvaro Omar Macias Fernandez (S'17) was born in Mexico City, in 1992. He received the B.S. degree in mechatronics engineering from the Tec de Monterrey, Guadalajara, Mexico, in 2015, and the M.S. degree in electrical engineering from the Université du Québec à Trois-Rivières, Trois-Rivières, QC, Canada, in 2018. He is currently working toward the Ph.D. degree in electrical engineering with the Université du Québec à Trois-Rivières, Canada. From 2015 to 2016, he was with Research and Development, Centro de Investigación y de Estudios Avanzados del Instituto Politécnico Nacional, Mexico. His current research interest includes the development of energy management strategies for fuel cell systems, passive and active system configuration, and fuel cell modeling.

Arash Khalatbarisoltani (S'18) received the bachelor's degree in electrical engineering from the Sadjad University of Technology, Mashhad, Iran, 2012, and the master's degree in mechatronics from Arak University, Arak, Iran, 2016. He is currently working toward the Ph.D. degree with the Hydrogen Research Institute (IRH) and the Department of Electrical and Computer Engineering, Université du Québec à Trois-Rivières (UQTR), Trois-Rivières, QC, Canada. His work deals with optimization, energy management of multipower source systems, modular systems, game theory, and decentralized control. His research interests include decentralized systems, fuel cell systems, energy management, fuel cell vehicles, and modular systems.

Hicham Chaoui (S'01–M'12–SM'13) received the Ph.D. degree in electrical engineering (with honors) from the University of Quebec, Trois-Rivières, QC, Canada, in 2012. His career has spanned both academia and industry in the field of control and energy systems. From 2007 to 2014, he held various engineering and management positions in the Canadian industry. From 2014 to 2016, he was an Assistant Professor with Tennessee Technological University, Cookeville, TN, USA. Since then, he has been a Faculty Member with Carleton University, Ottawa, ON, Canada. His research interests include adaptive and nonlinear control theory, intelligent control, robotics, electric motor drives, and energy conversion and storage systems. He has authored or coauthored more than 100 journal and conference publications. Dr. Chaoui was a recipient of the Best Thesis Award and the Governor General of Canada Gold Medal Award. He is a registered Professional Engineer in the province of Ontario. He is also an Associate Editor for the IEEE TRANSACTIONS ON VEHICULAR TECHNOLOGY.